AD NUMBER

AD841194

NEW LIMITATION CHANGE

TO

Approved for public release, distribution unlimited

FROM

Distribution authorized to U.S. Gov't. agencies and their contractors; Critical Technology; AUG 1968. Other requests shall be referred to Air Force Rocket Propulsion Lab., Attn: RPPR-STINFO, Edwards AFB, CA 93523.

AUTHORITY

Air Force Rocket Propulsion Lab. ltr dtd 27 Oct 1971

AFRPL-TR-68-143

ADVANCED COMPOSITE CARBIDE NOZZLES

R. P. Radtke and L. M. Swope
AEROJET-GENERAL CORPORATION

TECHNICAL REPORT AFRPL-TR-68-143

August 1968

Rocket Propulsion Laboratory
Research and Technology Division
Air Force Systems Command
Edwards, California

AFRPL-TR-68-143
August 1968

ADVANCED COMPOSITE CARBIDE NOZZLES

R. P. Radtke and L. M. Swope

31594T

FOREWORD

This final report was prepared by the Research and Technology Operations of the Aerojet-General Corporation, Sacramento, California, under USAF Contract AF 04(611)-11608.

The work was administered under the direction of the Air Force Rocket Propulsion Laboratory, Motor Development Branch, Edwards Air Force Base, California, with Captain E. M. Schneider and Lieutenant D. Zorich acting as project engineers.

L. M. Swope was the project manager and R. P. Radtke was the major investigator for this program. Contributions to the experimental effort were made by P. Booker, P. Dangel, R. Kreun, E. Spencer, J. Hoffman, R. Cobb, R. Knapp, W. Walker, C. Gracey, B. Baker, H. Effron, and T. Eckert. Technical direction was provided by Lrs. E. Rudy and S. Windisch.

The manuscript was released in August 1968 for publication as an Air Force Propulsion Laboratory Technical Report.

This technical report has been reviewed and is approved.

Lt. D. Zorich
Project Engineer
Air Force Rocket Propulsion Laboratory

ABSTRACT

The purpose of this program was to develop two thermal-shock-resistant composite carbide systems that could be reliably used with high-flame-temperature solid rocket propellants. The selected systems were (1) a microcomposite consisting of a tantalum/hafnium monocarbide and tantalum/hafnium alloy, and (2) a tantalum-carbide coated, tantalum carbide/graphite hypereutectic.

Fabrication procedures were developed, and ambient and elevated temperature properties were characterized for both the microcomposite and TaC-C hypereutectic systems. The composites were evaluated for thermal shock and chemical corrosion resistance in a hyperthermal environmental simulator using subscale inserts. The TaC-C composite exhibited outstanding thermal shock resistance, while the microcomposite showed excellent corrosion resistance.

Scale-up of the fusion casting of the TaC-C hypereutectic composite to produce 4.2-in.-dia by 3.0-in.-long billets was demonstrated. Two solid propellant motor firings using 6500°F propellant were conducted on nozzles containing TaC-C hypereutectic throat inserts.

TABLE OF CONTENTS

TABLE OF CONTENTS (cont.)

APPENDIX

TABLE LIST

FIGURE LIST

FIGURE LIST (cont.)

FIGURE LIST (cont.)

FIGURE LIST (cont.)

FIGURE LIST (cont.)

FIGURE LIST (cont.)

FIGURE LIST (cont.)

SECTION I

INTRODUCTION

This report presents the results of the Advanced Composite Carbide Nozzles Program conducted under Contract AF 04(611)-11608 and is organized into the five basic areas of work: (1) development of microcomposite, (2) development of tantalum carbide, lined-tantalum carbide/carbon hypereutectic composite, (3) thermal-shock-resistance evaluation, (4) chemical corrosion evaluation, and (5) demonstration firing tests.

A primary objective of this program was to develop thermal-shock-resistant composite carbides that can be reliably used as solid rocket nozzle inserts to successfully withstand solid rocket propellants having high flame temperatures (+6800°F) at a chamber pressure of 700 psi.

A. SIGNIFICANT FACTORS

The two most significant factors that influence the development and performance of carbide rocket nozzles are (1) material composition and (2) thermal shock resistance.

1. Material Composition

Composite carbides for rocket nozzle applications must incorporate a ductile matrix to increase thermal shock resistance and a carbide phase to provide high temperature capability. On this basis, consideration must be given to the following factors:

a. Only the monocarbides of tantalum, hafnium, and mixtures of the two have high enough melting points to withstand propellant flame temperatures in excess of 6800°F.

I, A, Significant Factors (cont.)

b. The ductile phase within the carbide matrix must be chemically and metallurgically stable. Low melting temperature phases must not form by reaction of the carbide structure with the ductile matrix. In early programs throughout the industry, this problem of internal reactions resulted in the failure of carbide composites.

c. The raw materials must not be contaminated. Impurities can reduce the melting temperatures of the high-temperature phases of the composites as well as inhibit the formation of desirable microstructures. In addition, impurities inhibit sintering and thus reduce the subsequent strength of the fabricated insert.

2. Thermal Shock Resistance Factors

Thermal shock failure in brittle materials occurs when excessively high stresses created by differential thermal expansion imposed by thermal gradients cannot be relieved by elastic or plastic flow. These stresses initiate cracks which propagate through the material and cause failure.

The thermal shock resistance of a material is not a material property but is dependent on complex interrelationships between the material properties and its environment. As a result, the thermal shock resistance of composite bodies cannot be clearly defined. A number of investigators have studied thermal shock and have established thermal shock and property relationships. Although these relationships cannot be determined with high reliability, there is some correlation of thermal shock relationships with thermal shock tests.

I, A, Significant Factors (cont.)

Bolmd and Walton (Reference 1) reviewed the subject of thermal shock and listed the five thermal shock parameters most frequently used:

$$R = \frac{S}{\alpha E}$$

$$R = \frac{S\ (1-\mu)}{\alpha E}$$

$$R = \frac{SK}{\alpha E}$$

$$R = \frac{SK\ (1-\mu)}{\alpha E}$$

$$R = \frac{Sa\ (1-\mu)}{\alpha E}$$

where

R = thermal shock resistance index
S = strength
E = Young's modulus
α = linear thermal expansion coefficient
μ = Poisson's ratio
K = thermal conductivity
a = thermal diffusivity = $\frac{K}{\rho c}$
where c = specific heat
ρ = density

The properties of tensile strength, modulus, and thermal expansion are the most significant properties, appearing in all five of the relationships. Though conductivity appears in only three of the relationships, its importance in establishing the thermal gradient makes it also a very significant property. Poisson's ratio, density, and specific heat can lead to a better understanding, but are of lesser importance.

I, A, Significant Factors (cont.)

For rocket nozzle applications, it is desirable to develop composites with high tensile strength because thermal shock cracking generally initiates in tension. The modulus of elasticity of the composite should be as low as possible to allow elastic deformation during the period of high thermally induced stress gradients. The development of composites with low thermal expansion properties results in a lower level of tensile stress in the cold material than for a high expansion material with the same temperature gradient profile. A composite with high thermal conductivity minimizes the thermal gradient problem which could create critical tensile stresses on outside-diameter of nozzle inserts.

B. COMPOSITE MATERIAL SELECTION

The composite materials evaluated during this program were selected from previous work at Aerojet. This work indicated that composite materials consisting of a metal phase and a carbide phase or graphite and a carbide phase have good potential for reasonably good thermal shock resistance at low temperatures, and at the same time maintaining refractory properties at firing temperatures. The metal phase provides low-temperature ductility and resistance to the propagation of cracks. Likewise, the graphite phase provides resistance to crack propagation. The carbide phase provides the high-temperature properties. A brief discussion of the two systems is as follows:

1. Microstructural Composite

The microstructural composite is based upon the Ta-Hf-C phase diagram developed by Aerojet (Reference 2) see Figure 1. Phase equilibria in the Ta-Hf-C system show that at the composition range near 10Ta/50Hf and 30Ta/40Hf at 37 to 40 at%C, there is chemical compatibility between metal alloy and refractory monocarbide over a wide temperature range, RT to 1850°C (3361°F). In addition, the monocarbide at this composition becomes

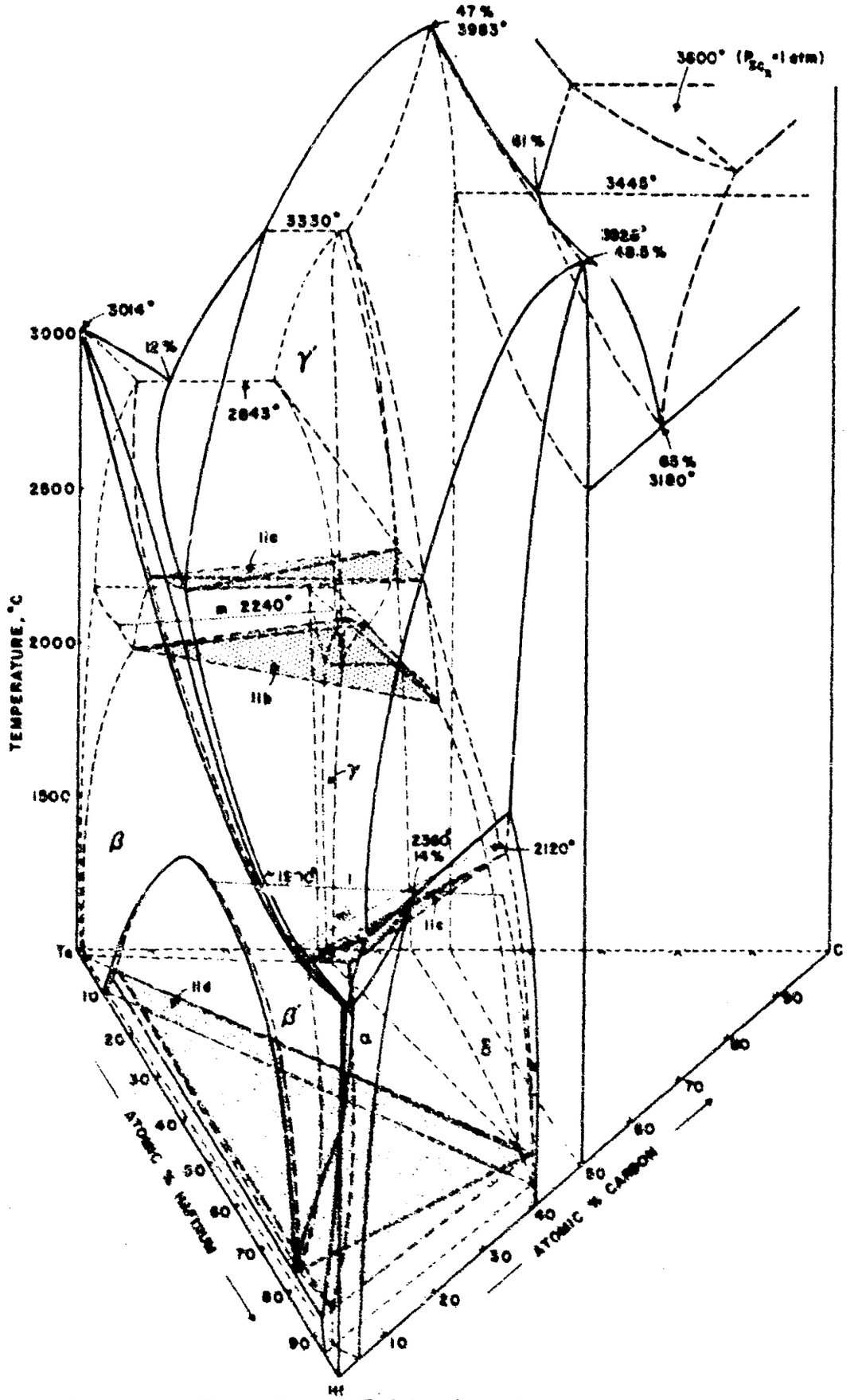

Figure 1. Phase Diagram Hafnium-Tantalum-Carbon

I, B, Composite Material Selection (cont.)

disproportionate on cooling below approximately 2000°C and the metal alloy precipitates within the carbide grains. The shifting equilibrium, shown by the shifting of the boundary line separating the monocarbide and the two phase (δ + β) can be seen by comparing Figure 2 and Figure 3, which are isothermal sections at 1850°C and 2000°C (3632°F).

Upon reheating of the microcomposite, the metal alloy phase becomes a disappearing phase by inverting to the monocarbide phase because of the increased solubility of the carbide for the metal phase. This phase relationship also occurs in the hafnium-carbon binary system. The increasing solubility of hafnium in the monocarbide on heating from ambient to 2360°C can be seen in Figure 1. Figure 4 is a set of photomicrographs typical of this concept and shows the most desirable two-phase composite structure as well as the single-phase structure resulting from heating above 2200°C (4000°F).

2. Tantalum-Carbide-Lined Hypereutectic Composite

The hypereutectic composite system consists of a high-density, thin-tantalum monocarbide (melting temperature approximately 3950°C or 7150°F) liner formed in situ on a tantalum carbide/graphite hypereutectic substrate. This substrate possesses good thermal shock resistance, has a minimum melting point of 3444°C (6230°F) (Reference 2), and has a thermal expansion that is compatible with that of the liner. The hypereutectic structure is characterized by dispersed graphite flakes in the monocarbide-graphite eutectic matrix (Figure 5).

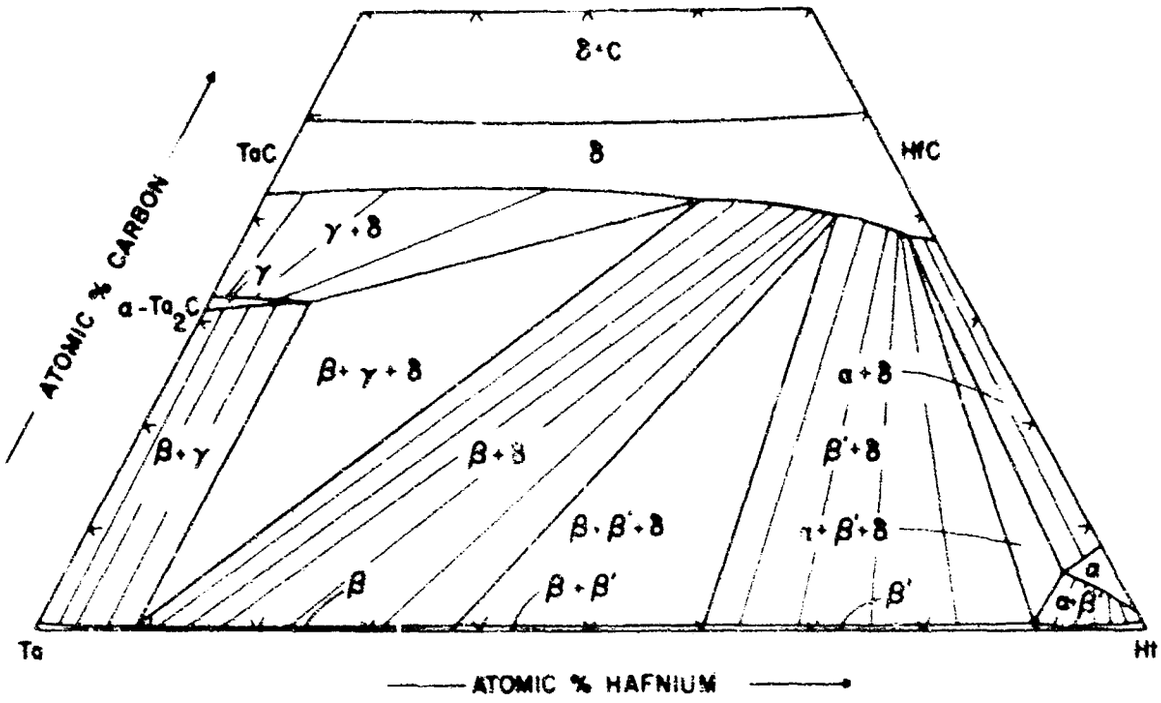

Figure 2. Temperature Section at 1850°C (3362°F)

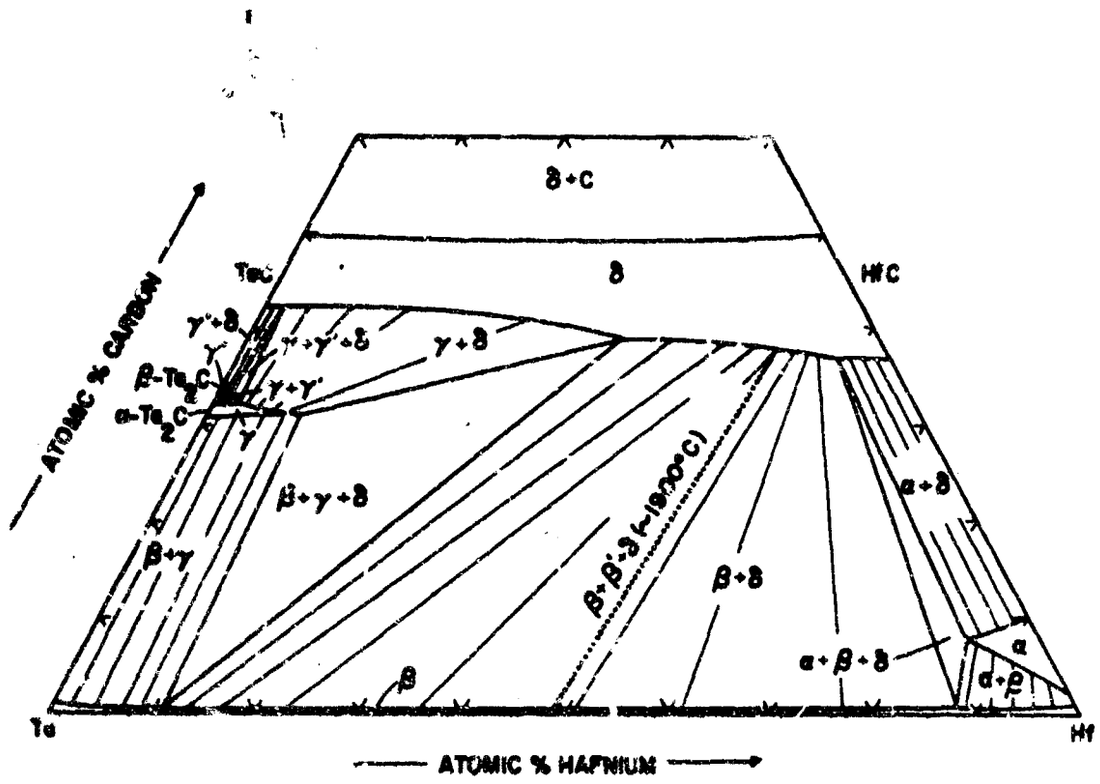

Figure 3. Temperature Section at 2000°C (3632°F)

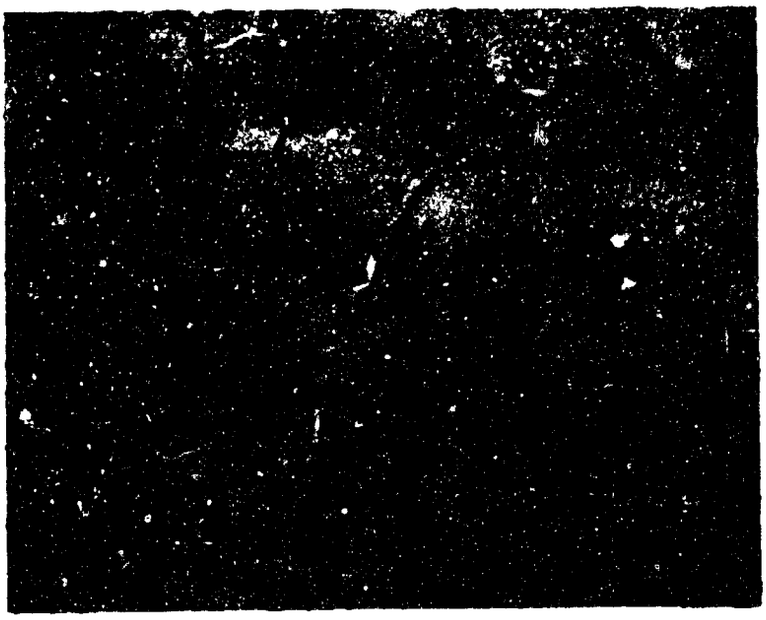

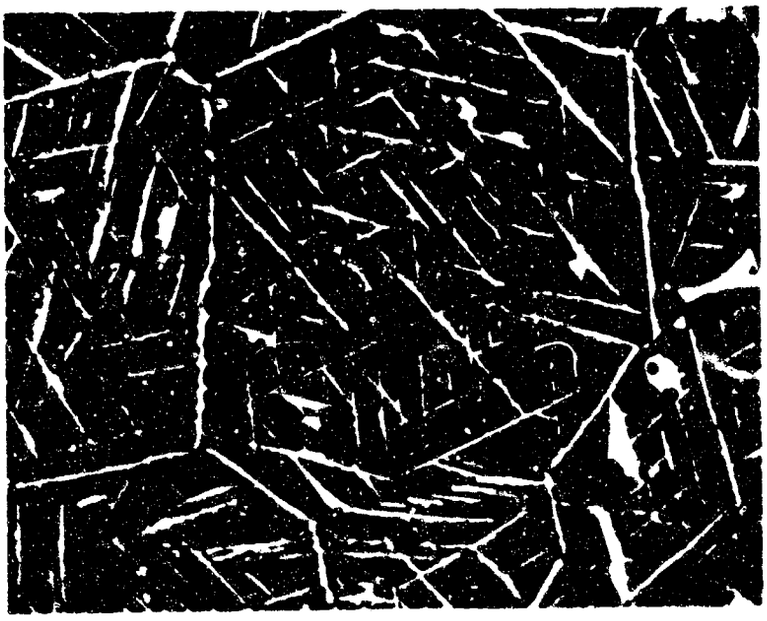

400X

Figure 4. Typical Microstructure of Two-Phase Composite Carbide Hf-C Matrix and Hf Metal (White Regions) Which Changes on Heating above 2200°C (4000°F) to a Stable Solid Solution Hf-C (Top)

Black Striated Regions are edges of graphite flakes — 100X

Figure 5. Typical Microstructure of Tantalum Carbide/Graphite Hypereutectic Structure (Melt-Formed at 3500°C)

SECTION II

SUMMARY

A. DEVELOPMENT OF MICROCOMPOSITE

1. Development of Fabrication Procedures

Tantalum, hafnium, tantalum-monocarbide, and hafnium-monocarbide powders were the starting materials for the microcomposite system. Six material compositions (18Ta-45Hf-37C, 13Ta-50Hf-37C, 8Ta-55Hf-37C, 13Ta-47Hf-40C, 10Ta-50Hf-40C, and 5Ta-55Hf-40C) were investigated along with two starting material metal ratios. Specimens were fabricated by hot pressing with varying sintering temperatures, times, cooling rates, and pressures to obtain the desired structures.

It was determined that density increased with time at temperature and a significant decrease in density occurred with increasing temperature as a result of carburization. Some latitude was found in the hot-press conditions required to produce the desired microcomposite microstructure from the three compositions containing 37 at%C. The hot-press temperature can vary from 2500 to 2700°C for pressing durations between 5 and 15 minutes. A relatively fast cooling rate, 500°C/minute, developed the desired fine needle-shaped metal alloy precipitation. Slow cooling rates, 50 to 100°C/minute, resulted in consolidation of the metal phase into both spherical and large needle shapes. Heat-treated was found to agglomerate the needle-shaped metal alloy precipitate. The three compositions with nominal 40 at%C contained no metal alloy phase.

2. Material Properties Characterization

Flexural strength, modulus of elasticity, density, and metal-alloy phase development were determined for the six microcomposite compositions. Applying the criteria for optimum thermal shock characteristics which favor

II, A, Development of Microcomposite (cont.)

high strength and low modulus of elasticity, two compositions, 6Ta-55Hf-37C and 8Ta-54Hf-38C, were chosen for elevated temperature properties, thermal shock, and chemical corrosion characterization. The elevated temperature tests showed that these two compositions had flexure strengths considerably higher than those reported for monocarbides. The thermal expansion and diffusivity data were comparable to the monocarbides.

B. DEVELOPMENT OF TANTALUM CARBIDE LINED-TANTALUM CARBIDE/CARBON HYPEREUTECTIC COMPOSITE

1. Development of Fabrication Procedures

The fabrication process utilized to produce the hypereutectic carbide composite was a fusion and drop-casting technique. Fabrication procedures were developed for four compositions (80 v/o TaC-20 v/o C, 70 v/o TaC-30 v/o C, 60 v/o TaC-40 v/o C, and 50 v/o TaC-50 v/o C). In initial scale-up studies, 1.5-in.-dia by 3.0-in.-long billets were produced. Final scale-up was to a billet size of 4.2 in. dia by 3.0 in. long. A diffusion process for forming a TaC liner on a TaC-C hypereutectic substrate was demonstrated.

2. Material Properties Characterization

Ambient and elevated temperature testing was conducted on specimens containing various carbon contents. The flexure strength and modulus of elasticity decreased with increasing carbon content. The strength of a given composition at the same test temperature could be correlated with the morphology of the graphite flakes. Flakes that are thin, short, and evenly dispersed are conducive to higher strength. The thermal expansion characteristics closely followed the expansion behavior for tantalum monocarbide.

II, Summary (cont.)

C. THERMAL SHOCK AND CHEMICAL CORROSION EVALUATIONS

Thermal shock resistance and chemical corrosion tests were conducted in a Hyperthermal Environmental Simulator (HES) at high cold wall heat flux levels (2800 to 4400 Btu/ft^2/sec) on two microcomposite compositions and on various TaC-C hypereutectic compositions. Both microcomposite compositions underwent fine thermal stress cracking; the 8Ta-55Hf-37C composition had better thermal shock resistance than the 8Ta-54Hf-38C composition. The hypereutectic composites had outstanding thermal shock resistance. Cracking was observed in only one specimen which was found to be of eutectic composition. The carbide composites were compared to G-90 graphite in the chemical-corrosion tests. The two microcomposite compositions were equal in resistance to attack and the surface regression rates were considerably lower than the G-90. The TaC-liued hypereutectic composites were approximately the same as the G-90 graphite. The better performance of the microcomposite was attributed to the formation of a higher melting oxide, HfO_2, on the flame surface of the microcomposite in comparison to the βTa_2O_5 formation on the hypereutectic.

D. FABRICATION OF NOZZLE INSERTS AND DEMONSTRATION FIRING TESTS

Five approximately 4.2-in.-dia by 3-in.-long nozzle inserts were fabricated: two microcomposites by hot pressing and three hypereutectics by casting. The first microcomposite insert cracked during hot-pressing. The second insert cracked during machining which was probably due to the existence of microcracks or high residual stresses during cooldown. Two hypereutectic inserts were fabricated, and the third was sectioned for laboratory examination. Two solid propellant motor firings were conducted using the AFRPL 36-in.-nominal-inside dia char motor to demonstrate the performance of the TaC-C hypereutectic system. The nozzle assembly for the first motor had a segmented throat insert. During test firing, the aft segment of the throat was ejected at 38 sec. The postfire analysis attributed failure to uneven material loss which

II, D, Fabrication of Nozzle Inserts and Demonstration Firing Tests (cont.)

resulted in buckling and ejection of the segment. In the second nozzle, a single piece throat was successfully test fired for 43 sec. The propellant had a 6300°F theoretical flame temperature, and the chamber pressure was 750 psi.

The regression rate (1.06 mil/sec) at the throat was very low and thermal shock resistance was excellent. This firing demonstrated a significant advancement in carbide technology for rocket applications and verified the potential of TaC-C hypereutectic composites for high-performance, solid propellant motors.

SECTION III

TECHNICAL DISCUSSION

A. TASK 1—DEVELOPMENT OF MICROCOMPOSITE

The objective of this work was to investigate the relationship of material and processing variables on phase configurations, to develop a fabrication technique suitable for scale-up, and to characterize mechanical and thermal properties at ambient and elevated temperatures.

1. Starting Material Characterization

Tantalum, hafnium, tantalum monocarbide, hafnium monocarbide, and graphite powders were the starting materials for the microcomposite. The sources of material were: tantalum and hafnium powders—Wah Chang Corporation; tantalum carbide—Wah Chang Corporation and Kawecki Chemical Corporation; hafnium carbide—produced at Aerojet; and graphite powder, Grade GP-48--carbon Products Division, Union Carbide Corporation.

a. Preparation of Hafnium Carbide

Hafnium carbide was produced by the carbothermic reduction of hafnium dioxide. The carbothermic reaction was conducted in a 100-kw Heraeus high vacuum induction furnace. Because of the high temperature thermodynamic stability of the Hf-O-C complex, high vacuum degassing at 2200°C was required to reduce the partial pressure of the evolved CO to bring the reaction to completion. Processing for approximately 8 hr at 2200°C reduced the CO evolution, and a final vacuum of 1×10^{-5} torr was achieved, resulting in an essentially oxygen-free carbide.

III, A, Task 1--Development of Microcomposite (cont.)

The first grinding of a batch of HfC for 12 hr by tungsten carbide ball milling with a carbon tetrachloride medium resulted in an increase in the oxygen content from 89 to 3066 ppm. Results of a grinding study showed that a minimum of 4 hr of ball-milling was required to comminute all the HfC to a particle size finer than 44 microns. The oxygen content increased detrimentally from 89 to 4380 ppm.

Dry grinding in an agate mortar was also evaluated as an expedient method for producing small batches of low-oxygen-content carbide for the microcomposite development work. This resulted in the oxygen content increasing from 89 to 268 ppm, which was satisfactory for developing the microcomposite, but approached the maximum allowable content. Ball-milling the carbide to the required particle size distribution, followed by a high vacuum degassing at 2200°C in the Heraeus induction furnace, was selected as the best approach. The batches of as-produced HfC were blended together, ball-milled for 12 hr to produce an average particle size less than 10 microns, and vacuum degassed at 2200°C. Final grinding was conducted in an inert atmosphere glove-box.

b. Results of Characterization Tests*

The following characterization tests were conducted on the starting materials:

Analyses	Material
Chemical	
a. Total carbon	TaC, HfC
b. Free carbon	TaC, HfC
c. Oxygen	Ta, Hf, TaC, HfC
d. Spectrographic	C, Ta, Hf, TaC, HfC, HfO_2
Particle size	C, Ta, Hf, TaC, HfC
X-ray diffraction	TaC, HfC

*A discussion of the test procedures used throughout the program for determining pertinent thermal, chemical, physical and structural properties is presented in the Appendix.

III, A, Task 1--Development of Microcomposite (cont.)

(1) Chemical Analysis

Table I shows the results of the chemical analyses on all the starting materials. For each material, with the exception of the graphite powder, an analysis was furnished by the supplier and a comparative analysis was conducted to verify the major concentration of impurities. Results from the two separate analyses were in satisfactory agreement.

(2) Particle Size

The average particle size of the starting materials as determined by Fisher subsieve analyses is given in Table II. The particle-size distribution by the Andreason sedimentation pipet method is plotted in Figure 6.

(3) X-Ray Diffraction

The lattice parameters for the HfC and Ta_2C obtained from the exposures with Cu-$K\alpha$-radiation were a = 4.635 Å and a = 4.445 Å, respectively, which are in good agreement with the reported literature (Reference 3).

2. Development of Fabrication Procedures

a. Experimental Procedures

To achieve a dense (exceeding 95% of theoretical) composite with the proper two-phase microstructure and composition, two fabrication steps were utilized: (1) hot-pressing and (2) heat treatment.

TABLE I

CHEMICAL ANALYSIS OF STARTING MATERIALS

Material:	HfO_2		HfC	Hf		Ta		Carbon		TaC	
Supplier:	Pittsburgh Plate		Aerojet	Wah Chang		Wah Chang		Carbon Products			
Impurity Element	Supplier's Analysis, ppm	Verification Analysis ppm	Analysis, ppm	Supplier's Analysis, ppm	Verification Analysis, ppm	Supplier's Analysis, ppm	Verification Analysis, ppm	Supplier's Analysis, ppm	Verification Analysis, ppm	Supplier's Analysis, ppm	Verification Analysis, ppm
Al	94	100	100	97	100	< 20	100	Not Furnished	10	< 25	< 10
B	0.3			< 0.2		< 1				2	< 100
C (Free)			0.23%	40		< 40				-	
C (Total)			6.316%							6.3%	6.3%
Ca	100									< 50	< ?
Cb	300 (est)			< 100						< 1	< < 100
Cd	0.3%			< 1		< 1				-	< 100
Co	5			< 5		< 20				< 5	< < 10
Cr	100	100		15		< 20				< 10	< 100
Cu	35	50	5%	< 40	50	< 10	50			< 2	
Fe	450	100	100	96	100	150				25	
H				9%							
Mg	20			< < 10		< 20				< 10	
Mn	20			< < 10		< 20				< 10	< 10
Mo	32	100		< < 10		< 20				< 10	-
N				130		55				35	
Ni				< 10		< 20				< 10	< 10
O			268 to 419*	850	520*	230	389*			420	< 100
Pb	20			< < 5					100	< < 5	
Si	275	500		< < 40	10	70	100			< < 10	< 1
Sn				< < 10		< 20				< < 10	< 100
Ta				< 200							
Ti	0.3 to 0.4%(est)	0.1 to 0.5%	0.1 to 0.5%	37	100	< 50	10			< 10	< 10
V	20			< 5						< 10	< < 100
W				< 25		< 10					
Zr***	0.62%	1.0 to 3.0%**	1.0 to 3.0%**	2.50%	1.0 to 3.0%**	< 50				< 50	< 10

* Determined by Luvak, Inc., Newton, Mass, for HfC the data presents the range of values on four batches of carbide.

** Limits of Detection

*** $\frac{Hf + Zr}{Total\ Metal} = 98.88\%$

$\frac{Hf}{Total\ Metal} = 98.26\%$

TABLE II

FISHER SUBSIEVE SIZER ANALYSES

	Average Particle Diameter, Microns
Tantalum carbide	6.5
Hafnium carbide	3.0
Hafnium	7.3
Tantalum	14.6
Carbon	3.0

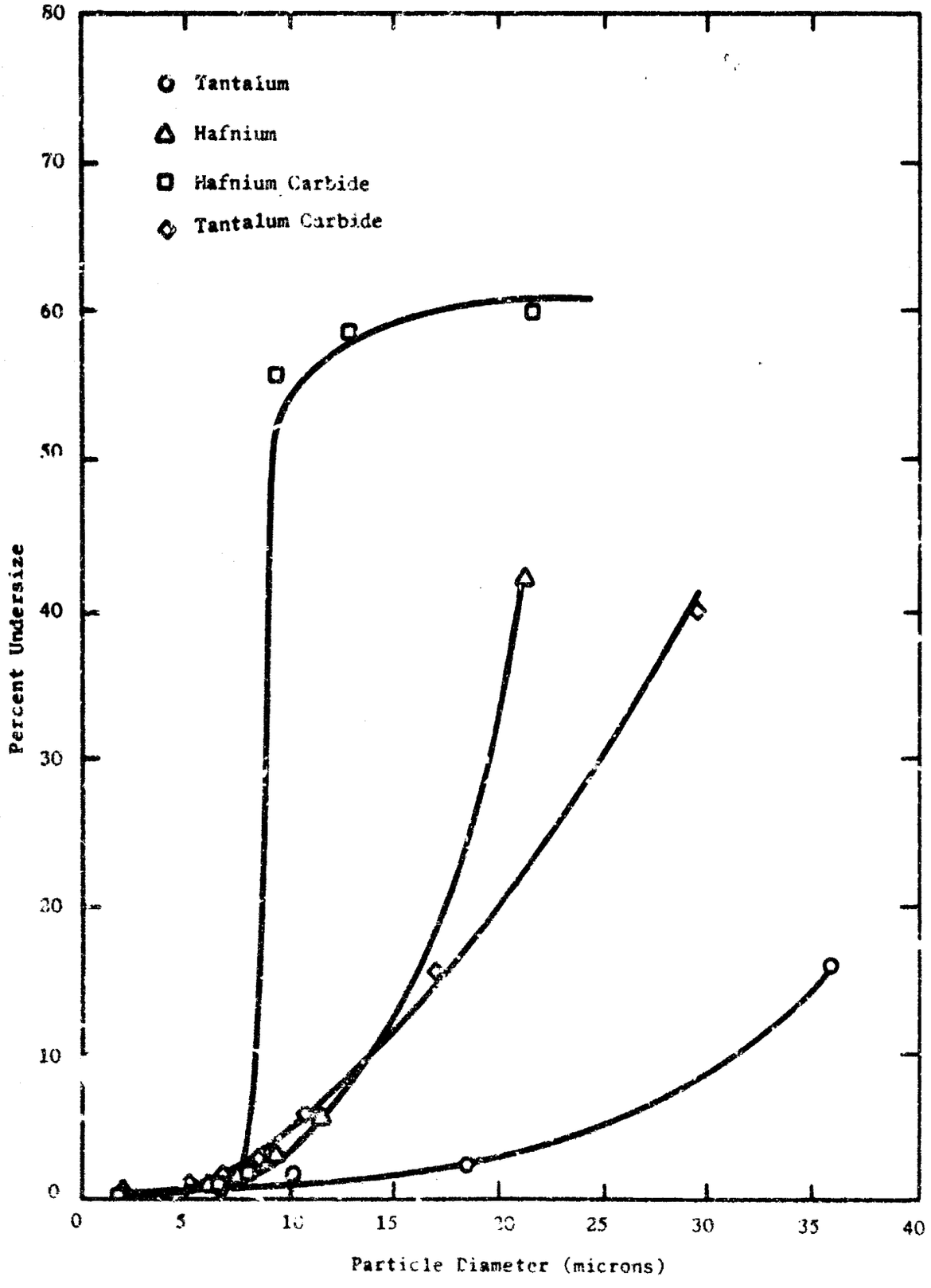

Figure 6. Andreason Pipet Particle-Size Distribution Curves

III, A, Task 1—Development of Microcomposite (cont.)

The developmental hot-pressing was conducted using a rapid heating hot-press which can reach a temperature of 3600°C in less than 5 minutes and maintain this temperature for prolonged durations. A schematic of the furnace arrangement is shown in Figure 7.

Temperatures were controlled by a variable rheostat used in conjunction with an optical pyrometer sighted on the surface of the die. The very fast heating and cooling rates minimize the reaction between the sample material and the die. Carbon analyses of the sample, after hot-pressing, were used to determine any change in carbon content during the hot-press operation.

The levels of fabrication variables that were evaluated are as follows:

Atomic Percent of Metal and Carbon Powder

Ta	Hf	C
18	45	37
13	50	37
8	55	37
13	47	40
10	50	40
5	55	40

Composition of Starting Material Metals Ratio*

80 Ta/20 Hf 50 Ta/50 Hf

Compaction Pressure, psi

500 and 3000 psi

*Ratio of Ta and Hf metal powders used in starting material formulation.

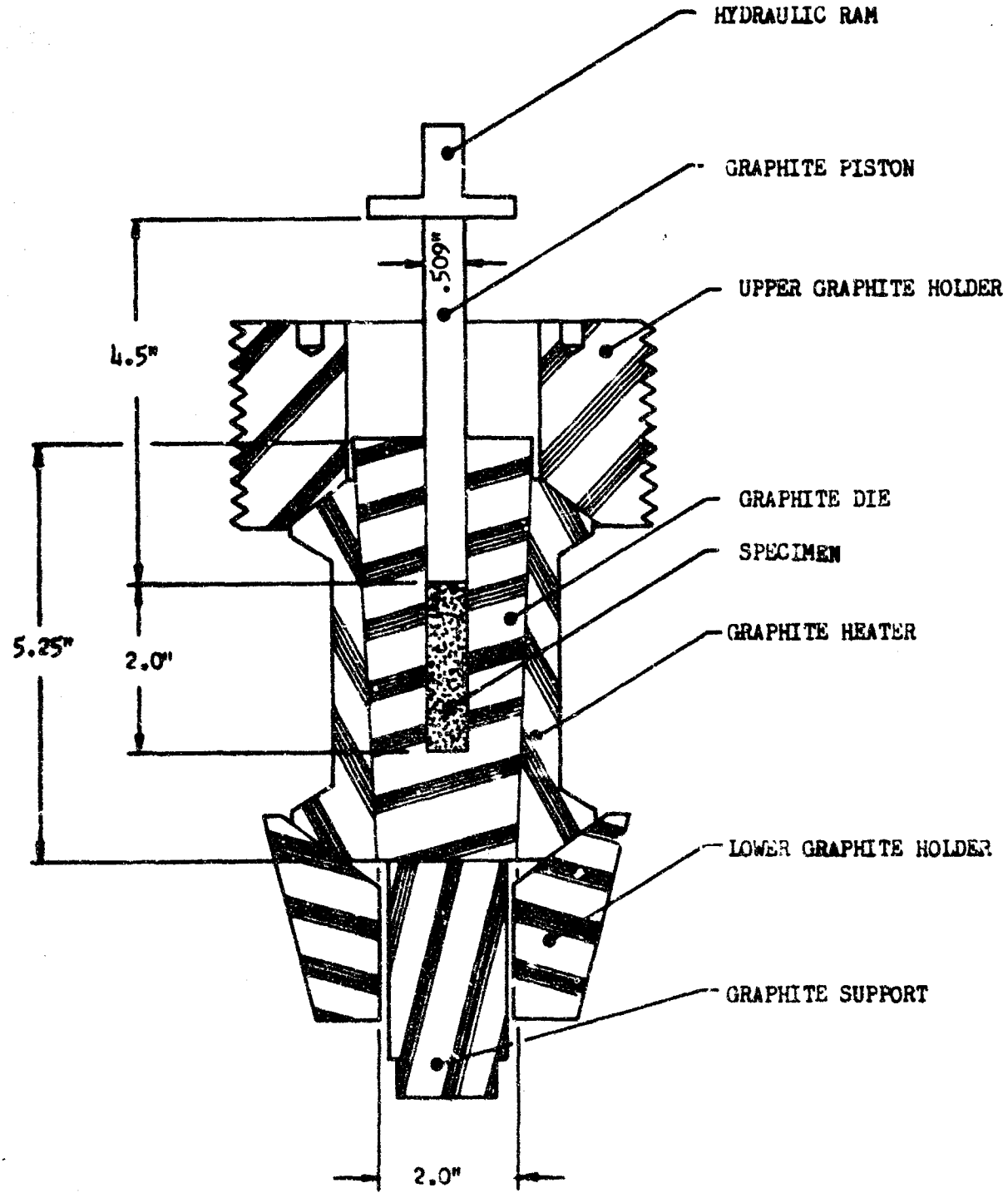

Figure 7. Schematic of Hot-Press Furnace

III, A, Task 1--Development of Microcomposite (cont.)

Sintering Cycle

Time, minutes: 2, 5, 10, 15, 20, 30, and 45

Temperature, °C: 2000, 2200, 2500, 2700, and 2800

Cooling Rate: 50°C/minute to 1500 and 1800°C
100°C/minute to 1500 and 1800°C

Heat Treatment

1600°C for 18 hr, 1800°C for 64 hr, 2200°C for 54 hr

Density and metallography were used to establish the effect of the processing variables on phase relationships. X-ray diffraction analyses were used to verify that the equilibrium metal and carbide composition had been achieved.

b. Experimental Results

(1) Carburization in Hot-Pressing

In initial hot-pressing experiments, the formation of a carburized layer on the microcomposite was observed. However, it could be minimized through proper control of time and temperature of the hot-pressing cycle. Typical carburized layer formations are shown in the microstructure of Figure 8, which is a specimen hot-pressed at 2800°C and 3000 psi for 15 minutes. The carburized layer developed as a function of temperature as shown graphically in Figure 9.

A comparison of the two curves, Figure 9, for samples hot-pressed for 15 minutes with starting material metal ratios of 20Ta/80Hf and 50Ta/50Hf showed no significant difference in carburization depths as a result of this composition variation. Also, the difference in carburization depths between 15- and 30-minute durations of hot-pressing

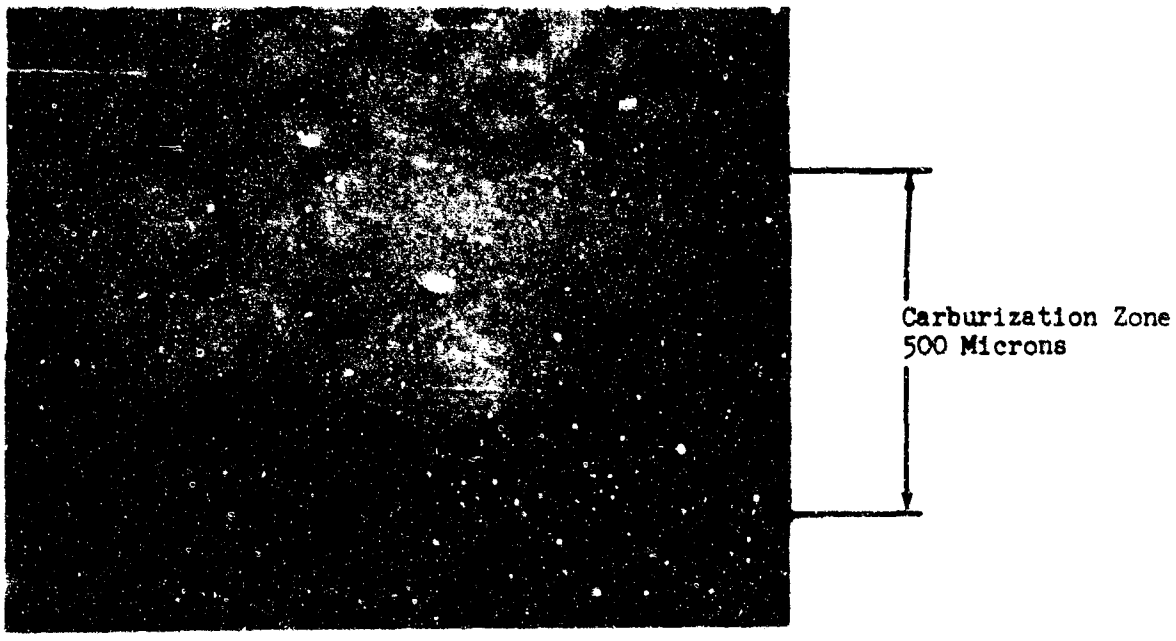

13Ta·50Hf·37C 100X

Figure 8. Typical Carburized Layer Formation (Specimen Hot-Pressed at 2800°C for 15 min at 3000 psi)

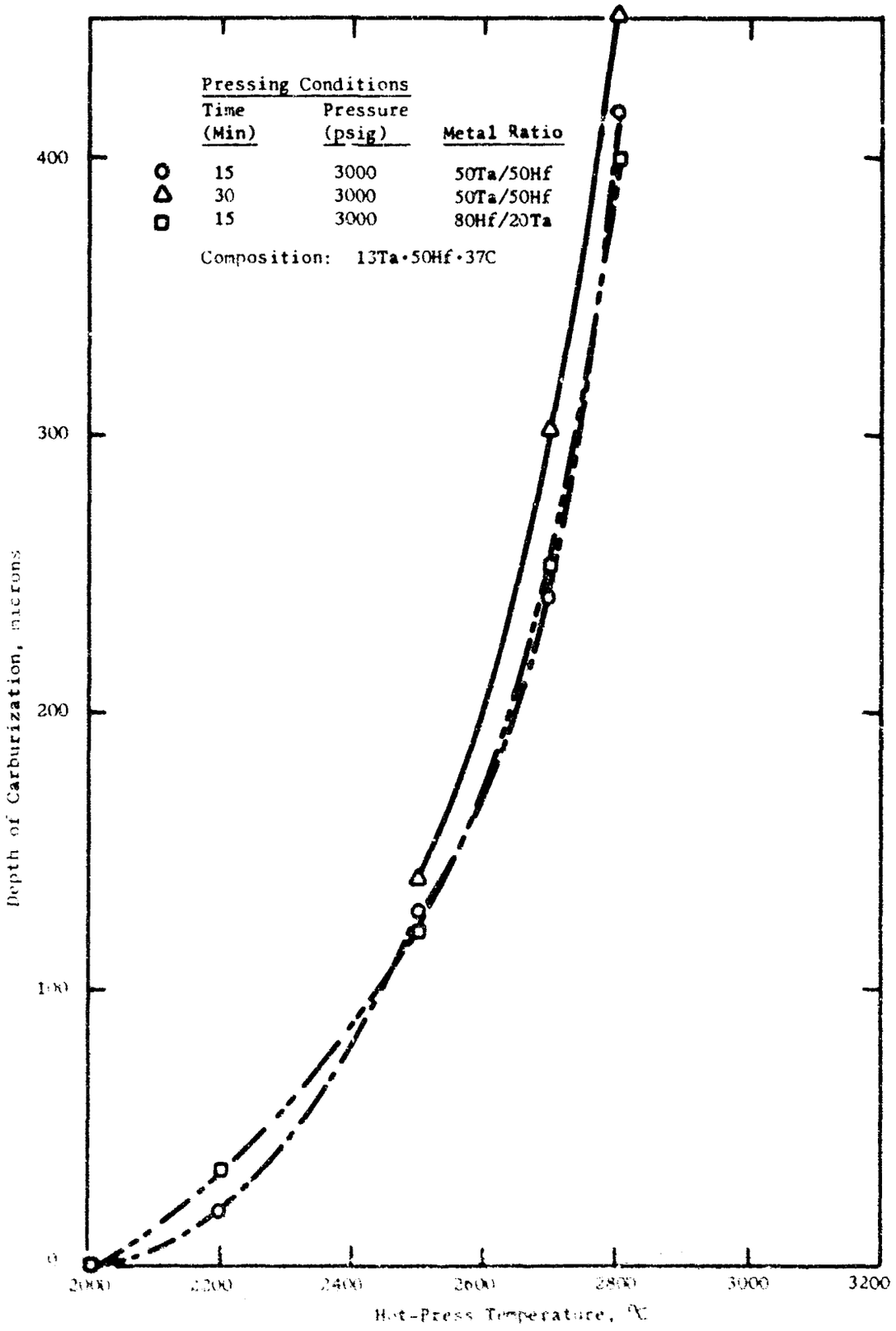

Figure 9. Depths of Carburized Layer Formation

III, A, Task 1--Development of Microcomposite (cont.)

was not as significant as the rapid increase in carburization depth with temperature. The carburized layer could be limited to approximately 0.5 mm, thus permitting the hot-press technique to be satisfactorily employed for fabricating the microcomposite structure.

(2) Composition Changes

Composition control of the microcomposite during hot-pressing was judged by the final carbon content after hot-pressing. Extreme care was necessary to obtain carbon analysis samples from the small 10-gm specimens without extracting a portion of the carburized layer containing high carbon concentrations. Table III shows the results of carbon analyses of specimens as affected by starting compositions and time at hot-pressing temperature. For short hot-pressing durations, 5 to 10 minutes, the compositions containing 37 at% carbon had net increases in carbon content ranging from 0.77 to 2.86 at%. The desired two-phase microcomposite structure was obtained with these 37.77 to 39.86 at% carbon compositions. Longer hot-press durations, 20 to 30 minutes, resulted in carbon content increases of 3.19 and 3.72 at%, respectively, and net increases in carbon contents for the composition 10Ta-50Hf-40C ranged from 1.0 to 5.13 at% carbon, which shifted the final compositions to the monocarbide region.

(3) Densification

Because of the deleterious effect of porosity on mechanical strength, the effects of hot-press temperature, time, heat treatment, and pressure on density were evaluated. Test results for the initial evaluation of the 13Ta-50Hf-37C composition, shown in Table IV, show that the density increased as the hot-press temperature and time increased. However, as solution and precipitation of the metal phase progressed, there was a corresponding change in the theoretical density, and the degree of densification was best judged

TABLE III

CARBON ANALYSES OF MICROCOMPOSITE COMPOSITIONS
AFTER HOT-PRESSING

Starting Material Composition[1]	Temp., °C	Total Carbon Contents, at % Hot-Press Durations, min				
		5	10	15	20	30
(1) 18Ta-45Hf-37C	2500			38.17*		
	2700	37.79*	38.77*	38.42		
	2800					
(2) 13Ta-50Hf-37C	2500			39.48*		
	2700	39.84	39.86	39.57	40.19	40.72*
	2800			39.31*		
(3) 8Ta-55Hf-37C	2500			39.43*		
	2700	38.96	39.36*	39.62*		
	2800					
(4) 10Ta-50Hf-40C	2500					41.00*
	2700			41.85*		41.54*
	2800			45.13*		43.00*

*Average of two determinations on same sample.
(1)20 Ta-80 Hf Metal Powder Ratio used in Starting Materials.

TABLE IV

DENSITY OF 13Ta-50Hf-37C MICROCOMPOSITES

Starting Material Composition	Hot-Pressing, 3000 psi Temperature, °C	Hot-Pressing, 3000 psi Density for Durations, gm/cm³		Heat Treatment 1800°C/62 hr Density for H.P. Durations, gm/cm³		Heat Treatment 2200°C/54 hr Density for H.P. Durations, gm/cm³	
		15 min	30 min	15 min	30 min	15 min	30 min
Metals ratio 20Ta/80Hf	2000	12.47		12.77			
	2200	12.32		12.66			
	2500	12.40	12.83	12.91			
	2700	12.72	12.87	12.97			11.76
	2800	12.94	12.88		12.81	11.15	12.60
Metals ratio 50Ta/50Hf	2000	12.22				10.86	
	2200	12.65				10.95	
	2500	12.75	12.84			11.84	11.36
	2700	12.75	12.87	12.97		10.72	
	2800	12.58	12.85	12.76			12.51

III, A, Task 1--Development of Microcomposite (cont.)

metallographically. Heat treatment of the hot-pressed specimens at 2200°C for 54 hr in vacuum tended to lower the density due to melting and loss of residual metal alloy phase (m.p. 2100°C), which was in excess of that which could be taken into solution in the carbide. This resulted in increased porosity. Heat treatment at 1800°C for 62 hr in vacuum increased the density.

Hot-pressing at 500 psi resulted in approximately 10% less density than at 3000 psi. Metallographic examination confirmed that nearly 10% porosity remained in the structures. By extending hot-press time at temperature to 30 minutes, the porosity was decreased to less than 5%. Increasing the time could have provided higher density, but 45 minutes resulted in extreme carburization depths which established that durations greater than 30 minutes were not considered practical.

The apparent densities of specimens hot-pressed from all the compositions investigated are listed in Table V. As determined in the initial tests, density increased with time at a constant temperature and pressure. The significant decrease in density with temperature as shown in Figure 10 is due to the increased carburization. Increasing tantalum content while decreasing the hafnium content by the same percentage at a constant carbon content resulted in an increased composite density because tantalum has a higher density. The three compositions containing 40 at% carbon had lower densities than those containing 37 at% carbon. The lower density was a result of higher porosities in the compositions containing 40 at% carbon.

(4) Microstructural Development

The six Ta-Hf-C compositions investigated covered the shaded region shown by the isothermal temperature section in Figure 11 of the ternary phase diagram. At this temperature, 1850°C, the composition is in

TABLE V

EFFECT OF PROCESSING VARIABLES ON APPARENT DENSITY OF MICROCOMPOSITES

Starting Material Composition	Hot-Pressing, 3000 psi Temperature, °C	Density for Durations, gm/cm³ 5 min	10 min	15 min	20 min	30 min
18Ta-45Hf-37C	2500	12.72	12.82	12.84		
	2700	12.43	12.50	12.48		
	2800		12.82	11.91		
13Ta-50Hf-37C	2500	12.678	12.57	12.95		12.73
	2700	12.41	12.50(7)*	12.75	12.83	12.52
	2800		10.84	12.55		12.53
8Ta-55Hf-37C	2500	12.54	12.49	12.49		
	2700	12.39	12.25	12.45		
	2800			11.93		12.02
13Ta-47Hf-40C	2500			12.33		
	2700	11.82	11.96	12.02		
	2800			11.41		
10Ta-50Hf-40C	2500			11.55		12.66
	2700			11.37		12.56
	2800					12.17
5Ta-55Hf-40C	2500			11.64		11.54
	2700	10.42	11.45(2)*	10.81		10.56
	2800			10.72		11.01

*( )Denotes the number of runs that were averaged.

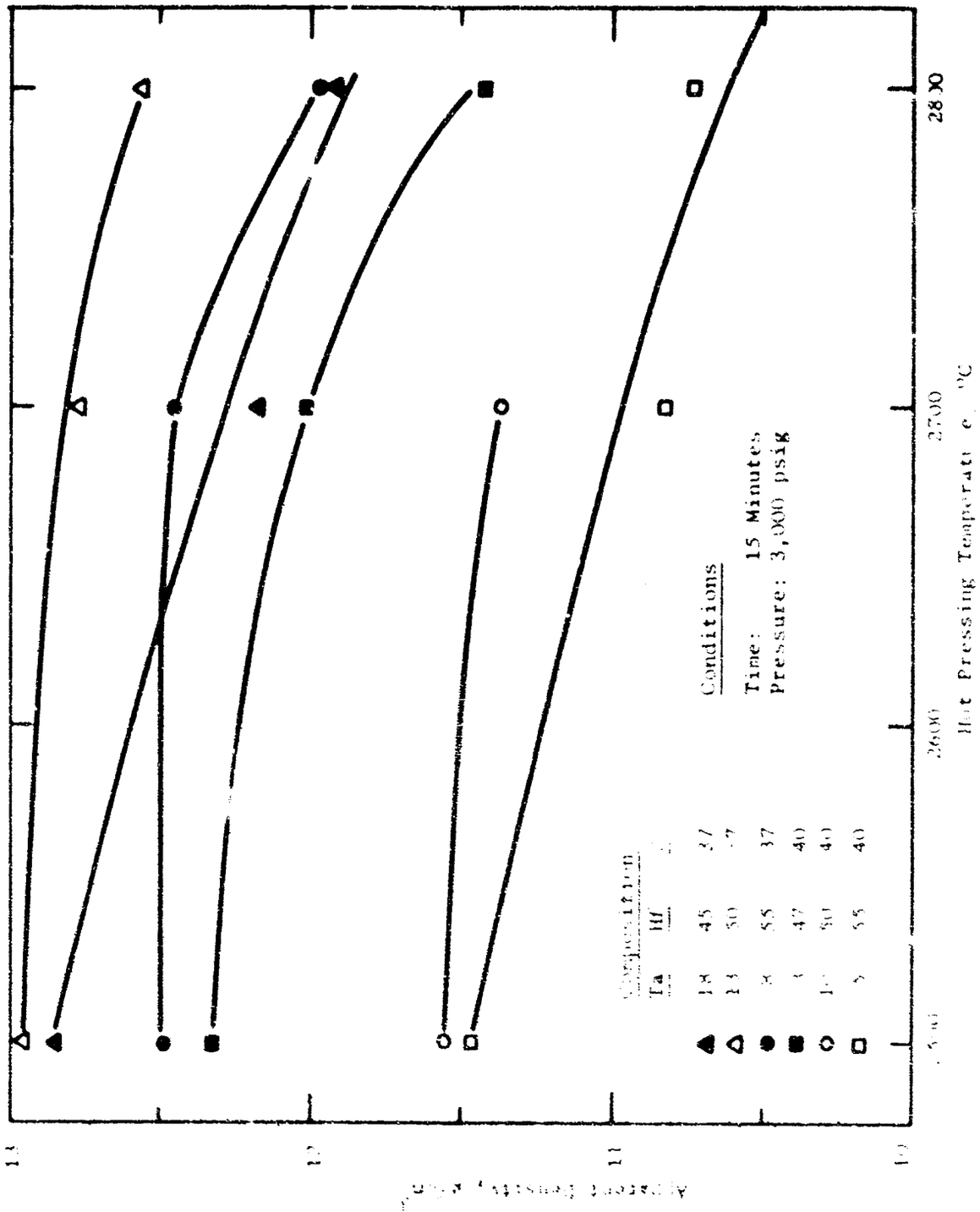

Figure 10. Effect of Hot-Pressing Temperature on Apparent Density of Microcomposite

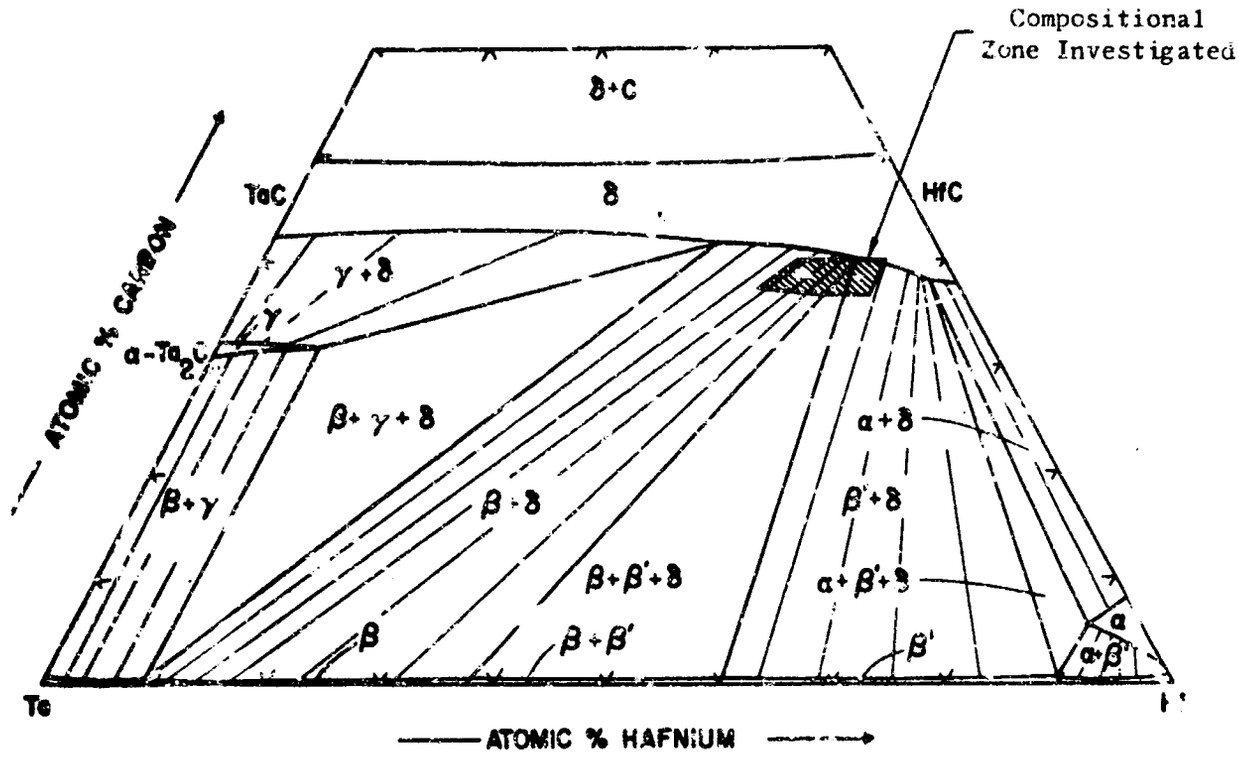

Figure 11. Temperature Section at 1850°C

III, A, Task 1--Development of Microcomposite (cont.)

the two-phase (tantalum-hafnium monocarbide δ + tantalum-hafnium metal, β) region. At higher temperatures, this composition range is in the monocarbide phase, δ, region as shown by the temperature section at 2000°C, Figure 12.

The development of the desired microstructure for the microcomposite required complete solution of the (Ta, Hf) monocarbide at the hot-pressing temperature and subsequent precipitation of the Ta-Hf metal phase within the carbide grains upon cooling.

(a) Composition: 13Ta-50Hf-37C

1 High Oxygen Content Material

In the preparation of the initial series of hot-pressed 13Ta-50Hf-37C specimens, high oxygen content, 2200 ppm, in the hafnium carbide inhibited solution and precipitation of the tantalum-hafnium metal alloy within the monocarbide grains. The oxygen atoms occupy the face-centered positions in the cubic carbide lattice and thus prevent the diffusion of the metal atoms into these sites.

Figures 13, 14, 15 and 16 are photomicrographs of specimens made with starting material containing high oxygen. The hot-pressing temperatures were successively increased from 2000 to 2800°C. Complete solution of the metal phase was nearly complete with a hot-press temperature of 2800°C for 15 minutes (Figure 15), but the high oxygen level of the HfC retarded diffusion of the metal alloy into the carbide lattice.

To achieve solution of the metal starting material in the carbide and subsequent precipitation of the metal alloy phase within the carbide grains, specimens hot-pressed at 2800°C for 30 minutes were

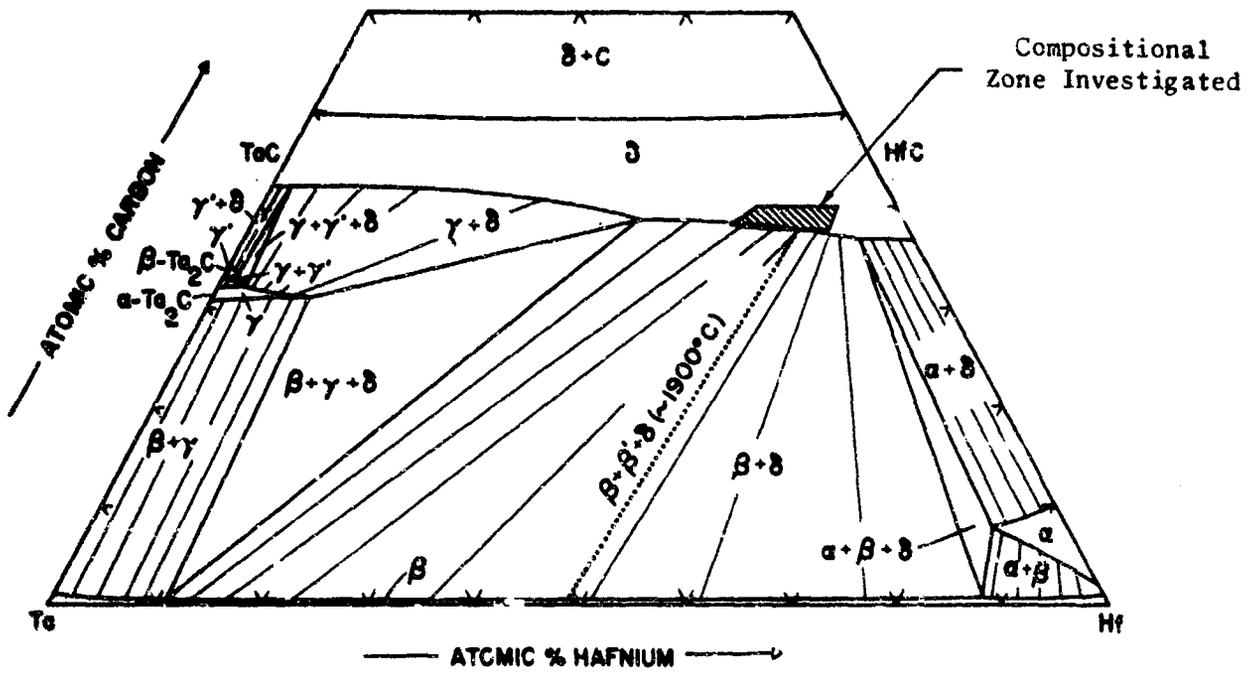

Figure 12. Temperature Section at 2000°C

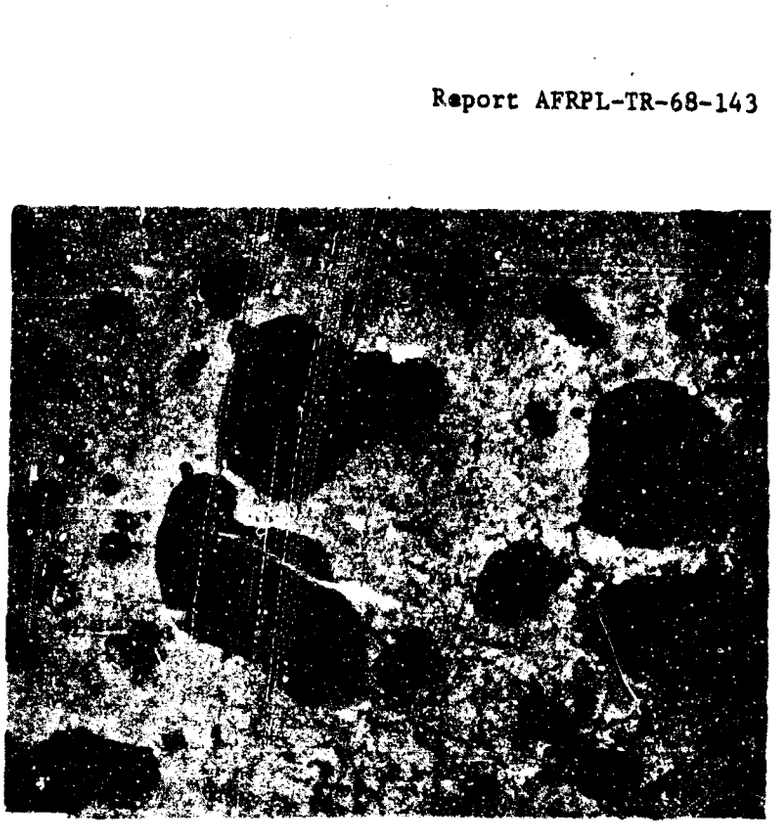

Black Pool Areas
Metal Alloy Phase

750X

a. Hot-Pressed at 3000 psi , 15 min , 2000°C

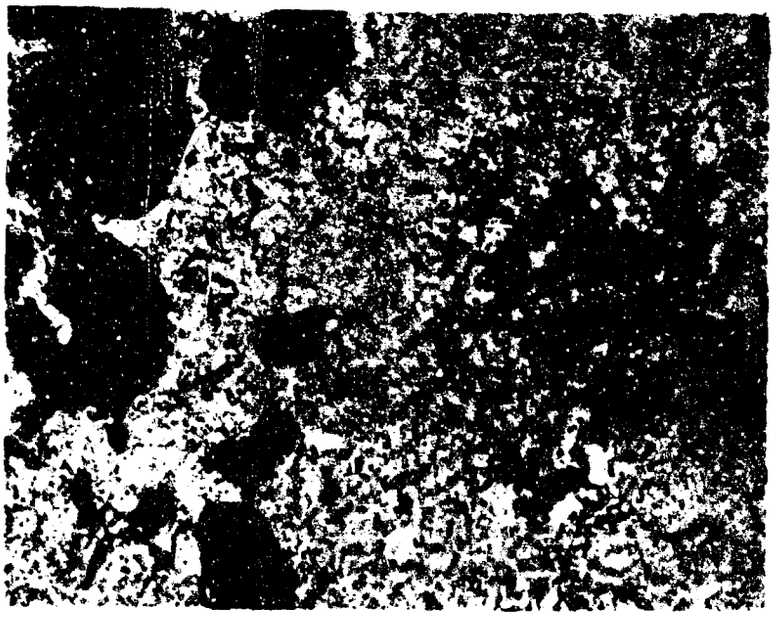

Black Pool Areas
Metal Alloy Phase

750X

b. Hot-Pressed at 3000 psi, 15 min, 2200°C

Figure 13. Photomicrographs of Composition 13Ta-50Hf-37C with Starting Material Metal Ratios 20Ta/80Hf (High Oxygen in HfC)

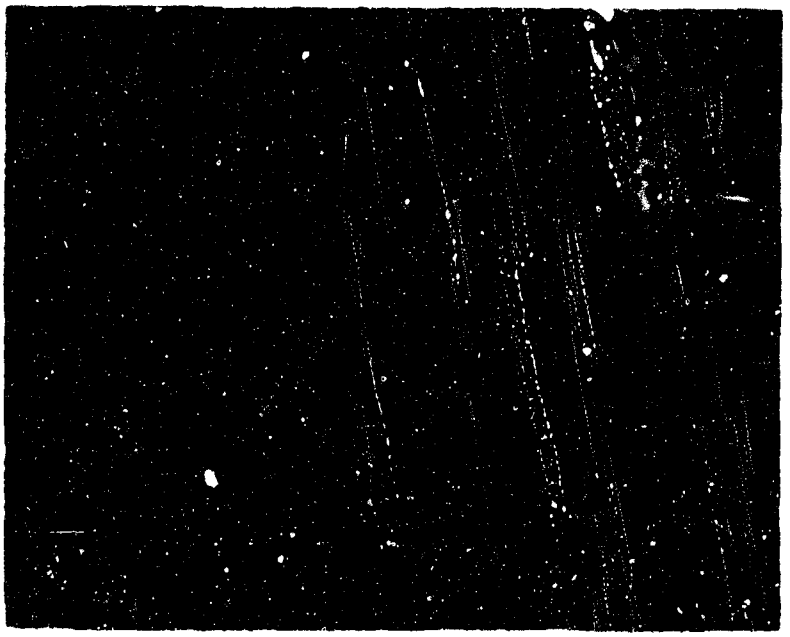

a. Hot-Pressed at 3000 psi, 15 min, 2500°C

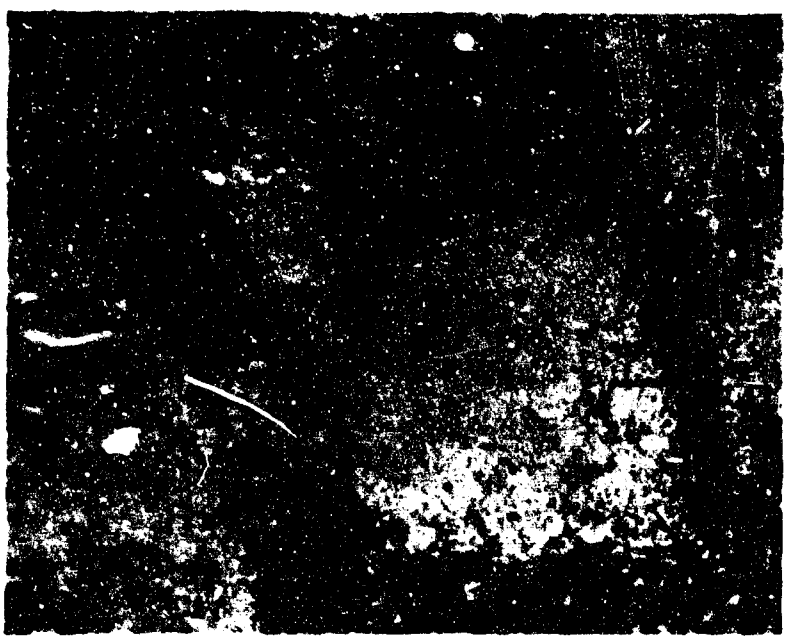

b. Hot-Pressed at 3000 psi, 15 min, 2700°C

Figure 14. Photomicrographs of Composition 13Ta-50Hf-37C with Starting Material Metal Ratios 20Ta/80Hf (High Oxygen in HfC)

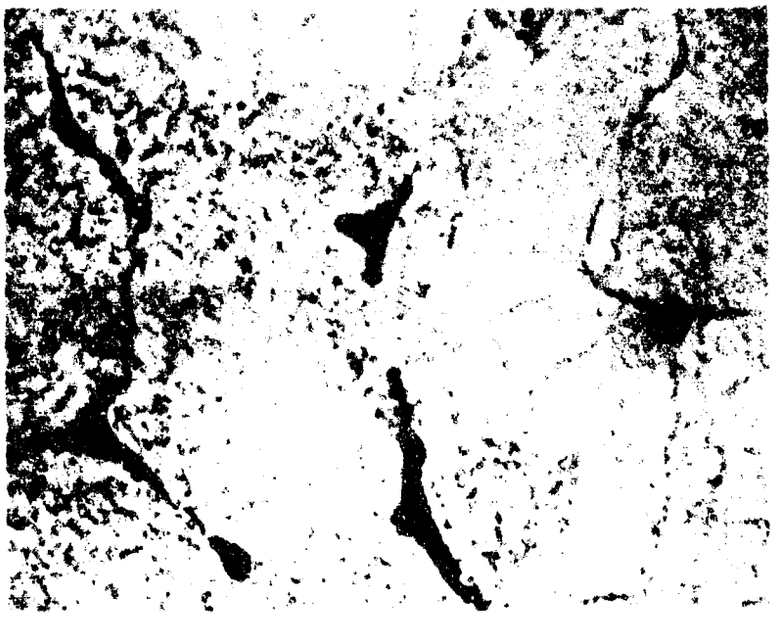

750X

Figure 15. Photomicrograph of Composition 13Ta-50Hf-37C with Starting Material Metal Ratio 20Ta/80Hf (High Oxygen in HfC) Hot-Pressed for 15 min, 3000 psi at 2800°C

Light Areas
Metal Diffusion
Zone

Dark Areas
(Ta, Hf) Monocarbide

150X

Figure 16. Photomicrograph of Composition 13Ta-50Hf-37C Material Metal Ratio 20Ta/80Hf Hot-Pressed at 2800°C, 30 min and 3000 psi (High Oxygen in Hf)

III, A, Task 1—Development of Microcomposite (cont.)

heat treated at 1800°C in vacuum (1×10^{-5} torr) for 64 hr. Homogenization and probably deoxidation occurred and a metal alloy was present in fine intergranular precipitations as shown in Figure 17.

2 Desired Oxygen Content Material

Low oxygen content, 268 ppm, hafnium carbide prepared by high vacuum degassing was used in subsequent studies. The microstructures of the 13Ta-50Hf-37C composition hot-pressed for 15 minutes, 3000 psi, and 2500, 2700, and 2800°C are shown in Figures 18a, 18b, and 18c, respectively. Some primary metal alloy remained at the grain boundaries (dark pool regions in photomicrographs) but a pronounced needle-shaped precipitation occurred within the carbide grains.

Heat treatment at 1600°C for 18 hr, in a vacuum of 10^{-5} torr, resulted in agglomeration of the metal alloy precipitate as shown in Figures 19a and 19b.

The effect of longer duration (30 minutes) at hot-press temperature on equilibration of the two-phase structure, i.e., complete absorption and precipitation of the metal alloy phase within the carbide grains, is shown in Figures 20a, 20b, and 20c. There was no evidence of more complete primary metal alloy solution but there was greater grain growth and segregation, particularly at 2700 and 2800°C.

The effect of hot-pressing time (5, 10, and 20 minutes) for the 13Ta-50Hf-37C composition hot-pressed at 3000 psi and 2700°C is shown in Figures 21a, 21b, and 21c, respectively. The desired uniform distribution of needle-shaped metal alloy precipitate was obtained in 5 and 10 minutes, as well as 15 minutes (Figure 18b) while in 20 minutes and longer (Figure 20b) the metal alloy phase tends to agglomerate.

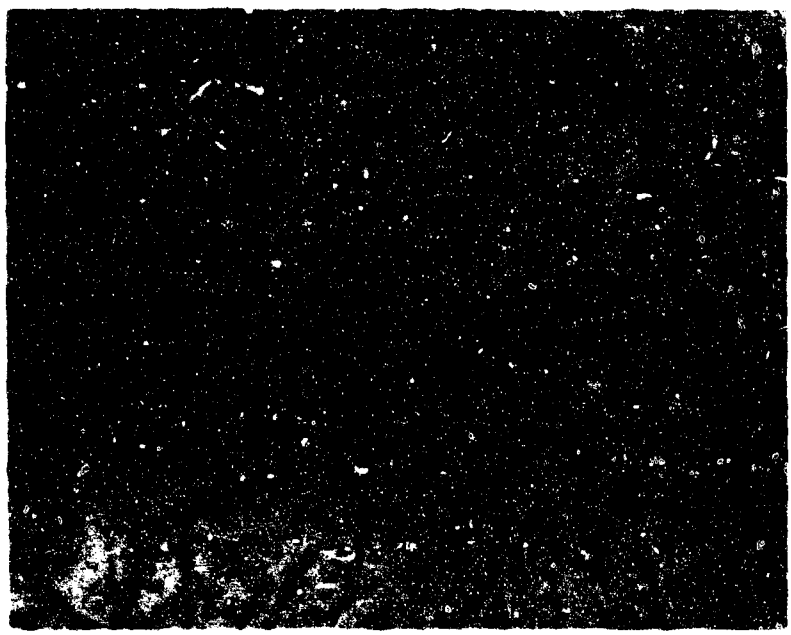

750X

Figure 17. Photom[illegible]f Composition 13Ta-50Hf-37C Material Metal [illegible]50Hf Hot-Pressed at 2800°C, 30 min and 3[illegible]t Treatment at 1800°C, 64 hr in Vacu[illegible]rr)

a. Hot-Pressed at 2500°C (Primary Metal-Black Pools) 750X

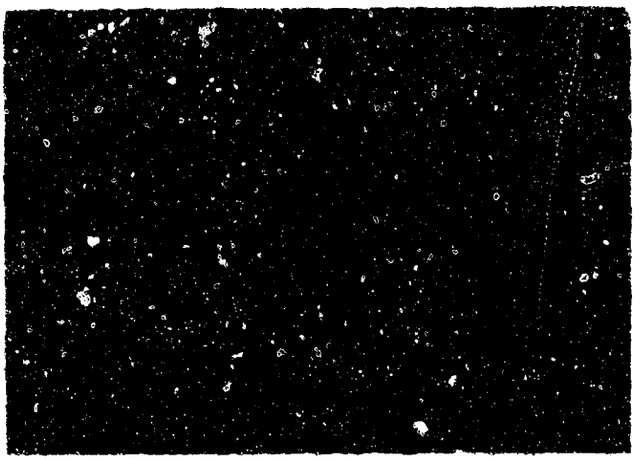

b. Hot-Pressed at 2700°C 750X

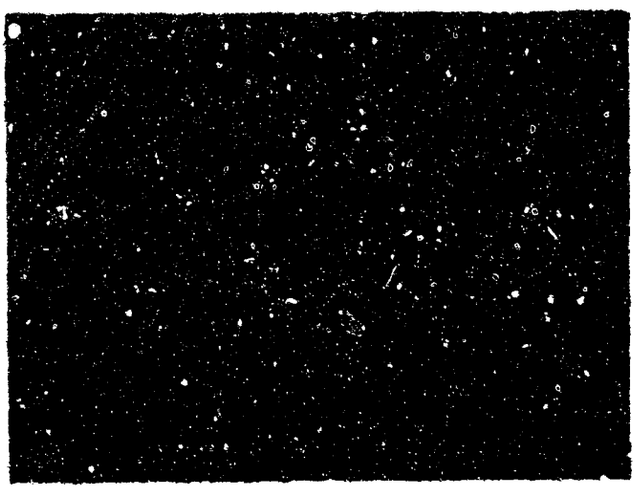

c. Hot-Pressed at 2800°C 750X

Figure 18. Photomicrograph of Composition 13Ta-5Hf-3C Hot-Pressed for 15 min. 3000 psi, at 2500°C, 2700°C, and 2800°C

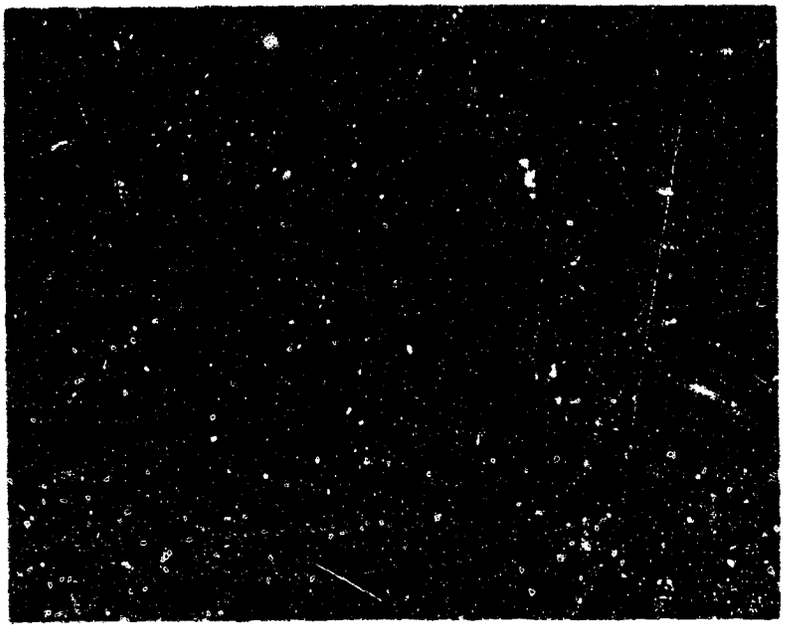

a. Hot-Pressed Prior to Heat-Treatment at 3,000 psi, 15 min, 2500°C — 750X

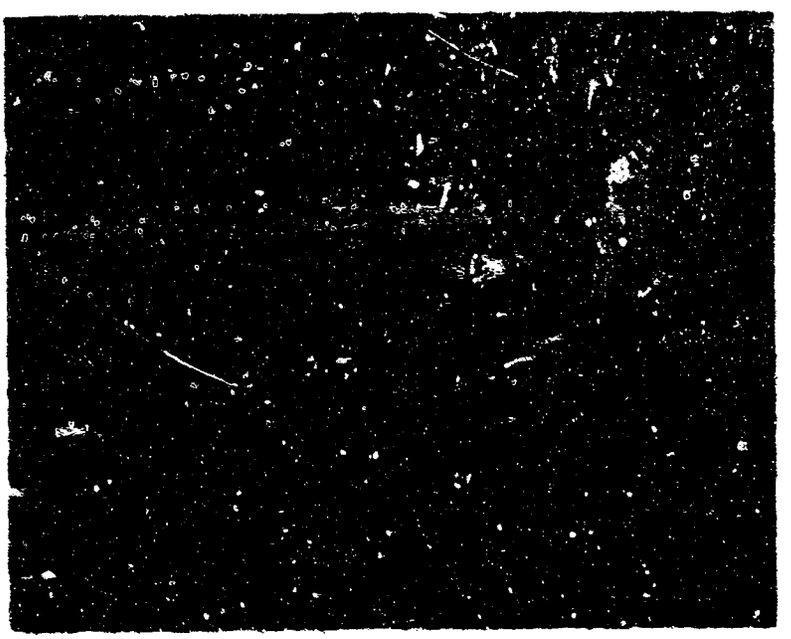

b. Hot-Pressed Prior to Heat-Treatment at 3,000 psi, 15 min, 2700°C — 750X

Figure 19. Photomicrograph of Composition 13Ta-50Hf-37C Heat-Treated at 1600°C, 18 hr in Vacuum (10^{-5} Torr)

a. Hot-Pressed at [illegible]°C 750X

b. Hot-Pressed at [illegible]°C 750X

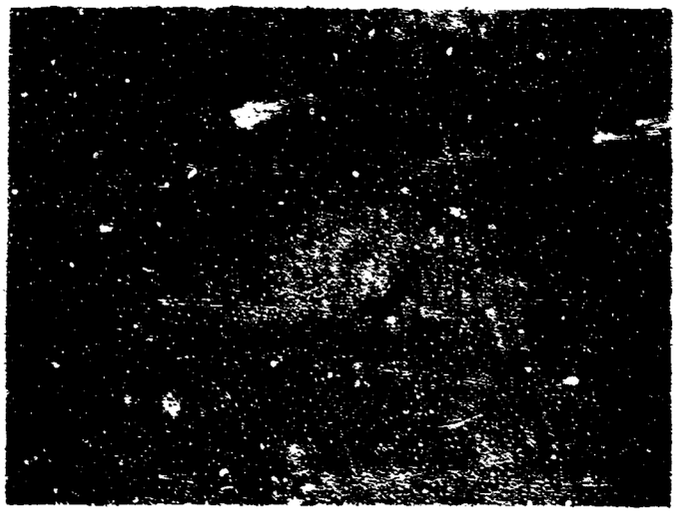

c. [illegible] X

Figure 21. [illegible]

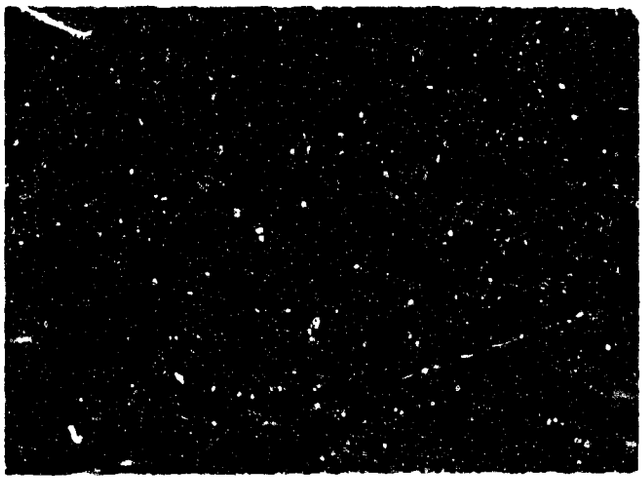

a. Hot-Pressed for 5 min 750X

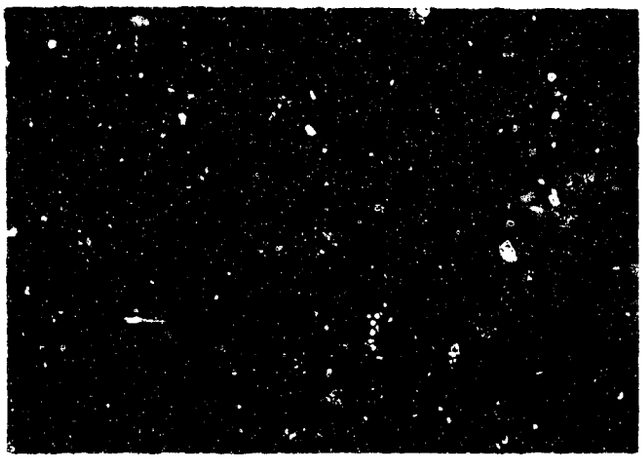

b. Hot-Pressed for 10 min 750X

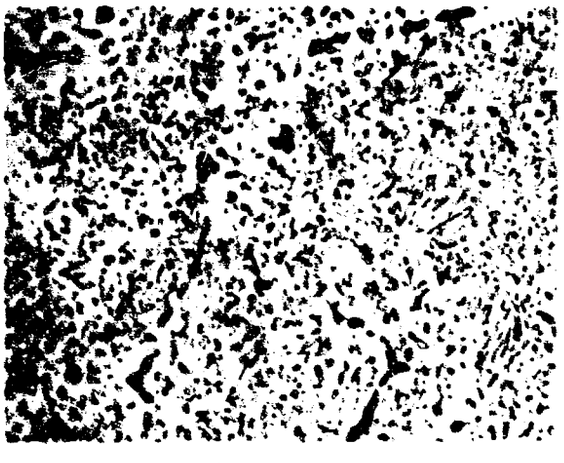

c. Hot-Pressed for 20 min 750X 3197

Figure 21. Photomicrograph of Composition 13Ta-50Hf-37C Hot-Pressed for 5, 10, and 20 min, 3000 psi, at 2700°C

III, A, Task 1--Development of Microcomposite (cont.)

The effects of controlled cooling rates and cycles on microstructural development were evaluated in the series of tests listed in Table VI. The fine needle-shaped metal alloy precipitation previously obtained in samples quenched from the hot-pressing temperature (approximately 500°C/minute) was not obtained at slower cooling rates. The metal alloy phase was consolidated into both spherical and large-needle configurations. Typical microstructures for the various slow cooling cycles are shown in Figures 22 through 25.

(b) Composition: 18Ta-45Hf-37C

The microstructural development of the 18Ta-45Hf-37C composition was found to be similar to that determined for 13Ta-50Hf-37C, with few exceptions. The microstructures of samples hot-pressed at 2500, 2700, and 2800°C for 15 minutes are shown in Figures 26a, 26b, and 26c, respectively. Needle-shaped metal alloy precipitation was obtained after each processing temperature; however, more primary metal alloy was retained around the carbide grain after processing at 2800°C.

Reducing the hot-pressed time at 2700°C to 5 and 10 minutes resulted in establishing that the 5-minute duration did not allow complete diffusion of the starting metal into the monocarbide grains as shown in Figure 27a. The 10-minute hot-pressing duration produced a finely dispersed needle precipitate (Figure 27b), but not as predominant as for the 15-minute duration shown in Figure 26b.

(c) Composition: 8Ta-55Hf-37C

After the extensive evaluation of the other 37 at% carbon compositions, the desired needle-shaped metal alloy precipitate for the 8Ta-55Hf-37C composition was readily produced by hot-pressing at 2700°C, 3000 psi, for 15 minutes, and is shown in Figure 28.

TABLE VI

HOT PRESSING/COOLING RATE STUDY

Composition	Hot Pressure Parameters: Pressure: 3000 psi Temp, °C	Time, min	Cooling Cycle: Cooling Rate, °C/min	Heat Treat Temperature, °C	Time, min
13Ta-50Hf-37C	2000	5	100	1800	Quench
	2200	5	100	1800	Quench
	2400	5	100	1800	10
		15	100	1800	10
	2500	2	100	1800	Quench
		10	100	1500	10
	2700	10	100	R.T.	Quench
		10	100	1500	Quench
		10	50	1500	10
		10	50	1500	20
		10	50	1800	10
18Ta-45Hf-37C	2500	10	50	1500	Quench
	2700	10	100	1500	Quench
8Ta-55Hf-37C	2500	5	50	1500	Quench
		10	50	1500	Quench
	2700	10	100	1500	Quench
		10	50	1500	Quench

750X

Figure 22. Photomicrograph of Composition 13Ta-50Hf-37C Hot-Pressed for 10 min, 3000 psi, at 2700°C, and Slow-Cooled at 100°C/min to 1800°C

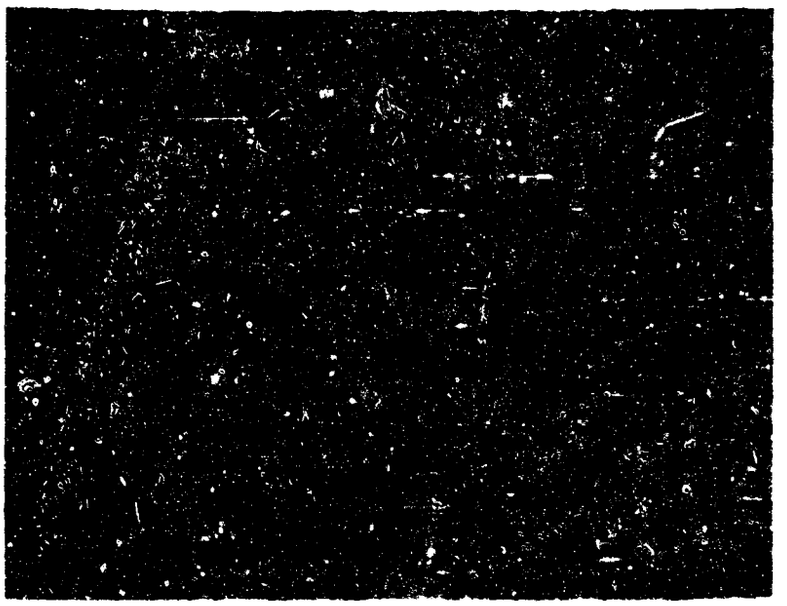

750X

Figure 23. Photomicrograph of Composition 13Ta-50Hf-37C Hot-Pressed for 10 min, 3000 psi, at 2700°C, and Slow-Cooled at 100°C/min to 1500°C

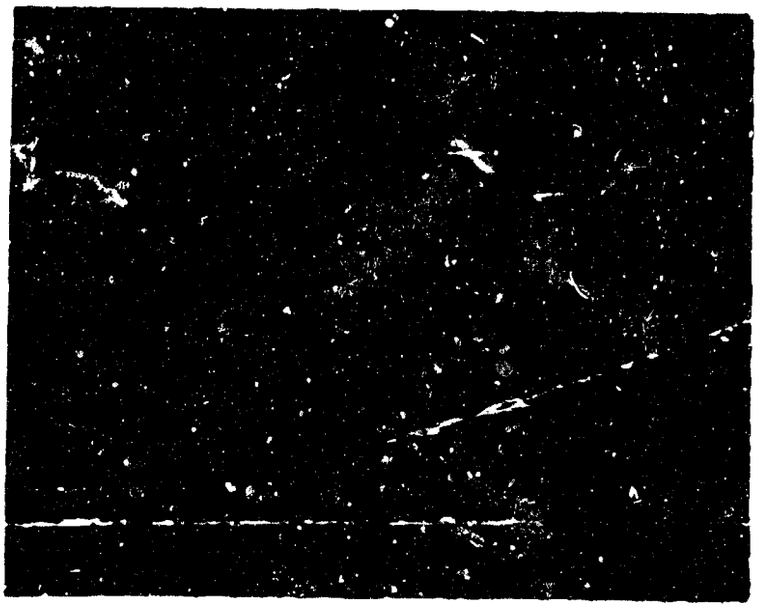

750X

Figure 24. Photomicrograph of Composition 13Ta-50Hf-37C Hot-Pressed for 10 min, 3000 psi, at 2700°C and Slow-Cooled at 100°C/min to 1500°C and Held for 20 min

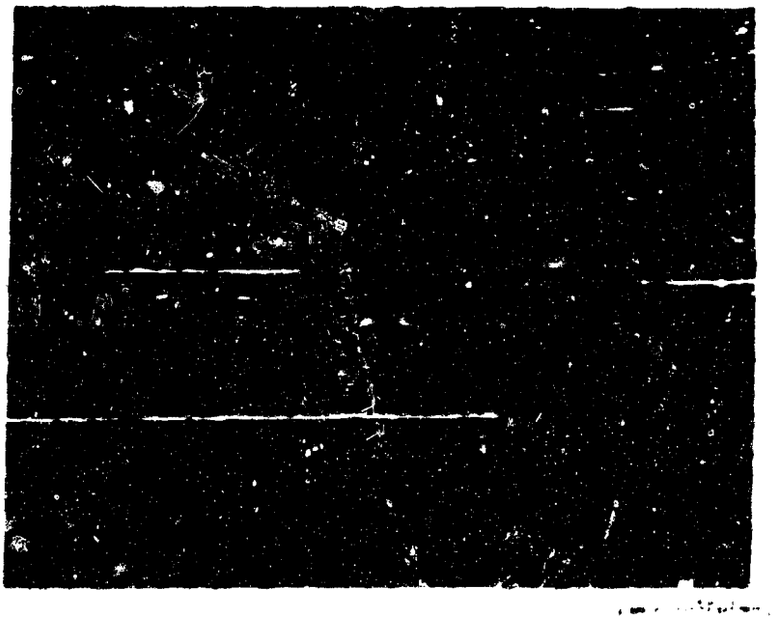

750X

Figure 25. Photomicrograph of Composition 13Ta-50Hf-37C Hot-Pressed for 10 min, 3000 psi, at 2700°C, and Slow-Cooled at 100°C/min to 1800°C and Held for 10 min

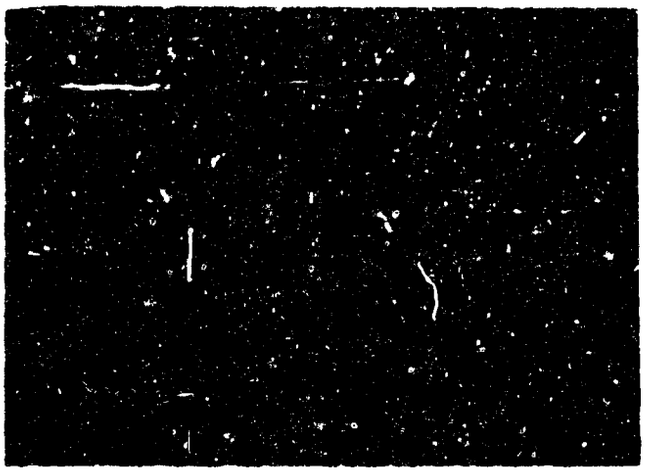

a. Hot-Pressed at 2500°C 750X

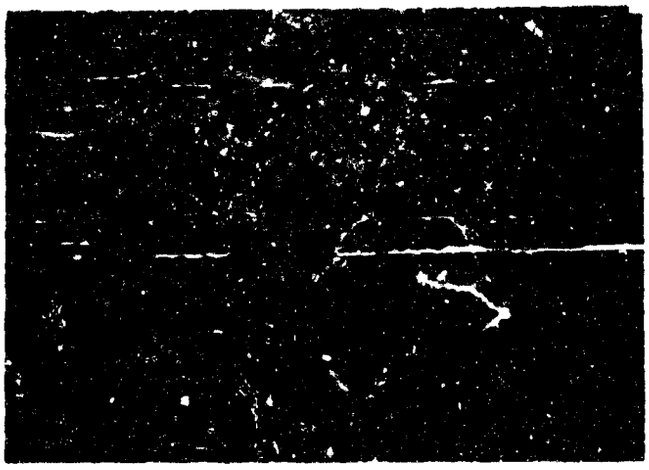

b. Hot-Pressed at 2700°C 750X

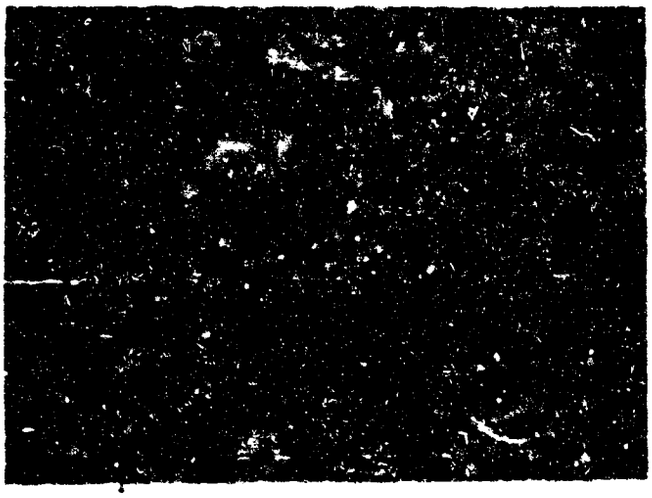

c. Hot-Pressed at 2800°C 750X

Figure 26. Photomicrographs of Composition 18Ta-45Hf-3.C Hot-Pressed for 15 min, 3000 psi, at 2500°C, 2700°C, and 2800°C

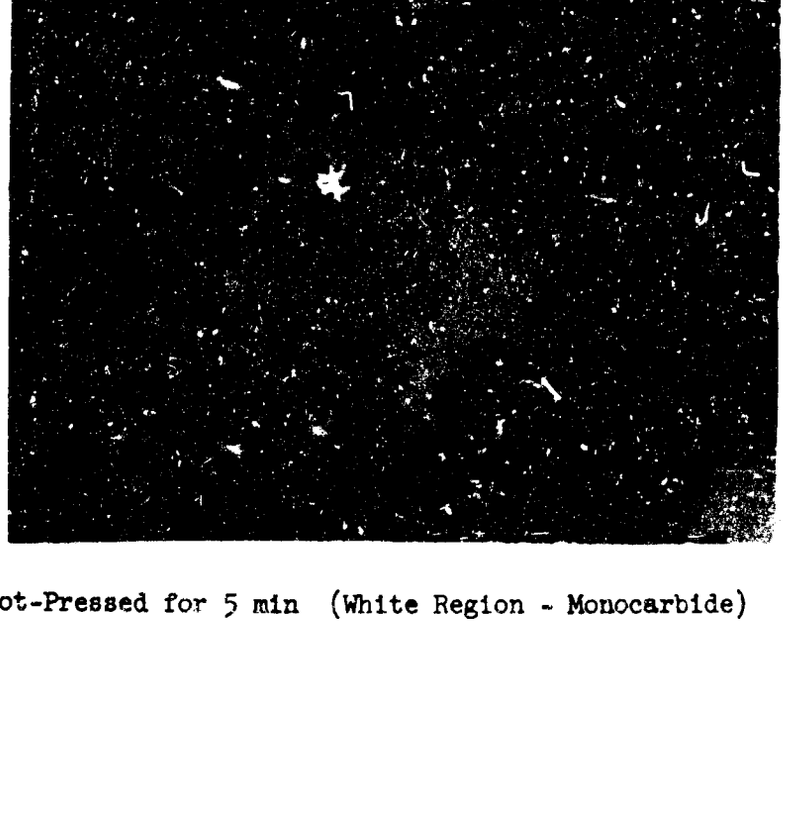

a. Hot-Pressed for 5 min (White Region - Monocarbide) 750X

b. Hot-Pressed for 10 min 750X

Figure 27. Photomicrographs of Composition 18Ta-45Hf-37C Hot-Pressed for 5 and 10 min, 3000 psi, at 2700°C

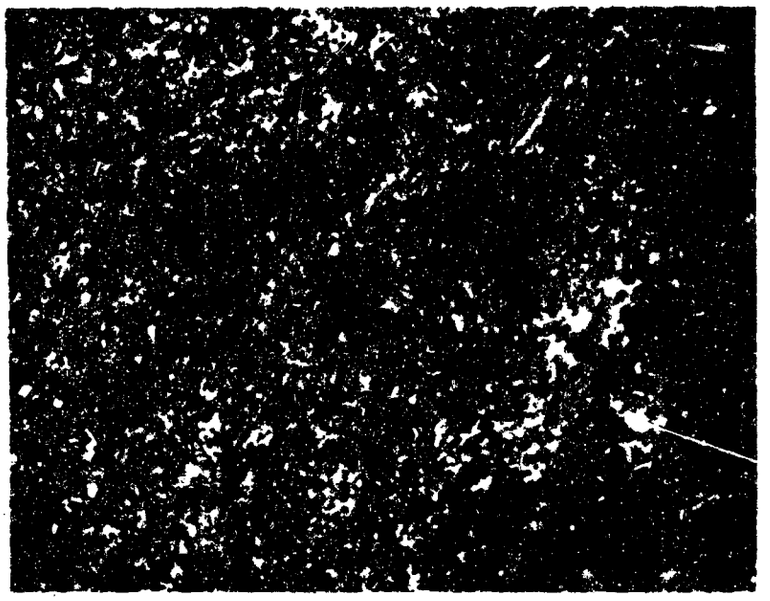

Figure 28. Photomicrograph of Composition 8Ta-55Hf-37C Hot-Pressed for 15 min, 3000 psi at 2700°C

III, A, Task 1—Development of Microcomposite (cont.)

3. Material Properties Characterization

a. Preparation of Test Specimens

The hot-pressing of specimens was conducted in graphite dies that were heated in the rapid heating hot-press previously described. The arrangement of the die and ram in the hot-press is shown schematically in Figure 29. Figure 30 shows the individual graphite components prior to assembly in the hot-press.

The technique used to load the powdered compositions into the die prior to hot-pressing was found to be very important to consistently produce crack-free specimens. A slight amount of the metal alloy phase could exude from the structure, infiltrate, and bond to the surrounding graphite die and ram. On cooldown, the specimen would crack in the die because of differential contraction between the graphite and the carbide specimen. This problem was eliminated by using a thin layer of lampblack on the floor of the die, compacting it, then filling the cavity with the selected composition. After another compaction, a thin layer of lampblack was added. This concept is illustrated in Figure 29. The use of the lampblack serves to absorb the major portion of the excess metal and the powdery structure does not bond to the specimen. By the use of this technique, two flexure specimens could be hot-pressed in the same die by using a layer of lampblack between the composition that is being hot-pressed.

Hot-pressing of all specimens was conducted at 2500°C, 3000 psi, for 10 minutes in a flowing argon atmosphere. After completion of the hot-press cycle, the graphite die was allowed to cool to ambient temperature in a flowing argon atmosphere. The flexure specimens were removed from the graphite die by partially sectioning the die and breaking it open as shown in Figure 31.

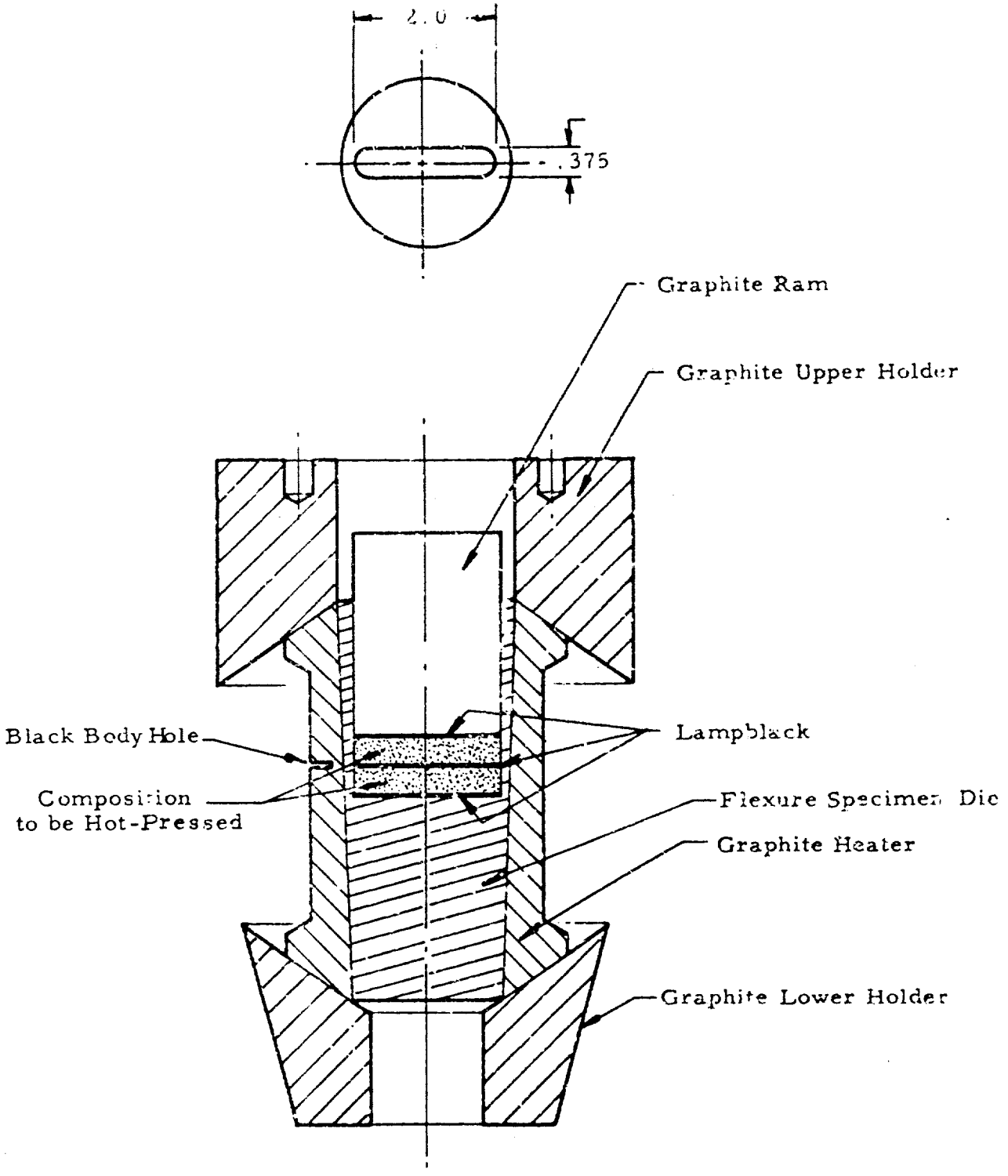

Figure 29. Schematic of Die and Ram Arrangement for Hot-Pressing Flexure Specimens

Figure 30. Graphite Components Used in Hot-Pressing Flexure Specimens

Figure 31. View of Flexure Specimen Die Split to Remove Specimen

III, A, Task I--Development of Microcomposite (cont.)

Figure 32 shows a typical flexure specimen blank as hot-pressed and the finished flexure specimen after diamond grinding. The size of the specimen after hot-pressing was approximately 0.37 in. wide by 0.30 in. deep by 2.0 in. long. The specimens were diamond ground until all visual surface contaminations or defects had been eliminated.

Machining of the specimens was accomplished by using a Thompson surface grinder with a 10-in.-dia, 100-grit diamond wheel. Table speeds of 40 to 50 ft/minute were used. Removal rates of 0.0005 to 0.001 in./pass were maintained with light finishing passes of 0.0001 to 0.0005 in. to obtain a finish of 8 to 10 rms.* Each specimen was examined under 20X magnification for visible flaws and chips. The specimens were then hand polished on a diamond metallographic wheel to slightly round the four corners along the length to eliminate any nonrepresentative corner flaws. The finished dimensions of the specimens were approximately 0.25 in. wide by 0.25 in. deep by 1.75 to 2.0 in. long. All surfaces along the length were maintained parallel within 0.001 in.

b. Ambient Temperature Screening Tests**

Seven compositions, 18Ta-45Hf-37C, 13Ta-50Hf-37C, 8Ta-55Hf-37C, 13Ta-47Hf-40C, 10Ta-50Hf-40C, 5Ta-55Hf-40C, and 13Ta-44Hf-43C, were tested at ambient temperature to determine the effect of composition on the strength, modulus of elasticity, and density.

*Root-mean-square average of surface roughness (microinches).
**A discussion of the test procedures used throughout the program for determining pertinent thermal, chemical, physical, and structural properties is presented in the Appendix.

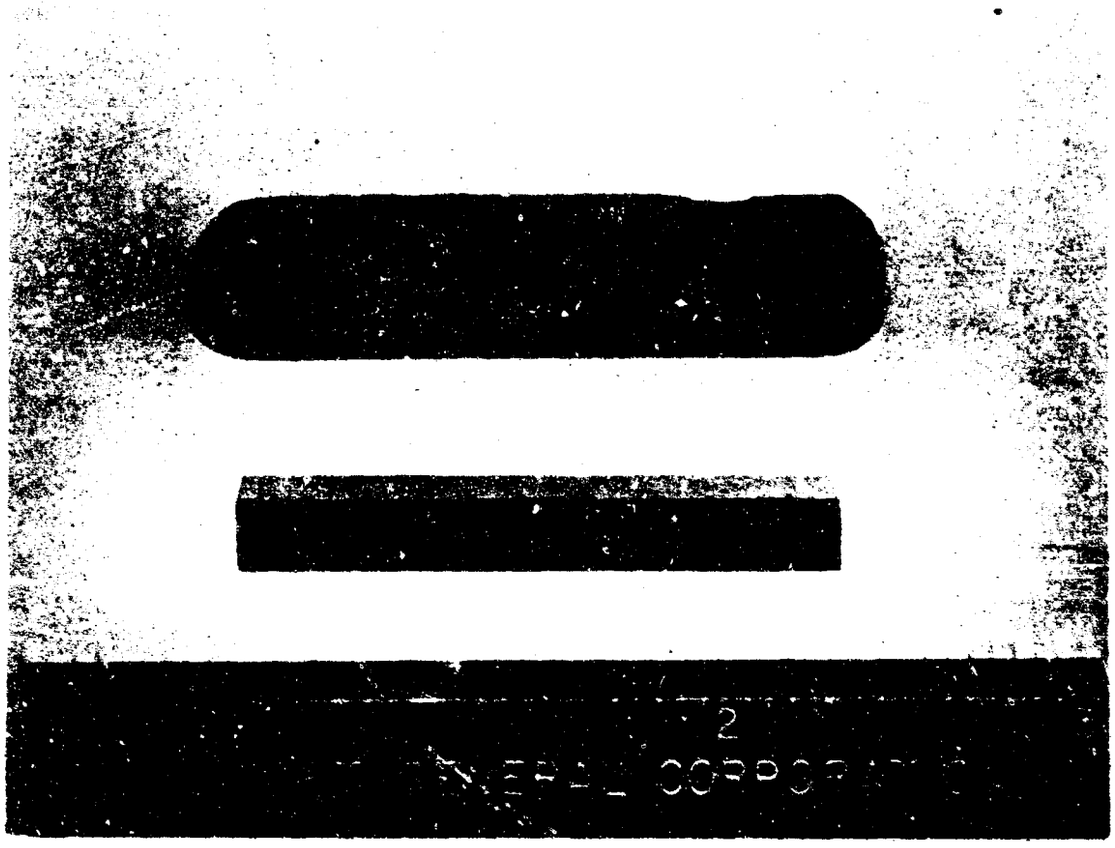

Figure 32. Flexure Specimen as Hot-Pressed and Final Machined

XII, A, Task 1—Development of Microcomposite (cont.)

(1) Flexure Strength

Flexure strength measurements were made using three-point loading with a 1.5-in. span. The crosshead travel rate was 0.02 in./minute. The results of each test are reported in Table VII. The arithmetic average and standard deviation are shown; however, a comparison of average strength values for the different compositions can be misleading. In each series of tests for a given composition, there were both high-strength and low-strength specimens. Therefore, there was no significant indication that strength differences existed at ambient temperature between the series of compositions.

A significant increase in ambient temperature strength of the microcomposite compositions was obtained in comparison to the typical reported values for the monocarbides of tantalum and hafnium (Reference 4).

The room temperature strength values for a given composition were not found to correlate with the variations in apparent density listed in Table VII. However, the variation in density was small and the density was always greater than 95% of theoretical.

Within a given composition, large differences in strength could be correlated in most cases with the appearance of the fracture surfaces. Specimens with high strengths (40 to 60,000 psi) had irregular fracture surfaces indicative of a higher degree of toughness than those specimens with low strength (20,000 psi) which had typical brittle fracture surfaces.

Figure 33 shows a photographic comparison of the two types of fractures surfaces on specimens made from the 13Ta-50Hf-37C composition. The brittle fracture surface corresponds to a specimen with

TABLE VII

AMBIENT TEMPERATURE

PHYSICAL PROPERTIES OF SIX MICROCOMPOSITE COMPOSITIONS

1. Composition: 8Ta-55Hf-37C

Specimen Number	Flexure Strength, psi	Standard Deviation, psi	Density, gm/cm^3	Modulus of Elasticity, 10^6 psi
212	53,400		12.7	38.7
213	59,500		12.7	39.4
214	20,700		12.7	37.0
218	33,600		12.5	37.3
225	55,600		12.6	39.7
226	57,000		12.6	41.1
308	43,200		12.6	Av: 38.8
310	66,300		12.6	
311	63,000			
Av:	50,300	15,000	Av: 12.6	

Relative Standard Deviation: 29.7%

TABLE VII (cont.)

II. Composition: 15Ta-50Hf-5?C

Specimen Number	Flexure Strength, psi	Standard Deviation, psi	Density, gm/cm^3	Modulus of Elasticity, 10^6 psi
199	18,700		12.8	41.7
207	18,300		12.8	41.5
224	50,500		12.8	41.6
243	69,900		12.8	41.4
252	31,300		12.8	41.2
253	30,500		12.7	39.5
254	35,600		12.8	41.8
255	39,100		12.8	41.1
256	41,600		12.8	41.4
257	41,600		12.8	41.0
Av:	37,500	15,200	Av: 12.8	Av: 41.2
		Relative Standard Deviation:	40.5%	

III. Composition: 18Ta-45Hf-37C

209	20,000		13.1	42.1
245	23,000		13.2	42.4
273	41,100		12.7	42.1
281	69,200		12.4	42.4
282	67,500		12.9	42.8
Av:	44,200	23,500	Av: 12.9	Av: 42.1
		Relative Standard Deviation:	53.1%	

TABLE VII (cont.)

IV. Composition: 10Ta-50Hf-40C

Specimen Number	Flexure Strength, psi	Standard Deviation, psi	Density, gm/cm^3	Modulus of Elasticity, 10^6 psi
222	18,600		12.6	45.7
223	53,800		12.7	44.8
267	14,400		12.5	44.0
268	24,700		12.5	40.0
361	12,500		12.5	47.4
362	49,800		12.2	42.1
Av:	29,000	18,200	Av: 12.5	Av: 44.0

Relative Standard Deviation: 62.7%

V. Composition: 13Ta-47Hf-40C

242	55,900		12.0	40.5
269	14,100		12.3	42.2
274	27,400		12.4	43.4
363	57,200		12.8	45.5
364	17,000		12.8	45.5
Av:	34,300	20,100	Av: 12.5	Av: 43.4

Relative Standard Deviation: 60.8%

TABLE VII (cont.)

VI. Composition: 18Ta-42Hf-40C

Specimen Number	Flexure Strength, psi	Standard Deviation, psi	Density, gm/cm^3	Modulus of Elasticity, 10^6 psi
247	60,000		12.7	43.7
249	54,100		12.8	44.5
251	30,700		12.7	35.2
365	71,000		13.0	46.6
366	57,200		13.0	46.4
Av:	55,000	14,000	Av: 12.8	Av: 43.2
		Relative Standard Deviation:	27.1%	

VII. Composition: 13Ta-44Hf-43C

231	21,200	—	12.7	50.1

500X

Microstructure showing less free metal in grain boundaries

500X

Microstructure showing large number of pools of free metal

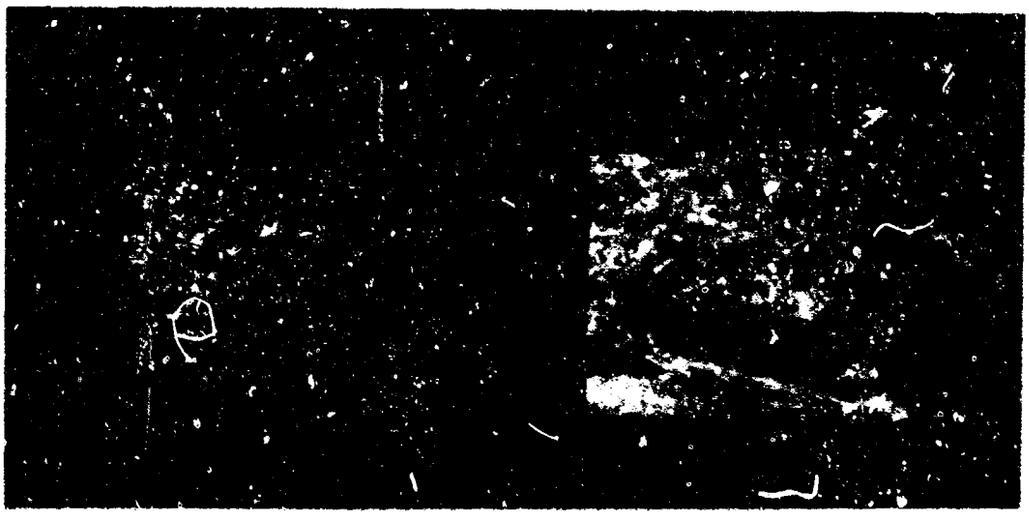

8X

Brittle type fracture surface
Flex Strength: 18,300 psi

8X

Fracture surface exhibiting toughness
Flex Strength: 69,900 psi

Figure 33. Macro and Microstructural Comparison of Flexural Specimens Exhibiting High and Low Strengths--Compositions 13Ta-50Hf-37C

III, A, Task 1—Development of Microcomposite (cont.)

18,300 psi flexure strength, while a greater degree of toughness was exhibited by the sample with a 69,900 psi strength. An examination of the corresponding microstructures for each of these two specimens (Figure 33) shows slightly more grain boundary metal present in the structure with higher strength and a greater degree of toughness. However, it is more likely that the strength difference was due to other factors as it also occurred in the specimens containing 40 at% carbon where little or no grain boundary metal phase was present. The compositions containing 40 at% carbon did, however, contain a finely dispersed metal phase compared to the heavier lamellar and grain boundary metal phase exhibited by compositions containing 37 at% carbon.

(2) Modulus of Elasticity

Sonic modulus of elasticity measurements were made on the flexure specimens prior to flexure testing. The sonic modulus data are presented in Table VII. The elastic modulus for those samples containing 37 at% carbon decreased with increasing hafnium content. Specimens containing 37 at% carbon had lower elastic modulus than those with 40 at% carbon and 43 at% carbon.

The modulus of elasticity of a two-phase composite material has been related to the proportion of each constituent in the structure. Investigators have reported the following elastic moduli for constituents in the Ta-Hf-C ternary compositions:

Constituent	Modulus of Elasticity (10^6 psi)	Reference
Hf	20	5
Ta	27	6
HfC	44 to 61	4
TaC	53 to 76	4

III, A, Task 1--Development of Microcomposite (cont.)

The lower elastic modulus for specimens with 37 at% carbon, 39 to 42 x 10^6 psi, in comparison to the higher values measured for materials containing 40 at% carbon, 43 to 44 x 10^6 psi, was due to the greater proportion of lower modulus tantalum-hafnium alloy present in the 37 at% carbon material. The decrease in modulus of elasticity values for materials with higher hafnium contents was probably due to the lower modulus of elasticity of the hafnium metal.

No correlation with modulus was found with increasing hafnium content for the three compositions containing 40 at% carbon. This was probably due to the small amount of metal precipitation existing in the microstructures of these compositions.

c. Selection of Microcomposite Compositions for Elevated Temperature Testing

Two microcomposite compositions were selected for elevated temperature testing based on the results of the ambient temperature tests. The first was the 8Ta-55Hf-37C composition. It had the lowest modulus which is desirable for thermal shock resistance. In addition, while the strengths of all six microcomposite compositions were comparable, this material had the least variability in strength.

The 37 at% carbon composition lies on the lower boundary of the monocarbide, δ, phase and melting occurs at 2120°C with lower carbon content as shown by the existence of liquid, L, in the 2130°C temperature section in Figure 34. As a result, this composition has to be closely controlled to prevent retention of excess metal alloy phase at the grain boundaries. A second composition, 8Ta-54Hf-38C, was selected to decrease the primary metal and ensure inversion to the monocarbide on heating and thus a higher temperature capability.

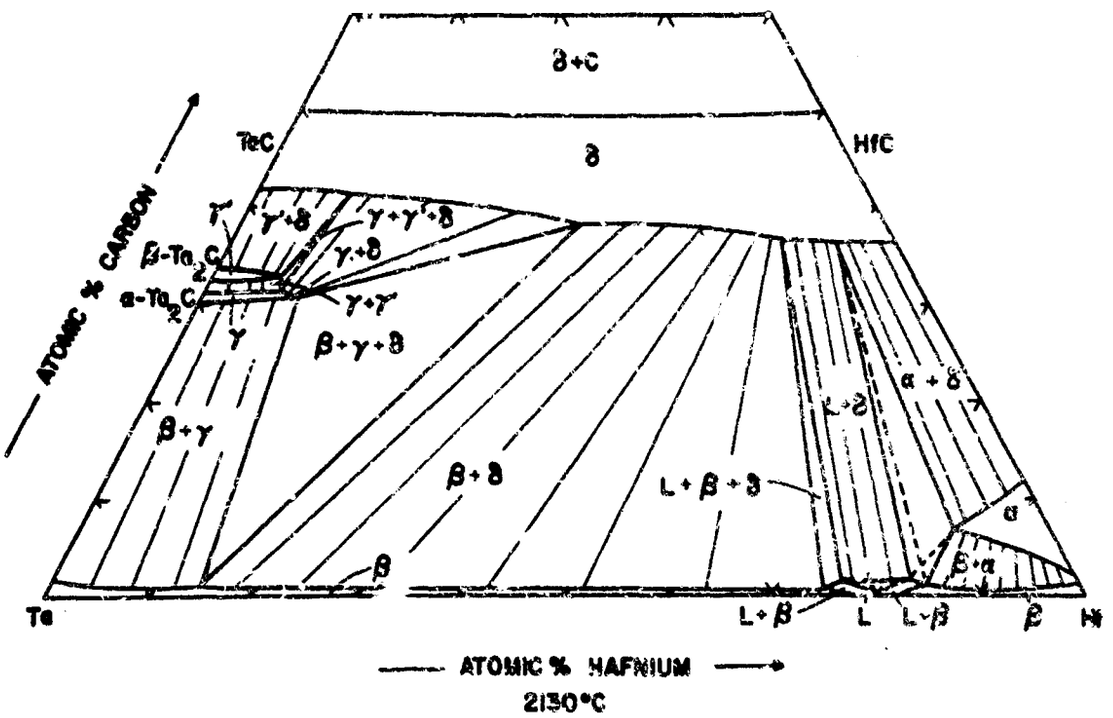

Figure 34. Temperature Section at 2130°C for Ta-Hf-C System

III, A, Task 1--Development of Microcomposite (cont.)

A phase equilibria study was conducted on both selected compositions to verify that the metal alloy phase would invert to the monocarbide. The Pirani melting point furnace described in the Appendix was used to equilibrate samples at a temperature above the metal alloy rich eutectic melting temperature of 2120°C. Metallographic examination of the 8Ta-55Hf-37C sample showed that a small amount of melt phase had formed as well as inversion of the major portion to the monocarbide. The composition 8Ta-54Hf-38C was similarly treated and metallographic examination confirmed that complete inversion to the monocarbide had occurred.

(1) Composition 8Ta-55Hf-37C

The strength and density of each specimen are reported in Table VIII. A plot of temperature vs strength is shown in Figure 35. At 540°C, the variation in strength from specimen to specimen was significantly less than at ambient temperature probably as a result of a decreased tendency for failure to initiate at surface flaws. Because of the low variation, the 540°C average was higher than at ambient. At 1100°C, where maximum strength was observed, an average strength of 135,600 psi was obtained. This strength level was more than three times the values reported for tantalum and hafnium monocarbides, as shown in Figure 36 (Reference 4). It is postulated that the strength improvement at 1100°C occurred because of plastic deformation through the initiation of creep of the metal alloy phase which enables the material to relieve critical failure stresses. Even though incipient cracking may begin in the matrix, the plastic deformation of the metal inhibits crack propagation.

At higher temperatures, 1650 and 2200°C, the strength decreased, which is characteristic of the carbides. Limited flexure testing was conducted at 2200°C because of the occurrence of high plastic deformation.

TABLE VIII

ELEVATED TEMPERATURE

FLEXURE STRENGTH OF MICROCOMPOSITE COMPOSITION 8Ta-55Hf-37C

Temperature, °C	Specimen Number	Flexure Strength, psi	Standard Deviation, psi	Density,[1] gm/cm^3
Ambient	212	53,400		12.7
	213	59,500		12.7
	214	20,700		12.8
	218	33,600		12.6
	225	55,600		12.7
	226	57,000		12.7
	308	43,200		12.6
	310	66,300		12.6
	311	63,000		12.6
	Av:	50,300	15,000	
			Relative Standard Deviation: 29.7%	
540	300	57,800		12.6
	306	49,300		12.7
	307	51,500		12.6
	313	54,400		11.6
	317	52,800		12.7
	320	53,300		12.6
	429	62,300		12.7
	430	60,400		12.8
	431	62,800		12.8
	432	65,500		12.7
	Av:	57,000	5,510	
			Relative Standard Deviation: 9.7%	

1. Determined on specimens after testing.

TABLE VIII (cont.)

Temperature, °C	Specimen Number	Flexure Strength, psi	Standard Deviation, psi	Density,[1] gm/cm³
1100	298	193,500		12.5
	299	164,200		12.6
	301	155,400		12.6
	305	117,000		12.6
	312	114,400		12.4
	427	153,700		12.7
	428	112,000		12.8
	434	74,300		12.8
		Av: 135,600	37,700	
			Relative Standard Deviation: 28%	
1650	302	19,800		12.5
	303	40,900		12.6
	304	32,900		12.6
	309	32,700		11.6
	331	13,200		--
	408	46,500		12.7
	409	54,700		12.8
	410	56,700		12.5
		Av: 37,200	15,500	
			Relative Standard Deviation: 41%	
2200	323	1,580		12.3
	435	593		12.6
	436	1,190		12.5
		Av: 1,120	497	
			Relative Standard Deviation: 44%	

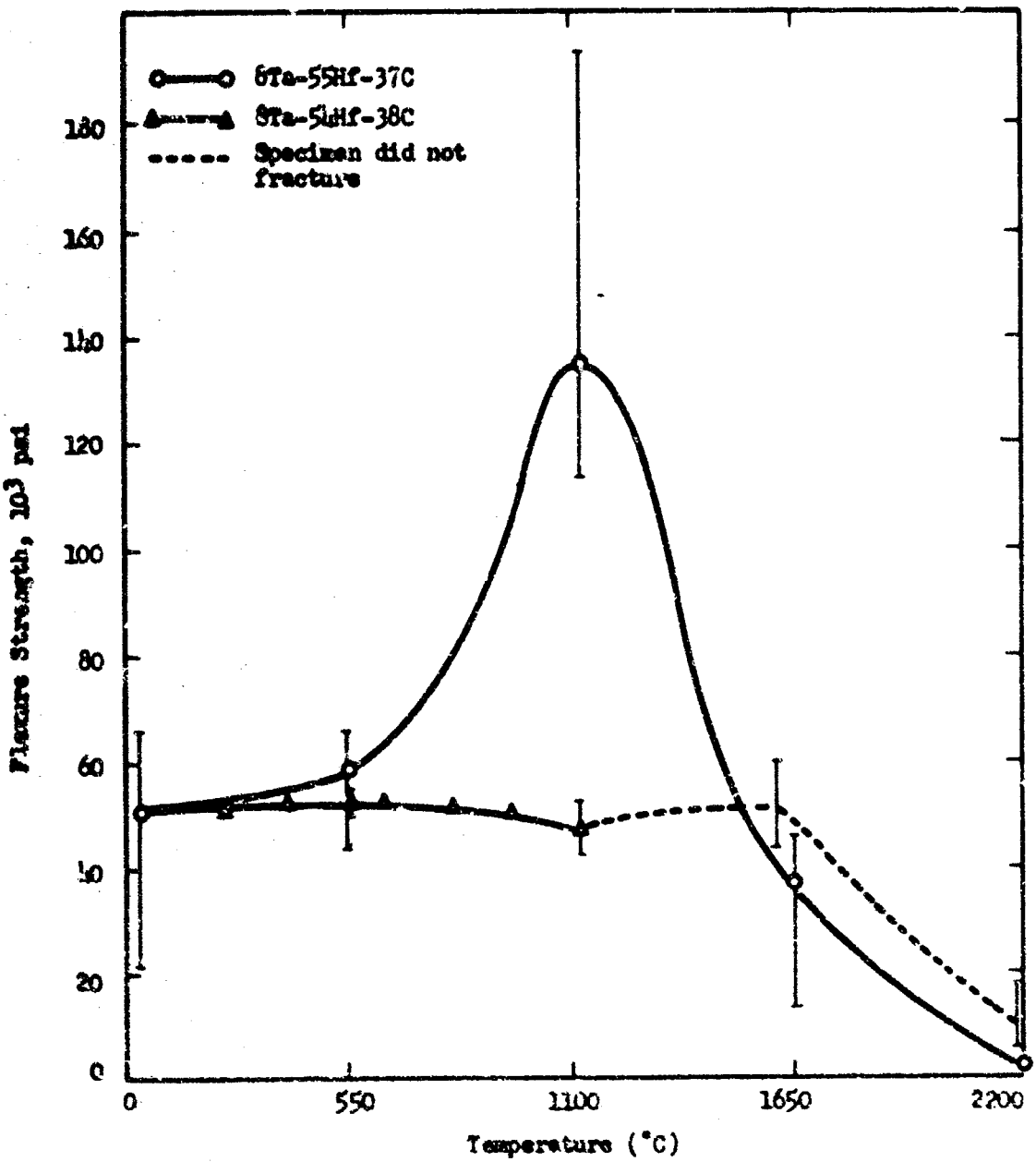

Figure 35. Comparative Elevated Temperature Flexural Strengths of Microcomposite—Compositions 8Ta-55Hf-37C and 8Ta-54Hf-38C

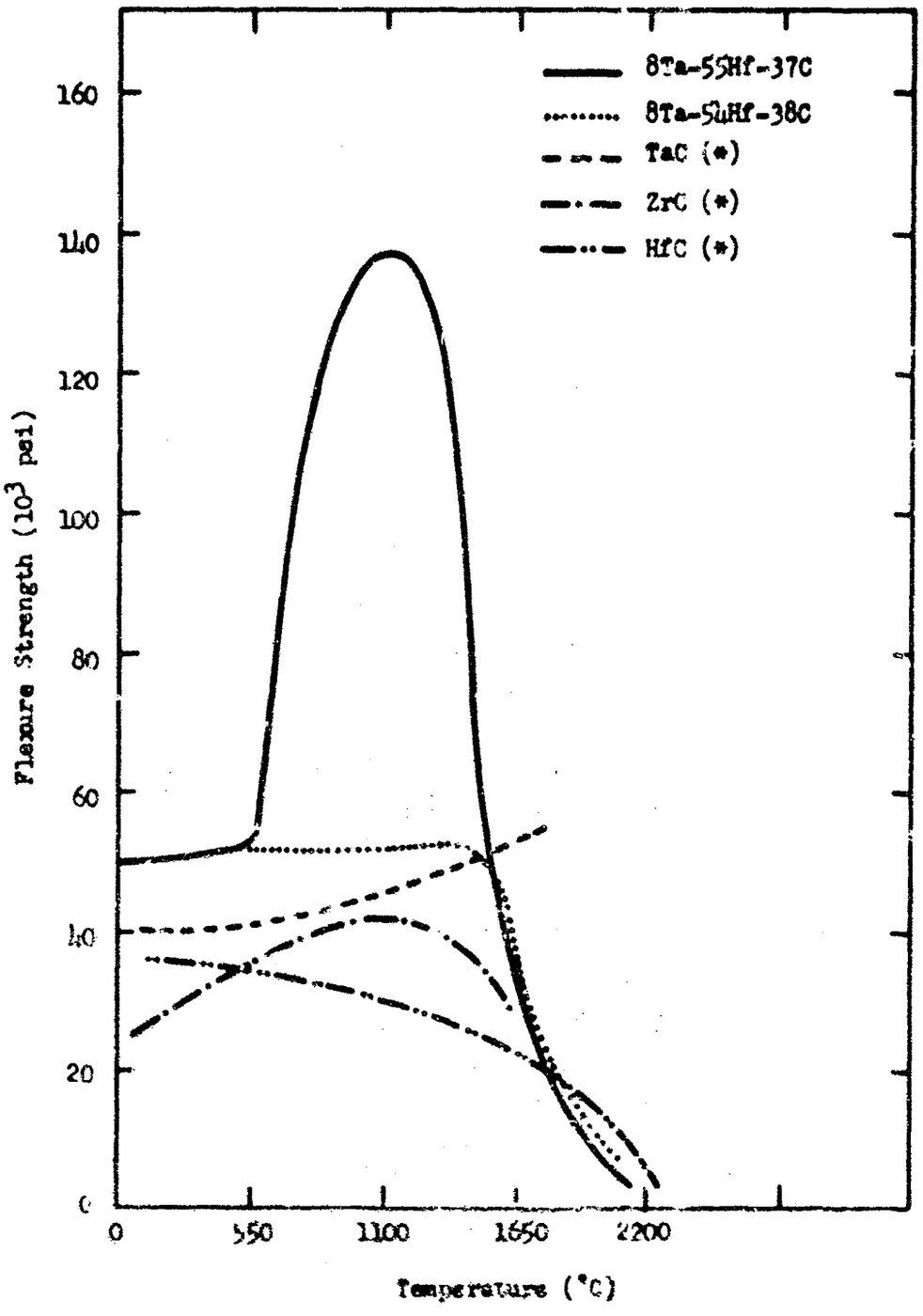

Figure 36. Comparative Elevated Temperature Flexural Strength of TaHf-C Microcomposite Compositions with Other High Melting Point Carbides

III, A, Task 1—Development of Microcomposite (cont.)

Strengths obtained on specimens in the plastic state are of a "relative value" since the flexural strength beam formula is not valid after bending has occurred.

A typical ambient temperature microstructure of a hot-pressed specimen produced from the 8Ta-5Hf-3C composition is characterized by grain boundary metal with a fine, acicular metal alloy precipitate within the carbide grains, as shown in Figure 37. The specimens, after testing at 540 and 1100°C, had a microstructure characterized by heavy precipitation of metal within the grains. Microstructures of specimens exhibiting a large percentage of grains having additional precipitation as compared to the room temperature structure had high strengths. Figure 38 shows a typical microstructure of a sample tested at 540°C where all flexural strengths were approximately 50,000 psi. Note that nearly every grain has the additional precipitation.

Figure 39 shows a grain in which additional precipitation has occurred. It may be seen that very little of the precipitate has a rounded shape and that most of the precipitate was of fine size and had a needle or plate shape. The gross properties associated with this extra precipitation are high strength, nil ductility, and isotropic properties. This structure was not found in any sample tested above 1100°C, nor was it found at room temperature.

One other structure that had a very high strength was observed in a sample tested at 1100°C. This structure was very fine grained, with most evidence of prior carbide grains having been obliterated by precipitation of fine metal particles within the carbide (Figure 40). The number and size of the metal pools remaining was still about the same as in the hot-pressed structure.

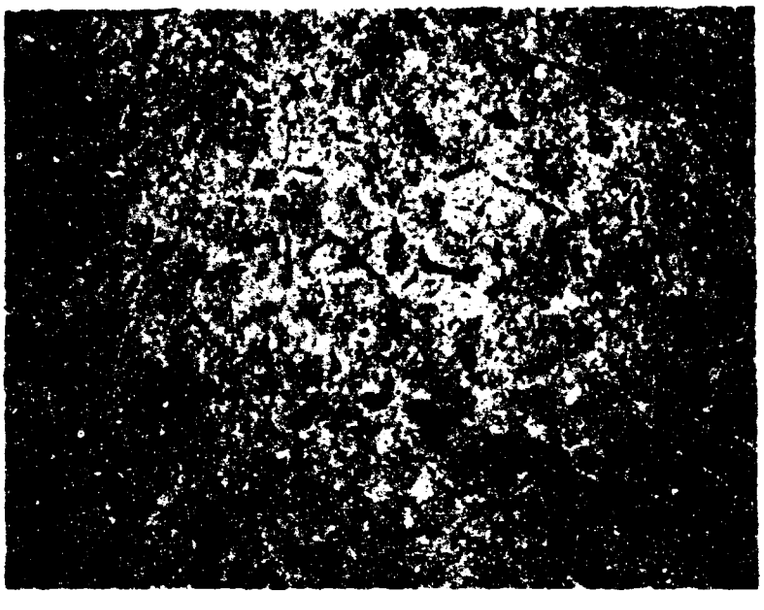

X100

Metal remains at the grain boundaries, but most of it has formed fine precipitates within the grains

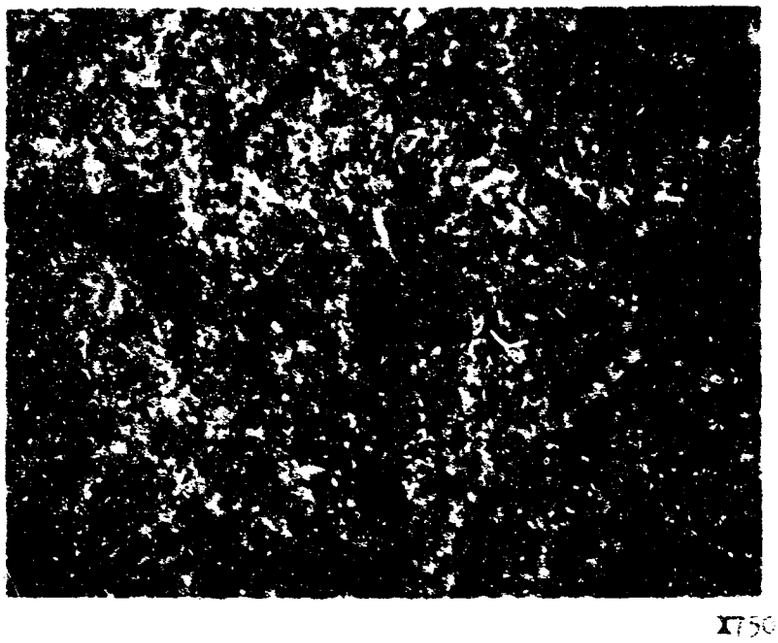

X750

Most of the precipitate is acicular, but near the edges of the grains the precipitates are rounded.

Figure 37. Typical Microstructures of Composition 8Ta-55Hf-37C at Ambient Temperatures

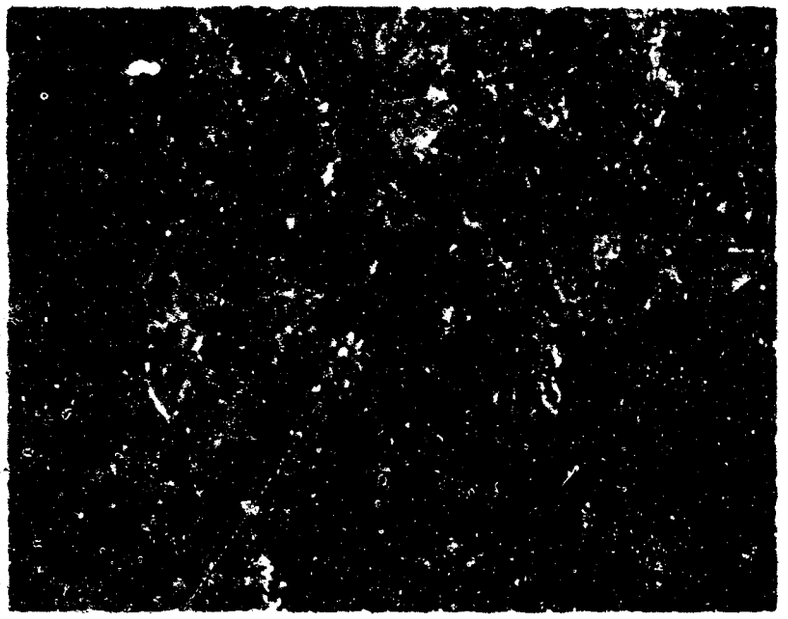

The precipitation in this sample is similar to that in Figure 42, except that in this sample precipitation occurred in every grain. If grains exist which lack such precipitation, mechanical properties are impaired. X100

Figure 38. Microstructure of Composition 8Ta-5Mf-3C Exhibiting a High Flexure Strength at 540°C

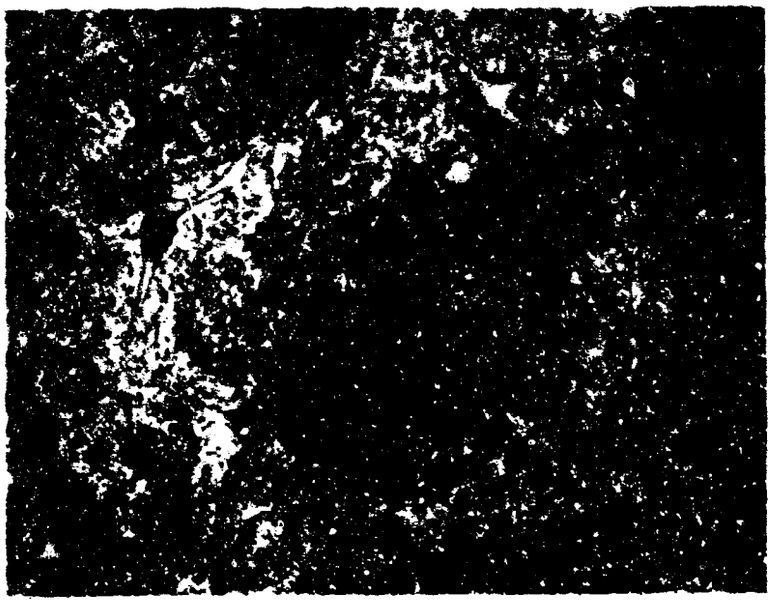

One grain fills over 90% of the picture. In the center of each grain the metal precipitate is platelet shaped. X500

Figure 39. Single Grain of Carbide of the Composition 8Ta-55Hf-37C Showing Fine Precipitation

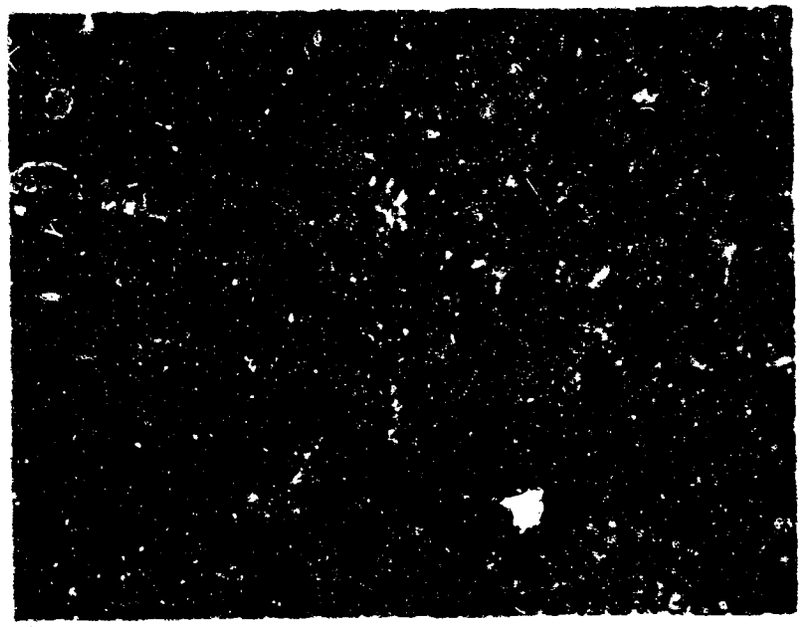

X100

Figure 60. Evidence of Prior Carbide Grains Nearly Obliterated by a Fine Precipitate of Metal

III, A, Task 1--Development of Microcomposite (cont.)

Flexure testing at elevated temperatures caused the microstructures of the specimen to change. At the highest temperatures of testing, 1650 and 2200°C, where marked plastic deformation occurred and the maximum stress before deformation occurs is low, the changes in microstructures were very noticeable. As temperature was increased from room temperature, very little metal dissolves until 1650°C. Then, between this temperature and 2000°C, all the metal would dissolve if equilibrium were attained.

After testing at 1650 and 2200°C, the grain boundary metal was essentially unchanged, but the precipitate within the grains had become heavier as shown in Figure 41. Specimens tested at 1650°C in which precipitation was lacking in a number of the grains resulted in lower flexure strengths. This type microstructure is shown in Figure 42. A sample which underwent heavy plastic deformation at 1650°C, but did not fracture, was sectioned at both the center where the deformation had occurred and at one end, where almost no plastic deformation had occurred. No difference was discernible in the two microstructures as they were both similar to the microstructure shown in Figure 43.

The large plastic deformation of flexure specimens tested at 1650°C suggested that creep might be occurring. Accordingly, a flexure specimen was tested at 1650°C in slow loading (crosshead rate at 0.02 cm/minute). The results are plotted in Figure 44. It appears that the relaxation was exponential with time. After testing, the specimen was badly cracked as shown in Figure 45 and all of the cracks had penetrated approximately the same distance into the sample and terminated near the neutral axis. Catastrophic failures did not occur at crosshead speeds of 0.01 cm/minute and 0.001 cm/minute, and the stress on the sample decreased nearly exponentially with time (Figure 46). As shown in Figure 47, a test run at 1650°C showed

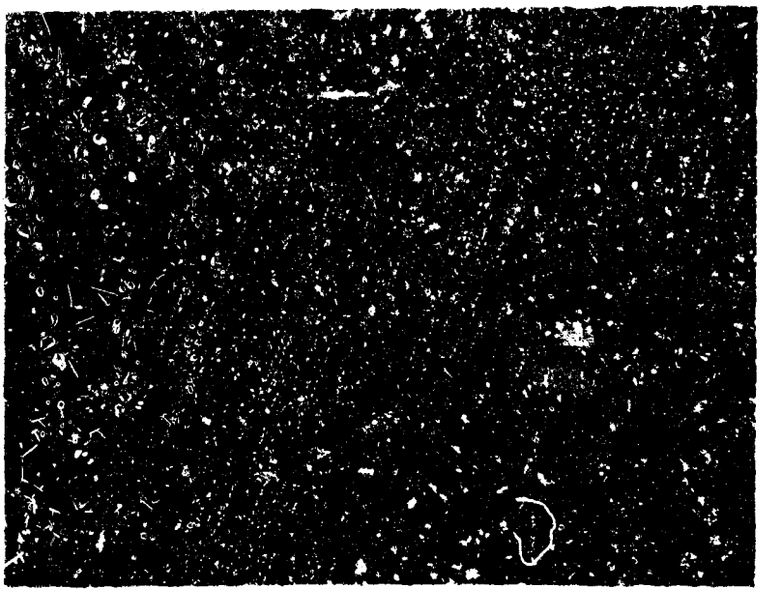

X100

Figure a. The metal pools are spheroidizing, and the precipitate in the grains have become heavier after testing at 1650°C.

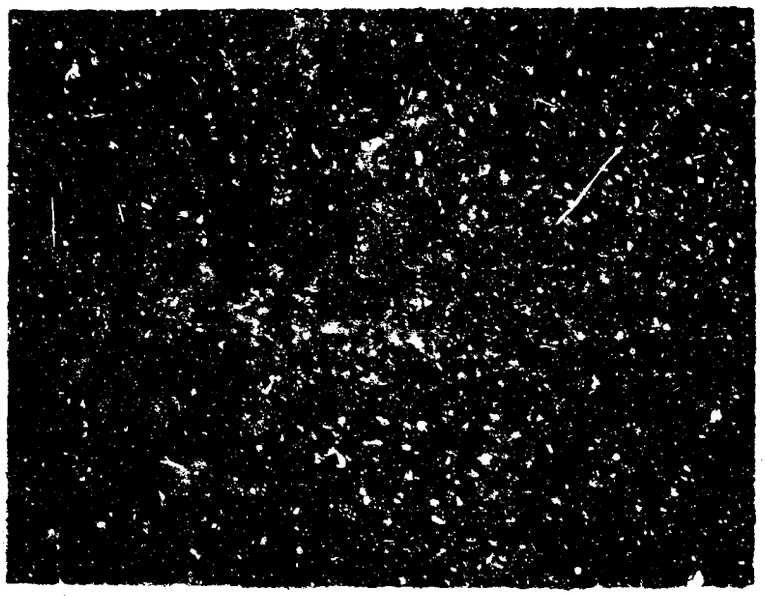

X500

Figure b. Soaked at 1650°C for 15 minutes and then tested. All the precipitates have ripened considerably compared to the ambient temperature microstructure.

Figure 41. Microstructures of Composition 8Ta-55Hf-37C After Testing at 1650°C

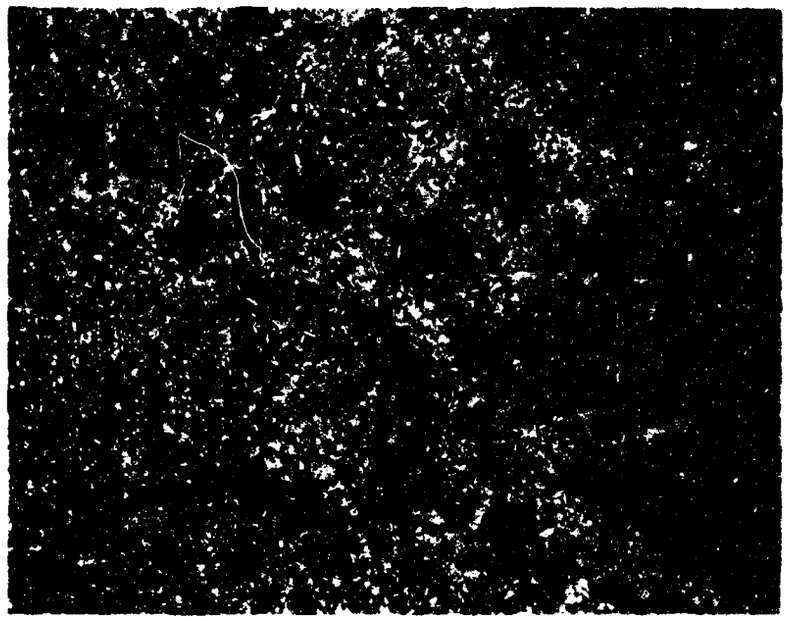

Dark areas are very heavy precipitation. The metal pools on the grain boundaries are depleted but have not begun to spheroidize.

X100

Figure 42. Microstructure of Composition 81a-35Hf-37C Exhibiting Low Flexure Strength at 1650°C

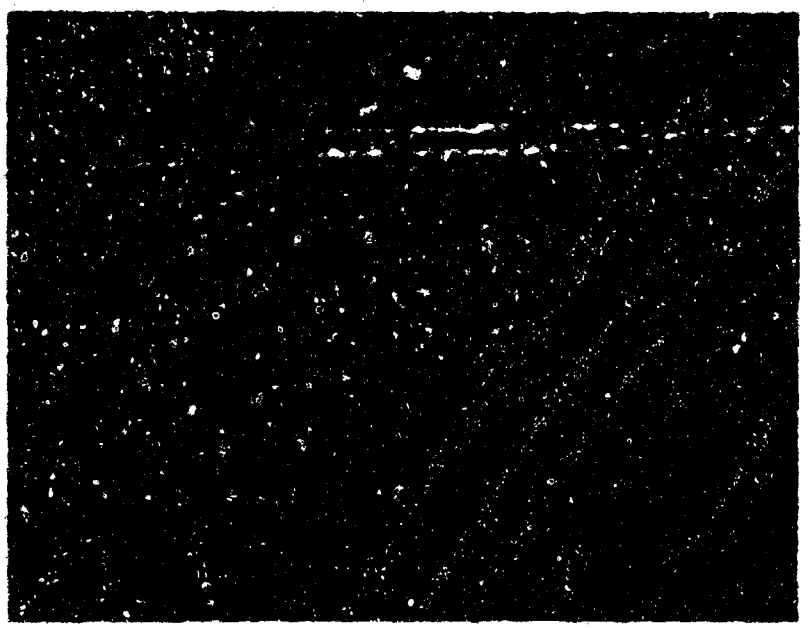

The metal pools at the grain boundaries are still present and the metal precipitate is spheroidising. Each carbide grain has been broken into subgrains. This picture is like Figure 57, but the sample was etched more heavily here. X500

Figure 43. Microstructure of Composition 8Ta-5Hf-3C After Testing at 1650°C

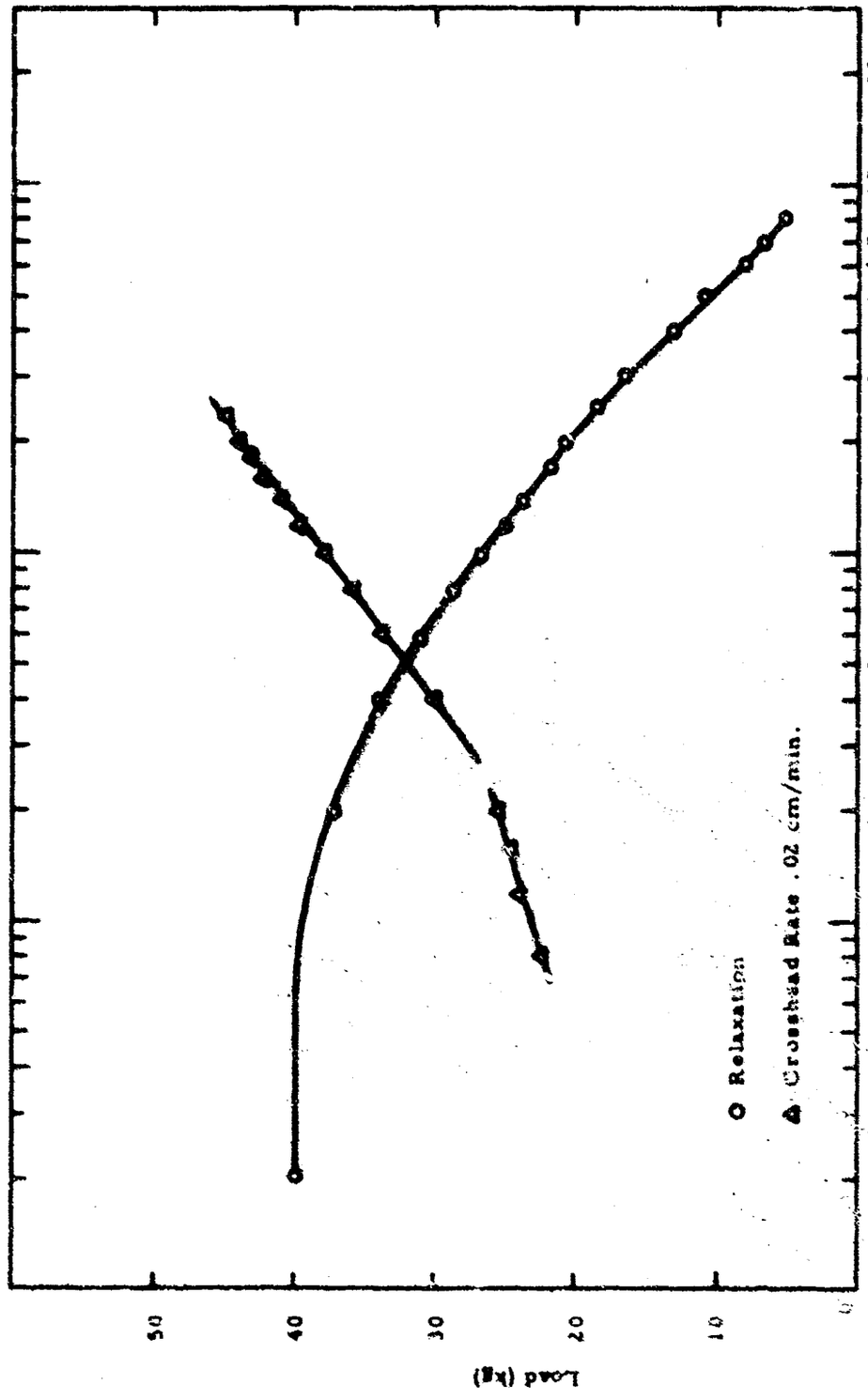

Figure 44. Stress Relaxation Curves for Flexure Specimen Tested at 1650°C--Composition 8Ta-55Hf-37C

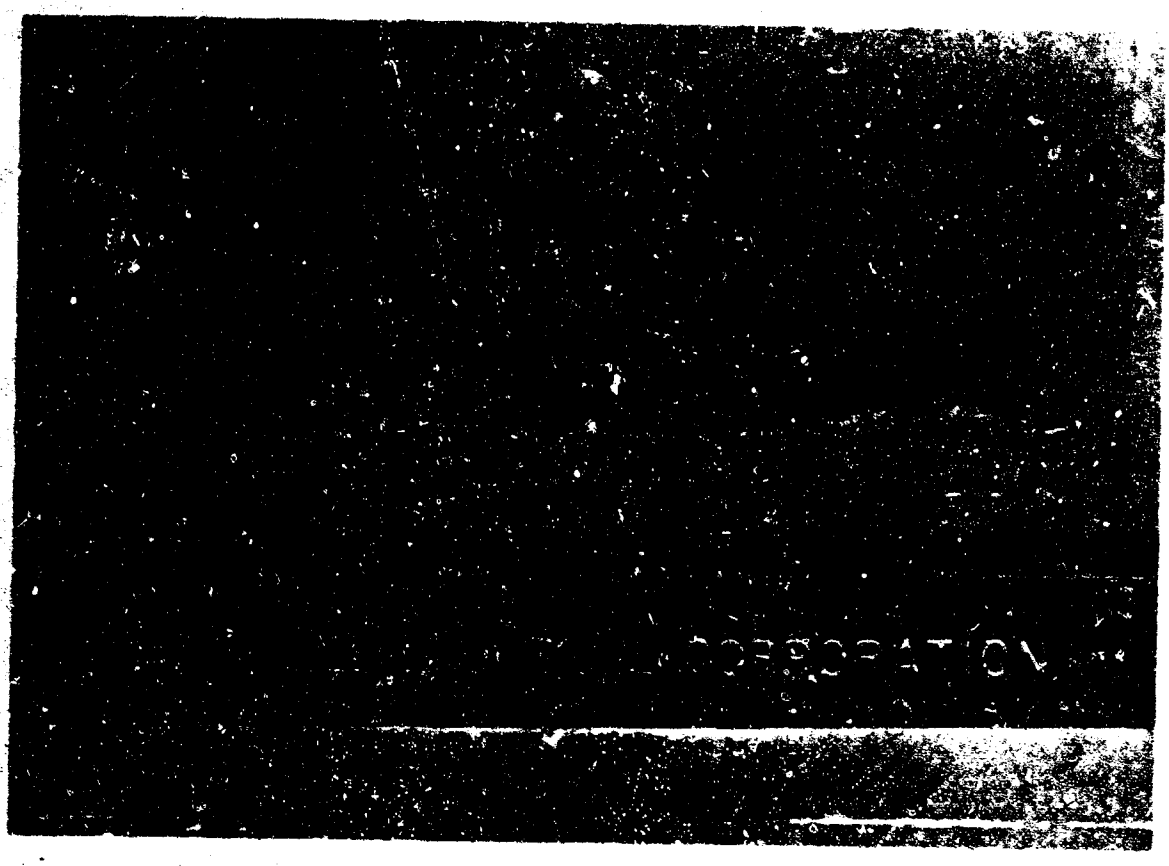

Figure 45. Effect of Deformation On a Flexure Sample Tested at 1650°C

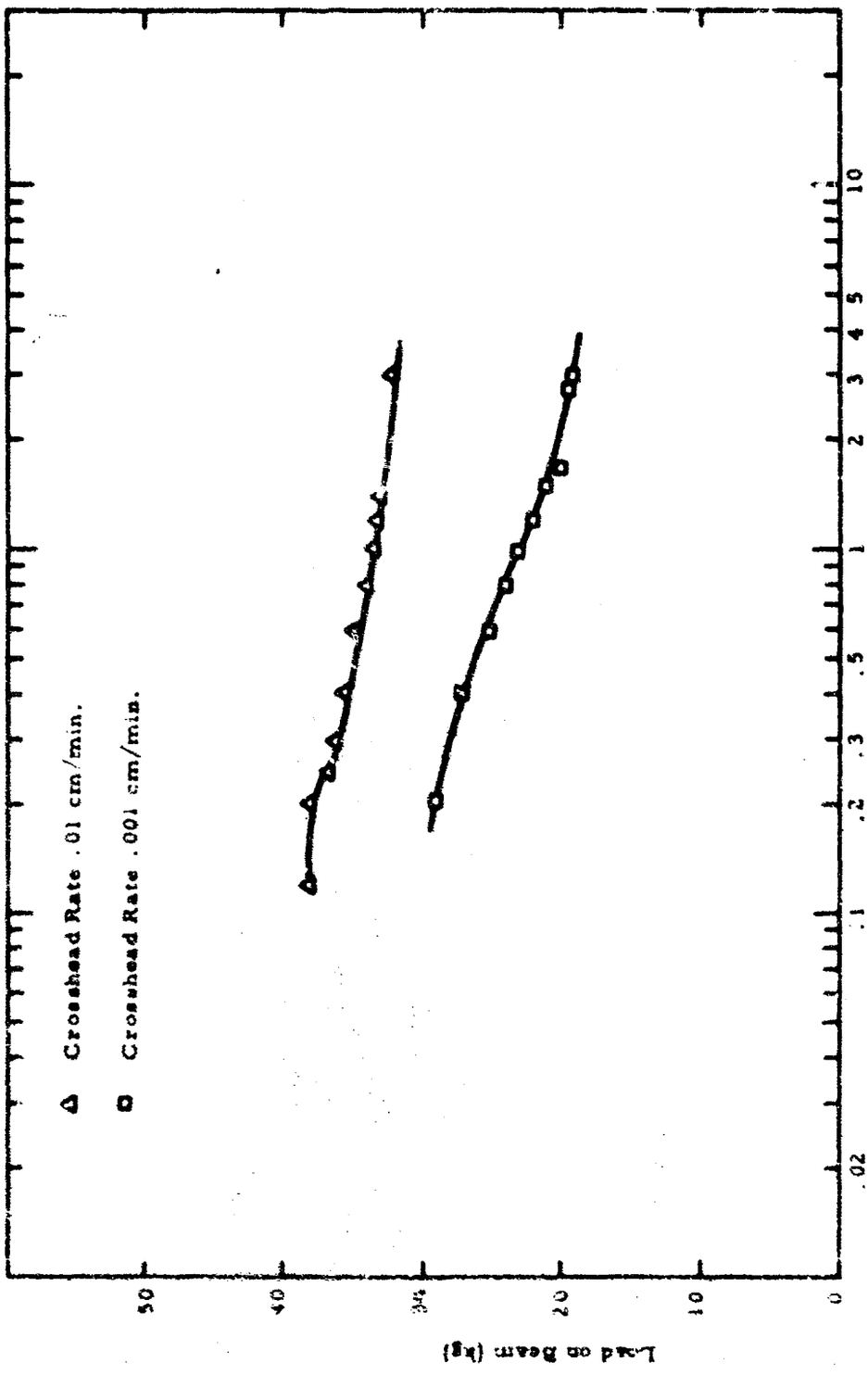

Figure 46. Stress Relaxation Curves for Flexure Specimen Tested at 1650°C--Composition 8Ta-5Hf-37C

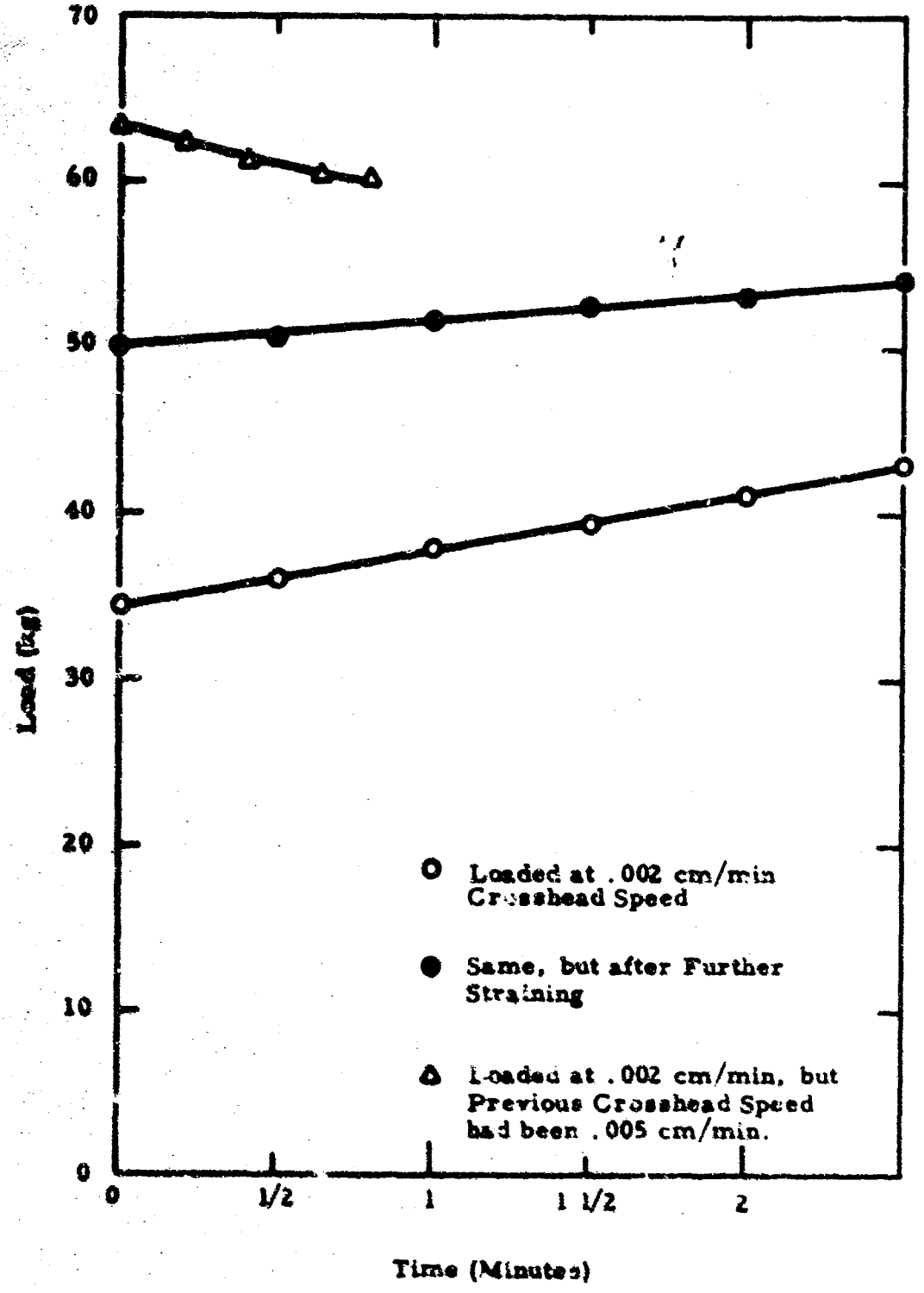

Figure 47. Stress Relaxation Curves for Flexure Sample Loaded at Constant Crosshead Speed at 1450°C—Composition HfB-35Hf-37C

III, A, Task 1—Development of Microcomposite (cont.)

that load increased as the crosshead advanced in two cases but decreased when the stress was at a slightly higher level (previous crosshead speed had been 0.005 cm/minute). At 1300 and 1200°C, the stress still relaxed exponentially with time as shown in Figures 48 and 49, respectively.

It was evident that, at elevated temperatures, the material did not exhibit brittle behavior because the cracks (Figure 45) did not propagate all the way through the sample. It was not possible to calculate creep parameters with the data because the nonhomogeneous deformation of the samples made it impossible for load to be converted into stress or strain. A Newtonian model, which is the model that describes a glass heated to the softening point, is not completely applicable at constant crosshead speeds. The load continues to increase without reaching a saturation value to accompany the almost constant strain rate produced by the crosshead. Another interesting feature of the results was that the relaxation time, which is the time required for the stress to fall to 37% of its initial value, did not behave like a thermally activated process of the type where stress relaxation is proportional to

$$\exp = \frac{\Delta H(\sigma, T, st)}{KT}$$

which Kebler and Aspinall (Reference 7) found to be the standard equation for creep. At 1650 and 1200°C, the relaxation time was about 30 minutes. At 1300°C, two runs had a relaxation time of 75 minutes, and a third had a relaxation time of 35 minutes. The minimum load necessary to produce creep was estimated to be 0 at 1650°C and 5000 psi at 1100°C. At stresses below this level, relaxation was too slow to be detected with existing equipment. It was established by these tests that below 1100°C creep does not occur. Above 1650°C, the strength was lower than 31,000 psi and at 2200°C, the strength was approximately 1500 psi.

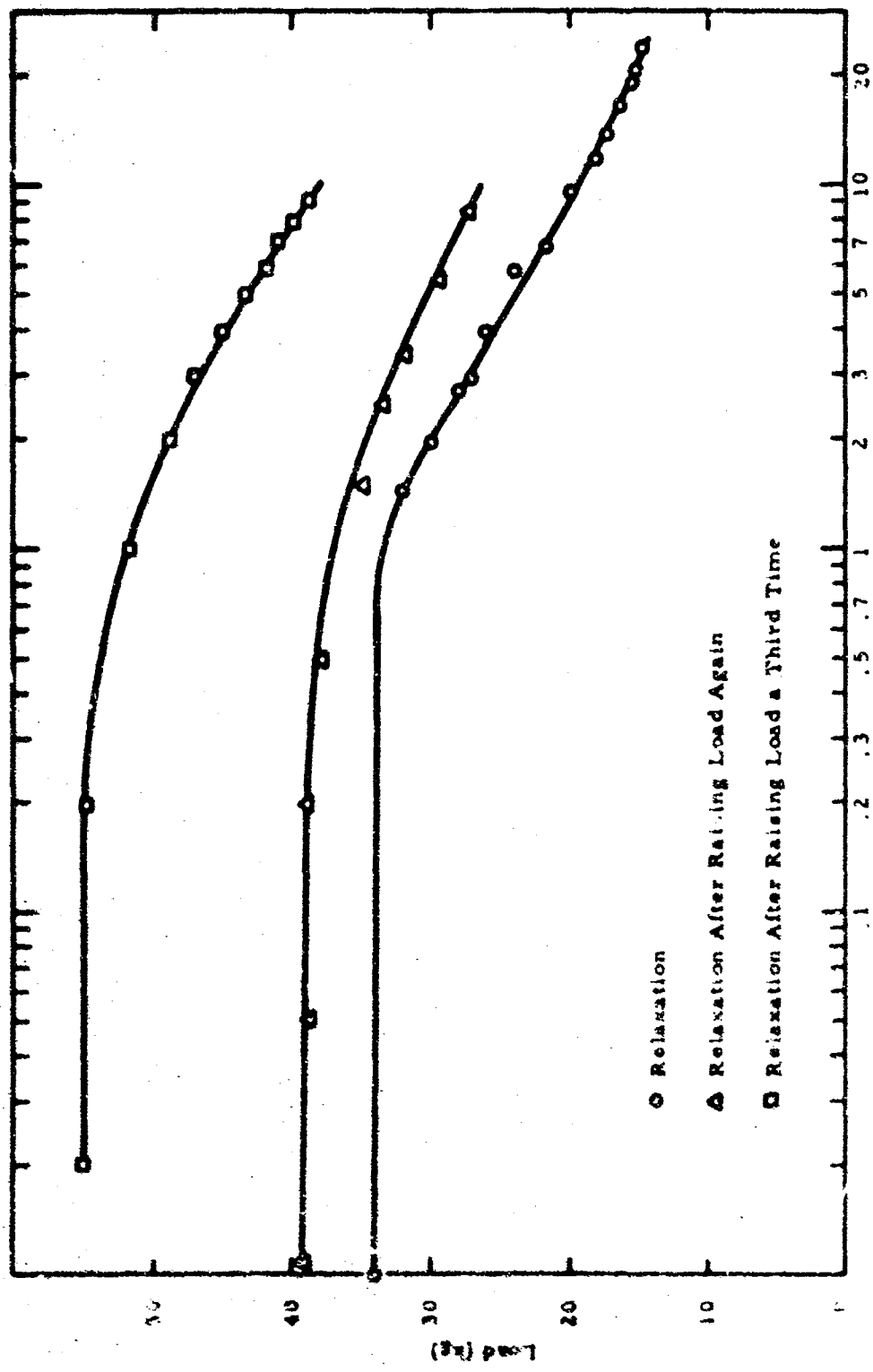

Figure 48. Stress Relaxation Curves for Flexure Specimen Tested at 1300°C--Composition 8Ta-5Hf-37C

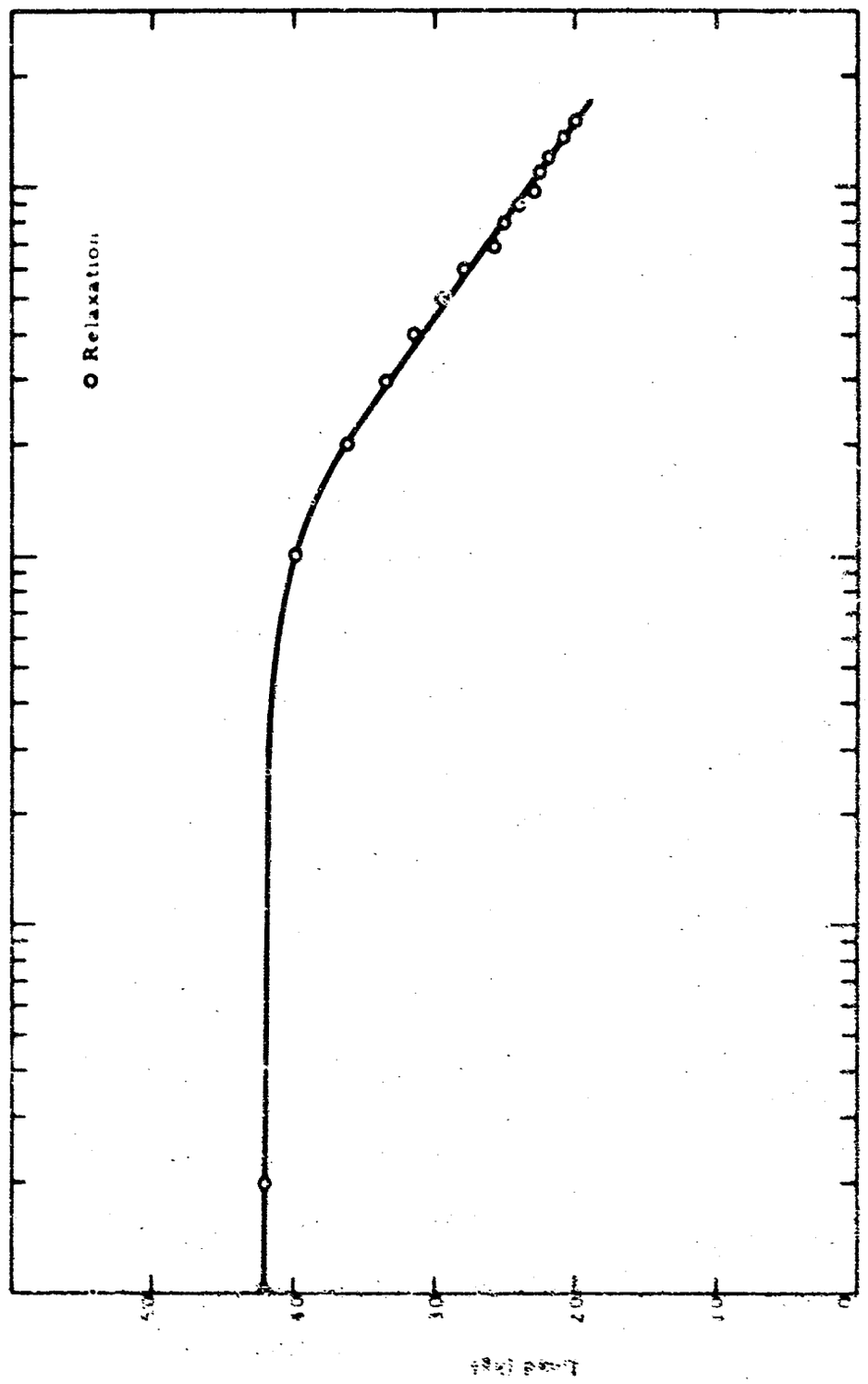

Figure 49. Stress Relaxation Curves for Flexure Specimen Tested at 1400°C--Composition 8Ta-55Hf-37C

III, A, Task 1—Development of Microcomposite (cont.)

Because deformation before rupture is small at 1200°C, it is expected that the metal pools at the grain boundaries were responsible for the deformation. No difference was seen in the microstructures of areas which had undergone large and small deformations at 1650°C; therefore, it may be assumed that the strain was distributed uniformly throughout the grains. The function of the metal precipitate which had not redissolved may be assumed to lower the stiffness of the carbide grains so that less deformation and cracking of the carbide grains would occur.

(2) Composition 8Ta-54Hf-38C

The flexure strength and density of the 8Ta-54Hf-38C composition are reported in Table IX. A plot of the average strength and the indicated range of strength for each test temperature is shown in Figure 35. Flexure testing at ambient temperature was not conducted for this composition. Results of previous tests showed no significant indication that any strength differences existed at ambient temperature between the series of compositions containing 37 and 40 at% carbon. A typical microstructure of this composition is shown in Figure 50. The metal alloy existed as precipitations within the carbide grains with little primary metal evident.

At 540°C, the average strength was 50,300 psi, which equalled the average strength of composition 8Ta-55Hf-37C at ambient temperature. The microstructure of a specimen after testing at 540°C is shown in Figure 51. At 1100°C, no increase in strength occurred as was the case for composition 8Ta-55Hf-37C. The average strength of 46,100 psi indicated a strength behavior characteristic of the carbides, wherein the strength was equal to or slightly lower than at ambient temperature. No differences were noted in the 1100°C microstructure, shown in Figure 52, when compared to the microstructure for the specimens tested at 540°C.

TABLE IX

ELEVATED TEMPERATURE

FLEXURE STRENGTH OF MICROCOMPOSITE COMPOSITION
8Ta-54Hf-38C

Temperature, °C	Specimen Number	Flexure Strength, psi	Standard Deviation, psi	Density,[1] gm/cm³
540	417	53,000		12.6
	418	48,100		12.6
	419	49,300		12.6
	420	50,900		12.7
	Av:	50,300	2,120	
			Relative Standard Deviation: 4.2%	
1100	414	42,500		12.6
	415	44,800		12.6
	416	51,400		12.7
	421	45,900		12.6
	Av:	46,100	3,780	
			Relative Standard Deviation: 8.2%	
1550	411	43,200[2]		12.6
	412	54,600[2]		12.5
	413	61,200[2]		12.8
	422	45,800[2]		12.7
2200	423	14,700[2]		12.2
	424	16,800[2]		12.2
	425	5,100[2]		12.5

1. Determined on specimens after testing.
2. Specimens did not fracture.

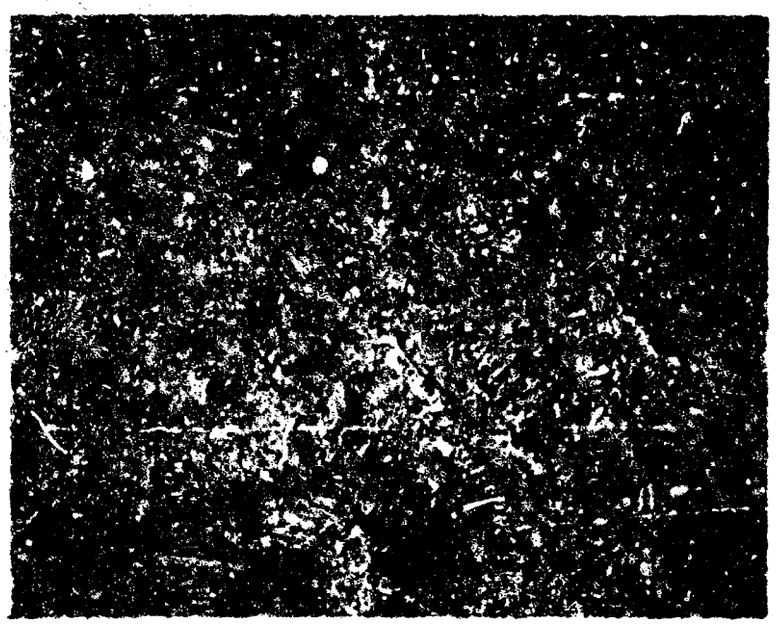

500X

Figure 50. Typical Microstructure of Composition BTa-54Hf-33C (Ambient Temperature)

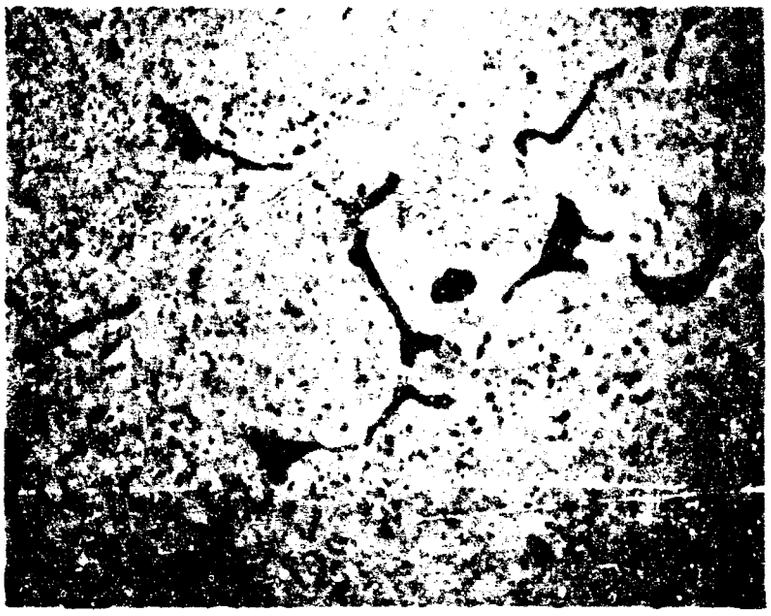

500X

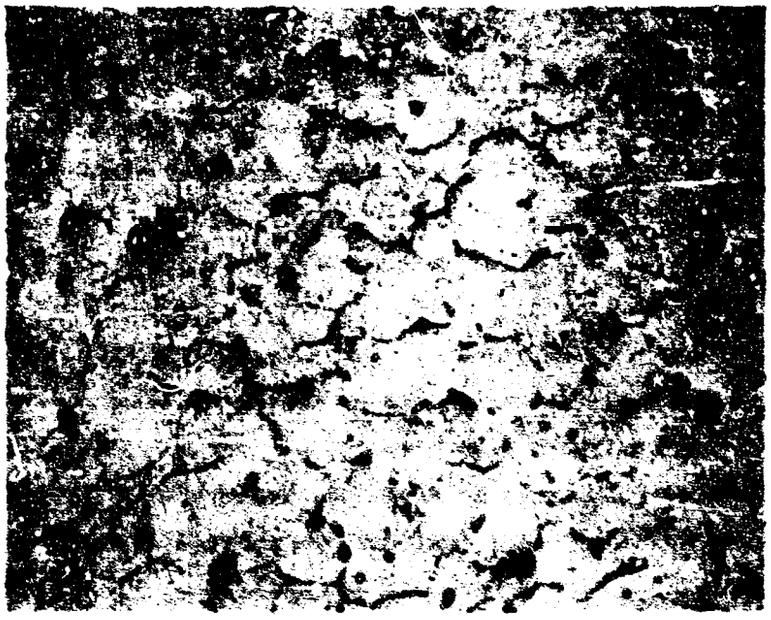

100X

Figure 51. Microstructure of Composition 8Ta-54Hf-38C after Testing at 540°C

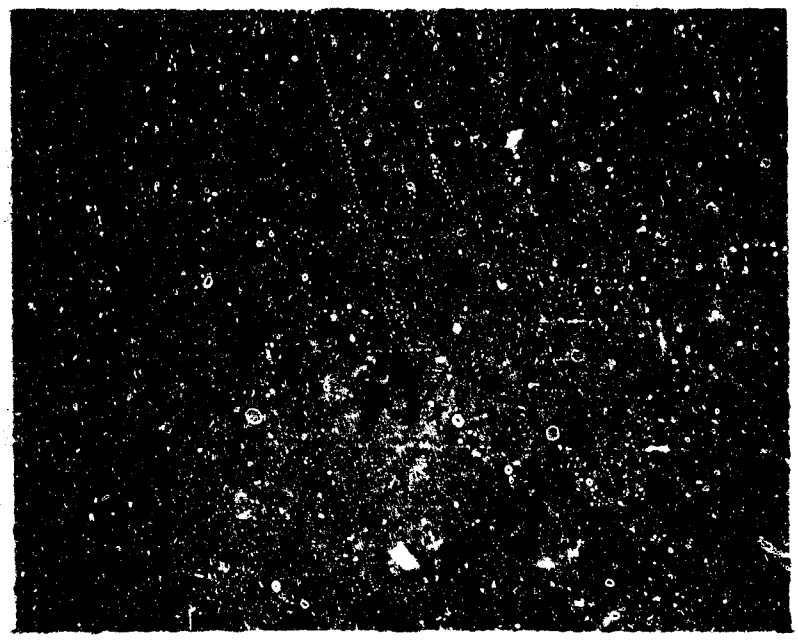

500X

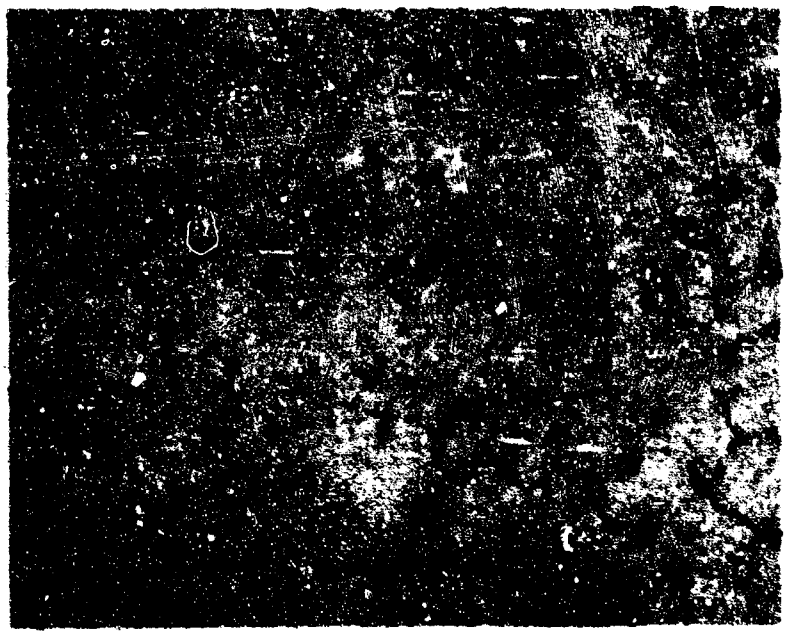

100X

Figure 52. Microstructure of Composition 8Ta-54Hf-38C after Testing at 1100°C

III, A, Task 1--Development of Microcomposite (cont.)

At 1650°C, one sample fractured when loaded to 61,200 psi, while the remaining samples were loaded from 43,200 to 54,600 psi before deflection of the sample exceeded the deformation allowed by the three-point load train. The latter test samples experienced "hot tearing" but did not fracture. Higher crosshead rates, up to 0.20 in./sec, did not result in fracture of the specimen. The microstructures of specimen No. 411, 43,200 psi strength, and No. 413, 61,200 psi strength, are shown in Figure 53.

At 2200°C, all specimens tested carried loads of 5100 to 14,700 psi to full deflection without complete fracture. Subsequent slow cooling resulted in a spheroidized metal precipitate within the grains. Figure 54 shows this typical microstructure.

d. Thermal Expansion Measurements

The linear thermal expansion of the two microcomposite compositions, 8Ta-55Hf-37C and 8Ta-54Hf-38C, was measured from 25 to 2047°C. The test results are presented in Table X.

Prior to the thermal expansion measurements on the specimens, calibration checks were made using sapphire and wrought tungsten rods for which expansion data have been accurately established in the literature. Figure 55 shows a plot of the thermal expansion of the two microcomposite compositions and the calibration checks on sapphire and tungsten. A thermal expansion curve for stoichiometric hafnium carbide has also been included for comparative purposes. These HfC data, as reported in the literature, were derived from X-ray diffraction "d" spacings (Reference 7).

A comparison of the curves in Figure 55 shows that both microcomposite compositions follow the expansion behavior of HfC to approximately 1600°C. Above 1600°C, the thermal expansion of both composites deviates slightly

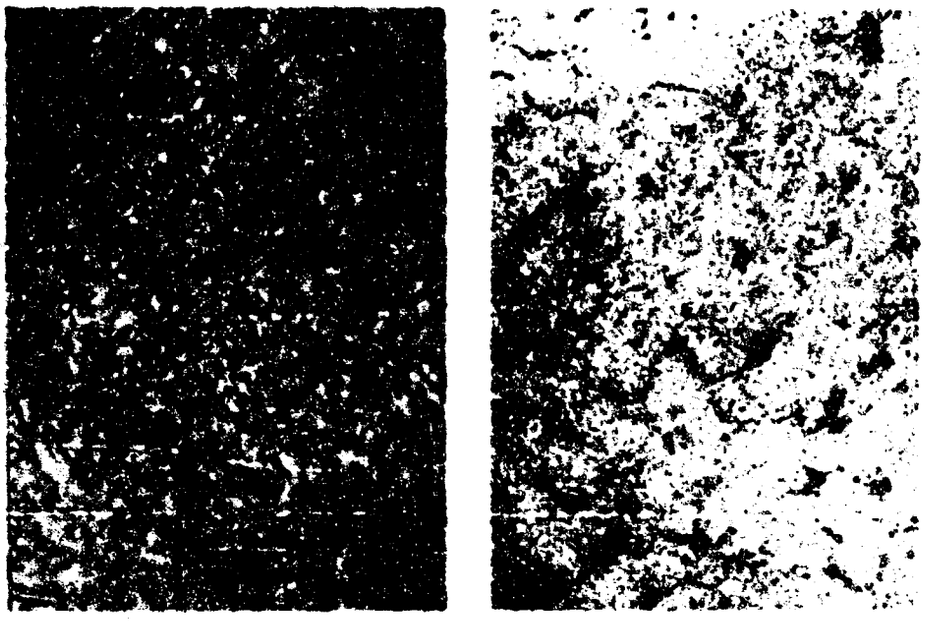

500X 100X

b. Specimen No. 413, minimum free metal in grain boundaries, Flexure strength 61,200 psi, Specimen fractured.

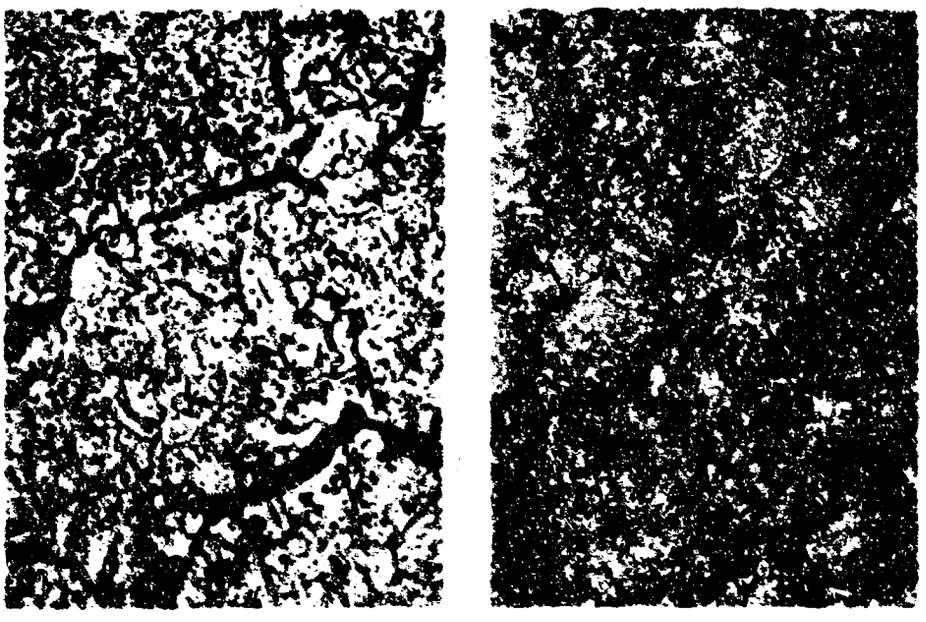

500X 100X

a. Specimen No. 411, abundance of metal at the grain boundaries, Flexure strength, 43,200 psi. Specimen did not fracture.

Figure 53. Microstructural Comparison of Composition 8Ta-54Hf-38C Exhibiting Low and High Strength after Testing at 1650°C

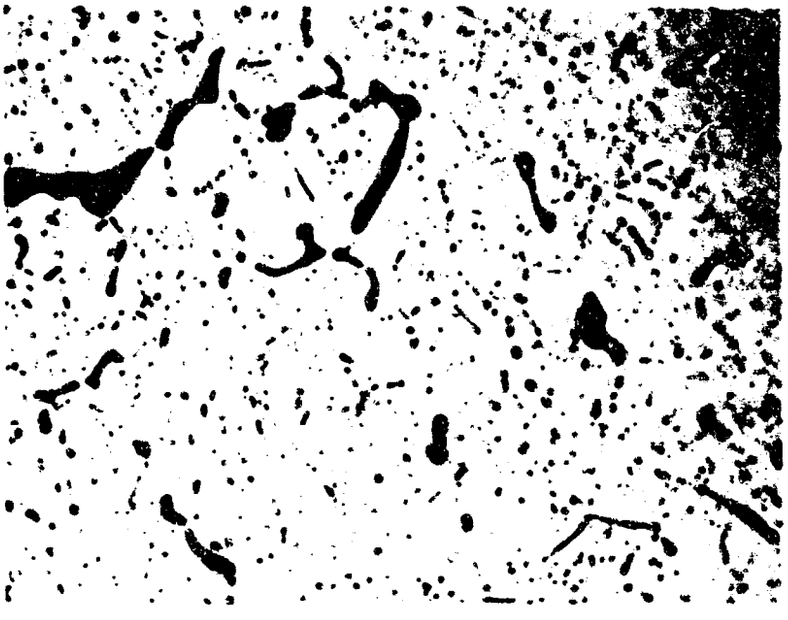

800X

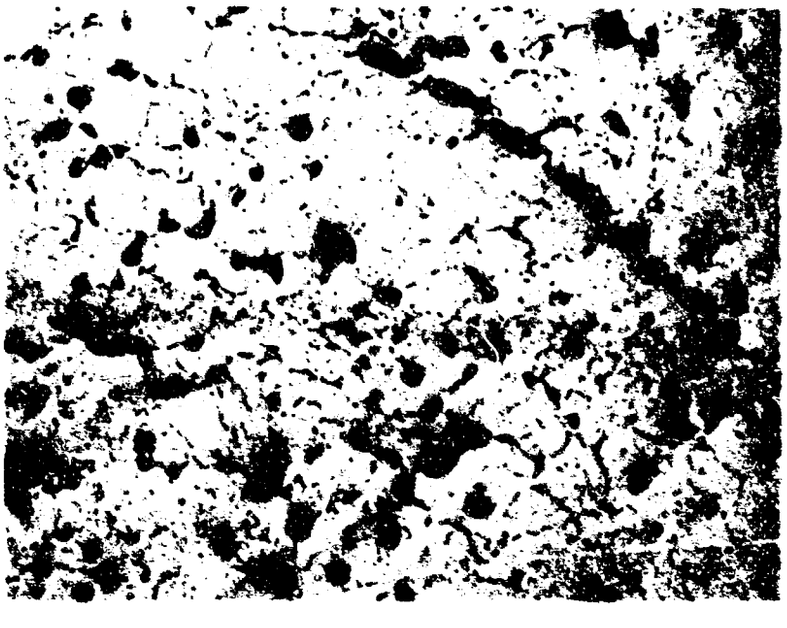

100X

Figure 54. Typical Microstructure of Composition 8Ta-54Hf-38C after Flexure Testing at 2200°C

TABLE X

LINEAR THERMAL EXPANSION MEASUREMENTS
FOR MICROCOMPOSITES

Composition: 8Ta-54Hf-38C

a. Corrected Measured Data

Specimen Temperature, °C	Specimen Expansion, in.	Thermal Expansion, in./in. x 10^{-3}	Percent Deviation from Least Squares Fit
848	0.00970	5.57	4.43
1024	0.01140	6.55	2.86
1202	0.01349	7.45	5.15
1368	0.01862	10.70	11.70
1598	0.01830	10.52	9.40
1810	0.02236	12.85	5.48
2857	0.02979	17.12	6.82

b. Least-Square-Fit of Data

Temperature, °C	Thermal Expansion, in./in. x 10^{-3}	Thermal Expansion Temperature Coefficient, in./in./°C x 10^{-6}
500	2.93	5.87
1000	6.55	6.55
1500	10.73	7.15
2000	15.43	7.72
2500	20.72	8.28
3000	26.53	8.84

TABLE X (cont.)

Composition: 8Ta-55Hf-37C

a. Corrected Measured Data

Specimen Temperature, °C	Specimen Expansion, in.	Thermal Expansion, in./in. x 10^{-3}	Percent Deviation from Least Squares Fit
828	0.00912	4.89	6.27
995	0.01190	6.38	8.60
1182	0.01375	7.37	0.68
1139	0.01561	8.37	5.37
1466	0.01716	9.20	8.43
1626	0.02036	10.92	6.41
1741	0.02235	11.98	7.04
2040	0.03458	18.54	13.70

b. Least-Square-Fit of Data

Temperature, °C	Thermal Expansion, in./in. x 10^{-3}	Thermal Expansion Temperature Coefficient, in./in./°C x 10^{-6}
500	2.41	4.83
1000	5.91	5.91
1500	10.38	6.92
2000	15.82	7.91
2500	22.24	8.89
3000	29.64	9.88

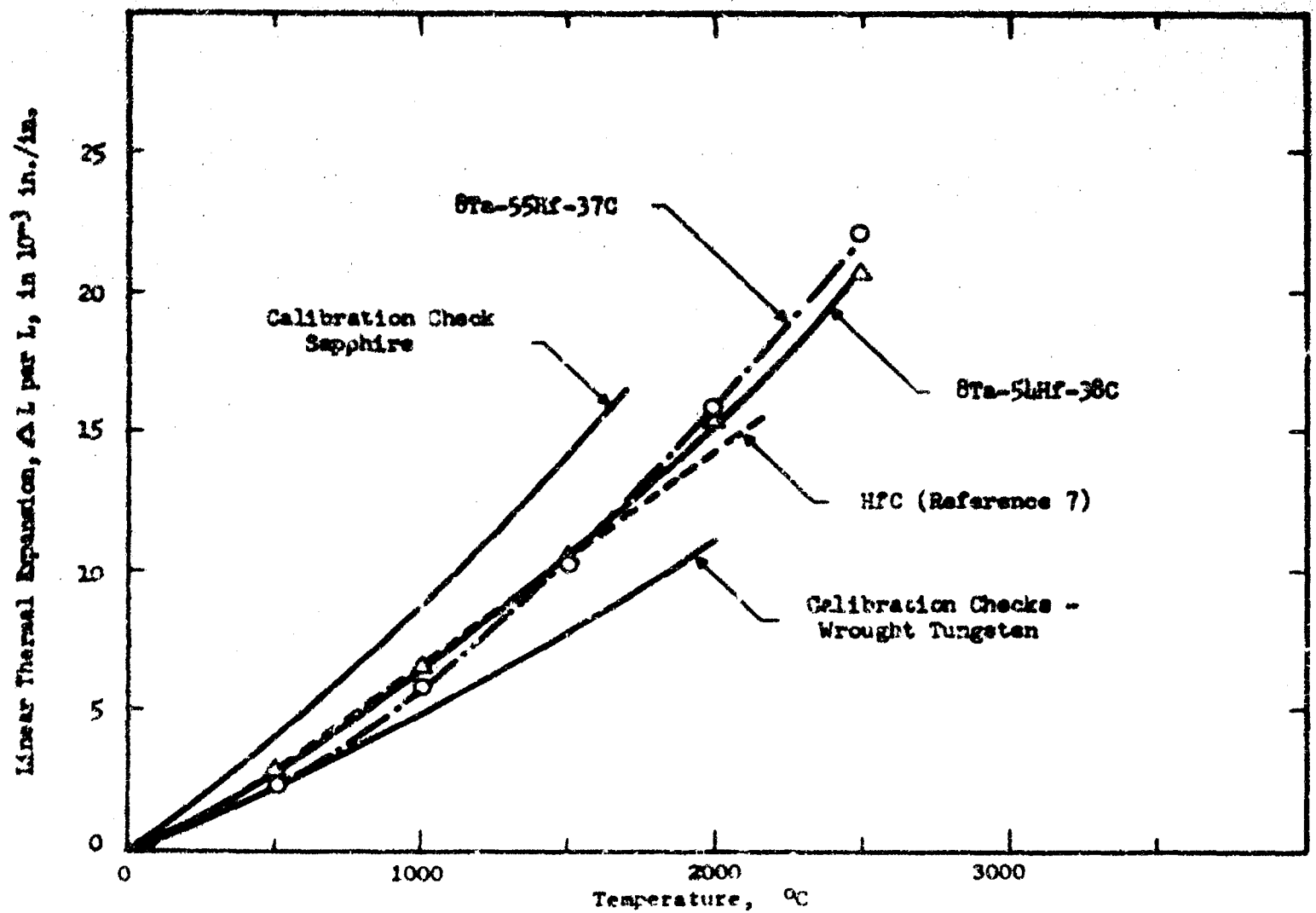

Figure 55. Elevated Temperature Linear Thermal Expansion Measurements on Microcomposite Compositions

III, A, Task 1--Development of Microcomposite (cont.)

from the expansion of hafnium monocarbide. The differences in expansion at the higher temperatures, 2000°C and over, are undoubtedly due to the inversion of the Ta-Hf alloy precipitate phase into the Ta-Hf monocarbide structure.

The thermal expansion of the two compositions can be expressed by the following equation:

$$\alpha = A_1 (T-25) + A_2 (T-25)^2$$

where α = linear thermal expansion
T = temperature, °C

For Composition 8Ta-54Hf-38C:
$A_1 = 5.685 \times 10^{-6}$ in./in./°C
$A_2 = 1.096 \times 10^{-9}$ in./in./°C

For Composition 8Ta-55Hf-37C:
$A_1 = 4.163 \times 10^{-6}$ in./in./°C
$A_2 = 1.949 \times 10^{-9}$ in./in./°C

e. Thermal Diffusivity

The results of thermal diffusivity measurements on three microcomposite compositions, 8Ta-55Hf-37C, 15Ta-50Hf-37C, and 18Ta-45Hf-37C, are presented in Table XI. No significant differences exist in the values at ambient temperature. At 540°C, the differences in data are considered to be typical of the scatter found in this determination. A comparison of these data with the literature (Reference 8) shows the data to be slightly lower than the reported value of 0.08 cm^2/sec for tantalum monocarbide and 0.04 cm^2/sec for hafnium carbide.

TABLE XI

THERMAL DIFFUSIVITY MEASUREMENTS ON MICROCOMPOSITE COMPOSITIONS

Sample No.	Composition, Ta-Hf-C	Temperature, °C	Thermal Diffusivity, cm^2/sec
205	8-55-37	Ambient	0.029
		Ambient	0.028
		540	0.033
306	8-55-37	Ambient	0.036
		Ambient	0.026
207	13-50-37	Ambient	0.027
		540	0.039
307	13-50-37	Ambient	0.023
218	18-45-37	Ambient	0.023
		Ambient	0.029
		540	0.029

III, A, Task 1—Development of Microcomposite (cont.)

4. Task Summary

The significant results of this work are summarized as follows:

a. A low oxygen content in the starting materials was found to be required to cause the desired solution and precipitation of the tantalum-hafnium metal alloy phase in the carbide grains.

b. The optimum conditions for fabricating the microcomposite are: hot-pressing temperature, 2500°C; time, 15 minutes; pressure, 3000 psi; and cooling rate, 500°C/minute.

c. The ambient and elevated temperature flexure strength of the microcomposite was significantly higher in comparison to typical strengths of tantalum and hafnium monocarbides.

d. Large differences in flexure strength for a given composition could be correlated in most cases with the appearance of the fractured surfaces of the specimens.

e. A significant decrease was obtained in the modulus of elasticity for the composition 8Ta-55Hf-37C. The modulus was found to decrease with increasing hafnium content because of the lower modulus of the hafnium.

f. The flexure strength of composition 8Ta-55Hf-37C was found to increase with temperature to 1100°C. This phenomenon is believed due to the occurrence of stress relief through the initiation of creep in the metal phase. This strength increase was nearly three times the ambient temperature strength.

III, A, Task 1--Development of Microcomposite (cont.)

g. Excellent crack arresting characteristics were exhibited at elevated temperatures because of the large amount of plastic deformation.

h. The thermal expansion characteristics closely followed the expansion behavior for hafnium monocarbide up to 1600°C after which some deviation occurred.

i. The thermal diffusivity data were slightly lower then the reported data for hafnium monocarbide.

B. TASK 2--DEVELOPMENT OF TANTALUM-CARBIDE-LINED TANTALUM CARBIDE/CARBON HYPEREUTECTIC COMPOSITE

The objective of this work was to investigate the major fabrication variables for forming the hypereutectic composite, to develop a fabrication process suitable for scale-up, characterize mechanical and thermal properties at ambient and elevated temperatures, and to develop a method for providing a TaC liner on a hypereutectic substrate.

1. Development of Fabrication Procedures for Hypereutectic Composite

a. Equipment

The hypereutectic carbide composites were formed by a direct resistance fusion and drop-casting technique. The hot-press and fusion-casting furnace is shown in Figure 56.

The furnace chamber is designed to be operated at 60 psi of flowing helium during the hypereutectic drop casting. Helium enters the two sight ports and flows through carbon sight tubes extending to within

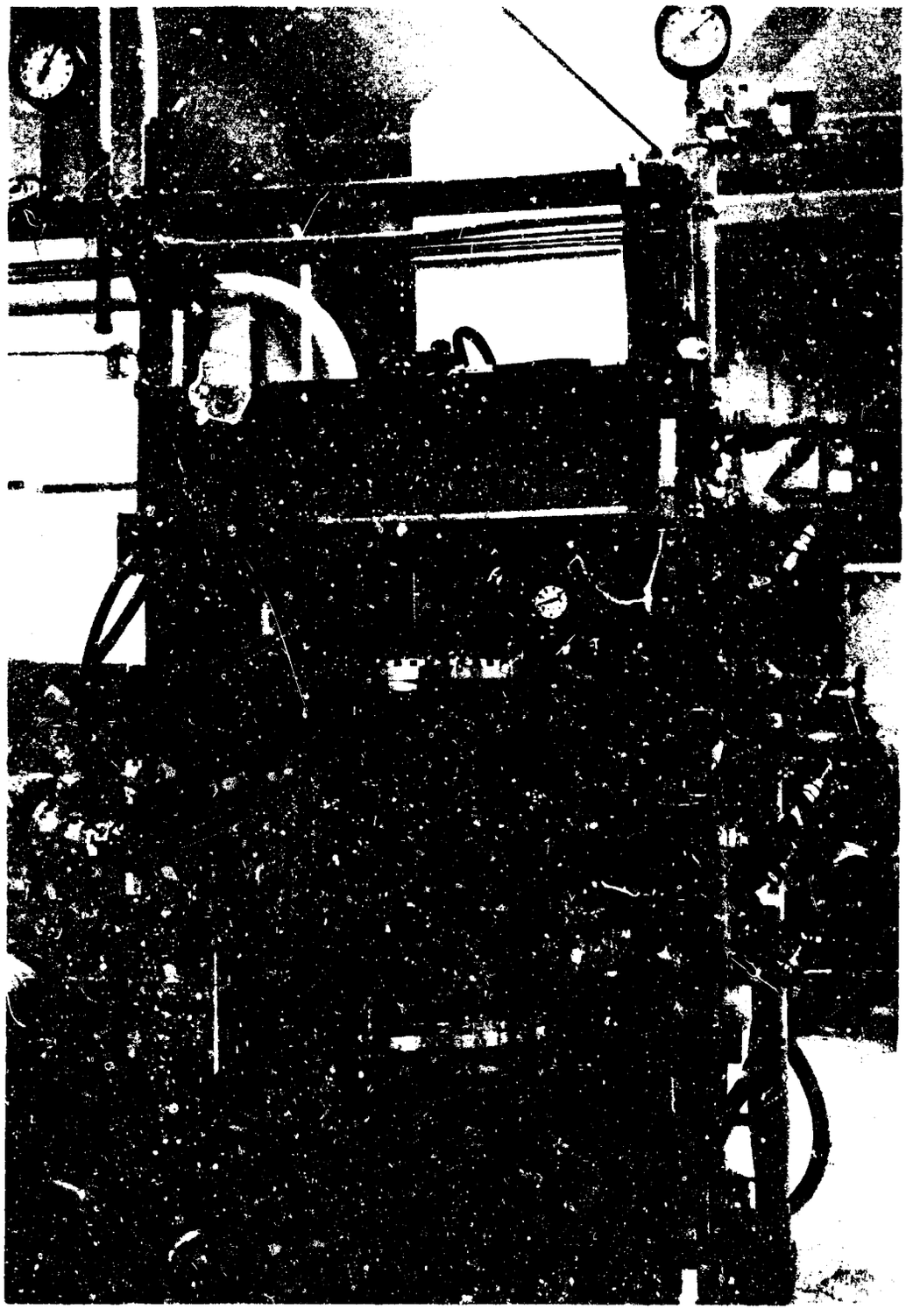

Figure 56. Close-up View of Hot Press and Fusion-Casting Furnace

XII, B, Task 2--Development of Tantalum-Carbide-Lined Tantalum Carbide/Carbon Hypereutectic Composite (cont.)

0.25 in. of the graphite die. The use of flowing helium during the furnace operation prevents the atmosphere within the tube from becoming cloudy with carbon vapor, thus enabling accurate temperature measurements in the black body hole within the graphite fusion casting mold. The pressurized system greatly reduces sublimation of the graphite and vaporization of the powders being melted, thus enabling good compositional control of the starting materials.

Temperature measurements are made through two calibrated quartz glass windows with a Model 95-E4 Pyro-Micro-Optical Pyrometer. Temperature is controlled by a powerstat which controls the input voltage to the saturable-core reactor. Figure 57 is a close-up view of the control panel showing the accessory controls. A temperature programmer has been built into the control circuit which permits controlled heating and cooling rates or constant temperature arrests to be automatically maintained within the furnace. Automatic operation of the controller is accomplished by a silicon photodiode sensor which measures total radiation from the black body hole. A closed-loop power control maintains a constant set power level to the furnace. Fine manual adjustments of the saturable core reactor can also be accomplished with the programmer.

For hot-pressing operations, double acting hydraulic rams are operated simultaneously or independently. Loads are transmitted from the rams to water-cooled, copper rams which extend through O-ring seals into the furnace chamber. Control of the two hydraulic rams is maintained by separate pressure gages and needle valves.

Power is supplied to the furnace by a 175 kw, 440 v, single-phase, stepdown transformer having an output of 8 v and a delivery capacity up to 22,000 amp. The output of the transformer is controlled by a saturable core reactor. Power is transmitted to the furnace by 1000 MCM super flexible welding cables.

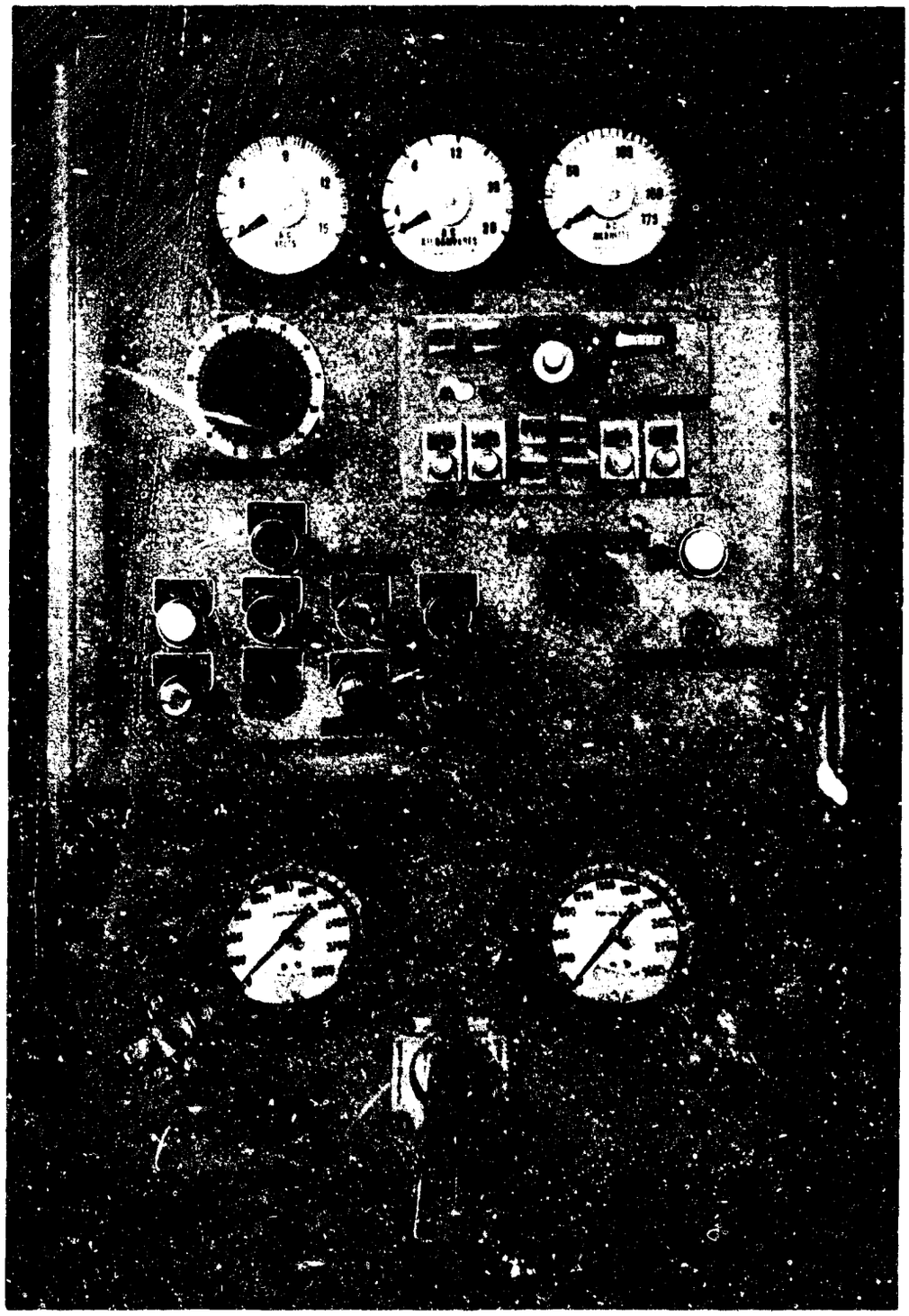

Figure 57. Close-up View of the Hot Press and Fusion-Casting Furnace Control Panel

III, B, Task 2--Development of Tantalum-Carbide-Lined Tantalum Carbide/Carbon Hypereutectic Composite (cont.)

b. Casting Procedure

The fusion and drop casting technique is performed in the following manner:

(1) Tantalum monocarbide powder is blended with graphite powder to the exact composition desired and hot-pressed to form a dense cylindrical compact in order to minimize the size of the melting crucible.

(2) The compact is inserted into a graphite crucible-mold-die which is direct resistance heated. A step in the inner diameter separates the crucible section from the mold cavity and retains the compact until melting occurs.

(3) The compact is uniformly heated to a temperature below the liquidus with the heating rate programmed to prevent overshooting of the desired temperature. As the compact is melted, the melt is gravity fed into the mold cavity below which it is then cooled at a controlled rate to produce graphite flakes of the desired shape, size, and distribution.

(4) After casting, the hypereutectic sample is removed by splitting the die.

c. Casting Development

(1) Temperature

The most critical processing parameter is the temperature of the melt. The temperature must approach but not exceed the liquidus temperature in the hypereutectic region. This region, as shown in

III, B, Task 2--Development of Tantalum-Carbide-Lined Tantalum Carbide/Carbon Hypereutectic Composite (cont.)

the tantalum-carbon phase diagram developed by Rudy and Harmon, Figure 58 (Reference 2), locates the eutectic temperature at 3445 ± 5°C. The liquidus temperature is approximate and is depicted by the dotted lines. Above the liquidus temperature, the melt will dissolve carbon from the graphite crucible, causing deviation from the required composition. At temperatures far below the liquidus, undissolved carbon will appear in the structure. In addition, insufficient temperature above the eutectic results in improper flow and too rapid solidification of the melt.

(2) Time at Temperature

The time required to equilibrate the carbide-graphite compact in the melting region of the graphite casting mold is dependent upon the temperature gradient that develops along the length of the graphite mold and the mass of the hypereutectic compact. It is imperative that the run be terminated once melting is completed to minimize reaction of the cast billet with the graphite mold.

(3) Graphite Casting Mold Design

Initial scale-up of the fusion casting of the TaC-C hypereutectic compositions required designing a mold capable of melting and casting billets 1.5 in. dia by 3.0 in. long. In establishing the mold design, the following criteria were satisfied:

(a) Provide sufficient total resistance to achieve and maintain temperatures from 3300 to 3600°C.

(b) Maintain a uniform temperature along the length of the melting cavity to assure uniform melting of the compact.

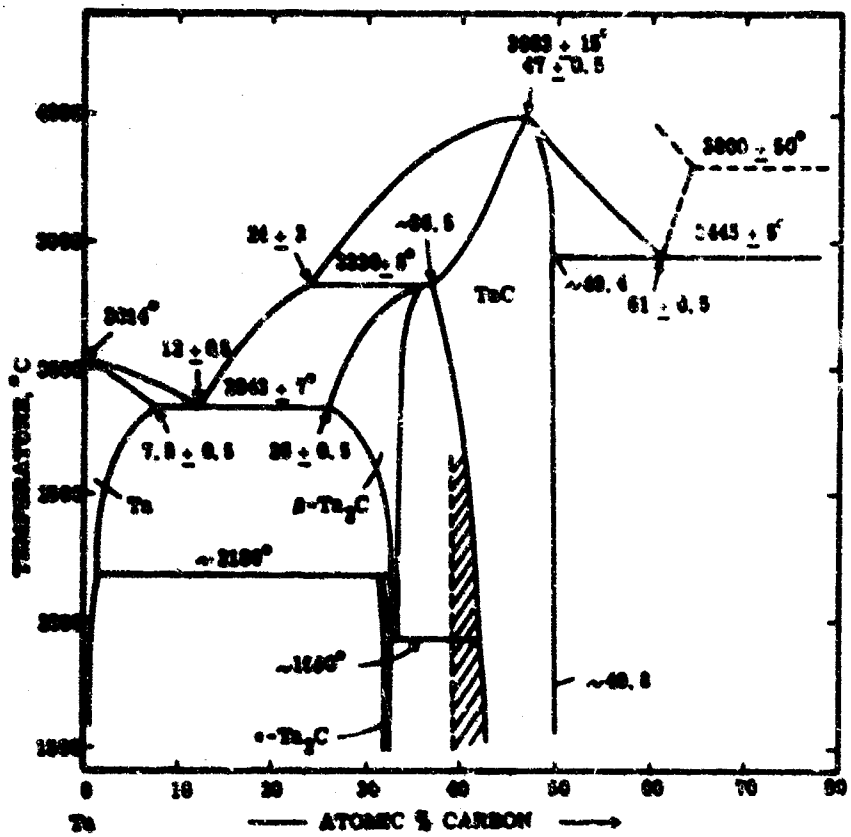

Figure 58. Phase Diagram, Tantalum-Carbon

III, B, Task 2--Development of Tantalum-Carbide-Lined Tantalum Carbide/Carbon Hypereutectic Composite (cont.)

(c) Develop a rapid quench of the melting in the casting cavity below the melting cavity.

(d) Provide an adequate wall thickness to account for graphite sublimation and to contain the melt.

(4) Castings 1.5 in. dia by 3.0 in. long

The appearance of a typical as-cast 1.5-in.-dia by 3.0-in.-long billet is shown in Figure 59a. The bottom of the billet, contained some "cold shut" extending approximately 0.5 in. Good temperature control minimized carbon pickup from the die and no reduction in the OD of the billet was necessary. The material on the top of the billet near the melting cavity increases in carbon content since the melt is hotter and more favorable for reacting with the graphite die. After cropping both ends, billets approximately 2.5 in. long, solid and defect free, as shown by the cross-sectional view in Figure 59b, were obtained. A total of 25 billets of this size were cast from the following compositions.

TaC, v/o	C, v/o	C, at%*	C, wt%**
80	20	62.2	3.873
70	30	67.9	6.461
60	40	73.2	9.702
50	50	78.2	13.879

*The balance being Ta.
**The balance being TaC.

The material required for the ambient and elevated temperature property characterizations and HES nozzle inserts for thermal shock and corrosion tests were obtained from these billets. This size billet can be cast with approximately 90% probability that a solid, usable billet will be attained.

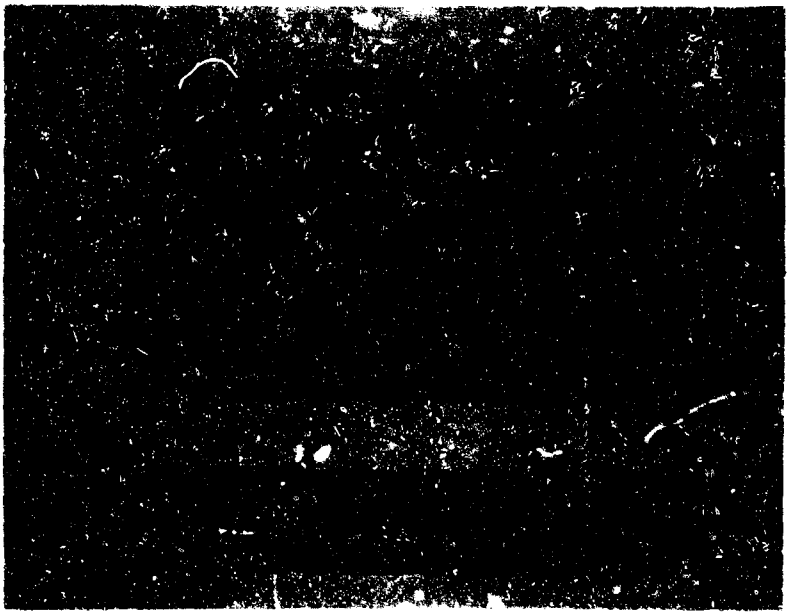

b. Cross-sectional view of billet

End Near Melting Cavity →

← End Cast First

a. As-cast Appearance, weight 1000 gm

Figure 59. [illegible] Billet of TaC-C Hypereutectic Composite

III, B, Task 2—Development of Tantalum-Carbide-Lined Tantalum Carbide/Carbon Hypereutectic Composite (cont.)

(5) Scale-Up to 4.2-in.-dia by 3.0-in.-long Castings

Scale-up to produce 4.2-in.-dia by 3.0-in.-long billets was accomplished in a graphite mold designed to satisfy the same criteria established for casting the 1.5-in.-dia billets. The mold design that evolved after taking these criteria into consideration was found to be very similar in configuration to the mold design used for casting the 1.5-in.-dia billets except a center tube was incorporated in the casting cavity to provide a hollow casting and to minimize ID machining of nozzle inserts.

The first trial casting was made with an 80 v/o TaC-20 v/o C compact weighing 2500 gm. A 4.2-in.-OD by 2-in.-ID by 1.2-in.-high billet was cast. Evidence of "cold shut" as shown in Figure 60 was found midway through the thickness of the billet. The melting temperature was increased and a successful casting was made as shown in Figure 61. Figure 62 shows a section view taken at the center of the billet. The grain structure is small and uniform throughout the wall thickness and there is no evidence of porosity.

Melting of compacts weighing 5000 gm was required to obtain the nozzle inserts. The as-cast appearance of a 5000-gm billet is shown in Figure 63. This 4.2-in.-OD by 2.0-in.-ID by 2.25-in.-high billet showed no evidence of "cold shut" or piping and minimal reaction with the graphite mold. However, melt leaked into the inner cavity of the graphite center tube during casting, leaving a cavity in the billet.

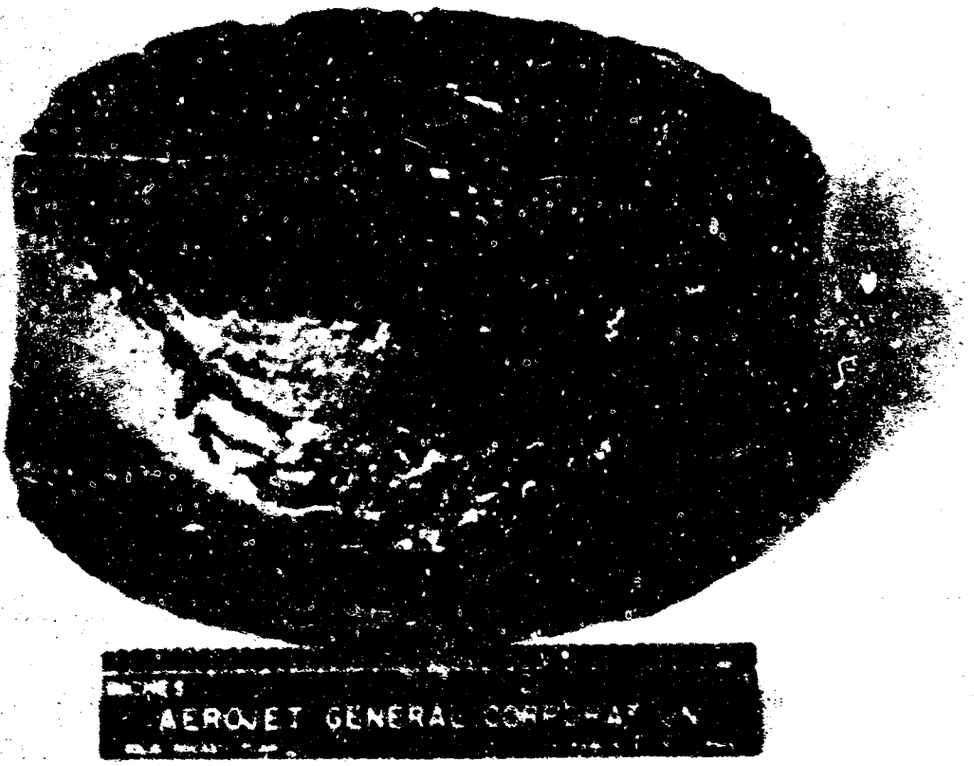

Figure 60. First Trial Casting of 4.2-in.-dia TaC-C Billet

b. Close-up Appearance of billet "as removed" from mold

a. Appearance "as removed" from mold

Figure 61. Current Trial Casting of Polyimide Carbon Billet

Figure 62. Sectional View of Second 4.2-in.-dia TaC-C Billet

Figure 63. As-Cast Appearance of 5000 gm, 4.2-in.-dia, TaC-C Billet

III, B, Task 2--Development of Tantalum-Carbide-Lined Tantalum Carbide/Carbon Hypereutectic Composite (cont.)

2. Material Properties Characterization for Hypereutectic Composites

a. Flexure Strength

Testing was accomplished on 0.25-in. by 0.25-in. by 2.0-in. specimens using three-point loading on a 1.5-in. span. A crosshead travel rate of 0.02 in./minute was used for all tests up to 1100°C. Above this temperature, a rate of 0.2 in./minute was used. Preparation of the specimens was the same as previously described for the microcomposite compositions. Tests were made at ambient, 540, 1100, 1650, 2000, and 2200°C.

The test results are reported in Table XII. The composition is reported as the volume percent (v/o) of graphite flake (the carbon in excess of the eutectic) for ease in correlation with microstructures. The eutectic composition is 61 ± 0.5 at% carbon (Figure 58). Expressing the eutectic in v/o TaC (containing ~49.4 at% carbon) and v/o carbon gives an 81 to 19% mixture, respectively. Figure 64 is a plot of volume percent of carbon and graphite flake versus atomic percent carbon. The composition of each sample was calculated from density measurements. A carbon analysis at the fracture surface was also determined on each specimen after testing. These analyses of the specimen at the fracture surface did not appear representative, probably because of the small amount of material used which was not representative of the carbon content in the sample. When a larger sample was removed from the specimen, a correlation was found between the carbon content derived by analysis and calculated from density measurements. Therefore, carbon compositions were derived by density measurements since this is the most economical measurement.

TABLE XII

PHYSICAL PROPERTIES OF TaC-C HYPEREUTECTIC COMPOSITIONS WITH VARYING CARBON CONTENTS

Temperature, °C	Specimen Number	Graphite Flake Content,* v/o	Flexural Strength, psi	Modulus of Elasticity,** 10^6 psi
Ambient	447A	8	17,650	38.2
	441B	9	14,810	31.5
	443A	8	14,540	33.0
	439E	12	6,310	20.0
	446C	15	6,090	20.6
	446A	15	5,640	24.8
	441C	9	5,190	30.9
	446B	15	4,610	25.1
	438B	15	4,150	17.8
	438C	18	3,970	13.2
	438A	11	3,260	28.0
	446D	17	2,860	22.8
	443F	20	2,120	14.3
	443D	19	1,480	13.5
	443B	17	820	13.1
540	451C	8	27,260	
	451E	9	9,400	
	451F	10	20,250	35.2
	460E	9	2,330	30.3
	460G	9	6,810	
1100	437A	9	7,940	
	437C	9	5,100	
	452A	9	6,370	
	460F	9	7,570	
	462A	11	2,040	
	462D	10	14,850	29.4
	463G	11	7,170	
1650	446E	14	14,240	24.7
	446F	12	26,190	
	462B	13	12,730	
	462I	10	14,020	
2000	443G	20	4,460	16.7
	461A	19	8,450	
2200	437A	9	16,130	
	443G	22	4,470	
	437E	10	16,140	
	443H	22	8,930	
	450A	13	14,163	
	462C	4	33,150	

*On the basis of density measurements.
**All moduli taken at ambient temperature.

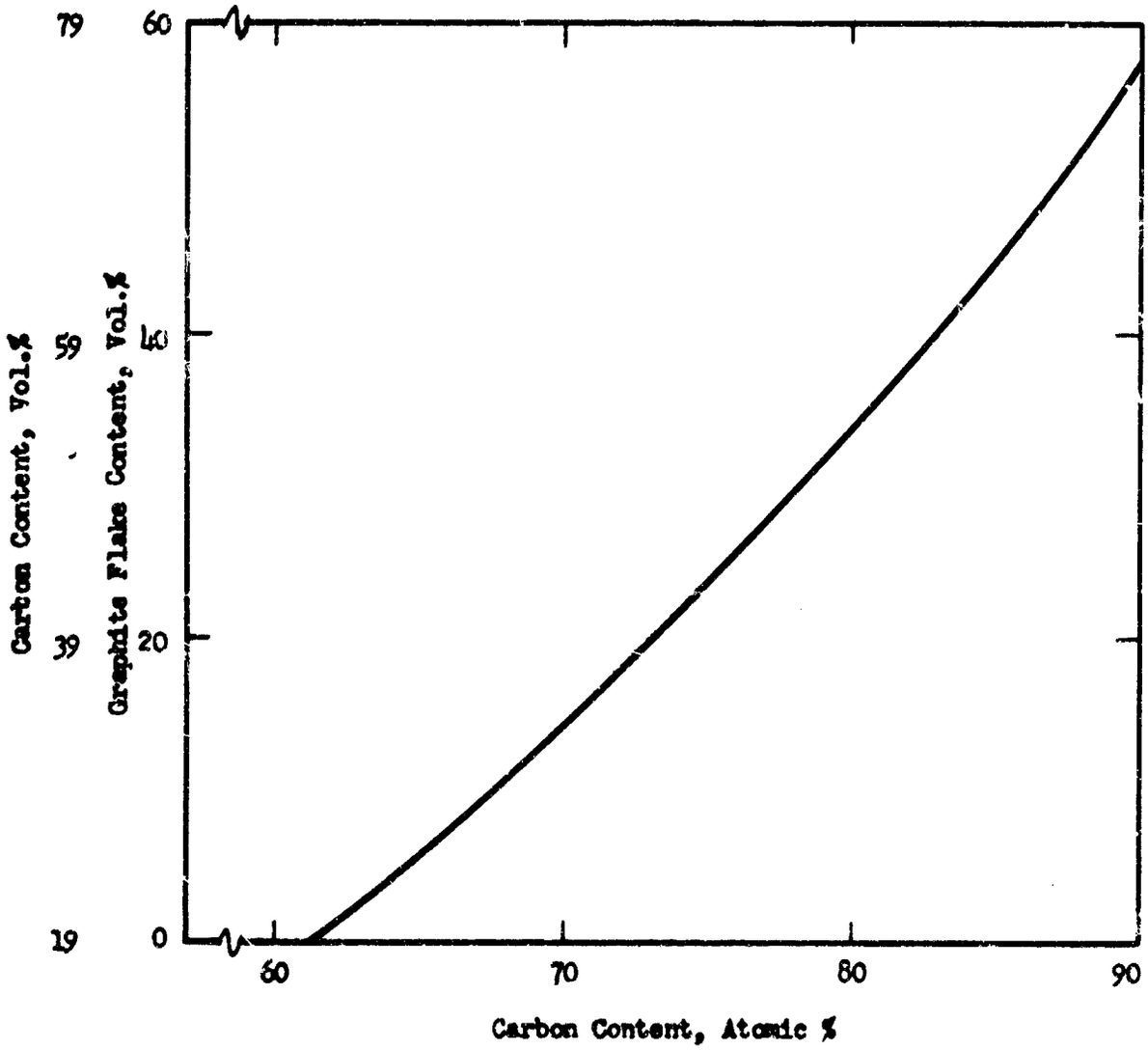

Figure 64. Correlation of Volume Percent Carbon and Graphite Flake with Atomic Percent Carbon for TaC-C Hypereutectic

III, B, Task 2--Development of Tantalum-Carbide-Lined Tantalum Carbide/Carbon Hypereutectic Composite (cont.)

A plot of ambient temperature strength data versus carbon content is shown in Figure 65. Ambient temperature specimens containing a low graphite flake content (8 to 9 v/o C) normally had high strengths, from 14,540 to 17,650 psi. The compositions containing high flake contents (19 to 20 v/o C) had low strengths in the range of 1480 to 2120 psi. Widespread differences in strength at the same compositions were found which led to evaluation of the microstructure of each specimen at the fracture surfaces to determine structural differences.

Specimen No. 451c, tested at 540°C, had a high flexure strength, 27,260 psi. The microstructure of this specimen shown in Figure 66a consisted of short, thin, and very evenly dispersed graphite flakes in the eutectic matrix. Specimen No. 460e had low strength, 2330 psi, and a microstructure with graphite flakes that were long, coarse, and randomly dispersed as shown in Figure 56b. The microstructural appearance of specimen No. 460g, which had an intermediate strength, 6810 psi, is shown in Figure 67a. The graphite flakes in this specimen are intermediate in size and distribution in comparison to flakes in those specimens (460e and 451c) having low and high strengths. Specimen No. 451e, with a strength of 9400 psi, had a microstructure (Figure 67b) which more closely resembles the microstructure characteristic of the high strength composite, specimen No. 451c. However, the light areas around the graphite flakes can be described as "divorced carbide." These areas were formed during solidification of the melt whereby graphite from the eutectic tends to diffuse to the graphite flake areas leaving single-phase tantalum carbide regions surrounding the primary graphite.

The specimens tested at 1100°C had fairly uniform strengths in the range of 6000 to 8000 psi. The microstructures of these specimens at the fracture surfaces were very similar in appearance to the microstructure of specimen No. 460f which is shown in Figure 68a. Specimen

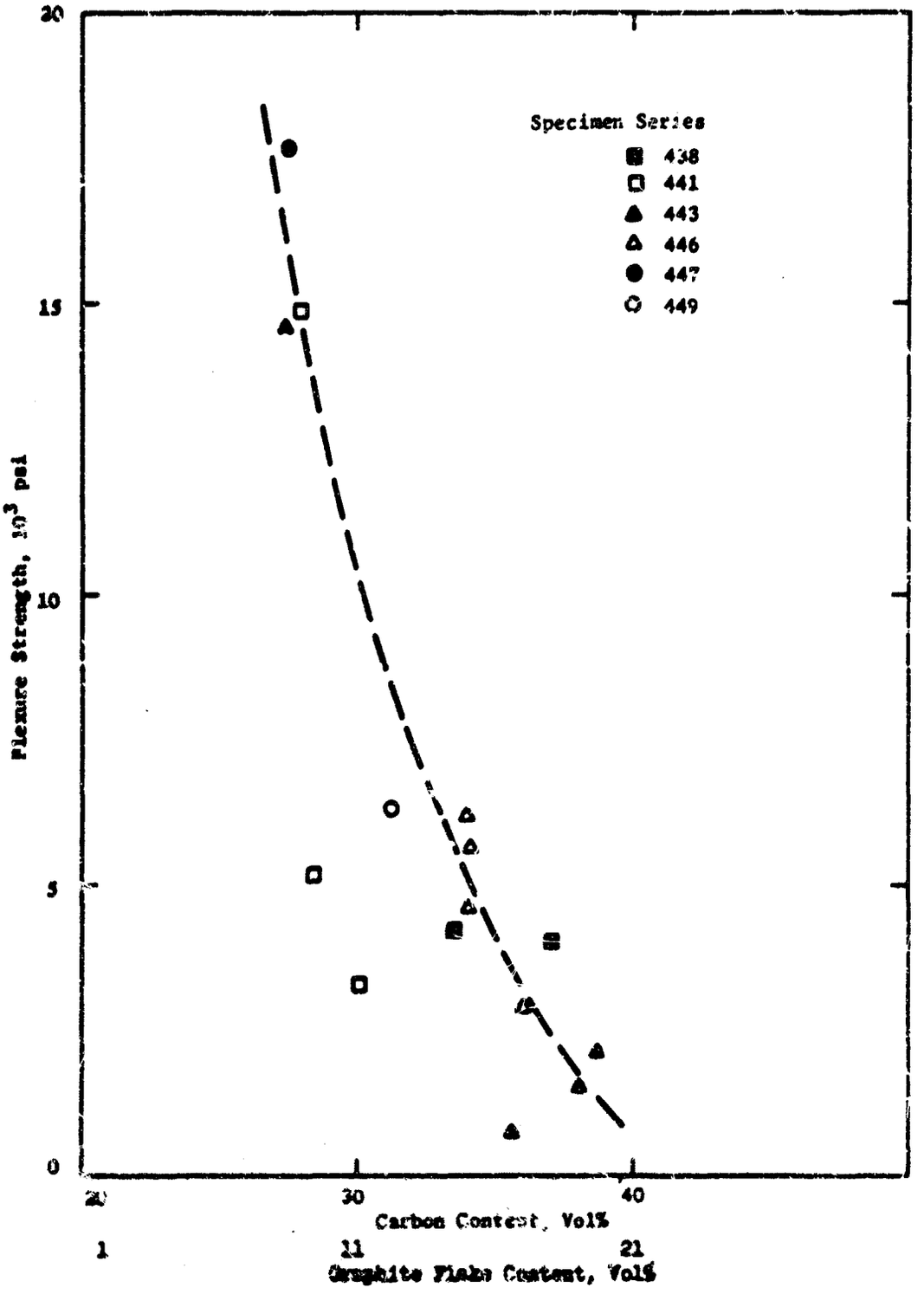

Figure 65. Ambient Temperature Flexural Strength of Various TaC-C Hypereutectic Compositions

50X

a. Specimen No. 451C, Composition: 8v/o Graphite Flake, Flexure Strength, 27,260 psi

50X

b. Specimen No. 460e, Composition: 9v/o Graphite Flake, Flexure Strength, 2330 psi

Figure 66. Microstructures of Two TaC-C Hypereutectic Specimens Having Low and High Strengths at 540°C

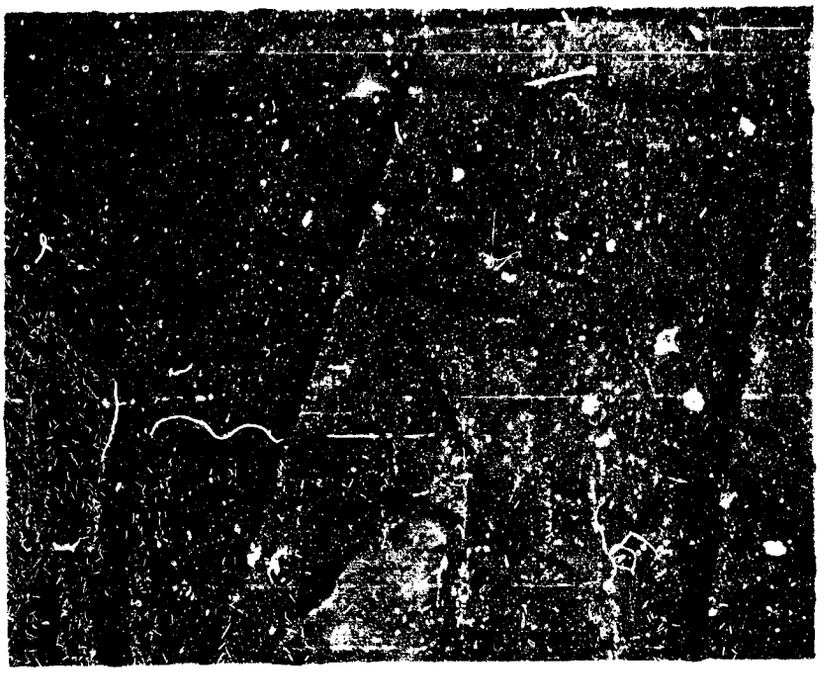

50X

a. Specimen No. 460g, Composition: 9v/o Graphite Flake, Flexure Strength, 6810 psi

50X

b. Sample No. 451e, Composition: 9v/o Graphite Flake, Flexure Strength, 9600 psi

Figure 67. Microstructural Comparisons of TaC-C Hypereutectic Composites Exhibiting Intermediate Strengths at 540°C

50X

a. Specimen No. 460F, Composition: 9v/o Graphite Flake, Flexure Strength, 7570 psi

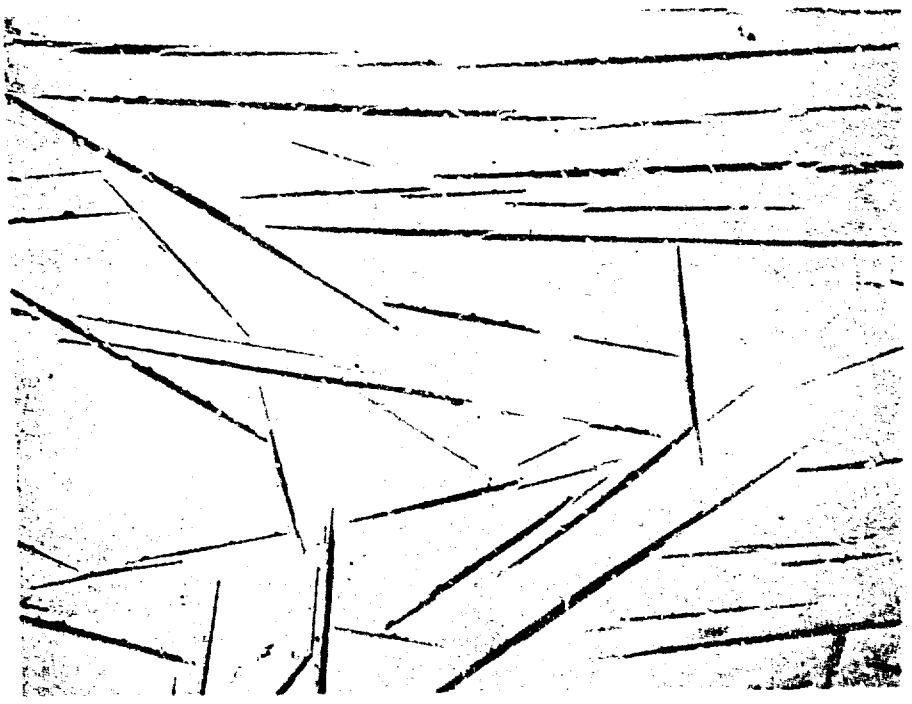

50X

b. Specimen No. 462a, Composition: 11v/o Graphite Flake, Flexure Strength 2040 psi

Figure 68. Microstructural Comparisons of TaC-C Hypereutectic Composites Tested at 1100°C

III, B, Task 2--Development of Tantalum-Carbide-Lined Tantalum Carbide/Carbon Hypereutectic Composite (cont.)

No. 462a had the lowest strength, 2040 psi, of the specimens tested in this series. The microstructure of this specimen shown in Figure 68b had a high concentration of long, randomly dispersed, graphite flakes in the region of fracture.

The specimens tested at 1650°C underwent noticeable plastic deformation. Strengths at this point become apparent values since the flexure formula is not valid. The specimens were capable of sustaining loads over a longer period of time than the microcomposite or other carbide composites previously tested. At this test temperature and at the lower temperatures, the hypereutectic composites exhibited outstanding resistance to crack propagation. The graphite flakes readily dissipate crack energies. A "stair-step" crack pattern occurs across the thickness of the specimens as shown in Figure 69. Figure 70a shows the microstructure of specimen No. 446f which had the highest strength at 1650°C, 26,190 psi. The flakes in this microstructure are relatively coarse because of higher carbon content; however, the length of the flakes was relatively short. Figure 70b shows the microstructure for specimen No. 462i, which had unusually short graphite flakes.

The specimens tested at 2200°C had considerable strength variation. The highest strength of 33,150 psi was obtained with specimen No. 462g which had a 4 v/o graphite flake. The microstructure of this specimen, Figure 71a, had relatively thin, short, evenly dispersed graphite flakes. The compositions having high carbon contents (12 v/o graphite) had extremely low strength. Figure 71b shows the heavy graphite flake distribution in specimen No. 443g which had the lowest flexure strength, 4470 psi.

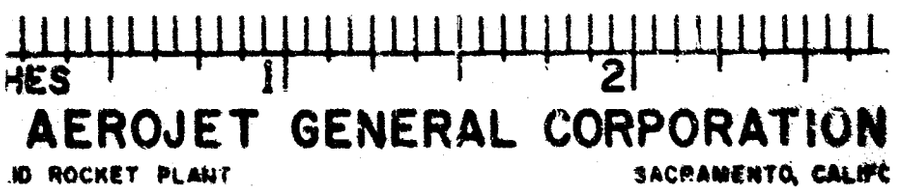

Figure 69. Fracture Pattern in TaC-C Hypereutectic Flexure Specimens

50X

a. Specimen No. 446f, Composition: 12v/o Graphite Flake, Flexure Strength, 26,190 psi

50X

b. Specimen No. 462k, Composition: 10v/o Graphite Flake, Flexure Strength, 14,020 psi

Figure 70. Microstructural Comparisons of TaC-C Hypereutectic Composites Tested at 1650°C

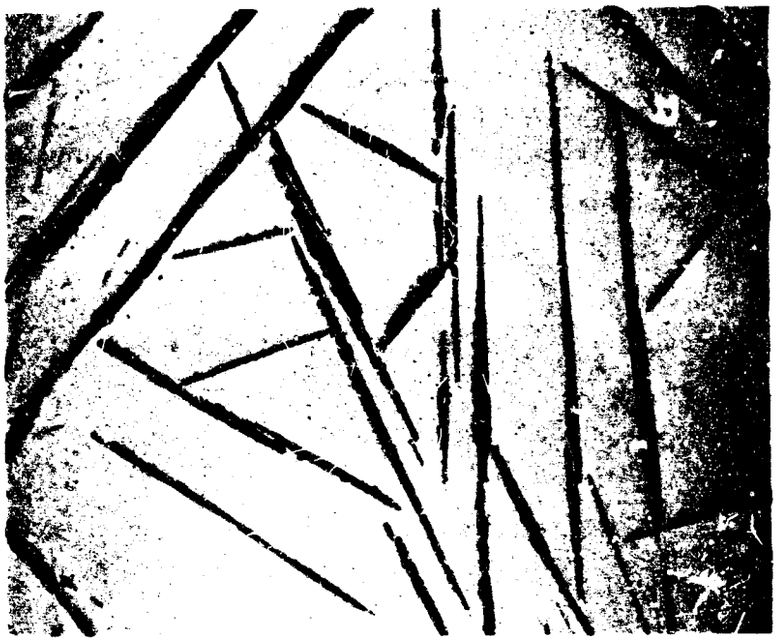

50X

a. Sample No. 462g, Composition: 4v/o Graphite Flake, Flexure Strength, 33,150 psi

50X

b. Sample No. 443g, Composition: 22v/o Graphite Flake, Flexure Strength, 4470 psi

Figure 71. Microstructural Comparisons of TaC-C Hypereutectic Compositions Tested at 2200°C

III, B, Task 2--Development of Tantalum-Carbide-Lined Tantalum Carbide/Carbon Hypereutectic Composite (cont.)

b. Modulus of Elasticity

Sonic modulus of elasticity measurements were made at ambient temperature on flexure specimens prior to flexure testing. The sonic modulus data are presented in Table XII. The correlation between the modulus of elasticity and carbon content is shown in Figure 72. Specimens with graphite contents of 9 to 11 v/o had moduli of approximately 30 x 10^6 psi. The modulus of elasticity decreased significantly with increasing carbon contents to a level of approximately 13 x 10^6 psi for compositions with 18 to 19 v/o graphite.

c. Thermal Expansion

Two hypereutectic compositions representative of the low and high carbon contents, 9 v/o and 16 v/o graphite flake, were selected for linear expansion measurements from 25 to 2172°C. These specimens were tested using the procedures and equipment previously described for thermal expansion measurements on the microcomposite. The test results are presented in Table XIII. In section b of both tables, the thermal expansion data have been expressed in terms of total thermal expansion, in./in. x 10^{-3}, and as a thermal expansion coefficient, in./in./°C x 10^{-6}.

A plot of the thermal expansion data for the two compositions as a function of temperature is shown in Figure 73. For comparative purposes, thermal expansion data for stoichiometric TaC as reported in the literature (Reference 7) and calculated from X-ray diffraction "d" spacings have been included in the figure. A comparison of the expansion curves shows that both compositions closely follow the expansion behavior of tantalum monocarbide. The 16 v/o graphite composition had a slightly higher expansion. Whether this difference can be attributed to differences in carbon content would require further investigation.

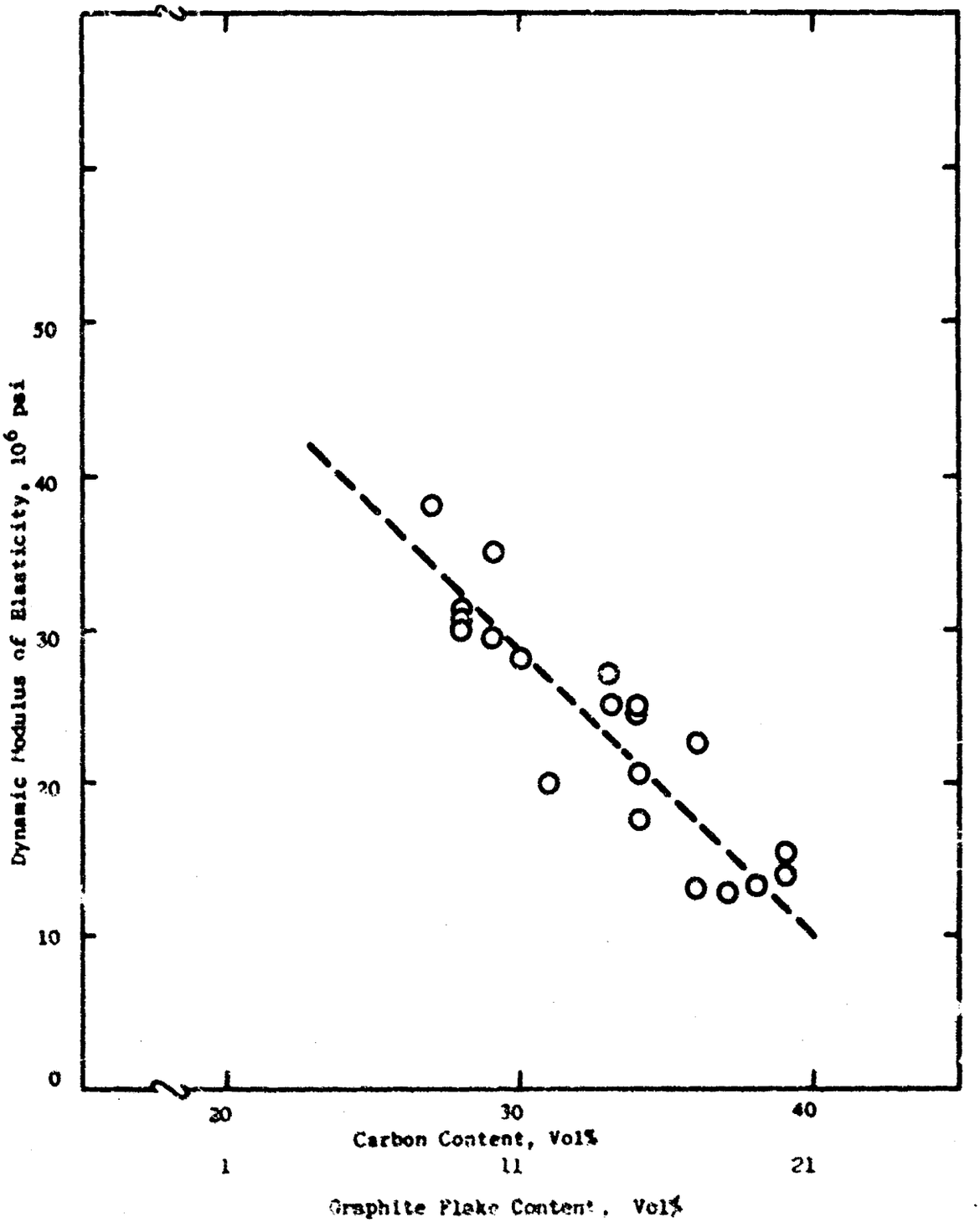

Figure 71. Relationship of Modulus of Elasticity and Graphite Flake and Carbon Content for Various TaC-C Hypereutectic Compositions

TABLE XIII

LINEAR THERMAL EXPANSION MEASUREMENTS FOR TaC-C HYPEREUTECTIC COMPOSITIONS

Composition: 16 v/o Graphite Flake

a. Corrected Measured Data

Specimen Temperature, °C	Specimen Expansion, in.	Thermal Expansion, in./in. x 10^{-3}	Percent Deviation from Least Squares Fit
783	0.01016	5.84	3.92
1024	0.01291	7.42	0.22
1225	0.01542	8.86	1.11
1420	0.01799	10.34	1.10
1626	0.01957	11.25	6.62
1839	0.02390	13.73	0.29
2115	0.02892	16.62	4.85

b. Least-Square-Fit of Data

Temperature, °C	Thermal Expansion, in./in. x 10^{-3}	Thermal Expansion Temperature Coefficient, in./in./°C x 10^{-6}
500	3.50	7.00
1000	7.25	7.25
1500	11.07	7.38
2000	14.95	7.47
2500	18.89	7.55
3000	22.90	7.63

TABLE XIII (cont.)

Composition: 9 v/o Graphite Flake

a. Corrected Measured Data

Specimen Temperature, °C	Specimen Expansion, in.	Thermal Expansion, in./in. x 10^{-3}	Percent Deviation from Least Squares Fit
737	0.00753	4.31	2.83
1081	0.01181	6.76	0.22
1253	0.01430	8.19	3.06
1460	0.01647	9.43	0.16
1684	0.01943	11.13	0.69
1873	0.02206	12.64	1.26
2172	0.02514	14.41	2.59

b. Least-Square-Fit of Data

Temperature, °C	Thermal Expansion in./in. x 10^{-3}	Thermal Expansion Temperature Coefficient, in./in./°C x 10^{-6}
500	2.91	5.82
1000	6.19	6.19
1500	9.71	6.47
2000	13.45	6.72
2500	17.42	6.96
3000	21.62	7.20

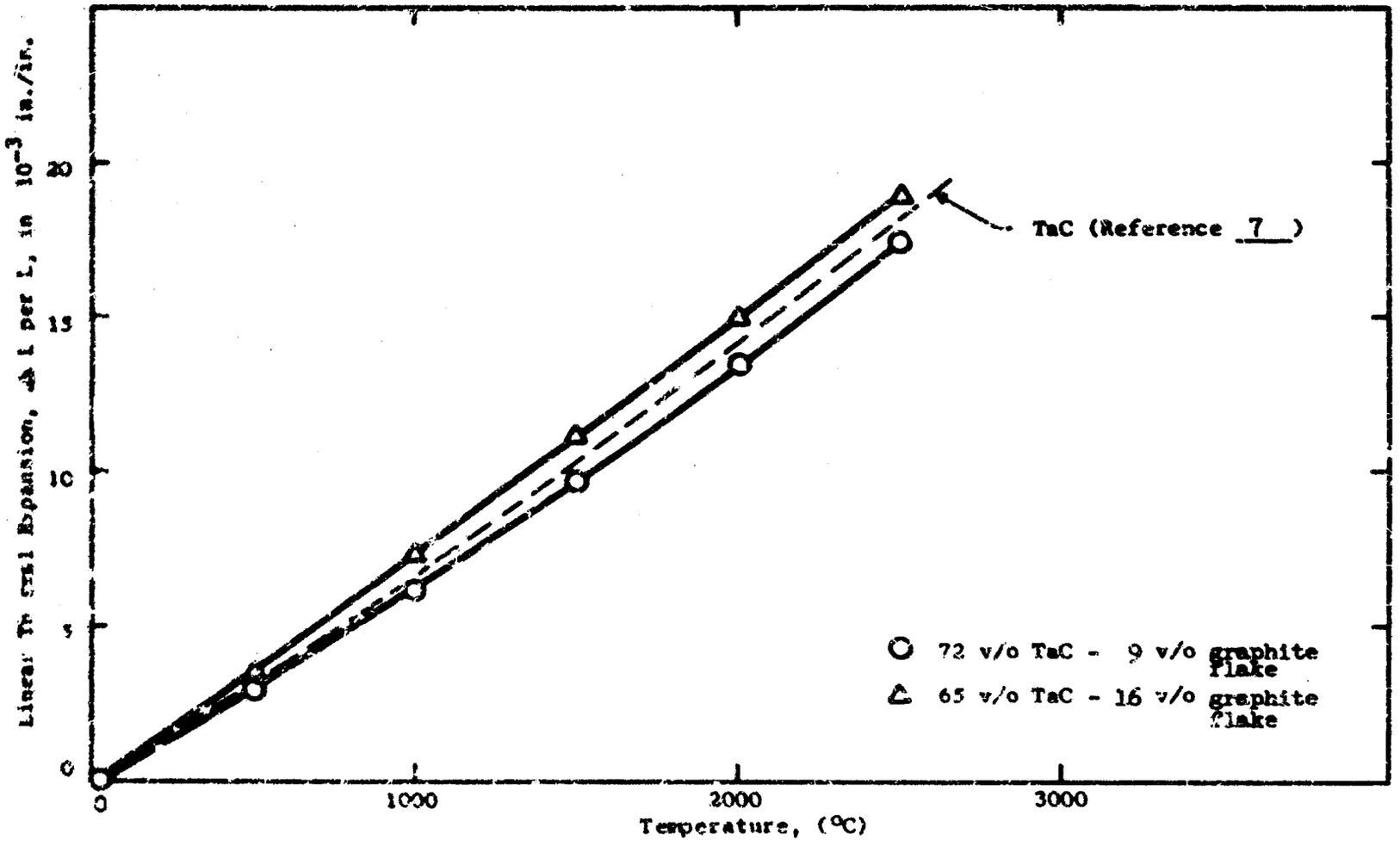

Figure 73. Elevated Temperature Linear Thermal Expansion of TaC-C Hypereutectic Compositions

III, B, Task 2--Development of Tantalum-Carbide-Lined Tantalum Carbide/Carbon Hypereutectic Composite (cont.)

Thermal expansion of the two compositions can be expressed by the following equation:

$$\alpha = A_1 (T-25) + A_2 (T-25)^2$$

where α = linear thermal expansion
T = temperature, °C

For Composition 9 v/o Graphite:
$A_1 = 5.90 \times 10^{-6}$ in./in./°C
$A_2 = 0.4562 \times 10^{-9}$ in./in./°C

For Composition 16 v/o Graphite:
$A_1 = 7.317 \times 10^{-6}$ in./in./°C
$A_2 = 0.1289 \times 10^{-9}$ in./in./°C

d. Thermal Diffusivity

The results of thermal diffusivity measurements on three TaC-C hypereutectic compositions is presented in Table XIV. The differences in data are considered to be typical of the scatter found in this determination. A comparison of these data with the literature (Reference 8) shows the data to be slightly lower than the reported value of 0.08 cm^2/sec for tantalum monocarbide.

3. Development of Diffusion Forming Technique for TaC Liner

Data published on the diffusion rates in the Ta-C binary system are limited. Diffusion coefficients for carbon in TaC between 1700 and 3700°C were determined by Resnick and Seigle (Reference 9). A value of 5.25×10^{-8} cm^2/sec was observed at 2600°C. Brizes (Reference 10) determined the diffusion coefficients of carbon in TaC between 2100 and 2650°C and reported a value of 2.22×10^{-7} cm^2/sec at 2400°C.

TABLE XIV

THERMAL DIFFUSIVITY MEASUREMENTS
ON TaC-C HYPEREUTECTIC COMPOSITES

Specimen No.	Composition v/o Graphite Fiber	Temperature, °C	Thermal Diffusivity, cm^2/sec
452 I	8	Ambient	0.059
		540	0.040
		775	0.048
		775	0.048
452 II	7	Ambient	0.055
		540	0.050
		775	0.054
459	8	Ambient	0.055
		540	0.046
		540	0.046
		775	0.035
		775	0.035

III, B, Task 2—Development of Tantalum-Carbide-Lined Tantalum Carbide/Carbon Hypereutectic Composite (cont.)

The diffusion coefficient of carbon in Ta metal was determined to be 6.58×10^{-5} cm^2/sec at 2600°C by Kalinovich, et al. (Reference 11). This value, along with those reported for carbon diffusion in TaC, indicates that the tantalum metal reaction with TaC-C hypereutectic should not proceed at a high enough rate to provide a TaC coating of suitable thickness. However, Reference 11 also showed that the diffusion coefficient, D, was linear dependent on temperature, log D = f (1/T), up to 1800°C and then showed a positive deviation from linear dependence up to 2600°C. Should this deviation continue above 2600°C, the diffusion rates could be adequate for providing a diffusion-formed TaC coating of suitable thickness. This deviation is attributed to an increasing activation energy, E, with temperature. The result is an increasing value for the diffusion coefficient with temperature.

a. Carbon Diffusion in Tantalum Metal

To establish whether a suitable TaC coating on a TaC-C hypereutectic substrate could be achieved, the process parameters of time and temperature were studied by reacting Ta metal with graphite. These data were considered to be of the same order of magnitude as those for Ta reacting with the TaC-C hypereutectic. Diffusion couples were made of Ta and carbon and annealed at temperature from 2600 to 3200°C.

The tantalum metal used in this investigation was 325 mesh powder of 99.99 + wt% purity. The chemical analysis of the powder is shown in Table I. The powder was packed in a 0.5-in.-dia hole drilled in an ATJ grade graphite block and placed in a graphite heater which in turn was inserted into the resistance furnace shown in Figure 56. The furnace was outgassed while being heated to 2000°C under vacuum, backfilled to 4 atm of helium, and then heated to the desired diffusion anneal temperature at 200°C/minute. The temperatures were measured with a Leeds and Northrup optical pyrometer on the graphite heater at a point 1 in. above the sample. After diffusion, the thicknesses of the carbide layers were measured on photomicrographs taken at 50 to 200X.

III, B, Task 2--Development of Tantalum-Carbide-Lined Tantalum Carbide/Carbon Hypereutectic Composite (cont.)

The carbide layer growth data, listed in Table XV, show the resulting Ta_2C and TaC layer thicknesses. A review of these data indicates that the TaC layer growth was minimal, <0.1 cm at 2600, 2850, and 3000°C, for all durations up to 23 minutes. In addition, a Ta_2C layer was formed. The phases present in the diffusion layer developed at 3100°C for 2 minutes are shown in a photomicrograph in Figure 74. A TaC layer 0.1 cm thick was formed at 3200°C in 10 minutes along with appreciable Ta_2C.

b. Tantalum Diffusion in TaC-C Hypereutectic

TaC liners were formed by reacting Ta metal with TaC-C hypereutectic substrates on the ID of 0.75-in.-OD by 0.20-in.-ID by 0.5-in.-long specimens. The process temperature was 3300°C and duration was 10 minutes. Although the temperature approached the melting temperature of the substrate (3443°C) and was therefore a difficult process, a 0.1-cm-thick coating as shown in Figure 75 was obtained. The undesirable Ta_2C layer formation was absent.

4. Task Summary

The results of this work are summarized as follows:

a. The ability of the fusion and drop casting process to melt and cast TaC-C billets up to 4.2 in. in diameter has been demonstrated.

b. Strength variations for a given composition at the same test temperature can be correlated with the morphology of the graphite flake. Flakes that are thin, short in length, and evenly dispersed are conducive to higher strengths for a given composition.

TABLE XV

SUMMARY OF DIFFUSION DATA FOR CARBON IN Ta AND TaC-C HYPEREUTECTIC

System	Diffusion Temperature, °C	Diffusion Time, min	W_{TaC} (cm)[1]	W_{Ta_2C}(cm)
Ta-C	2600	5	N.D.[2]	1.8×10^{-3}
	2850	1	3.8×10^{-3}	1.4×10^{-2}
	3000	1	1.9×10^{-2}	1.5×10^{-2}
	3000	2	2.4×10^{-2}	4.2×10^{-2}
	3000	5	3.2×10^{-2}	5.3×10^{-2}
	3000	10	4.3×10^{-2}	6.4×10^{-2}
	3000	23	8.9×10^{-2}	8.8×10^{-2}
	3100	2	2.6×10^{-2}	---
	3200	1	2.1×10^{-2}	2.8×10^{-2}
	3200	3	6.0×10^{-2}	---
	3200	10	1.1×10^{-1}	---
(TaC-C)-Ta	3300	10	1.1×10^{-1}	nil

1. W = Width of carbide layer
2. Not detectable

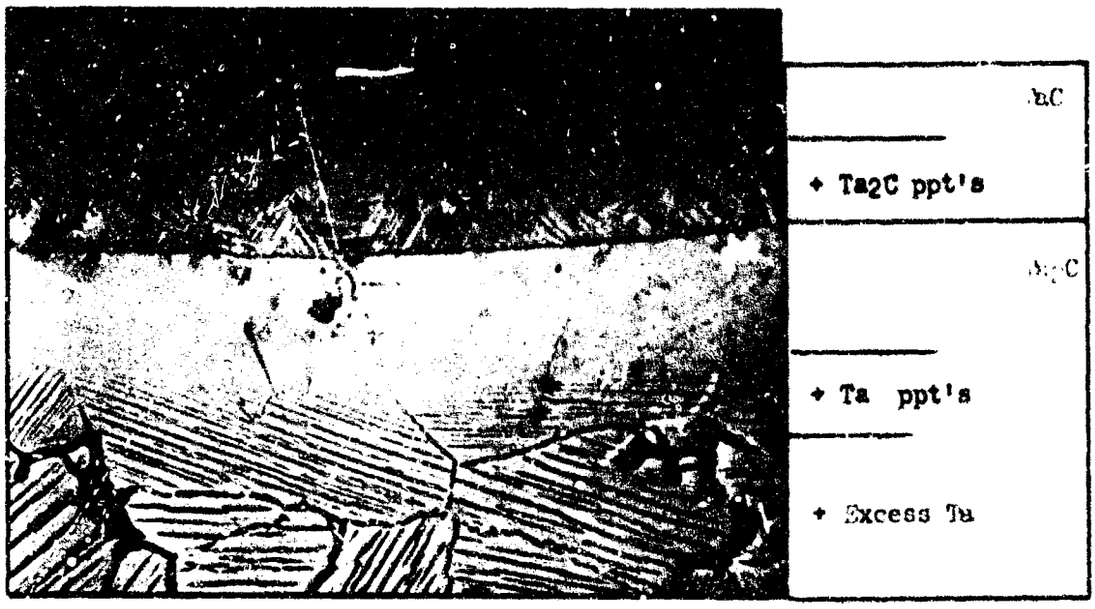

100X Unetched

Figure 74. Typical Diffusion Zone of Ta-C Sample-3100°C for 2 minutes

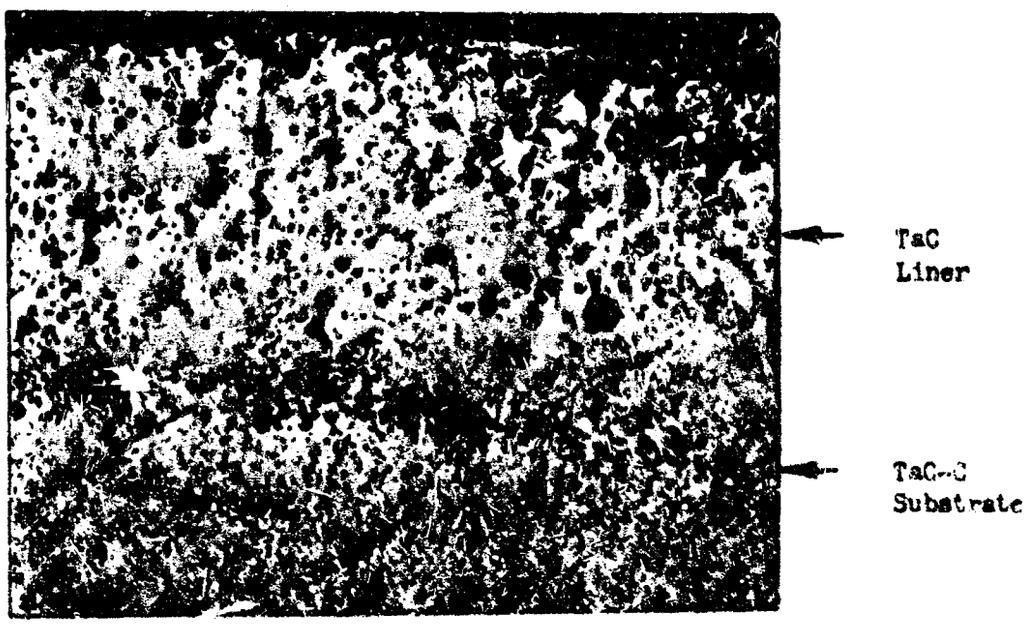

50X Unetched

Figure 75. Typical Diffusion Formed TaC Liner on TaC-C Hypereutectic Substrate

III, B, Task 2—Development of Tantalum-Carbide-Lined Tantalum Carbide/Carbon Hypereutectic Composite (cont.)

c. The strength and modulus at ambient temperature decreased significantly with increasing carbon content. This same conclusion regarding elevated temperature strength data is not readily apparent because of the limited number of tests.

d. The thermal expansion characteristics closely followed the expansion behavior for tantalum monocarbide.

e. The thermal diffusivity data were slightly lower than the reported data for tantalum monocarbides.

f. A diffusion process for forming a TaC liner on a TaC-C hypereutectic substrate was successfully demonstrated.

C. TASK 3—THERMAL SHOCK RESISTANCE EVALUATIONS

The objective of this task was to determine the thermal shock resistance of the microcomposite and TaC-C hypereutectic compositions and from this thermal shock resistance establish their suitability for high-temperature, solid propellant nozzle applications. Two microcomposite compositions, 8Ta-55Hf-37C and 8Ta-54Hf-38C, and TaC-C hypereutectic compositions, with variations in graphite flake contents from 7 to 20 v/o, were evaluated.

1. Experimental Setup in Hyperthermal Environmental Simulator

The Hyperthermal Environmental Simulator (HES), shown in Figure 76, was used for the thermal shock testing. The HES is a high-pressure, 1-megawatt plasma generator facility, developed for material studies in which controlled rocket motor combustion environments and thermal stress conditions can be simulated. The HES system can be operated at pressures up to 500 psig,

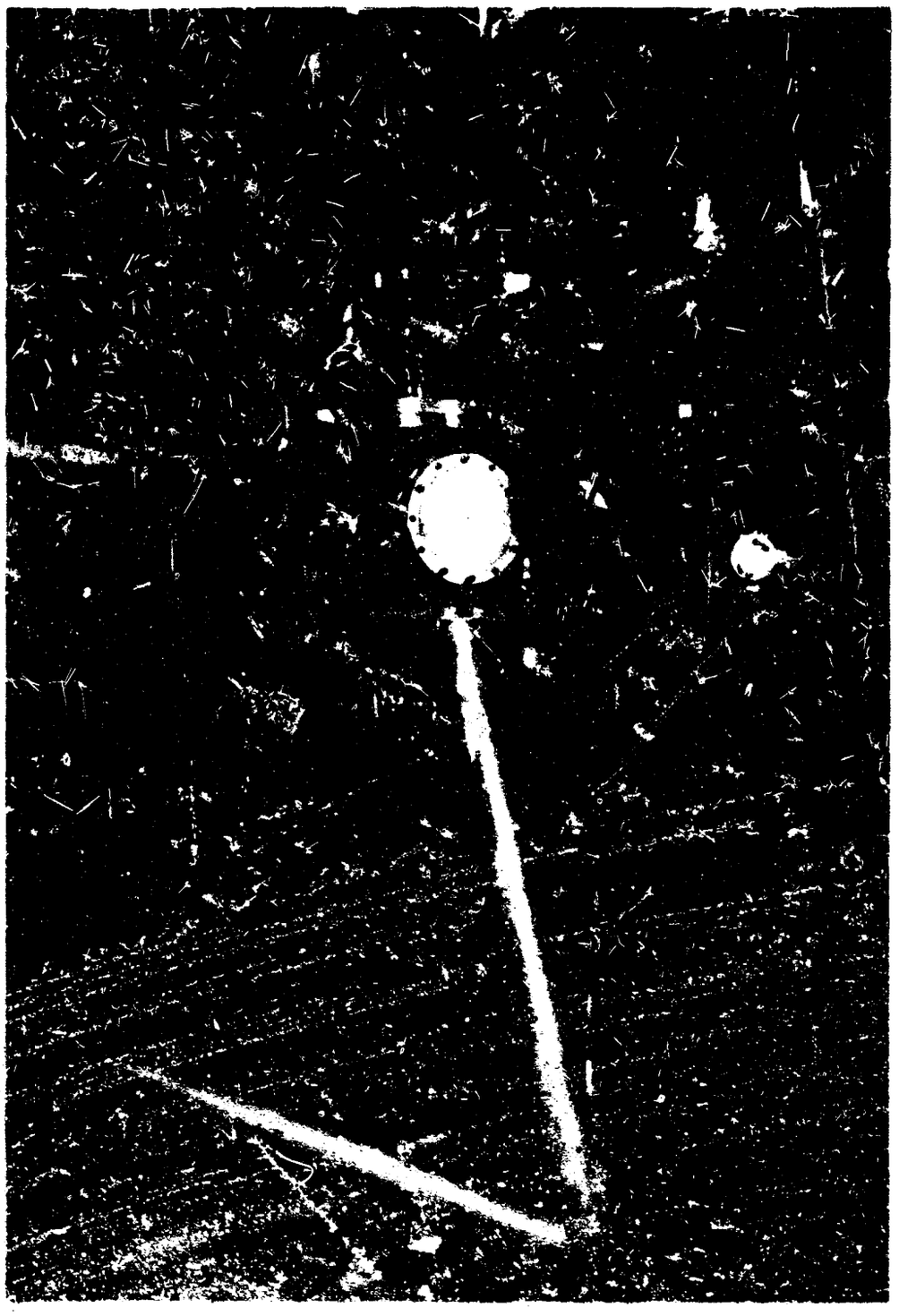

Figure 74. HRS Plasma Generator and Test Chamber

III, C, Task 3—Thermal Shock Resistance Evaluations (cont.)

at gas temperatures to 10,000°F, and at flow rates between 1 and 20 lb/minute, depending on the gas composition and enthalpy required. At maximum power, in excess of 1.2 megawatts, the system is capable of being operated for durations up to 5 minutes. The unit can be operated with nitrogen, nitrogen-hydrogen mixtures, and simulated propellant combustion mixtures including carbon dioxide, carbon monoxide, hydrogen, hydrogen chlorine, nitrogen, oxygen, and water. To duplicate the thermal shock environment of a rocket engine, initial heat flux to the sample must be high. The test procedure for HES thermal shock tests is to start N_2 gas flow at full flow rate and then to start the arc at the full power level. The resulting start transient is similar to a rocket motor start transient.

The candidate composite bodies selected for thermal shock verification were prepared as small, tubular specimens with an ID of 0.20 in., OD of 0.75 in., and a length of 0.75 in. for the microcomposites and 0.5 in. for the hypereutectic composites. Each composite specimen was press-fitted into an ATJ graphite backup. The insert/graphite assembly was pressed into a cylindrical silver-infiltrated tungsten holder. The use of a holder possessing a high strength and a high modulus of elasticity was found to be required to prevent the graphite backup from cracking during firing due to the higher expansion of the carbide insert.

The arrangement of the specimen in the graphite backup after attachment to the HES nozzle is shown schematically in Figure 77. The overall schematic arrangement of the HES test setup is shown in Figure 78. As shown, the specimen was attached to the nozzle of the HES unit and thermal shock testing was accomplished by passing the hot plasma consisting of a nitrogen/helium gas mixture through the specimen. A 7.5 wt% addition of helium was added to the nitrogen plasma stream to increase the heat flux to the required minimum level of 2800 Btu/ft^2/sec. Cold-wall heat fluxes developed during the duration of the test were measured by the copper calorimeter affixed at the exit end of the specimen.

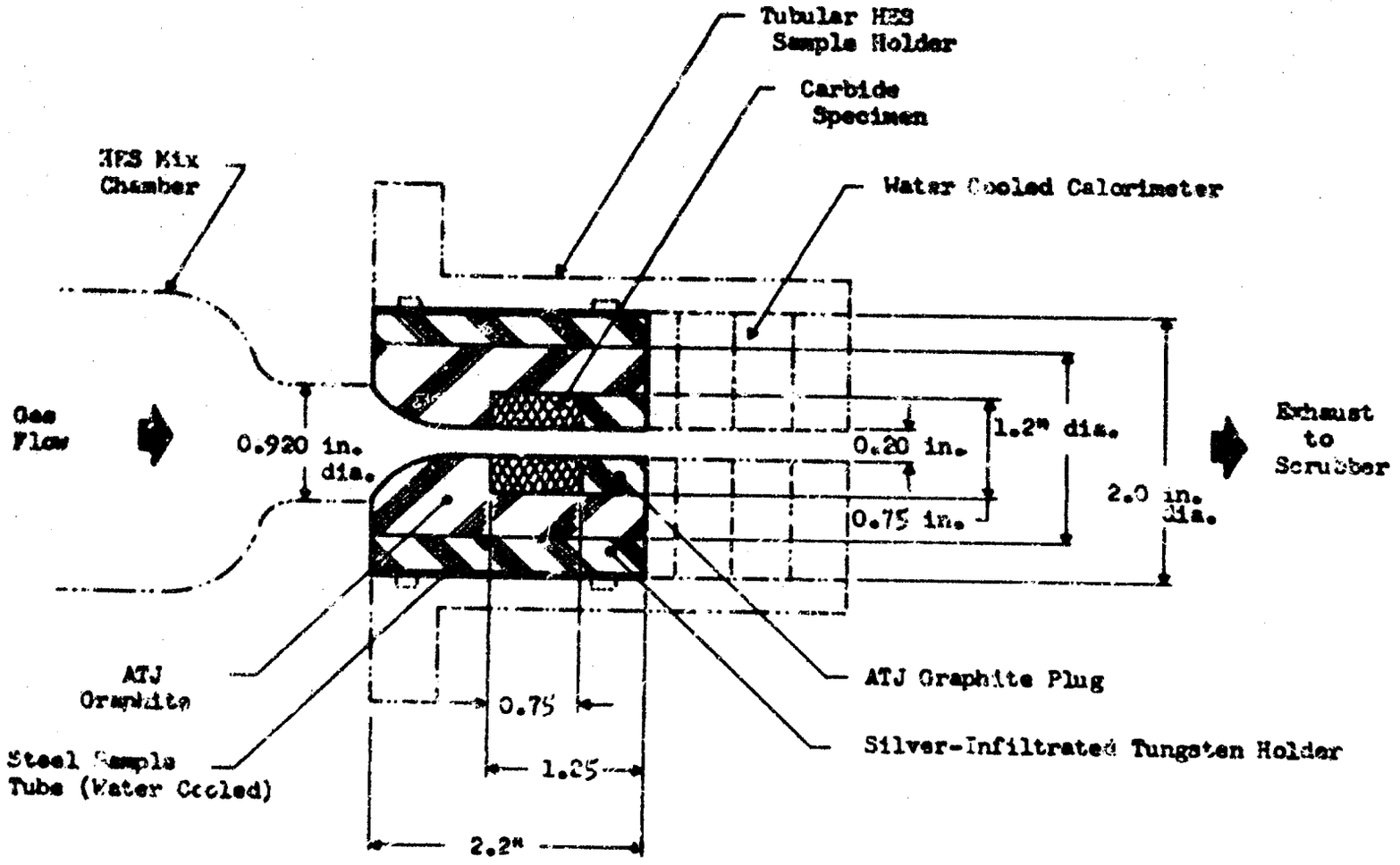

Figure 77. Schematic Showing Attachment of Test Specimen to H&S Nozzle

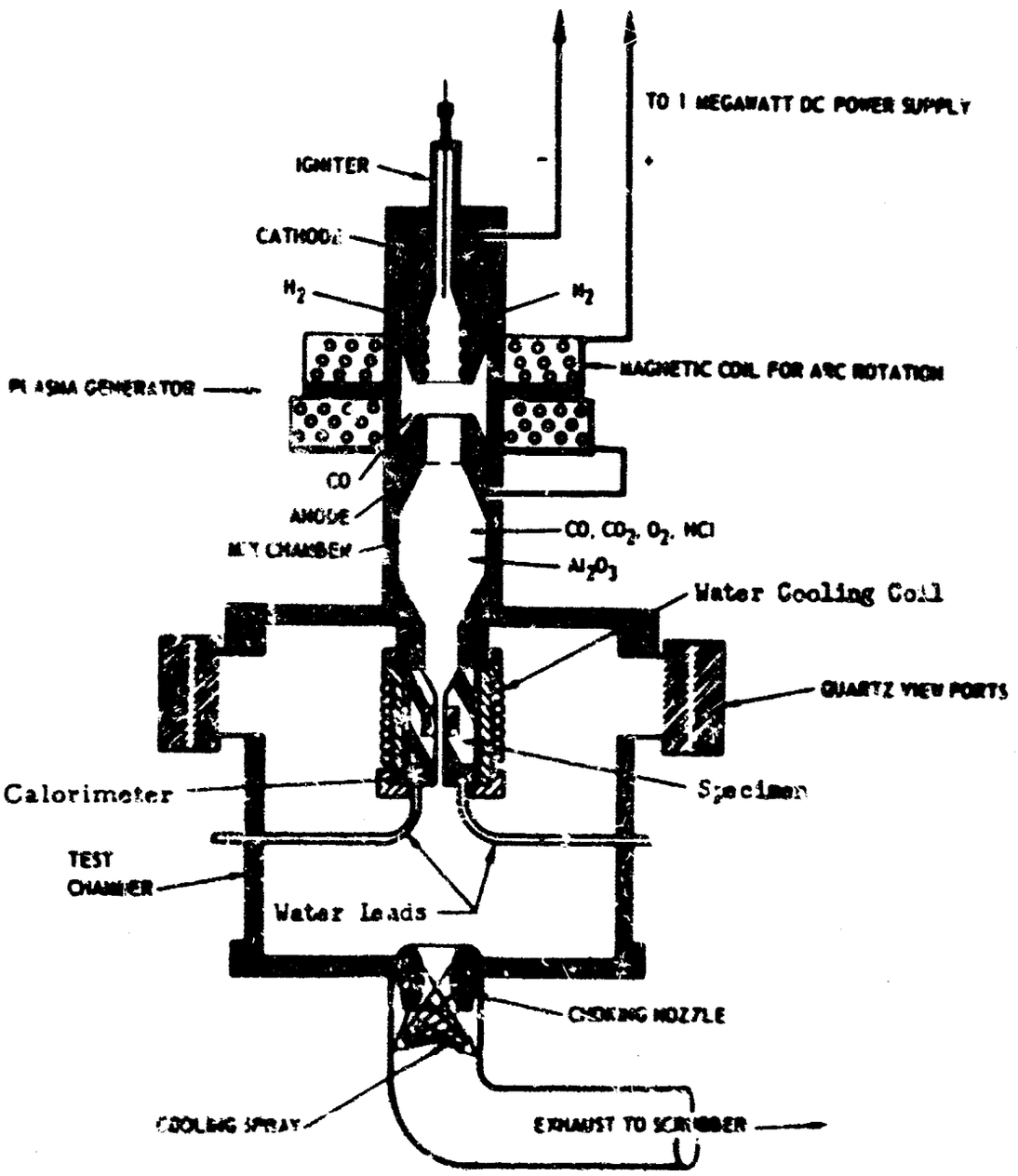

Figure 78. Schematic of HES Plasma Head with Test Specimen

III, C, Task 3--Thermal Shock Resistance Evaluations (cont.)

2. Design of Insert for Thermal Shock Tests

The most important criteria in the design of the thermal shock insert was to assure that the material being tested would undergo a critical test and properly simulate the conditions under which the material will be tested in the full-scale nozzle. Establishing this design involved deriving detailed thermal and stress analysis of various designs to establish the optimum wall thickness necessary to minimize thermal gradients and reduce critical stress. The properties of the microcomposite carbide were used in these analyses.

Three wall thicknesses, 0.10, 0.15, and 0.275 in., were considered in the design of the HES insert. The selection of these thicknesses was based upon fabrication considerations, subscale to full-scale scaling factors in relation to stress conditions and expected material regression during the tests. The full-scale nozzle design that was analyzed was similar to that discussed in a subsequent section, Demonstration Firing Tests. Varying wall thicknesses, 0.25, 0.5, and 1.0 in., for the throat insert were included in the analysis. Both the HES and full-scale inserts were analyzed with graphite backups.

An Aerojet computer program which permits use of a large number of concentric cylinders and allows input of different material properties for each cylinder was utilized in the stress analysis. In this computer program, the anisotropy of each material in the three principal directions--hoop, longitudinal, and through the thickness--is taken into account. Input of various end constraint conditions are also provided for as well as internal pressure. To advantageously use this computer program, the physical and thermal properties of the material must be carefully selected as typical and effective for nozzle thermal shock conditions before insertion into the computer program. The triaxial stresses which appear critical are investigated by the octahedral shearing stress failure criterion shown as follows:

III, C, Task 3--Thermal Shock Resistance Evaluations (cont.)

$$\sigma_{C\ max} = 1/\sqrt{2}\sqrt{(\sigma_1 - \sigma_2)^2 + (\sigma_2 - \sigma_3)^2 + (\sigma_3 - \sigma_1)^2} = \frac{\sqrt{2}}{3} \times \frac{\sigma_s}{M}$$

where σ_s is taken as the short-time failure strength of the material at temperature, and the factor M provides a safety or correlation factor when corrections for stress concentration, surface roughness due to machining, or other extraneous influences appear to affect σ_s.

The elevated-temperature flexural strength input data used in this program are shown in Figure 79. The values estimated for Poisson's ratio and the modulus of elasticity as a function of temperature are given in Figures 80 and 81, respectively. A stress analysis, using these estimated values, showed that extremely high tangential tensile stresses would develop on the outer surfaces of both the subscale and full-scale inserts. The values obtained were well above the ultimate strength of the material.

Subsequent analyses were conducted using stress-strain characteristics under rapid "thermal shock" type loading. From knowledge of the stress-strain behavior of the microcomposite at slow strain rates, creep data, and the behavior of other refractory materials, an estimate was made of the stress-strain behavior of the microcomposite composition 8Ta-55Hf-37C at high load rates. These estimated stress-strain curves from ambient to 4000°F are presented in Figure 82. Analyses using these properties indicated that the time at which the maximum thermal gradient existed in the insert was not necessarily the time at which critical stresses were developed. Therefore, it became apparent that a more realistic expression of the variation of stress with time was required.

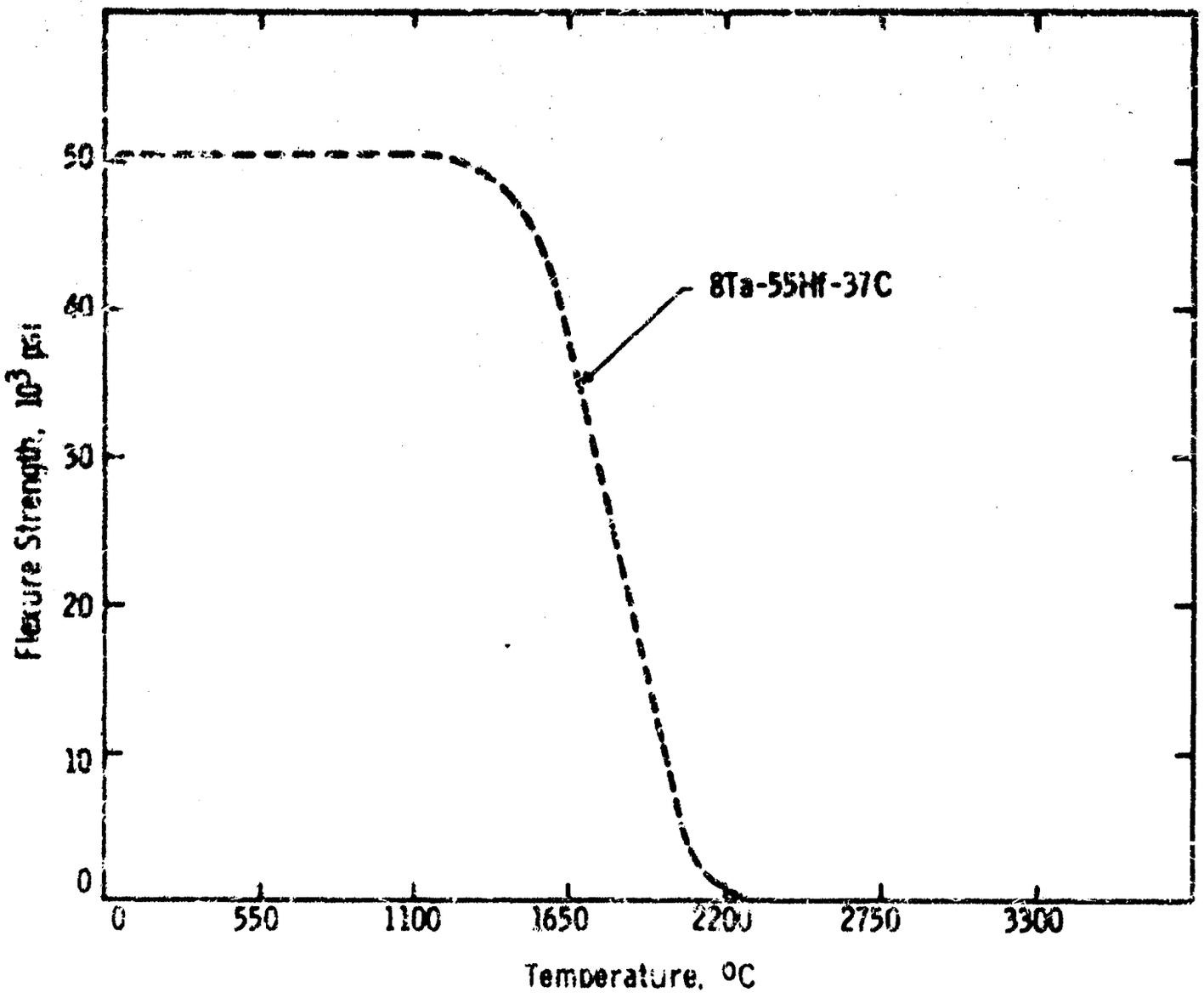

Figure 79. Elevated Temperature Flexural Strength Data Input for Stress Analysis

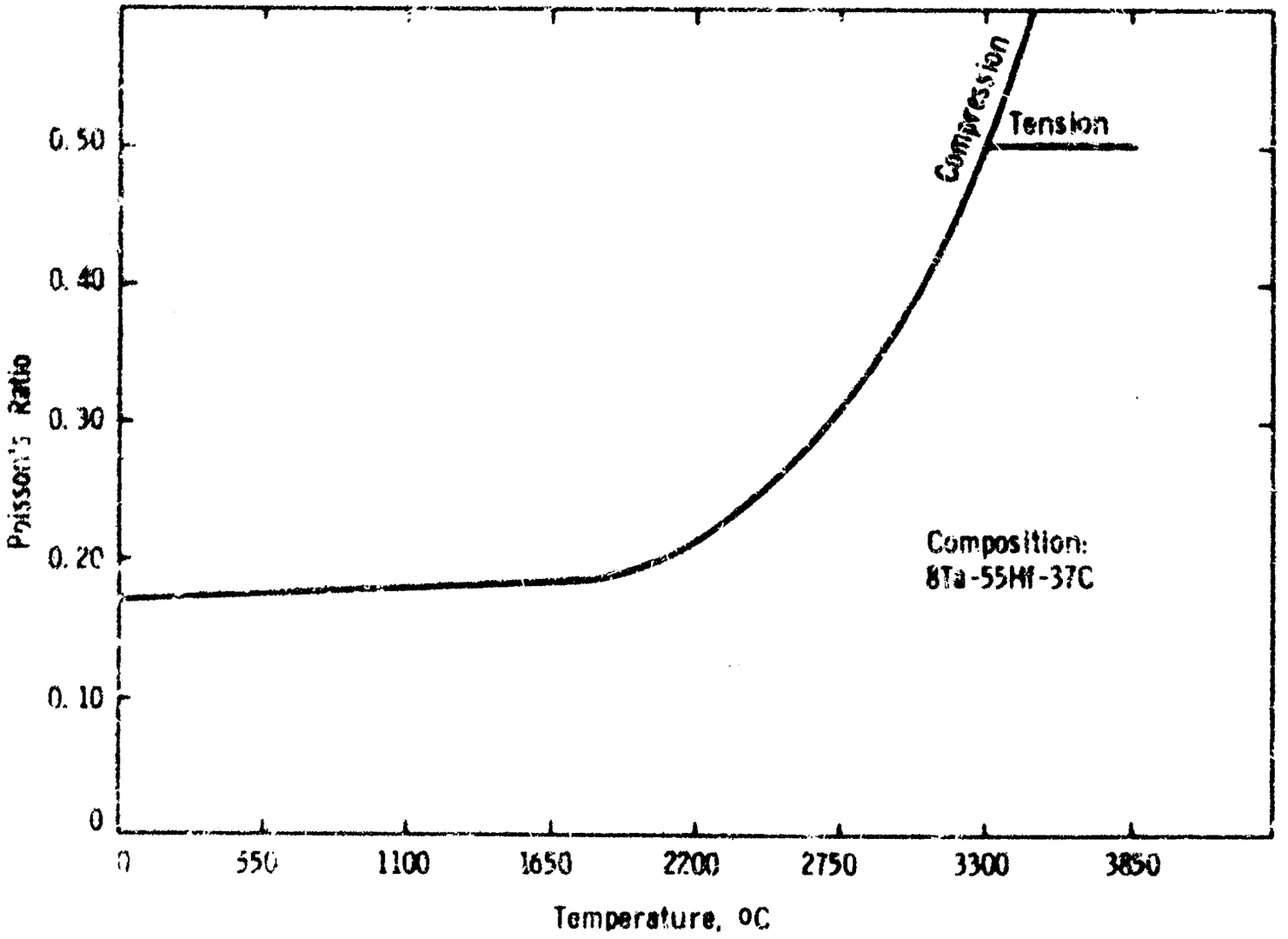

Figure 80. Elevated Temperature Estimate of Poisson's Ratio for Microcomposite for Stress Levels Below Yield Point

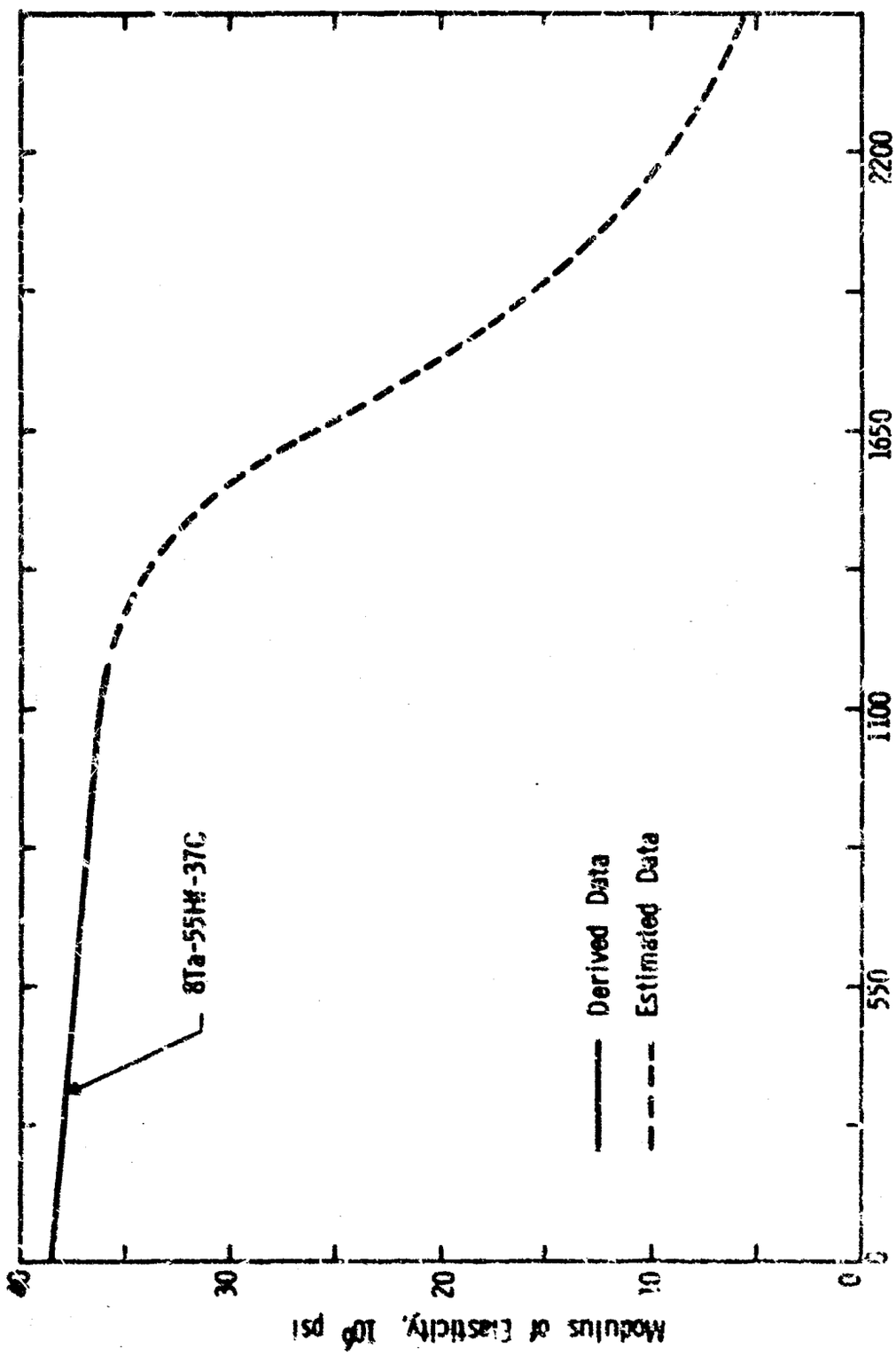

Figure 81. Elevated Temperature Estimate of Modulus of Elasticity for Microcomposite

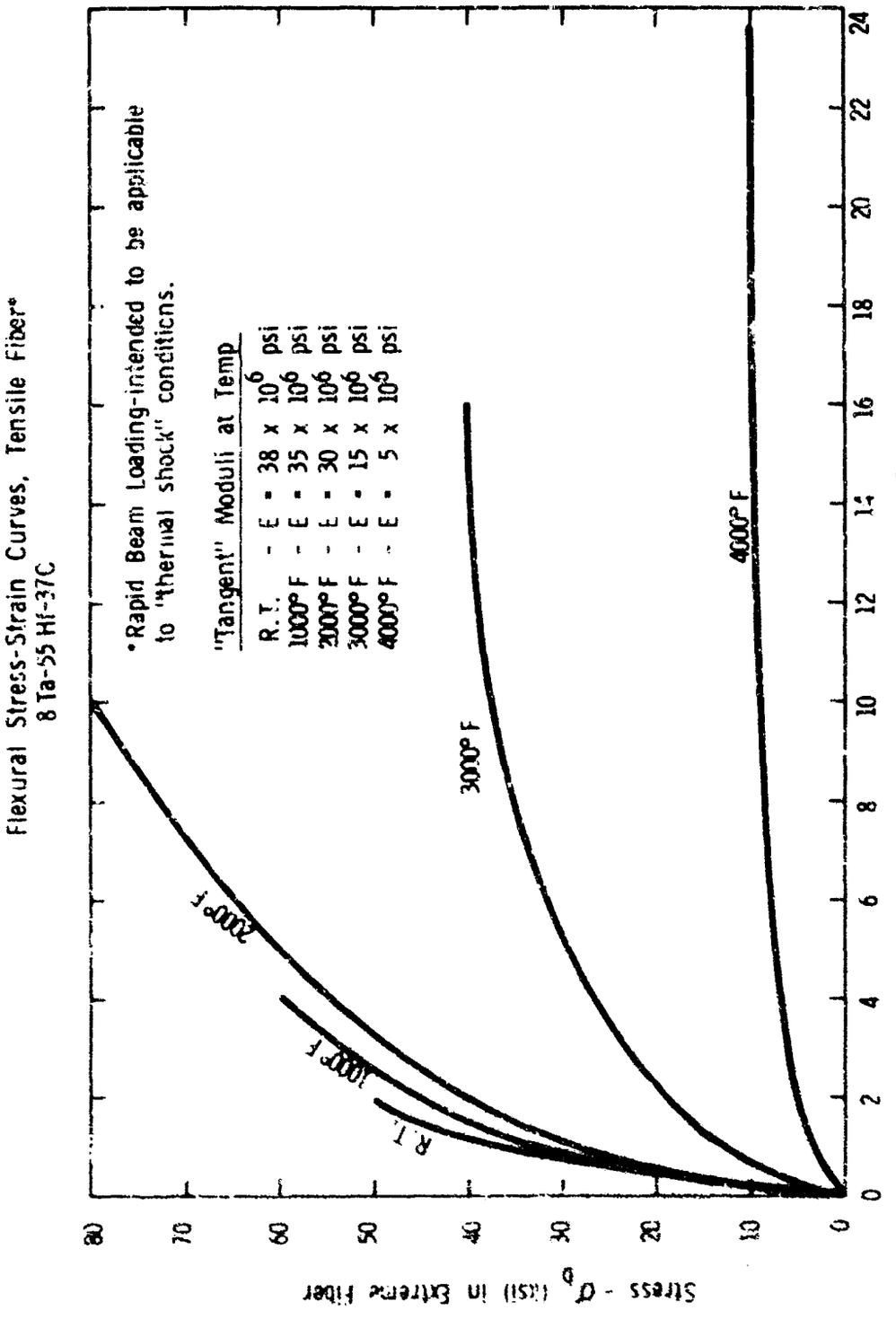

Figure 82. Flexural Stress-Strain Curves (Tensile Fiber) under Rapid Loading for Microcomposite Composition 8Ta-55Hf-37C

III, C, Task 3--Thermal Shock Resistance Evaluations (cont.)

The parameter chosen to reflect these variations was as follows:

$$K = (\Delta T)\ (E_{sec})\ (P)$$

where T = temperature gradient
E_{sec} = secant modulus of elasticity which is time dependent
P = geometrical term which varies only with the thickness of the inserts.

The thermal coefficient of expansion, α, is also important in determining the magnitude of stress. Its variability, however, with time is not as significant as the factors ΔT and E_{sec}. Analysis of the full-scale nozzle insert is shown graphically in Figure 83. The results show that K decreases with thickness, even though ΔT increases, because of the decreases in E_{sec} and P.

The HES insert designs, with wall thicknesses of 0.10, 0.15 and 0.275 in., were analyzed in terms of the variation of the parameter K with time. The magnitude of the stresses which develop on the OD of the insert during the initial seconds of the HAS test are presented in Table XVI. As shown by the data, the insert with a 0.275-in. wall thickness had the lowest OD stresses after 0.6 sec and therefore has the best chance of surviving. This wall thickness was therefore selected for the HES insert.

The data from a similar analysis of the full-scale insert with varying thicknesses is presented in Table XVII. The variation of the parameter K with time is shown graphically in Figure 84. The insert with a 0.5-in. wall thickness was determined to develop the lowest OD stress of 55,400 psi after 2 sec of firing. The critical stresses for all thicknesses at some point in time were found to be near the ultimate strength of the microcomposite. When a graphite backup is used, the stress values are reduced by an estimated 10 to 20%.

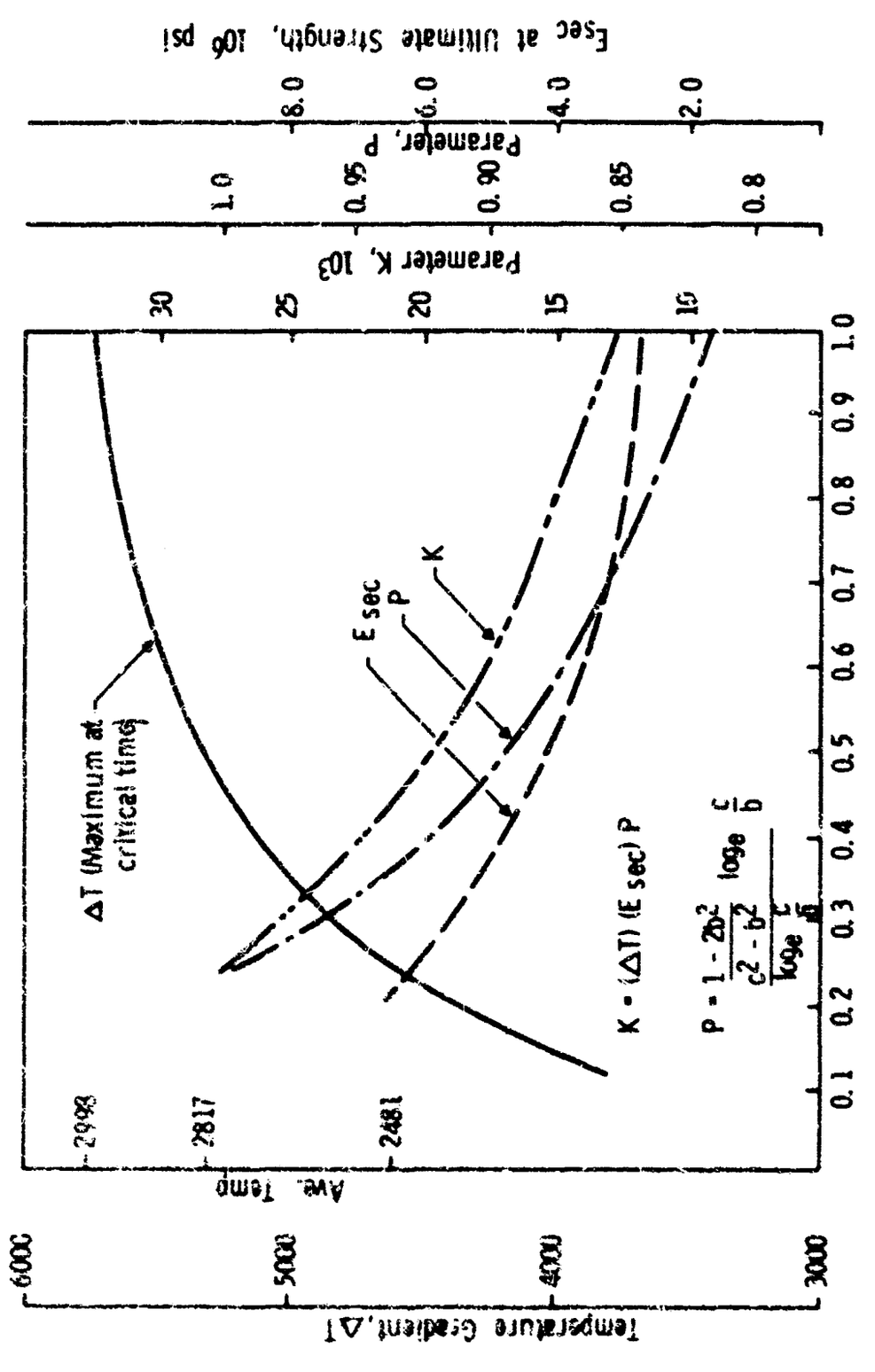

Figure 83. Variation of Parameter K as a Function of Insert Thickness for Full-Scale Nozzle Insert

TABLE XVI

SUBSCALE NBS NOZZLE INSERT
VARIATION OF PARAMETER, K, WITH TIME

$$K = (\Delta T)(E_{sec})\,P \quad \text{where: } E_{sec} = \text{Secant Modulus at Failure}$$

$$P = \frac{\frac{1-2b^2}{c^2-b^2}\log_e \frac{c}{b}}{\log_e \frac{c}{b}}$$

Time, sec	ΔT, °F	Av Temp, °F	E_{sec}, 10^6	K, 10^6	a, 10^{-6}	OD Stresses, psi
A. 0.275-in.-thick Insert P = 0.602; $\frac{a}{2(1-\nu)} = \frac{a}{1.64}$						
0.6	3321	1741	13.3	26,600	3.05	49,500
1.0	3583	1878	12.5	27,000	3.2	52,600
2.2	3833	2110	12.0	27,700	3.45	58,300
2.6	3783	2198	12.0	27,350	3.5	58,400
3.2	3845	2241	8.13	18,800	3.56	40,800
B. 0.15-in.-thick Insert P = 0.710; $\frac{a}{2(1-\nu)} = \frac{a}{1.64}$						
0.4	3058	1637	13.2	28,600	2.95	51,500
0.6	3166	1818	12.5	28,100	3.1	53,100
0.8	3291	1909	12.0	28,100	3.2	54,800
1.2	3317	2089	12.0	28,250	3.42	59,000
1.8	3282	2251	8.13	18,900	3.57	41,100
C. 0.10-in.-thick Insert P = 0.778; $\frac{a}{2(1-\nu)} = \frac{a}{1.64}$						
0.2	2549	1403	16.4	32,600	2.7	53,600
0.4	2857	1735	13.3	29,500	3.05	54,900
0.6	3047	1859	12.5	30,000	3.18	58,200
1.0	2858	2147	12.0	26,650	3.45	56,100
1.4	2690	2256	8.13	17,000	3.58	37,100

TABLE XVII

FULL-SCALE NOZZLE INSERT
VARIATION OF PARAMETER, K, WITH TIME

$$K = (\Delta T)(E_{sec})\, P \quad \text{where: } E_{sec} = \text{Secant Modulus at Failure}$$

$$P = \frac{\frac{1-2b^2}{c^2-b^2}\log_e \frac{c}{b}}{\log_e \frac{c}{b}}$$

	Time, sec	ΔT, °F	Average Temperature, °F	E_{sec} (10^6)	K (10^6)	α (10^{-6}	OD Stresses, psi
A.	1-in.-thick Insert	P = 0.815;	$\frac{\alpha}{2(1-\nu)} = \frac{\alpha}{1.64}$				
	1.0	2356	1258	16.2	31,100	2.55	48,500
	3.0	2660	1410	15.7	34,100	2.70	56,000
	7.0	5596	2879	3.96	18.100	4.25	47,000
	10.0	5701	2936	3.04	14,130	4.30	37,100
	14.0	5757	2999	2.66	12,500	4.40	33,500
	20.0	5718	3101	2.34	10,900	4.50	29,900
B.	0.5-in.-thick Insert	P = 0.893;	$\frac{\alpha}{2(1-\nu)} = \frac{\alpha}{1.64}$				
	2.0	5088	2625	5.0	22,700	4.0	55,400
	4.0	5315	2815	3.96	18,800	4.2	48,200
	6.0	5255	2997	2.86	13,400	4.35	35,500
	10.0	4952	3302	2.18	9,650	4.70	27,700
C.	0.25-in.-thick Insert	P = 0.968;	$\frac{\alpha}{2(1-\nu)} = \frac{\alpha}{1.64}$				
	1.0	4622	2481	6.33	28,900	3.8	67,000
	2.0	4571	2842	3.46	15,600	4.25	40,400
	5.0	3957	3503	1.32	5,160	4.9	15,400
	9.0	3537	3814	1.0	3,500	5.5	11,730

Variation of Parameter, K, with Time (Full Scale Nozzle Insert)

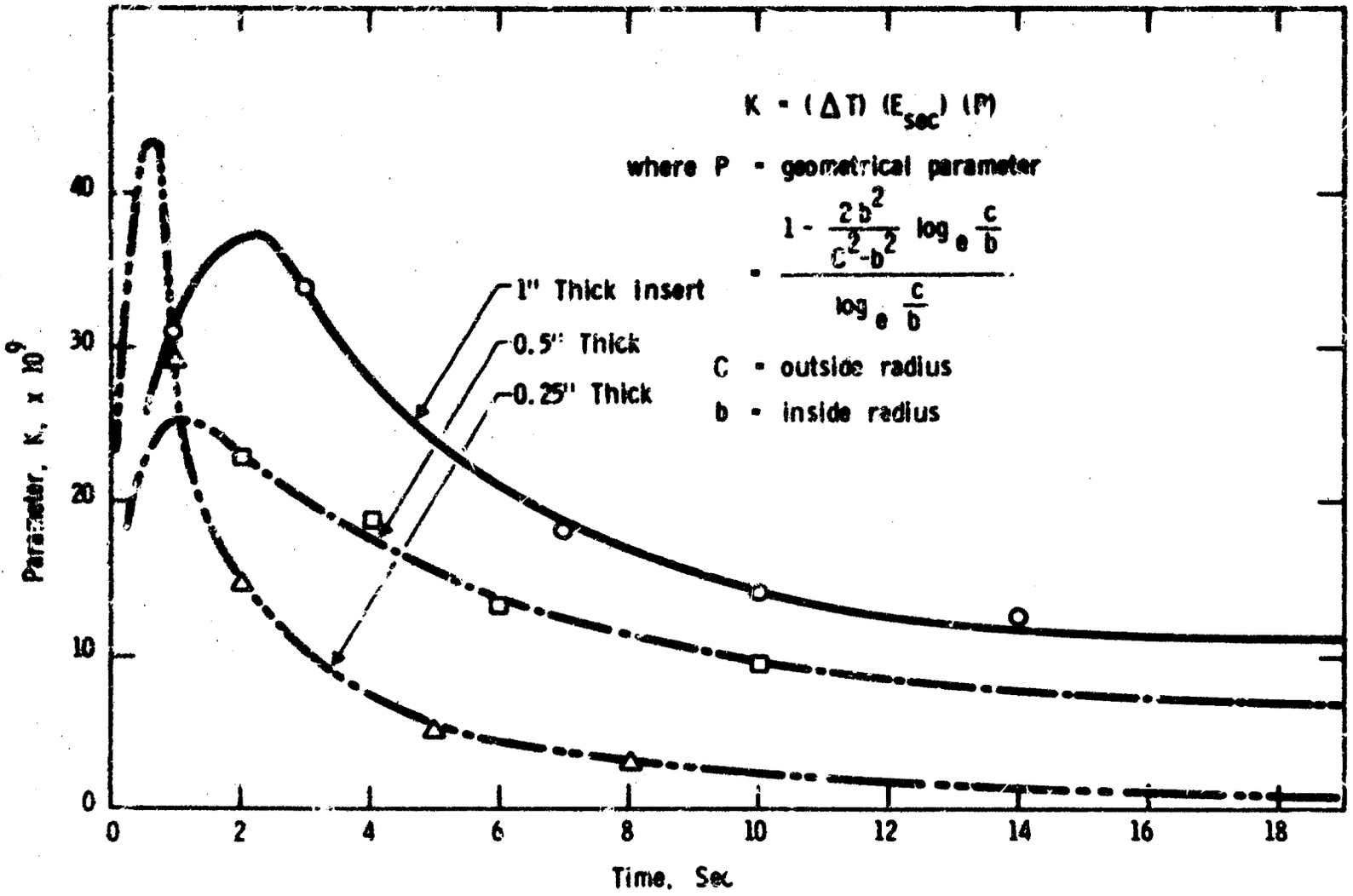

Figure 84. Variation of Parameter K, with Time for Full-Scale Nozzle Insert

III, C, Task 3—Thermal Shock Resistance Evaluations (cont.)

3. Experimental Results

a. Microcomposite

Duplicate thermal shock tests were conducted with the two compositions, 8Ta-55Hf-37C and 8Ta-55Hf-38C. The test conditions, regression rate, and weight loss are shown in Table XVIII. For each composition, one test was planned for a duration of 20 sec and the other for 60 sec. Three tests were as planned; the fourth was terminated after 26 sec due to overheating of an exhaust tube in the HES unit.

The typical posttest appearance of an insert from each composition is shown in Figure 85. All specimens contained radial cracks, which extended the length of the specimen. The 8Ta-55Hf-37C specimens remained physically intact after removal from the graphite backups. The radial crack patterns could be observed in the graphite backup as a result of the carbide expanding into the graphite during the firing. This observation established that cracking occurred during heatup rather than during the rapid cooldown. The 8Ta-54Hf-38C specimens contained more radial cracks than the 8Ta-55Hf-37C specimens and fractured into small mosaic segments between the radial crack planes. As shown in Table XVIII, no material regression was experienced in the throat region and the amount of weight loss was insignificant.

Examination of the microstructure of the 8Ta-54Hf-38C specimens showed a monocarbide zone 0.060 in. deep on the flame surface. Metal alloy existed in large pools within the grain boundaries of the monocarbide. Below this zone, there was a gradual transition over a distance of approximately 0.030 in. from the monocarbide phase to the characteristic microcomposite structure with the metal precipitated throughout the grains.

TABLE XVIII

RESULTS OF THERMAL SHOCK TESTS ON MICROCOMPOSITE COMPOSITIONS

Composition	Insert Number	Density, gm/cm^3	Material Regression: Regression Rate, mils/sec	Material Regression: Weight Loss, %	Test Conditions: Duration, sec	Test Conditions: Pressure, psig	Test Conditions: Heat Flux, $Btu/ft^2/sec$	
8Ta-55Hf-37C	467	12.62	0.0	0.8	20	440	2800	Radial cracks developed
8Ta-55Hf-37C	466	12.50	0.0	0.0	60	455	2800	Radial cracks developed
8Ta-54Hf-38C	470	12.58	0.0	N.D.	20	420	2800	Specimen fractured during removal from graphite backup.
8Ta-54Hf-38C	468	12.53	0.0	0.75	28	450	2800	Small mosaic cracks developed between radial cracks.

N.D. = Not Determined, See Comments

3X 3X

b. Composition 8Ta-54Hf-38C

3X 3X

a. Composition 8Ta-55Hf-37C

Figure 85. Posttest Appearance of Microcomposite Inserts after Thermal Shock Testing

III, C, Task 3--Thermal Shock Resistance Evaluations (cont.)

Examinations of the microstructure of the 8Ta-55Hf-37C specimens showed that the radial cracks initiated at the OD and terminated near the flame surface. The photomicrograph in Figure 86 shows the termination of a crack near the flame surface in an insert. The characteristic precipitated-metal alloy phase existed throughout the thickness of the inserts. Some of the metal alloy melted and flowed into the cracks that originated at the OD of the insert during heating.

The results of the performance evaluation on this series of thermal shock tests on the two microcomposite compositions, 8Ta-55Hf-37C and 8Ta-54Hf-38C, are summarized as follows:

(1) No material regression occurred for either composition; therefore, microspalling or erosion effects do not appear to be a problem.

(2) No gross material loss by "chunking" or ejection of large segments occurred for either composition.

(3) Fine thermal stress cracking occurred in both compositions during test firing. Cracking was less severe for the composition 8Ta-55Hf-37C. This is believed to be a result of the greater volume of Ta-Hf metal alloy in the grain boundaries in comparison to 8Ta-54Hf-38C.

b. TaC-C Hypereutectic Composites

In the thermal shock resistance evaluation of the TaC-C hypereutectic composites, eight tests were conducted to evaluate variations in carbon content and coherence of the TaC flame liner on the TaC-C substrate. The compositions tested together with test conditions, regression rates, and weight loss for each run are presented in Table XIX.

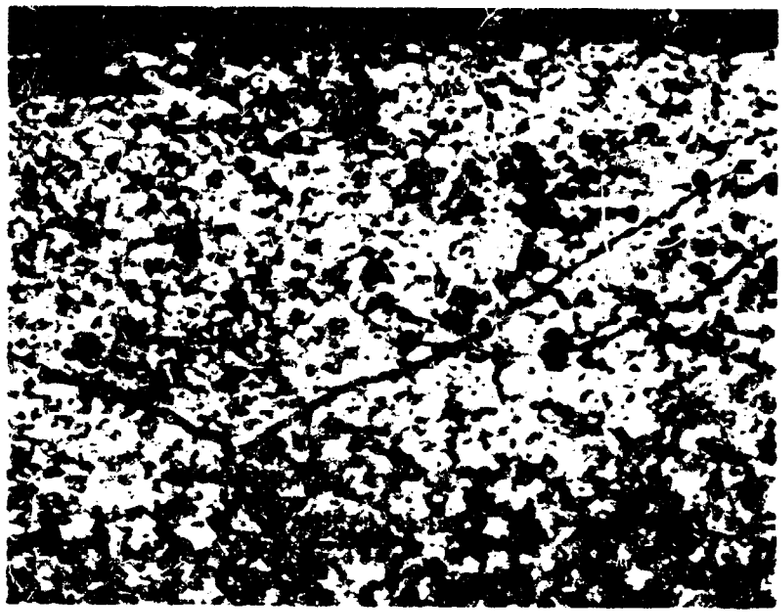

50X

b. Close-up View of Area where Cracking Terminated

Flame Surface →

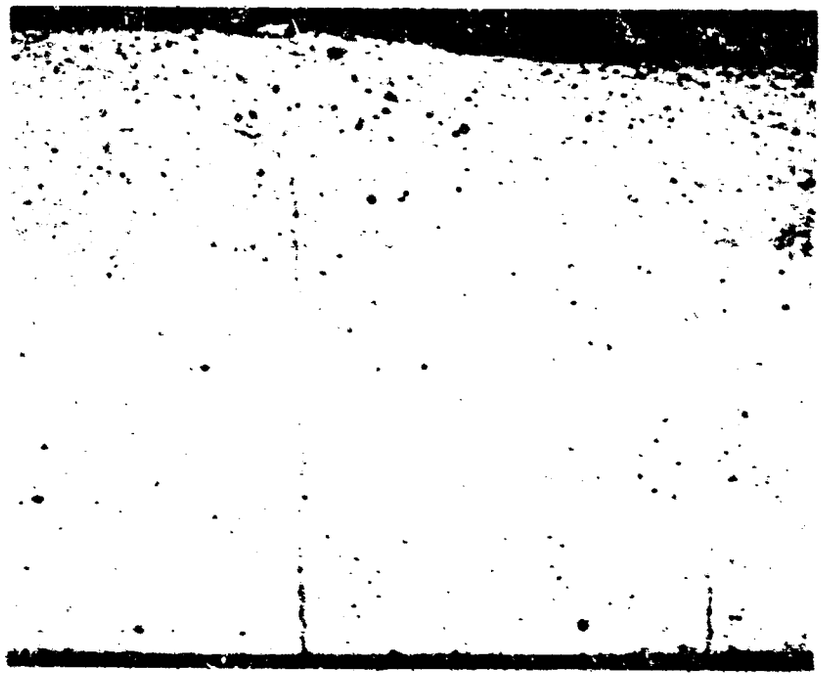

↳ ID of Insert 20X

a. View of Wall Thickness

Figure 84. Photomicrograph of a Cross-Section of a Microcomposite Insert, Composition 91a-9Hf-3C, Showing Crack Termination near ID

TABLE XIX

RESULTS OF THERMAL SHOCK TESTS ON TaC-C HYPEREUTECTIC COMPOSITES

Type of Insert	Composition Graphite Flake w/o	Insert Number	Density (gm/cm³)	Material Regression: Regression Rate mils/sec	Material Regression: Weight Loss %	Jet Conditions: Duration, sec	Jet Conditions: Pressure, psia	Jet Conditions: Heat Flux, Btu/ft²-sec	Remarks
A. No TaC liners (solid)	7	439-1	11.3	0.0	0.0	60	405	2800	
	7	441-2	11.3	0.0	0.0	60	405	2800	
	15	451-1	10.3	0.0	0.22	60	440	2800	
	17	453-1	10.1	0.0	0.4	60	450	2800	
B. TaC lined inserts	8	458-1	11.2	0.0	0.77	60	400	2800	Radial cracks developed at one end.
	13	450-2	10.3	0.0	2.33	60	415	2800	
	19	458-2	9.8	0.0	5.4	60	400	2800	
	19	441-1	9.8	0.0	1.0	60	430	2800	

III, C, Task 3--Thermal Shock Resistance Evaluations (cont.)

In the first series of tests which were conducted on inserts without a TaC liner, the variation in carbon content was expected to provide a variation in resistance to thermal shock. However, none of the four inserts tested cracked. There was no significant material regression. Figure 87 shows the excellent posttest appearance of the insert from composition 7 v/o graphite flake, which was typical of all the inserts tested in this series.

The second series of four thermal shock evaluation tests was conducted on inserts which had a TaC liner formed in situ on the ID flame surface. The hypereutectic substrates were of varying graphite contents, 8, 15 and 19 v/o. No surface regression occurred. However, a slight weight loss was noted. These minor losses were believed to be a result of the material loss during the sectioning of the insert from the graphite backup and not during firing. Examinations of the thin TaC liners showed no evidence of spalling or cracking. The coatings remained integrally bonded to the hypereutectic substrates. No evidence of cracking was found in the three inserts with the high graphite flake contents, 15 and 19 v/o graphite. The remaining insert, No. 452-1, which had a graphite flake content of 8 v/o, had a slight amount of radial cracking in the exit portion of the insert as shown in Figure 88. The microstructure in this region was found to be of the eutectic composition. The absence of primary graphite flakes accounts for the poor thermal shock resistance of the material in this region.

4. Task Summary

The results of the performance evaluation on this series of eight thermal shock tests are summarized as follows:

a. The TaC coated or uncoated hypereutectic inserts experienced no significant material regression from microspalling, chunking, ejection of the TaC coating, or erosion.

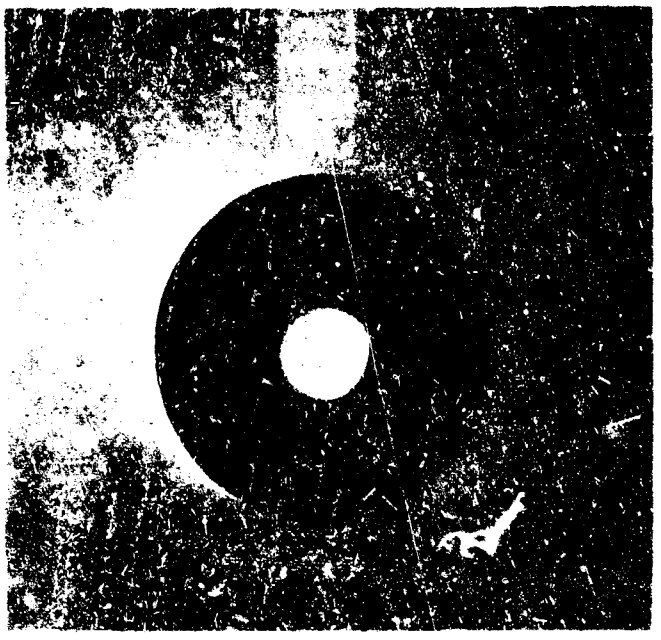

2.8X

a. Exit View of Insert No. 459-1, Showing no Structural Degradation

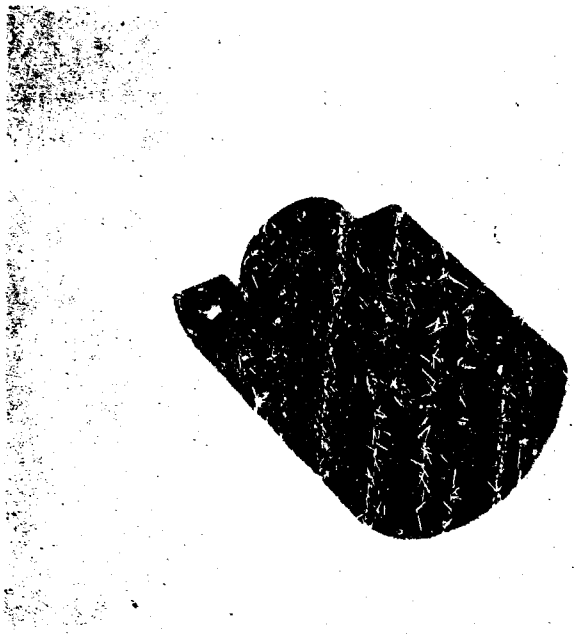

1.2X

b. Sectioned View of Insert in Graphite Holder

Figure 87. Appearance of Hypereutectic Insert, Composition 7 v/o Graphite Flake, After Thermal Shock Testing

1.2X

b. Sectional View of Insert in Graphite Holder, Spec. No. 452-1

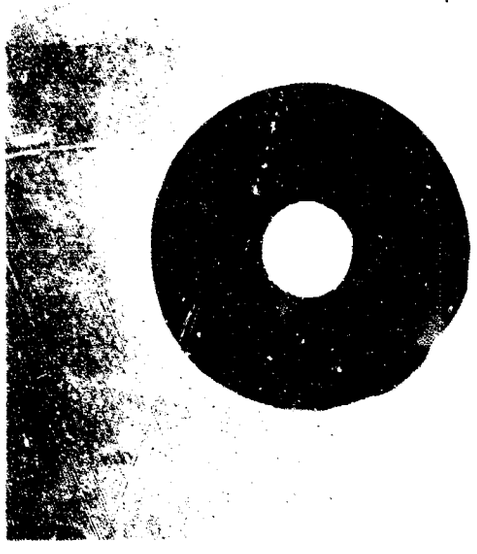

2.8X

a. Exit View of Insert No. 452-1 Showing Radial Cracks

Figure 88. Appearance of TaC-Coated Hypereutectic Insert, Composition 8 v/o Graphite Flake, Showing Radial Cracks after Thermal Shock Testing

III, C, Task 3--Thermal Shock Resistance Evaluations (cont.)

b. The uncoated hypereutectic inserts, both low carbon contents (7 v/o graphite flake) and high carbon contents (15 to 17 v/o graphite flake), did not experience thermal stress cracking.

c. The TaC coated hypereutectic inserts with carbon contents from 15 to 19 v/o graphite flake exhibited no thermal cracking. One coated insert containing 8 v/o graphite flake developed radial cracks in a region which was found to be of eutectic composition.

D. TASK 4--CHEMICAL CORROSION EVALUATIONS

The objectives of this work were to determine the relative corrosion resistance of the two candidate microcomposite and TaC-C hypereutectic composites: (1) in an environment simulating the exhaust-gas chemistry of the motor tests to be conducted in a subsequent task, and (2) to characterize the two composites in varied propellant-gas chemistries to define the environmental capabilities of the material systems.

1. Test Procedures

Testing was accomplished in the hyperthermal environmental simulator (HES) in a manner similar to the thermal shock testing previously described. Regression rates were measured at specified locations in the carbide insert and in the entrance and exit sections of the ATJ graphite holder. These numerical locations are shown in Figure 89. In the rocket motor simulation tests, the specimens were evaluated by simulating the propellant and firing conditions to be used in the full-scale motor firings. The solid propellant simulated in these tests had a flame temperature of 6500°F and 13 mole% oxidizing gases in the propellant exhaust gas. The principal oxidizing gases considered corrosive to the carbides are H_2O, CO_2 and OH.

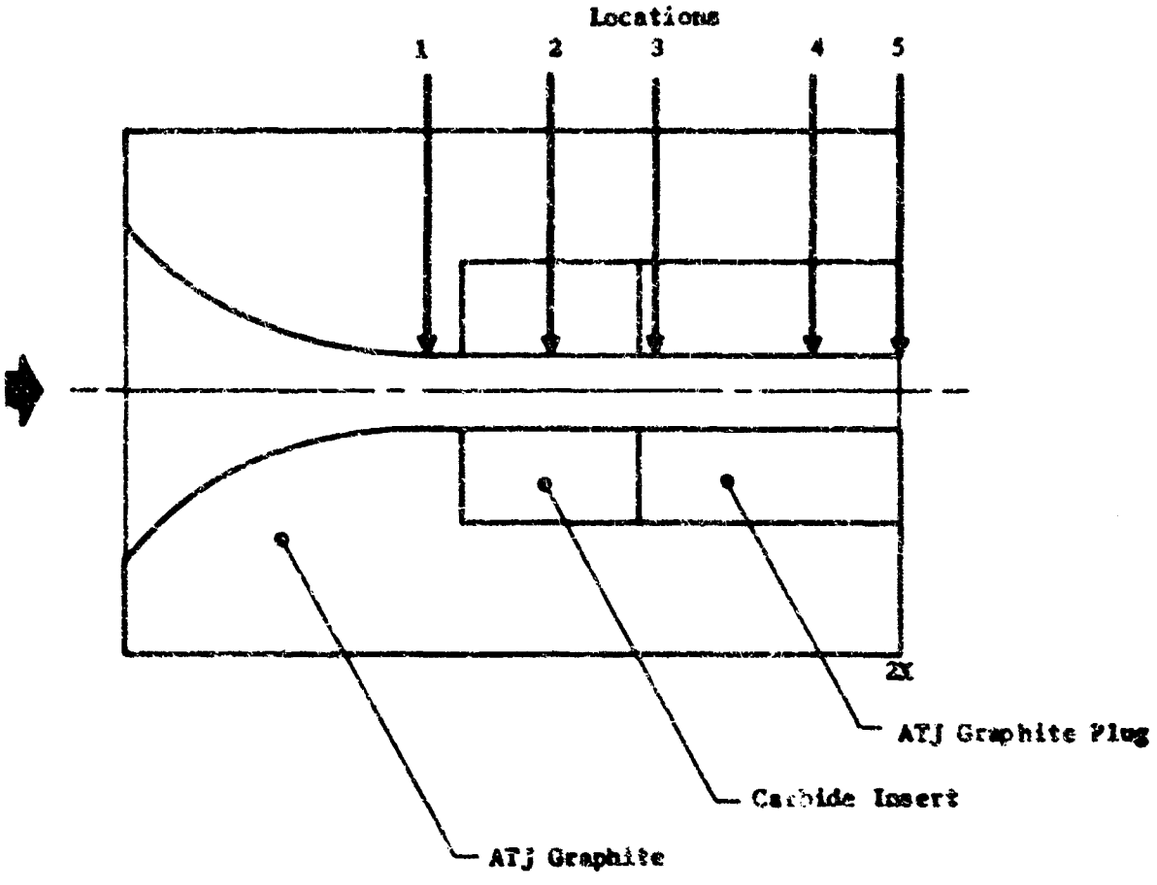

Figure 89. Cross-Sectional View of Insert Showing Locations where Regression Rate Measurements were Obtained

XII, D, Task 4--Chemical Corrosion Evaluations (cont.)

Al_2O_3 (liquid) is also corrosive but the effect of variations in the gases obscures the effect of variations in Al_2O_3 content. The corrosive effects of liquid Al_2O_3 on both the microcomposite and TaC-C hypereutectic composites are discussed in Reference 12. A separate program under AFRPL sponsorship was conducted at the Equipment Laboratories, Thompson-Ramo-Wooldridge, Cleveland, Ohio, to primarily establish the magnitude of the reactivity problem between Al_2O_3 and these carbide composites.

In the environmental capability tests, three solid propellants were simulated with higher oxidizing potentials than in the first series of tests. The oxidant levels were 9, 18, and 24 mole% with flame temperatures of 6300, 6500, and 5800°F, respectively. The third series of tests, comparative tests, were conducted using inserts of Carborundum's Grade G-90 graphite.

2. Experimental Results

a. Rocket Motor Simulation

A compilation of the test conditions and material regression rates are reported in Section A of Table XX.

The initial test conducted was with the composition 80Ta-5Hf-15C, Insert No. 472. This test was stopped after 20 sec due to a burn-through within the sample and graphite holder which allowed gases to escape into the water-cooled sample holder. A posttest examination of the sample and the graphite holder revealed that the higher thermal expansion of the carbide insert caused the graphite backup to crack longitudinally in the entrance region. This allowed the plasma gas to flow through the crack and damage the stainless-steel sample holder. This problem was alleviated by using a silver infiltrated tungsten tube as shown in Figure 77. The carbide-graphite inserts were press-fitted into the tungsten tube. The use of the

TABLE XX

RESULTS OF CHEMICAL CORROSION TESTS

Test Series	Specimen/Item	Insert Number	Density, g/cm³	Propellant Oxidant Content, Mole %	Corrosion Rates: Entrance Location (1), mils/sec	Corrosion Rates: Center Location (2), mils/sec	Corrosion Rates: Location (3), mils/sec	Corrosion Rates: Exit Location (4), mils/sec	Weight Loss, %	Test Conditions: Duration, sec	Test Conditions: Pressure, psia	Test Conditions: Heat Flux, Btu/ft²/sec	Comments
[illegible]	Inserts												
A. Rocket Motor Simulation Tests	8-58-37	479	18.5	13	N.D.	N.D.	N.D.	N.D.	N.D	80	400	3800	Burn through occurred in graphite holder.
	8-58-38	471	18.5	13	N.D.	0.83 (see Comments)		N.D.	18.3	60	390	3800	Oxidizer inlets in #25 were partially plugged. Lower oxidant content than 13 mole %.
	8-55-37	473	12.6	13	N.D	N.D	N.D	N.D	0.12	60	400	3800	Oxidizer inserts in #13 completely plugged. No oxidants introduced.
	8-58-39	481	19.6	13	0.67	0.80	0.82	0.78	37.5	[illegible]	400	3800	
	8-55-37	474	17.6	13	0.80	1.06	1.04	0.88	6.7	35	430	3800	
B. Environmental Capabilities	8-58-38	475	19.6	18	1.57	1.58	1.1	0.9	53.1	60	410	4300	
	8-58-38	476	12.6	24	1.49	1.42	1.37	1.13	66.7	60	430	4300	
[illegible][1]	Graphite Plate, Item 4												
A. [illegible] Motor Simulation Tests	11	447-2	10.8	13	0.77	1.75	2.44	3.82	49.7	57	395	3800	
	13	458-3	10.5	13	0.60	1.93	2.50	3.13	36.6	60	400	3800	
	17	451-2	10.1	13	N.D.	N.D.	N.D.	N.D.	N.D.	60	435	3800	Specimen shattered during removal from RSS holder.
	19	458-1	9.8	13	0.6	1.73	2.67	3.13	58.5	60	395	3800	
B. Environmental Capabilities	16	448-1	10.2	8	1.08	1.1	1.41	1.82	80.6	60	430	4400	
	18	445-2	10.1	18	2.18	1.90	2.42	1.66	58.7	60	395	4300	
[illegible]													
A. Rocket Motor Simulation Tests	0-60 Graphite	479	1.90	13	0.43	0.98	-	0.8[illegible]	-	60	390	3800	
B. Environmental Capabilities	0-60 Graphite	477	1.90	18	1.17	2.0	-	2.18	-	60	430	4300	
	0-60 Graphite	476	1.90	24	1.43	3.03	-	2.38	-	60	405	4300	

(1) All inserts were TaC lined on flame surface

N.D. = Not Determined - See Comments

III, B, Task 4--Chemical Corrosion Evaluations (cont.)

tungsten with a higher modulus of elasticity allows the tube to partly constrain the thermal growth of the graphite holder, thus preventing the holder from cracking.

In the next two tests with compositions 8Ta-54Hf-38C and 8Ta-55Hf-37C (Inserts No. 471 and No. 473, respectively), problems were encountered in obtaining the 13 mole% oxidant level in the plasma gas. Partial plugging of the oxygen inlets to the mix chamber had occurred with insert No. 471 and the inlets became completely plugged with Insert No. 473. This happens very seldom and, therefore, was not detected until after the test with Insert No. 473 when a low pressure decay was noted in the oxygen line.

In the fourth test with composition 8Ta-54Hf-38C, Insert No. 481, all of the test conditions were achieved. The regression rate of the carbide insert was 0.80 mils/sec. The graphite in the exit region of the insert, locations 3 and 4, had regression rates of 0.82 and 0.78 mils/sec, respectively, which were approximately the same rate as the carbide insert. The graphite located in the entrance section of the insert, location 1, had a slightly lower regression rate (0.67 mils/sec). The insert weight loss was 37.5% for the 60-sec test. A posttest microstructural examination showed that the insert developed the same type of mosaic cracking previously discussed for this composition in the section on thermal shock tests. Microstructural examinations showed a thin oxide film on the flame surface. Below this film was a thin layer (<0.050 in. thick) of monocarbide. Below this zone, there was a gradual transition over a distance of 0.100 in. to the characteristic microstructure containing the precipitated alloy phase.

The last of the tests on the microcomposite compositions was with composition 8Ta-55Hf-37C, Insert No. 474. This test was terminated after 25 sec due to overheating of a tube used to duct the exhaust gases into a water scrubber. However, the test conditions and data were not jeopardized.

III, D, Task 4--Chemical Corrosion Evaluations (cont.)

The regression rate of the carbide insert was 1.08 mils/sec, slightly higher than previously obtained for the composition 8Ta-54Hf-38C, Insert No. 481. The graphite in the exit sections had regression rates of 1.04 and 0.88 mils/sec, which are also higher than that obtained with Insert No. 481.

Posttest examinations showed the same type of radial cracking which was observed for this composition in the thermal shock tests. Microstructural examinations showed a slight oxide film on the flame surface. The characteristic metal alloy phase existed at all depths from the flame surface.

Using the same gas composition as for the previous microcomposite tests, the TaC coated (approximately 0.010 in. thick) TaC-C hypereutectic compositions were evaluated. The backup materials were 11, 13, 17 and 19 v/o graphite flake. Throat measurements from which regression rates were calculated were not obtained for the one composition 17 v/o graphite, Insert No. 451-2, because the graphite holder and sample were shattered in the process of being pressed from the tungsten sample holder. The regression rates for the other three were 1.73, 1.75, and 1.93 mils/sec for the carbide inserts. No correlation with respect to composition could be established for the hypereutectic compositions. Indications were that the thin TaC coatings were removed in 5 to 10 sec, leaving the hypereutectic substrate exposed. The regression patterns were not uniform and all three of the inserts underwent high material losses, ranging from 36.6 to 58.5 wt%, for the 60-sec test duration.

Figure 90 shows the appearance after testing of the composition 19 v/o graphite, Sample No. 458-1, which had a regression rate of 1.73 mils/sec and had the highest material loss, 58.5 wt%. More uniform material regression was experienced with the composition 13 v/o graphite,

2.0X

a. Exit View of Insert No. 458-1, Regression Rate 1.73 mils/sec, wt. Loss 58.5%

1.2X

b. Sectional View of Insert in Graphite Holder

Figure 90. Appearance of TaC Coated Hypereutectic Insert, Composition 10 v/o Graphite Flake, After Rocket Motor Simulation Test (Propellant 13 Hole I Oxidants)

III, D, Task 4--Chemical Corrosion Evaluations (cont.)

Insert No. 453-3, which had a regression rate of 1.93 mils/sec and a weight loss of 36.6%. The appearance of this insert after testing is shown in Figure 91.

The AXJ graphite plugs behind the carbide inserts experienced significantly higher regression rates than the carbide inserts. These regression rates at locations 3 and 4 varied from 2.42 and 3.82 mils/sec and are considerably higher than anticipated based upon the results of the microcomposite tests. The regression rates in the graphite entrance ranged from 0.6 to 0.77 mils/sec, which is comparable to the regression rate obtained with microcomposite insert No. 481.

The comparative results of the rocket motor simulation tests on both the microcomposite and the TaC-C hypereutectic composites are summarized as follows:

(1) The two microcomposite compositions exhibited approximately equal material regression rates with the recorded difference due to slightly different test gas compositions as indicated by the graphite entrance and exit regression rates.

(2) The four TaC lined TaC-C hypereutectic composites had similar regression rates. No correlation between the rate of material regression and hypereutectic composition was obtained.

(3) The TaC-C hypereutectic composites had material regression rates 70 to 100% higher than the rates obtained for the two microcomposite compositions. This difference can be attributed to the formation of the higher melting oxide, HfO_2, on the flame surface of the microcomposite in comparison to Ta_2O_5 formation on the hypereutectic.

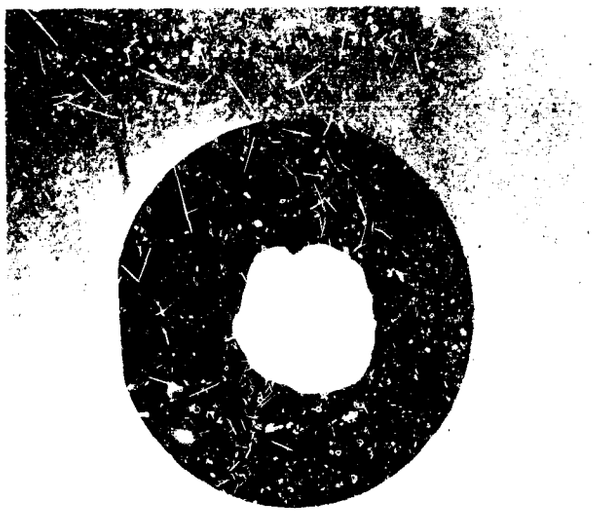

2.8X

a. Exit View of Insert No. 458-3 Regression Rate 1.93 mils/sec, wt. Loss 36.6%

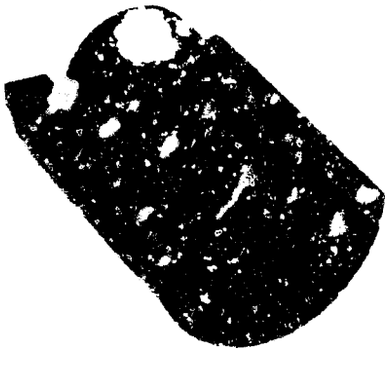

1.2X

b. Sectional View of Insert in Graphite Holder

Figure 91. Appearance of TaC Coated Hypereutectic Insert, Composition 15 v/o Graphite Flake, After Rocket Motor Simulation Test (Propellant 13 Mole % Oxidants)

III, D, Task 4--Chemical Corrosion Evaluations (cont.)

(4) A comparison of the regression data obtained from the thermal shock tests and the rocket motor simulation tests clearly establishes that the mechanism of material regression for both composite carbide systems is chemical corrosion.

b. Environmental Capabilities

In this series of tests (Table XX), the microcomposite composition 8Ta-54Hf-38C and the TaC lined TaC-C hypereutectic compositions, 17 and 16 v/o graphite, were evaluated with simulated solid propellant exhausts having oxidant levels of 8, 18, and 24 mole%. The more oxidation resistant microcomposite composition was tested at oxidant levels of 18 and 24 mole%. The hypereutectic composites, because of poorer oxidation resistance, were tested at oxidant levels of 8 and 18 mole%.

Microcomposite Insert No. 475, which was tested at 18 mole% oxidants, had a regression rate of 1.58 mils/sec and a weight loss of 53.1%. Insert No. 475, which was tested at 24 mole% oxidants, had a slightly lower regression rate, 1.42 mils/sec, but as expected, a higher weight loss of 64.7%. This lower than expected regression rate for this insert is believed to be a result of the nonuniform regression that occurred in the specimen, in addition to the fact that measurements were taken at one specified location.

At the lower 8% oxidant level, the hypereutectic Insert No. 469-1 exhibited a regression rate of 1.1 mils/sec and a weight loss of 20.6%. Figure 92 shows the appearance of this insert after testing. The second insert, No. 465-2, which was evaluated at the 18% oxidant level, had a regression rate of 1.90 mils/sec and a weight loss of 82.7%. This excessive amount of material regression can be seen from the appearance of

1.2X

b. Sectional View of Insert in Graphite Holder

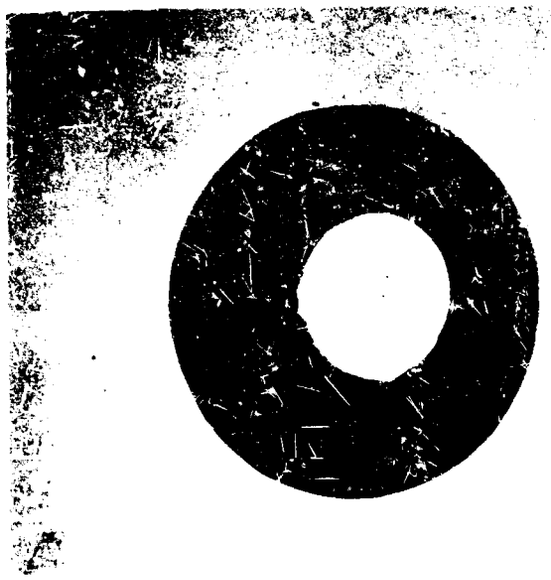

2.8X

a. Exit View of Insert 469-1 Regression Rate 1.1 mils/sec, wt. Loss 20.6%

Figure 92. Appearance of TaC Coated Hypereutectic Insert, Composition 16 v/o Graphite Flake, After Corrosion Test (Propellant 8 Mole % Oxidants)

III, D, Task 4--Chemical Corrosion Evaluation (cont.)

the insert shown in Figure 93. The ATJ graphite behind these inserts corroded at higher regression rates in a manner similar to that experienced in the previous series of rocket motor simulation tests. In the 18% oxidant test, the graphite in the entrance section experienced a regression rate higher than the insert.

c. Comparative Tests

The comparative tests (Table XX) on Grade G-90 graphite were run at oxidant contents of 13, 18 and 24 mole%. Figure 94 shows a plot of the graphite regression rates taken at location 2 as a function of propellant oxidant content. Regression measurements at this location permit a valid comparison between the regression rates of graphite and the carbides. The regression rates increased rapidly from 0.98 mils/sec at an oxidant content of 13%, to 2.0 mils/sec at a content of 18%, and finally to 3.03 mils/sec at an oxidant content of 24%.

Figure 95 shows a similar correlation for all of the microcomposite tests at the three oxidant levels of 13, 18, and 24%. The regression rates and weight of material loss are strictly a function of the oxidant content of the propellant.

The same type of correlation is shown for the TaC-C hypereutectic composites in Figure 96. However, higher regression rates and higher material losses at the same oxidant levels were experienced by these composites in comparison to the results from the microcomposite tests.

Figure 97 shows a very significant comparison of the regression rates obtained for all the tests on the microcomposite, hypereutectic, and graphite inserts under the various simulated propellant exhausts.

1.2X

b. Sectional View of Insert on Graphite Holder

2.8X

a. Exit View of Insert 465-2, Regression Rate of 1.90 mils/sec, wt. Loss 82.7%

Figure 93. Appearance of TaC Coated Hypereutectic Insert, Composition 17 v/o Graphite Flake, After Corrosion Test (Propellant 13 Mole % Oxidants)

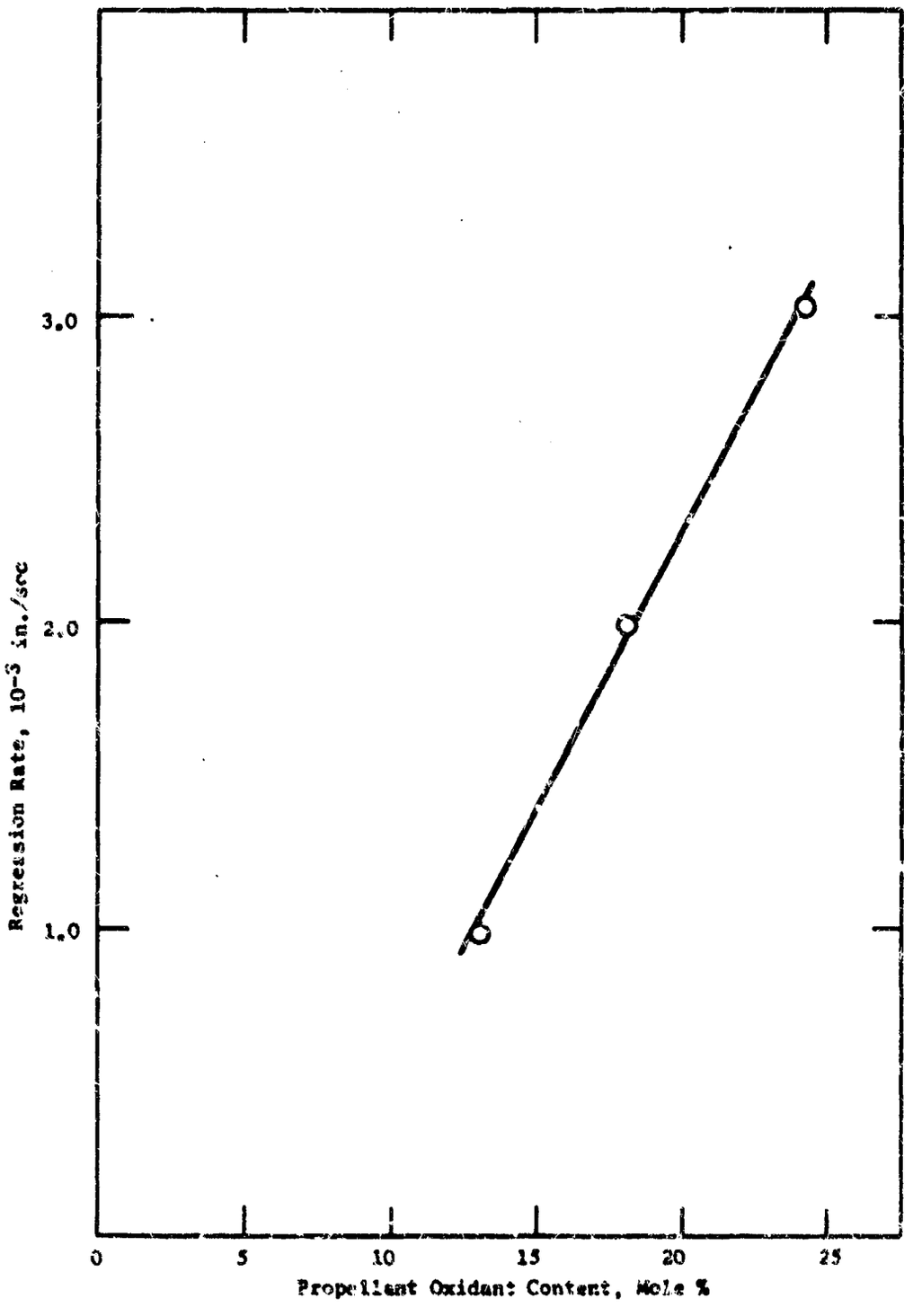

Figure 94. Effect of Oxidant Content in Solid Propellants on the Material Regression of Grade G-90 Graphite

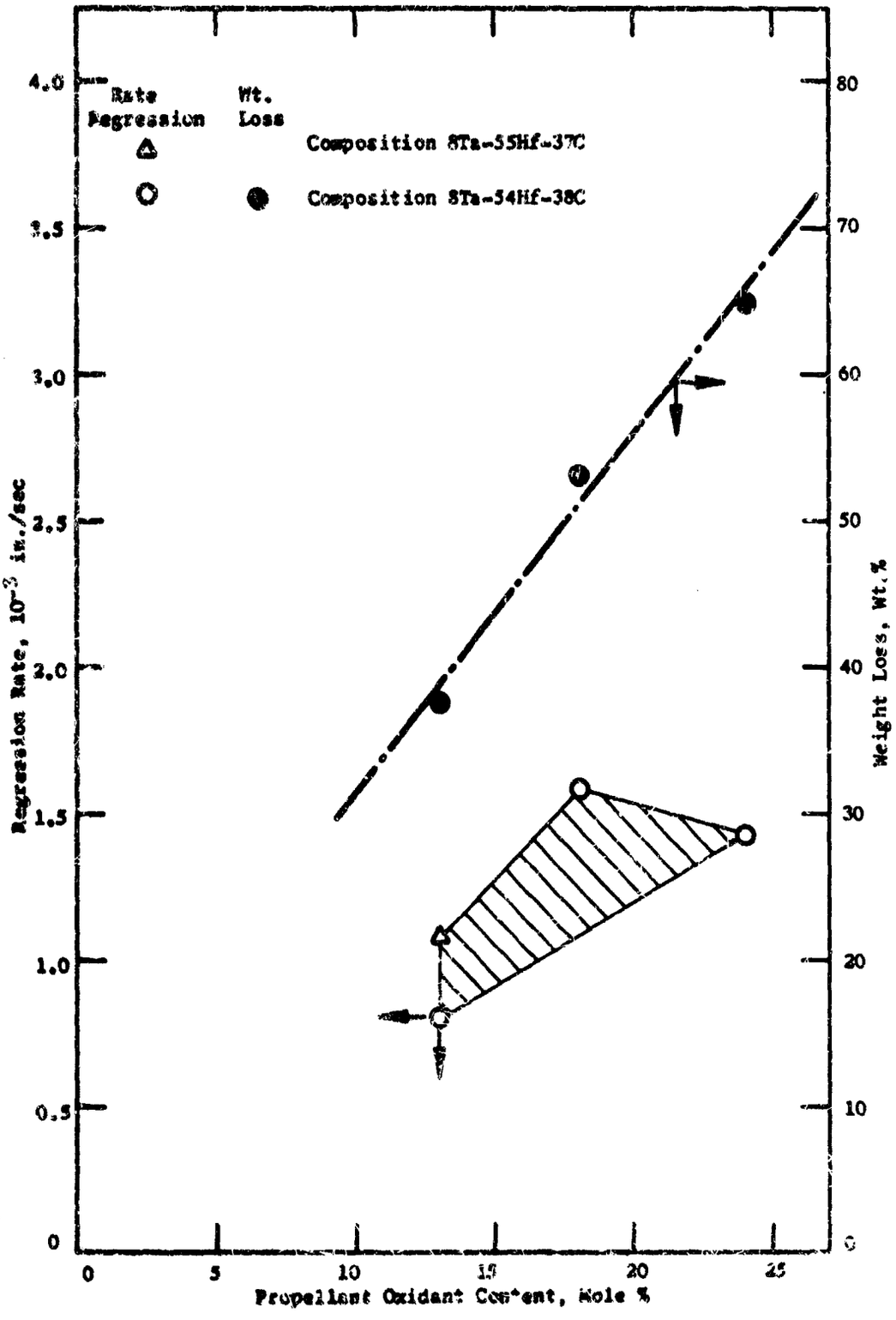

Figure 95. Effect of Oxidant Content in Solid Propellants on the Material Regression of Microscopic Inserts

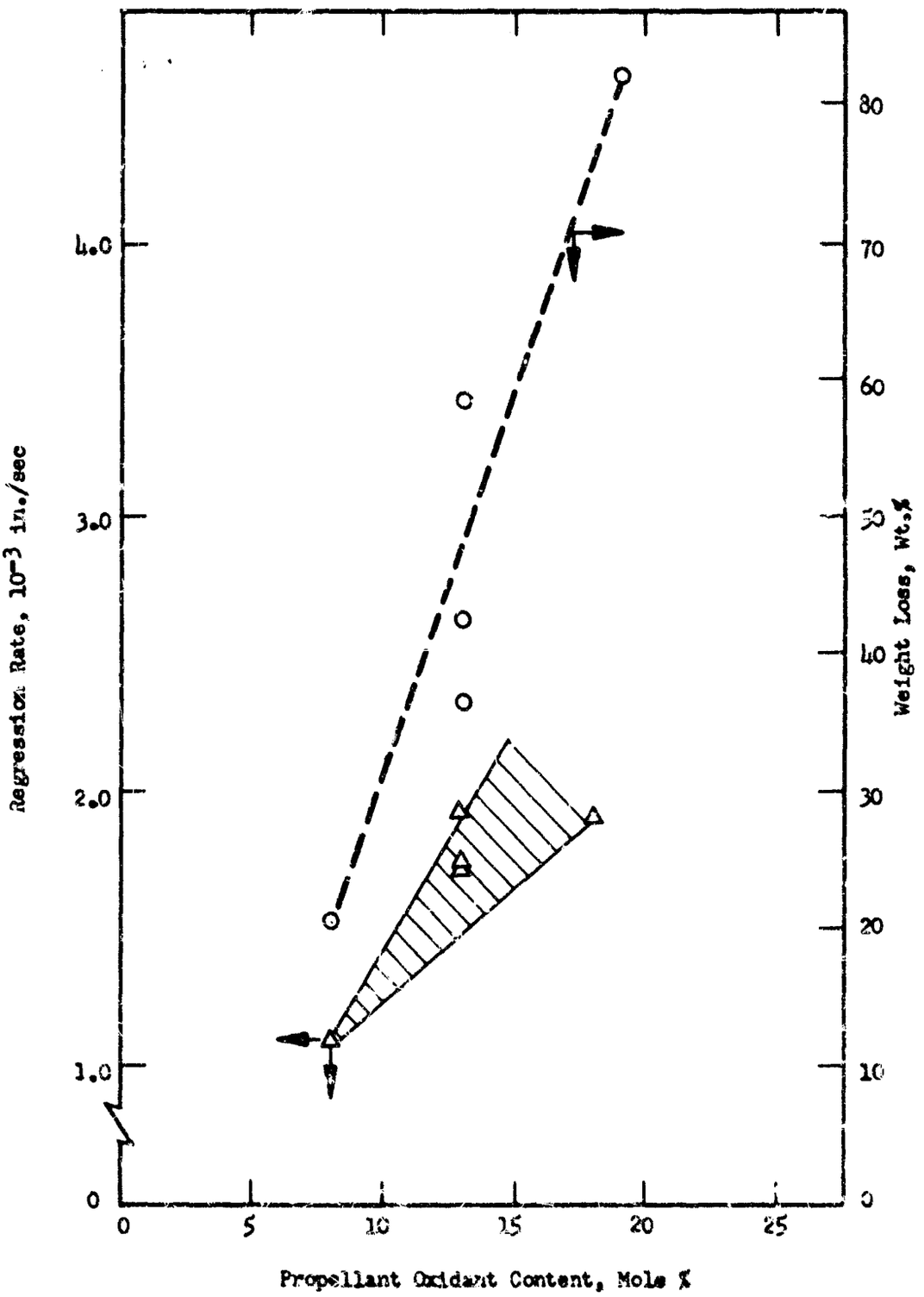

Figure 96. Effect of Oxidant Content in Solid Propellants on the Material Regression of TaC-C Hypereutectic Inserts

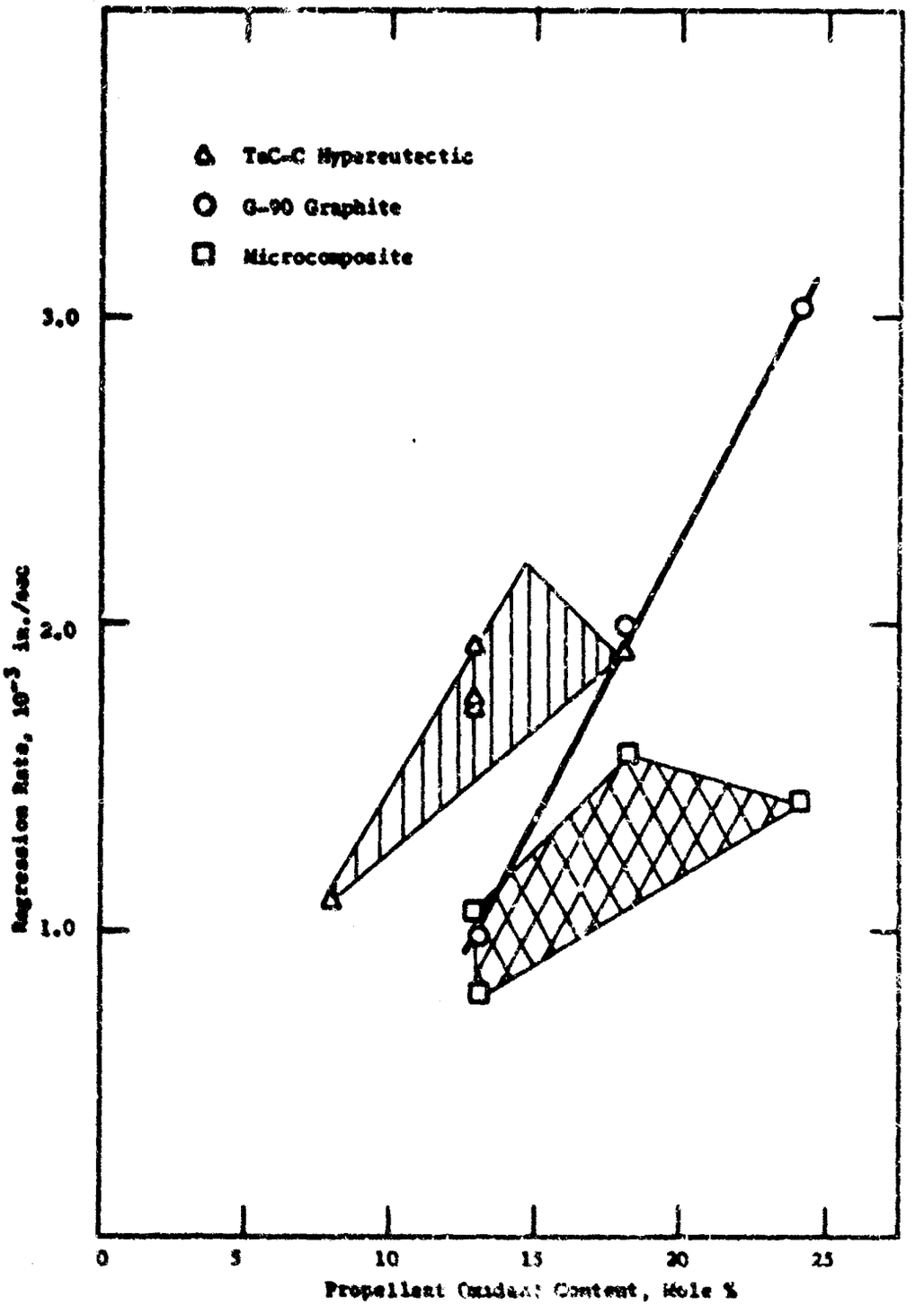

Figure 97. Comparison of [illegible] Rates for G-90 Graphite, Microcomposite [illegible] Hypereutectic Composites Under Differe[illegible]t Exhaust Chemistries

III, D, Task 4--Chemical Corrosion Evaluation (cont.)

As shown in Figure 97, the TaC-C hypereutectic composites had the highest regression rates of the three materials. The microcomposite had the lowest material removal rates. The low regression rates of the microcomposite became quite significant with the highly corrosive propellants containing 18 and 24 mole% oxidants.

3. Task Summary

The conclusions derived from propellant corrosion tests on the microcomposites, the TaC-C hypereutectic carbides, and the Grade G-90 graphite can be summarized as follows:

a. Chemical Corrosion Resistance

(1) The principal mechanism responsible for material regression in the two carbide composites was chemical corrosion caused by oxidants in solid propellant exhausts.

(2) The microcomposite carbide exhibited regression rates significantly lower than the rates obtained from the TaC-lined TaC-C hypereutectic composites and the Grade G-90 graphite, particularly for propellants with oxidant contents of 18 and 24 mole%.

b. Propellant Selection Criteria

(1) For minimal material regression in a rocket nozzle, the TaC-C hypereutectic composite should be used with propellants containing low total oxidants in the exhaust gases. A recommended maximum level would be 13 mole%.

III, D, Task 4—Chemical Corrosion Evaluation (cont.)

(2) The microcomposite has excellent resistance to corrosion due to the in situ formation of an oxide film on the flame surface. This composite can be used with solid propellants containing high contents of oxidants in the exhaust. It appears that propellants with oxidant contents up to 18 mole% could be used with the composite when minimal surface regression would be desired. The composite could be used with higher oxidant content propellants, depending upon the pressure and thermal environment of the insert.

E. TASK 5—DEMONSTRATION FIRING TESTS

The objective of this work was to design and fabricate nozzle throat inserts of the microcomposite and TaC-C hypereutectic composite systems, and to conduct demonstration firings employing the TaC-C hypereutectic composite system.

1. Nozzle Design

The nozzle was designed for use in AFRPL's 36-in.-dia chamber. The motor operating parameters were a 6500°F propellant having a total oxidant content of 13 mole%, a nominal operating chamber pressure of 700 psi, and durations up to 60 sec. The following factors were considered in the design of the nozzle:

a. Provision was made for the excessively high tensile stresses developed in the backup member due to the higher thermal expansion of the carbide insert.

b. An effective gas seal was necessary between the carbide insert and the backup structure.

III, E, Task 5--Demonstration Firing Tests (cont.)

c. The carbide insert had to be of a proper design symmetry to reduce thermal shock cracking or cracking due to notch sensitive areas.

d. The throat insert had to be reliably retained to prevent the ejection of segments should cracking occur.

Three throat insert designs were used in the program, one microcomposite and two TaC-C hypereutectic. The basic design of the nozzle is shown in Figure 98. This design was based upon thermal and stress analyses using the properties of the microcomposite, since this composite had greater tendency for thermal stress cracking in the HES thermal shock test. The thermal stress analysis took into account component geometry, boundary conditions, and pressure loads as well as the thermal profile and material properties. A finite element computer program was utilized which has the capability for solutions in the plastic range. The plastic solution is required particularly for high modulus materials such as the carbides as elastic solutions indicate thermal stress failures when none occur. To perform the plastic solution, the stress-strain relationship as a function of temperature as well as the coefficient of thermal expansion and Poisson's ratio are required. The analysis performed used the temperature profile selected at a duration where the highest temperature gradient was predicted.

The design included a 0.016-in.-thick copper spacer positioned circumferentially between the carbide insert and the graphite backup, as shown in Figure 98, to reduce the stresses in the graphite backup. The concept being that, as the insert expands during the firing, the copper softens and extrudes thus minimizing the strain induced in the graphite backup. The use of tapered mating surfaces between the carbide and the graphite backup provides retention of the insert, maintains a gas seal, and allows the insert to shift aft as the copper extrudes. In turn, the tapered surface between the graphite insert exit cone and the aft insulation assures retention of the graphite.

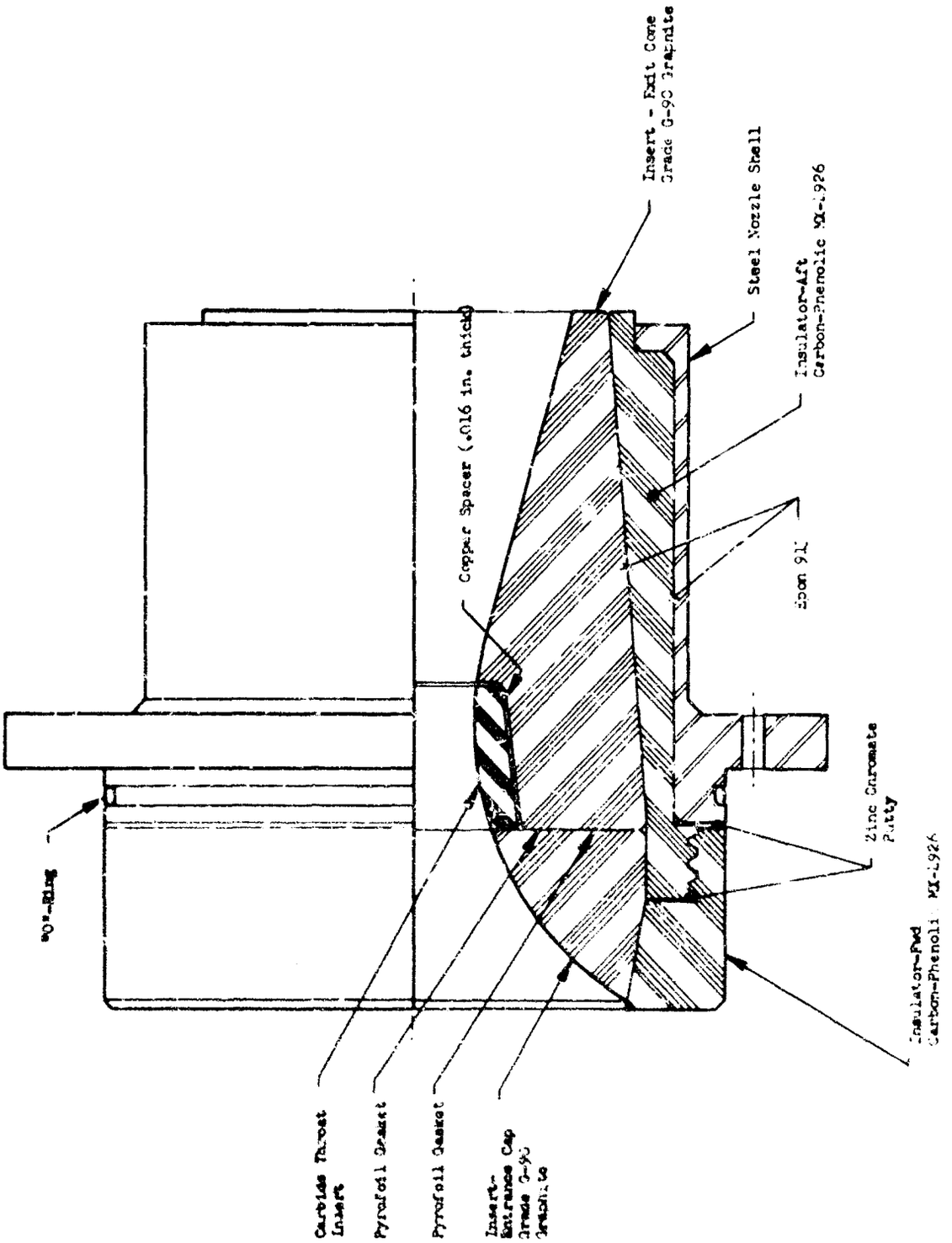

Figure 98. Design of Nozzle

III, E, Task 5--Demonstration Firing Tests (cont.)

The use of a two-piece, threaded forward and aft insulator provided ease of assembly of the carbide insert and the two graphite components. Tightening of the forward insulation assured a positive contact between the tapered mating components. All mating surfaces between the tapered graphite and carbon-phenolic components and between the steel nozzle shell and the insulators were bonded with Epon 913 to provide a gas seal. In addition, "Pyrofoil" gaskets, produced by Carbon Products Division of Union Carbide Corp., were positioned between the graphite entrance cap and the insert exit cone to further ensure a gas-tight joint. The graphite used for the entrance cap and the insert exit cone was Carborundum's Grade G-90 graphite, which is an extruded, high density, premium missile grade graphite. The material used for the tape-wrapped forward and aft insulators was carbon-phenolic MX-4926 produced by Fiberite.

2. Throat Insert Fabrication

a. Microcomposite Inserts

The fabrication of the microcomposite nozzle insert from the 8Ta-55Hf-37C composition was accomplished by hot-pressing, using the parameters previously established during the development phase for this composite system. One trial insert was initially fabricated to establish a process whereby the insert could be hot-pressed to the approximate dimensions required by the insert design shown in Figure 99. During hot-pressing of this insert, a mixture of lampblack and graphite chips was used as a core material in the center of the insert to provide a hollow cylindrical compact. This insert cracked radially at four positions approximately 90 degrees apart. An analysis of the failure indicated that the carbon powder in the core densified during hot-pressing and restricted the shrinkage of the carbide insert during cooldown.

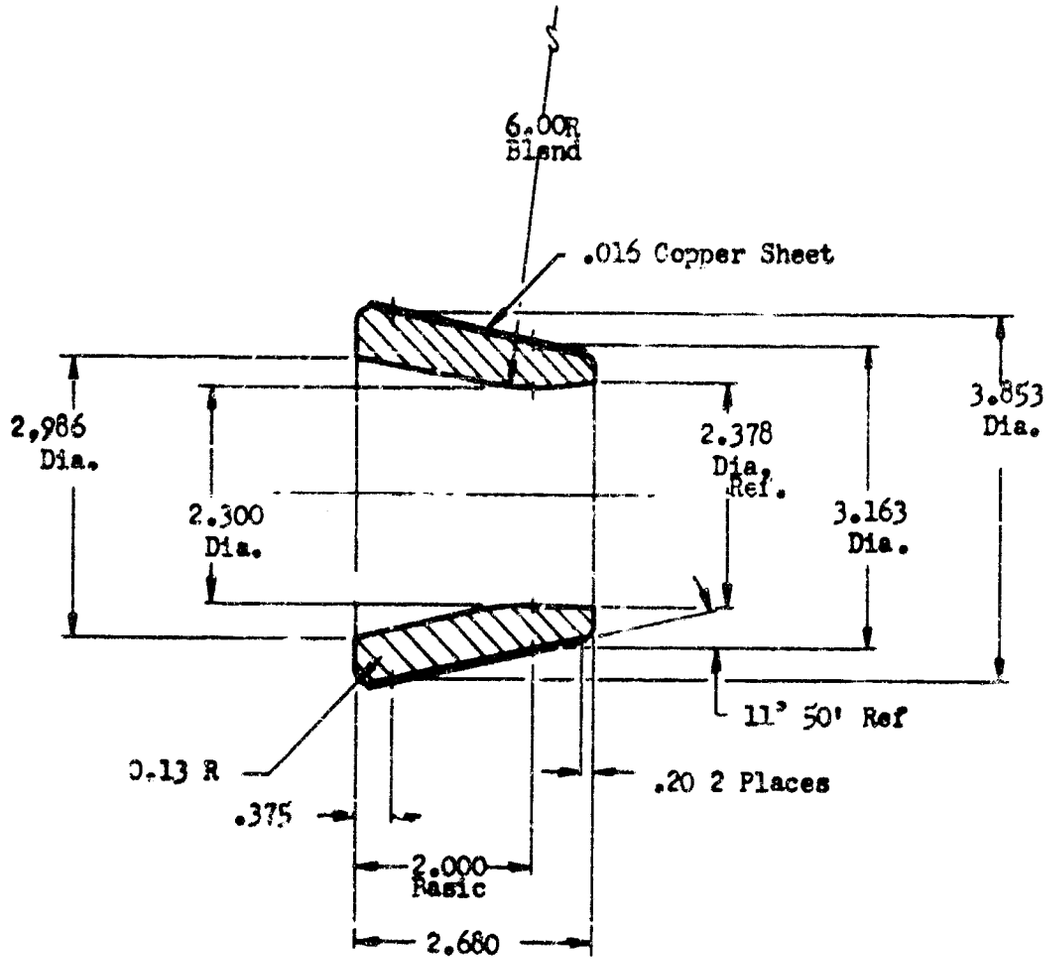

Figure 99. Design of Microcomposite Throat Insert

III, E, Task 5--Demonstration Firing Tests (cont.)

Fine powdered lampblack was used for the core material while pressing the first nozzle insert. This same powder had been used successfully in hot-pressing TaC composites with ID cavities. Pressure was relieved very slowly after the end of the cycle and the cooldown rate was carefully controlled. The mold was sectioned for easy removal from the insert to eliminate any possibility of cracking the insert during mold removal. This insert was much improved but had two radial cracks approximately 80 degrees apart. The cracks initiated on the OD and propagated to the core.

For the fabrication of the second nozzle insert, a thin graphite tube was used in lieu of the powder to form the ID. The upper and lower rams were slip-fitted to the tube to allow compaction to occur during hot pressing. During cooldown, the carbide insert collapsed the tube and prevented the insert from cracking. An insert, 4.2-in. OD by 2.0-in. ID by 3.0-in. long, was successfully hot-pressed using this technique. However, during machining to remove the graphite ID mandrel, the insert cracked longitudinally. The failure was probably due to the existence of microcracks or high residual stresses during cooldown. Microstructural examinations showed that the metal alloy phase was coarser, Figure 100, than the typical, finely divided acicular structure characteristic of the microcomposites made in smaller sizes.

Two flexural specimens were machined from the insert and tested at ambient temperature. The flexural strengths of 80,080 psi and 75,020 psi were significantly higher than the typical values of 50,000 psi previously obtained for this composition. This high strength and density of 12.7 gm/cm^3, which is in the characteristic density range of 12.6 to 12.7 gm/cm^3 for this composite, confirmed that the quality of the microcomposite had not deteriorated because of scale-up. However, because of the success of the TaC-C hypereutectic nozzle inserts discussed in the next section, further work to prevent cracking of the microcomposite inserts during handling was discontinued.

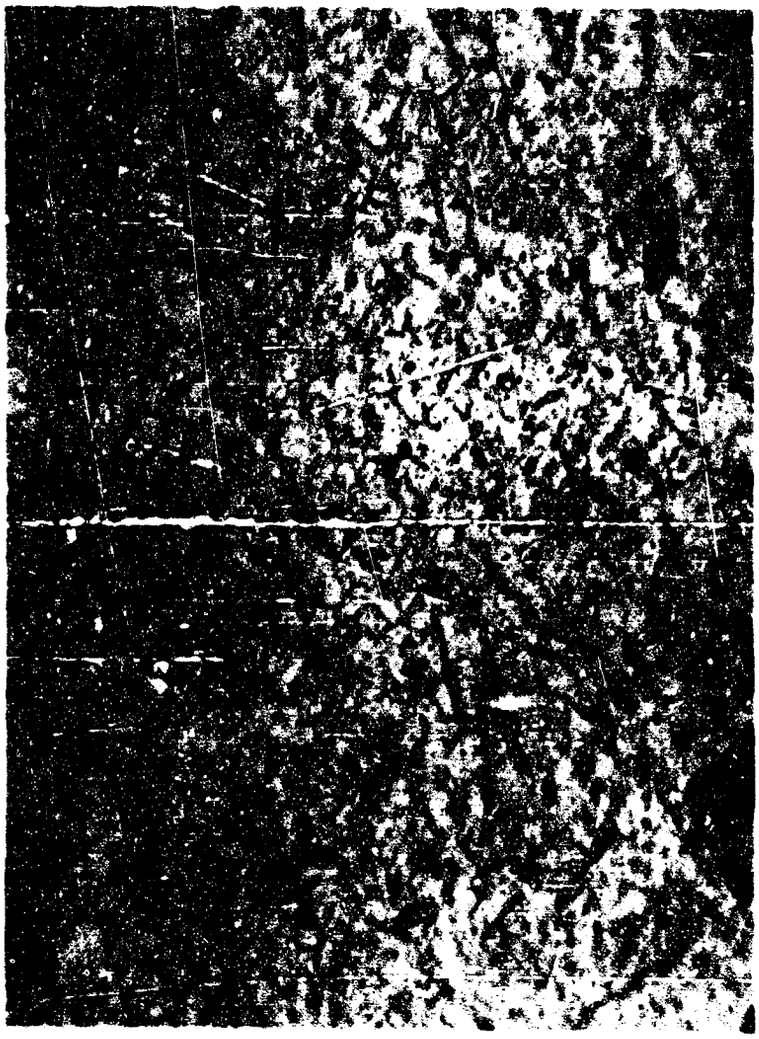

750X

Figure 100. Microstructure of Hot-Pressed Insert Composition 8Ta-55Hf-37C, Showing Coarse Metal Precipitate

III, E, Task 5--Demonstration Firing Tests (cont.)

b. TaC-C Hypereutectic Inserts

The diffusion-formed TaC liner previously discussed for the TaC-C hypereutectic substrate was not incorporated into the insert design because of a reduction in the anticipated propellant flame temperature (6800 to 6500°F). The heat transfer analysis conducted on the nozzle with the 6500°F flame temperature indicated that the surface temperature would not exceed 5800°F, well below the 6230°F melt temperature of the TaC-C hypereutectic. Two designs were used for the throat inserts, a segmented design and a single-piece design.

(1) Segmented Throat Insert Design

Because of difficulties encountered during the melting of the large compacts required for a single-piece throat, the first throat insert was fabricated in two segments as shown in Figure 101. The segment used for the entrance section was 1-in. long while the segment containing the throat was 1.7-in. long. A composition near the eutectic was selected to provide the best resistance to regression. The appearance of the segmented insert after machining is shown in Figure 102.

(2) Single Throat Insert Design

The second throat was fabricated from a single segment as shown in Figure 101. In this design, the length of the insert was shortened and the angle of the taper at the OD was reduced to provide a more uniform wall thickness in comparison to the segmented throat insert. As the chamber pressure obtained during the firing of the segmented throat insert was higher than desired, the throat diameter for the single segment design was increased from 2.300 in. to 2.370 in. A 9 v/o graphite flake composition was

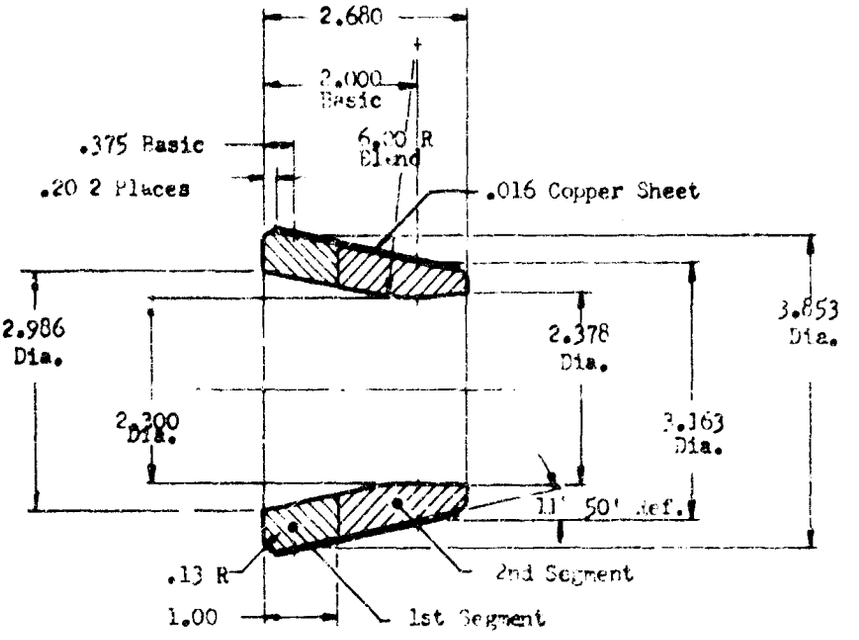

Segmented Throat Design

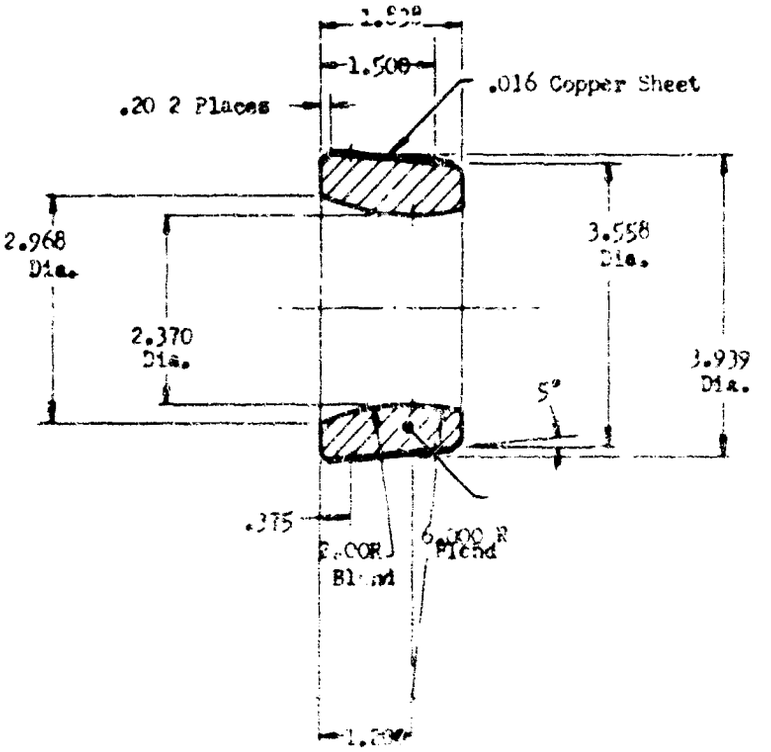

Single Throat Design

Figure 101. Design of TaC-C Throat Insert

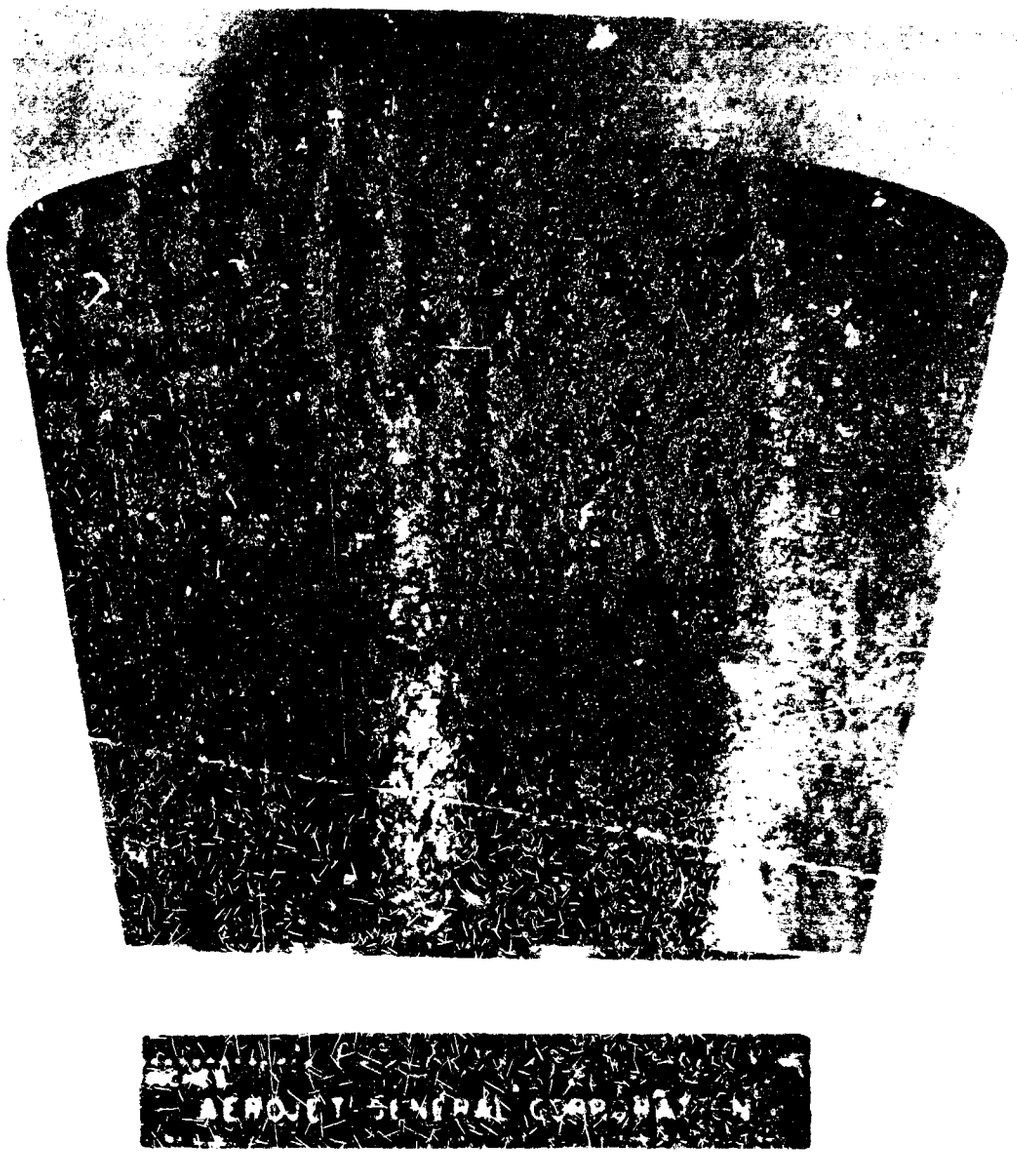

Figure 102. View of [illegible] TaC-C Hypereutectic Throat Insert

III, E, Task 5--Demonstration Firing Tests (cont.)

selected for this insert on the basis of its excellent overall performance in the HES subscale thermal shock and corrosion tests. The appearance of the insert after machining is shown in Figures 103 and 104.

3. Motor Test Firings

The two TaC-C hypereutectic nozzle throat inserts were assembled into nozzles and test fired at the Air Force Rocket Propulsion Laboratory, Edwards, California, using the 36-in. char motor. Measurements of chamber pressures, thrust, and thermocouple readouts were recorded for the duration of each test. The significant test conditions for both firings are contained in Table XXI. A brief summary of each firing is presented below.

a. Segmented Throat Insert

The chamber pressure vs firing duration is shown in Figure 105. The chamber pressure on ignition rose from 808 psi to a maximum of 834 psi after 16 sec. From 16 to 38.16 sec, small fragments were observed to be randomly ejecting from the nozzle. This occurrence was confirmed by the linear decay in chamber pressure to 665 psi at 38.16 sec at which time a large number of fragments were observed. An instantaneous rise in the thrust trace confirmed the ejection of a structural member of the nozzle. The maximum thrust obtained on the motor was 5856 lb at 15.8 sec. The data obtained from the chromel-alumel thermocouple were erroneous and therefore could not be utilized.

b. Single Throat Insert

The firing performance of this nozzle closely followed theoretical predictions. As shown in Figure 106, the chamber pressure decreased slightly from 750 to 711 psi over the 43-sec firing duration. A maximum thrust of 5514 lb at 5.9 sec was recorded.

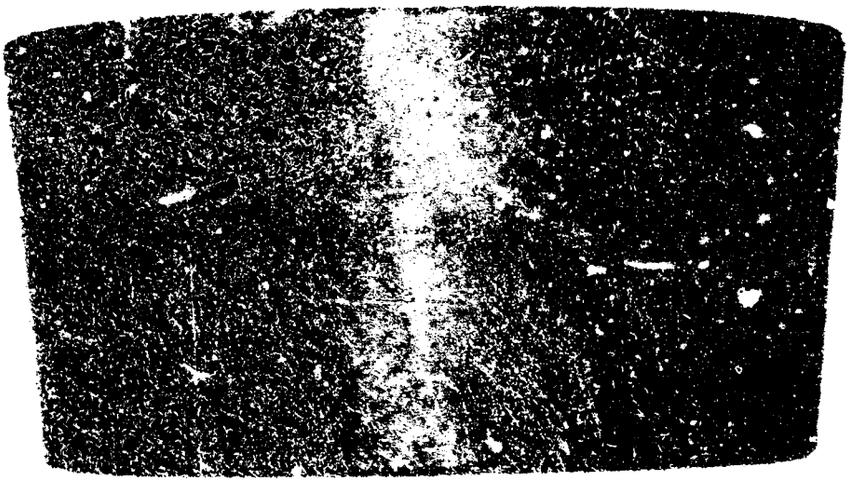

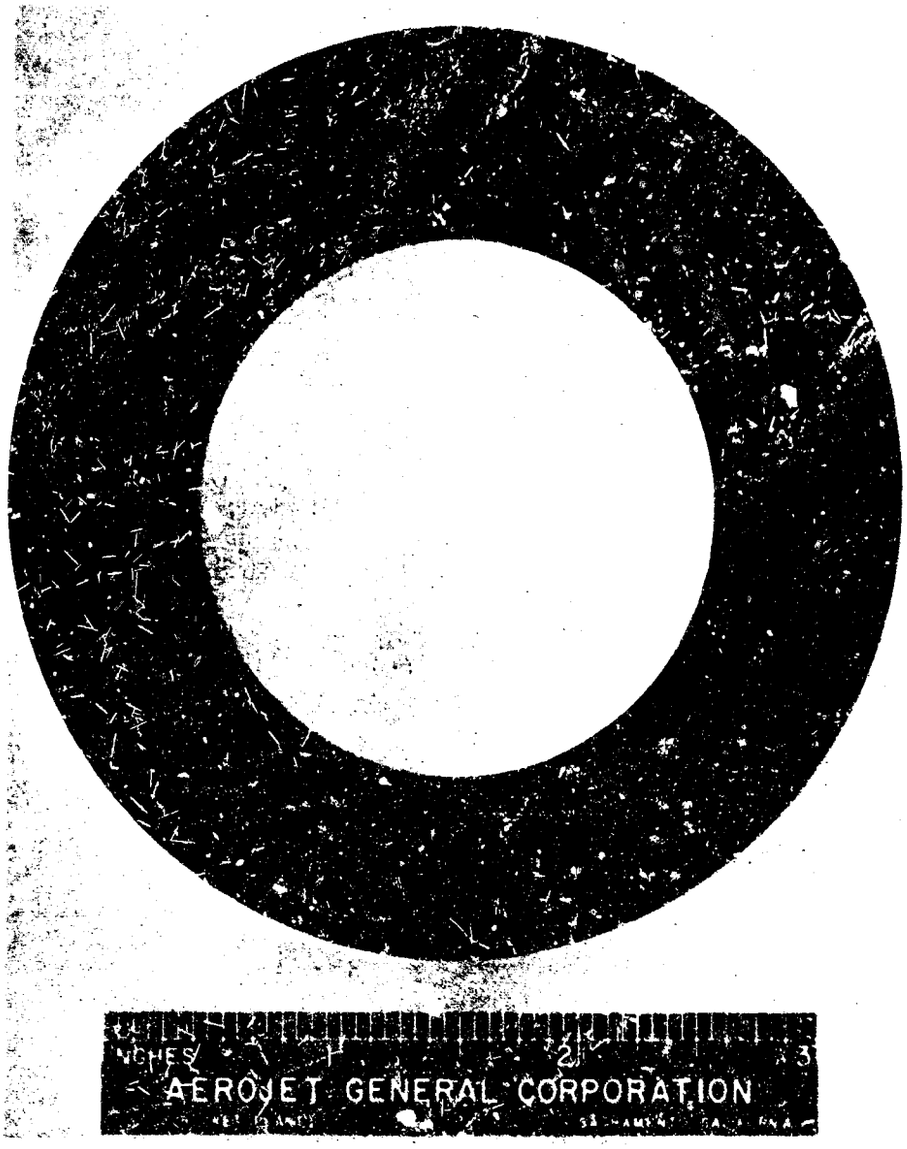

Figure 104. End View of TaC-C Single Throat Insert

TABLE XXI

MOTOR TEST CONDITIONS

	Type of Insert	Throat Diameter, in.	Propellant Flame Temperature, °F	Duration, sec	Chamber Pressure After Ignition, psi	Chamber Pressure Prior to Tailoff, psi	Maximum Thrust, lb	Type of Thermocouple	Comments
1.	Segmented TaC-C Hypereutectic	2.300	6500	38.16 (See comment)	803	665	5856	Chromel-alumel Located 1 in. below flame surface of throat	Second segment of throat insert ejected at 38.163 sec
2.	Single TaC-C Hypereutectic	2.370	6500	43	750	[illegible]	5514	Chromel-alumel Located 1 in. below flame surface at the throat	

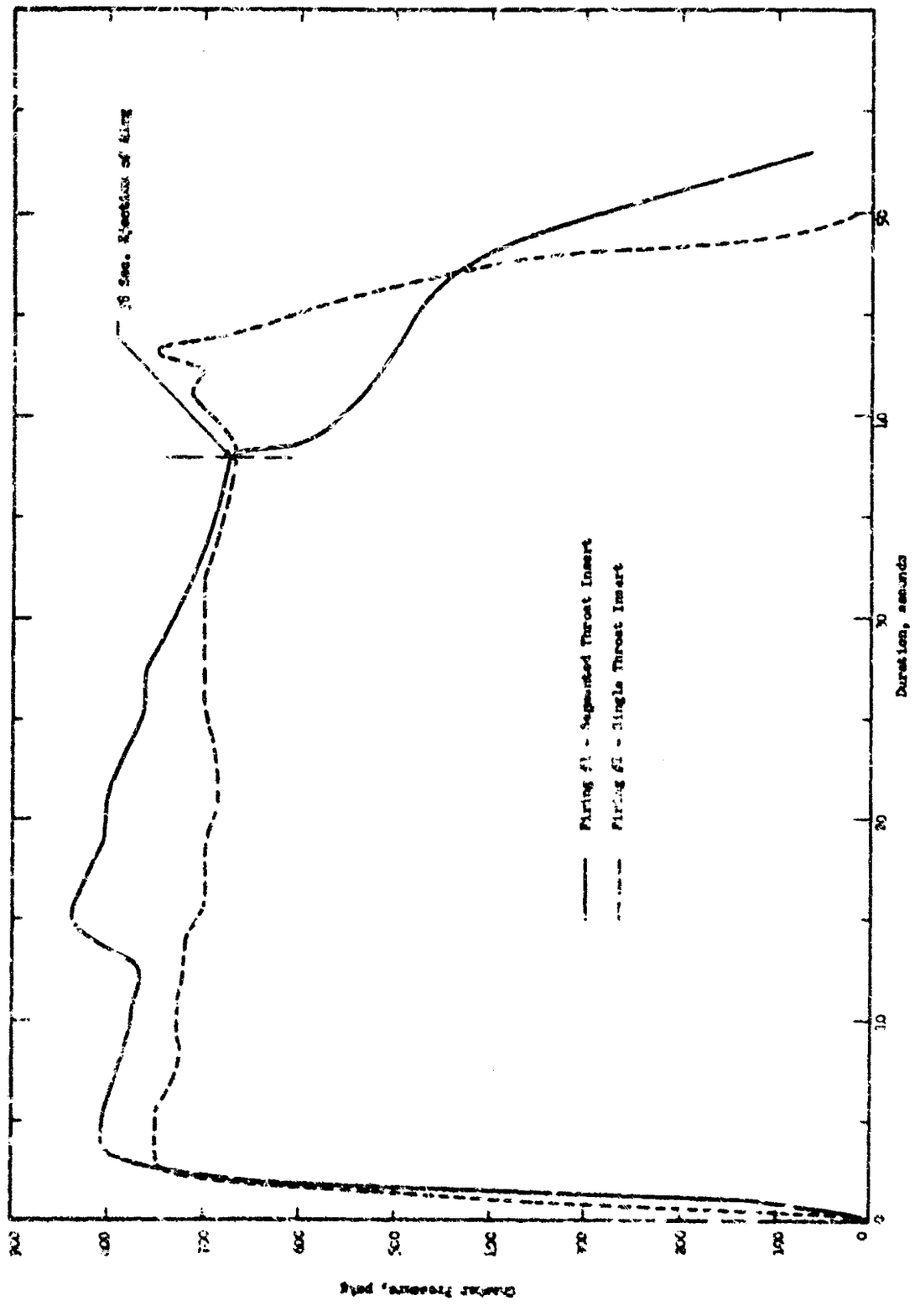

Figure 105. Chamber Pressure vs Duration for TaC-C Nozzles

III, E, Task 5--Demonstration of Firing Tests (cont.)

A continuous readout was obtained from the chromel-alumel thermocouple located 1 in. below the flame surface of the throat. A correlation of these data with the theoretical analysis is discussed in the following section.

4. Postfire Analyses

a. Segmented Throat Insert

The postfire examination of the nozzle revealed that the throat segment (No. 2) had been ejected and the graphite exit cone heavily eroded.

The appearance of the nozzle as viewed from the exit cone is shown in Figure 106. Severe graphite regression was noted in the region where the throat segment had been ejected and in the exit cone. The G-90 graphite entrance cap revealed numerous radial cooling cracks as shown in Figure 107. The entrance segment of the throat (No. 1 insert) was removed intact and showed minimal structural degradation. Figure 108 shows the excellent appearance of the insert as viewed from both surfaces. Four equally spaced cooling cracks running longitudinally developed around the circumference. The occurrence of these cracks on cooldown was established by the sharp and noneroded edges along the crack paths at the flame surface.

The regression profile of the nozzle components is shown in Figure 109. The G-90 graphite entrance cap underwent a significantly higher material regression ranging from 0.09 to 0.19 in. in comparison to the TaC-C hypereutectic entrance segment which had a total regression of 0.025 in. around 80% of the circumference. The remaining 20% of the circumference underwent uneven and higher removal rates ranging from 0.1 to 0.175 in. This corresponds to a regression rate of 0.66 mils/sec for the major portion of the

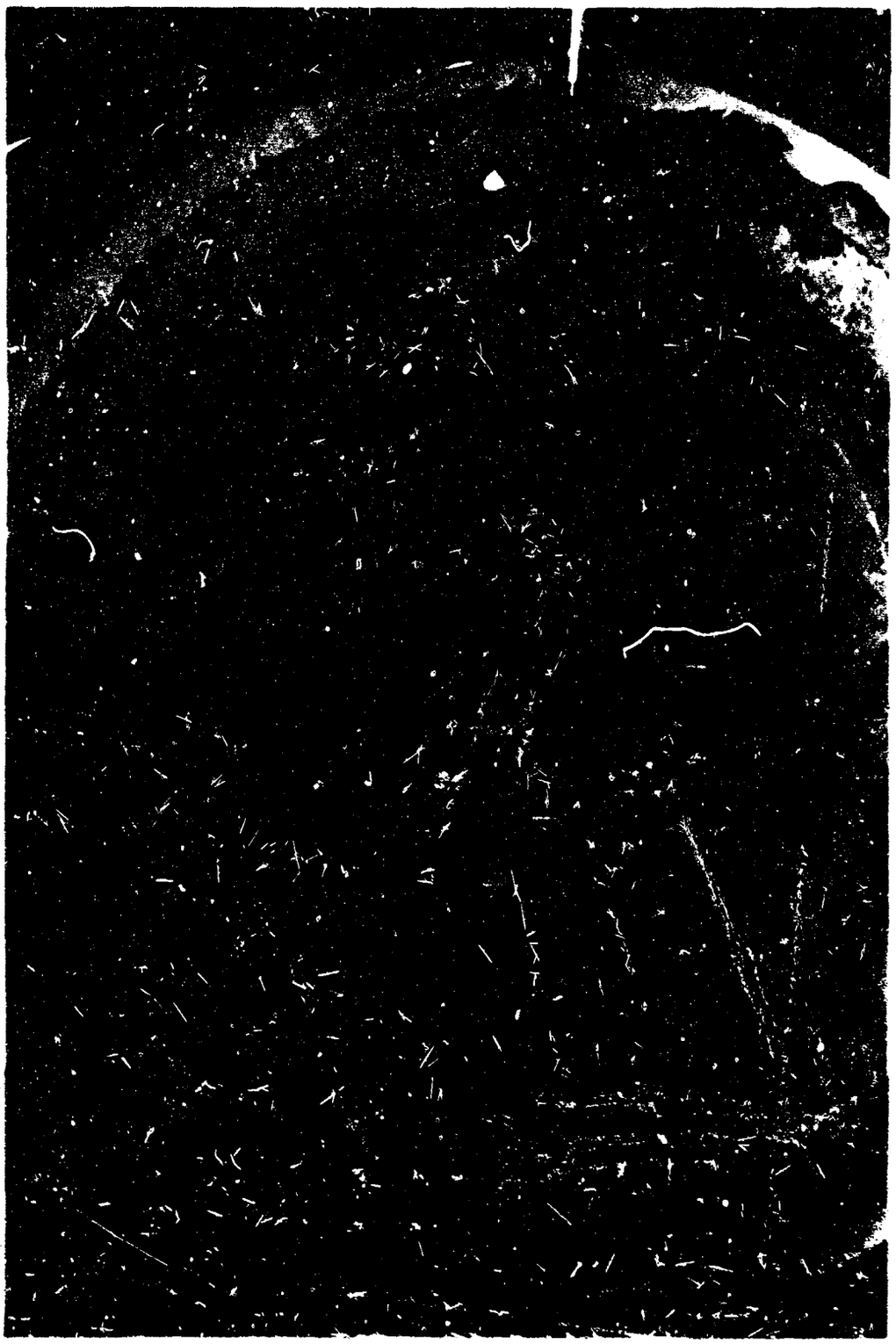

Figure 106. Exit View of Segmented Nozzle After Firing

Figure 107. Cool Down Cracking in G-90 Graphite Entrance Cap of Segmented Throat Nozzle

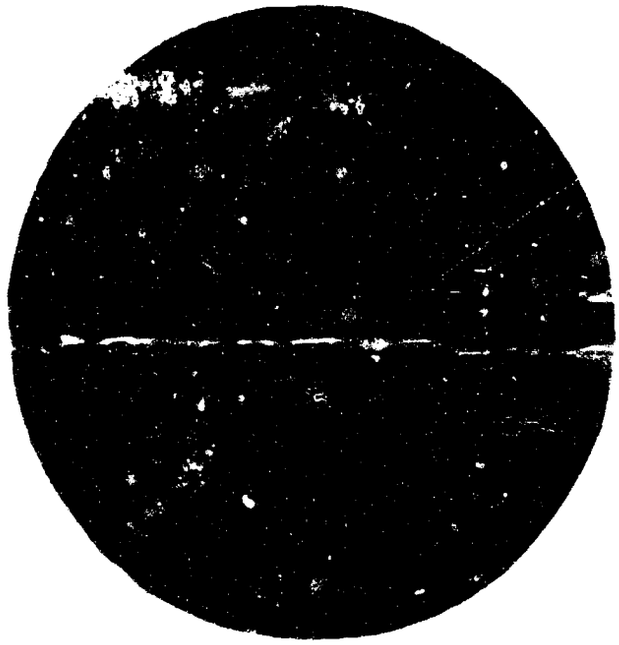

a. View of Entrance Region

L-503

b. Exit View of Segment (Interface between First and Second Segment) Cracks developed on Cool-Down

Figure 108. Views of the First Segment of the TaC-C Hypereutectic Throat Insert after Testing

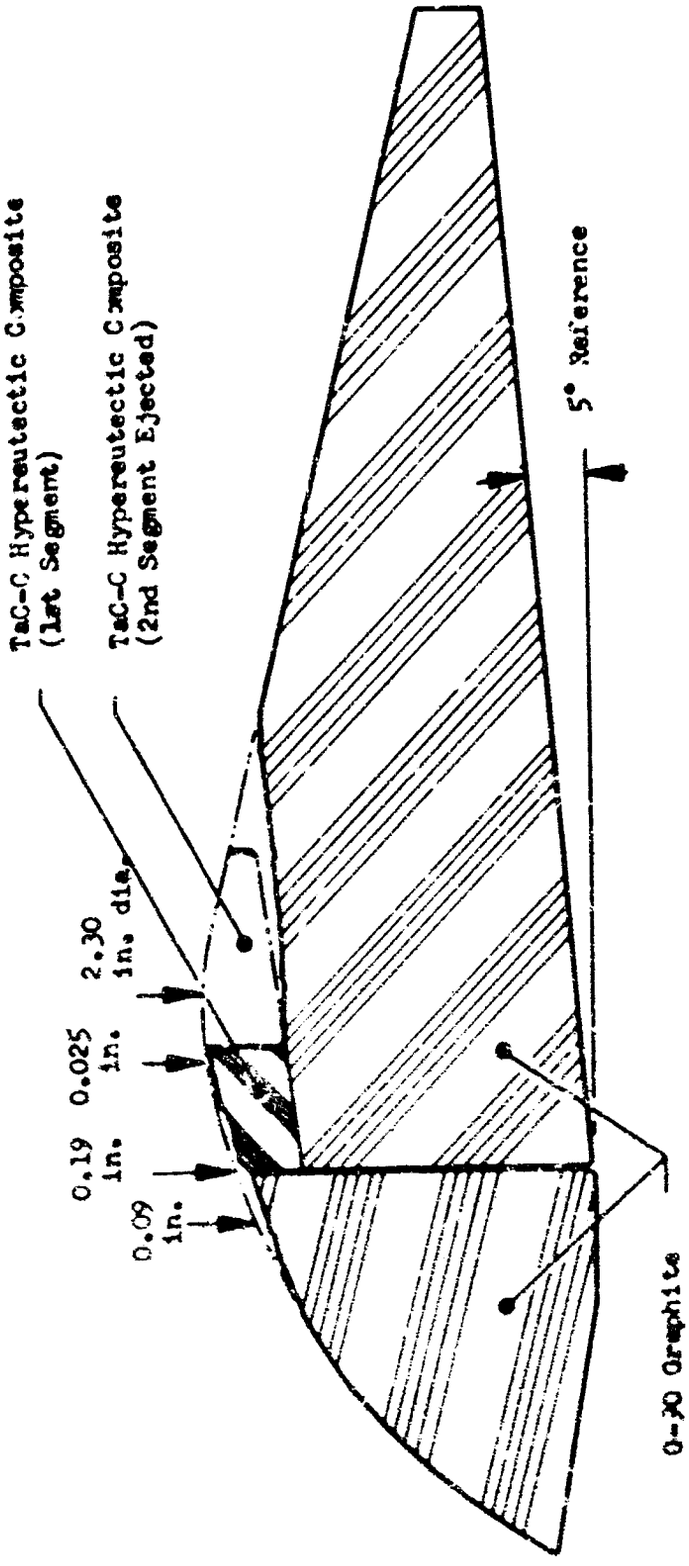

Figure 109. Regression Profile of Segmented TaC-C Hypereutectic Nozzle

I.F, E, Task 5--Demonstration of Firing Tests (cont.)

carbide insert and a range of 2.4 to 5.0 mils/sec for the graphite entrance cap. The graphite exit cone was heavily eroded because of the turbulence of the flow after the throat segment was ejected.

The carbide entrance segment was sectioned longitudinally at locations 120 degrees apart. Metallographic examinations supplemented by carbon analyses and density measurements were used to evaluate the material at these locations. Results of these tests indicated that the major portion of the entrance segment was near the eutectic composition in the range from 2 to 7 v/o graphite flake. The portion of the segment that experienced high material regression had a high carbon content region of approximately 19 v/o graphite flake.

A cross-sectional view and corresponding microstructures of the entrance segment in this high carbon content region is shown in Figure 110. The material in Region A had a typical eutectic composition as shown by the microstructure in Figure 110b, while the material in Region B contained a high graphite flake content as shown in Figure 110c. The primary graphite flakes in this region were abnormally long as shown in Figure 110a. Some microcracking was observed along the planes of the flakes. The flame surface in this high carbon region appeared to have been eroded by small fragments being cleaved along the planes of the large graphite flakes.

Since none of the material from the ejected throat segment was found, the mode of failure of this component had to be postulated based upon what information could be obtained from the other components. As the design of the nozzle was based upon the carbide insert being under a compressive load all during the firing, excessive or uneven material loss in the throat region such as experienced in the entrance segment could have resulted in buckling and ejection of the throat segment. The throat segment was more susceptible to this type of failure because it was thinner than the entrance segment.

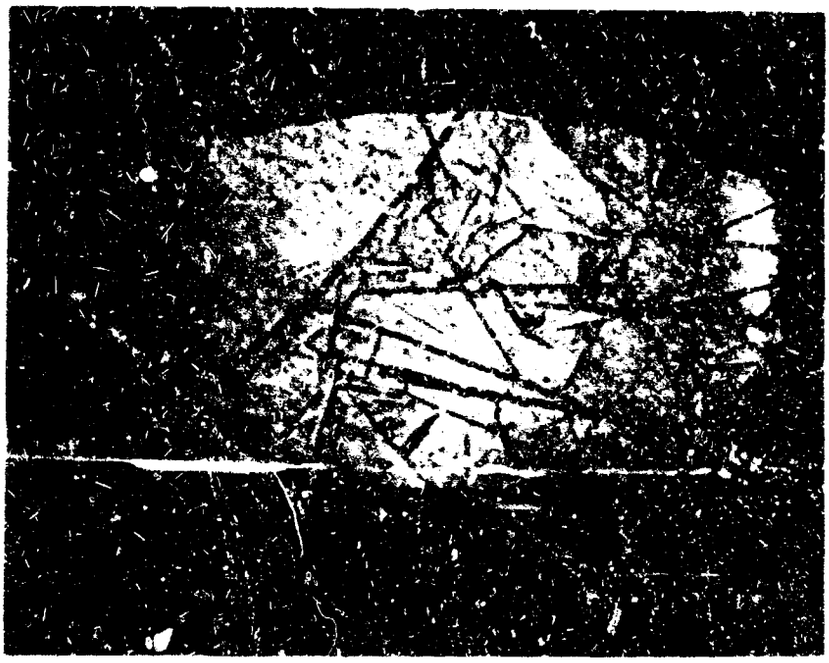

a. Cross-sectional View of Entrance Segment where Material Regression was Excessive

b. Typical Eut[illegible] Matrix [illegible] Region A

c. Typical Hypereutectic Matrix [illegible] Region B

Figure 110. Cross-Sectional View of Nozzle Segment and Related Microstructures Taken at the Region of High (19 v/o) Graph[illegible]e Flake

III, E, Task 5—Demonstration of Firing Tests (cont.)

b. Single Throat Insert

The appearance of the nozzle as viewed from the entrance segment is shown in Figure 111. The G-90 graphite in the region adjacent to the throat insert underwent a significant amount of material regression in comparison to the throat insert. Numerous radial cracks developed on cool-down in the graphite. A view of the throat insert through the exit cone is shown in Figure 112. The white region in this figure indicates where a thin segment of the carbide insert adjacent to the graphite exit cone was ejected during the firing.

Views of the insert after removal from the nozzle are shown in Figures 113 and 114. The material loss in the entrance section was very small. Localized surface pitting occurred in several regions in the entrance section. Four very fine, longitudinal cracks developed in the insert during cooldown. A very irregular, circumferential crack pattern developed on the OD and extended approximately halfway around the circumference as shown in Figure 115. This crack extended to the flame surface just aft of the throat. The eroded edges along the crack indicated that this cracking occurred during the firing. Fine hairline cracks also developed randomly over the entire OD, Figures 113 and 116. Despite these cracks, the insert remained solidly intact after removal from the nozzle.

Spectrographic and X-ray diffraction analyses were made on residue removed from the interior of the cracks to establish whether cracking occurred during the firing. No evidence of combustion products such as Al_2O_3 was found within the cracks. As would be expected, the existence of Al and Si compounds were detected on the flame surface of the insert. The white coating on the aft end surface of the insert where a fragment was ejected was identified as HfN_2O_5.

Figure 111. [illegible] View of Nozzle with [illegible] Throat Insert

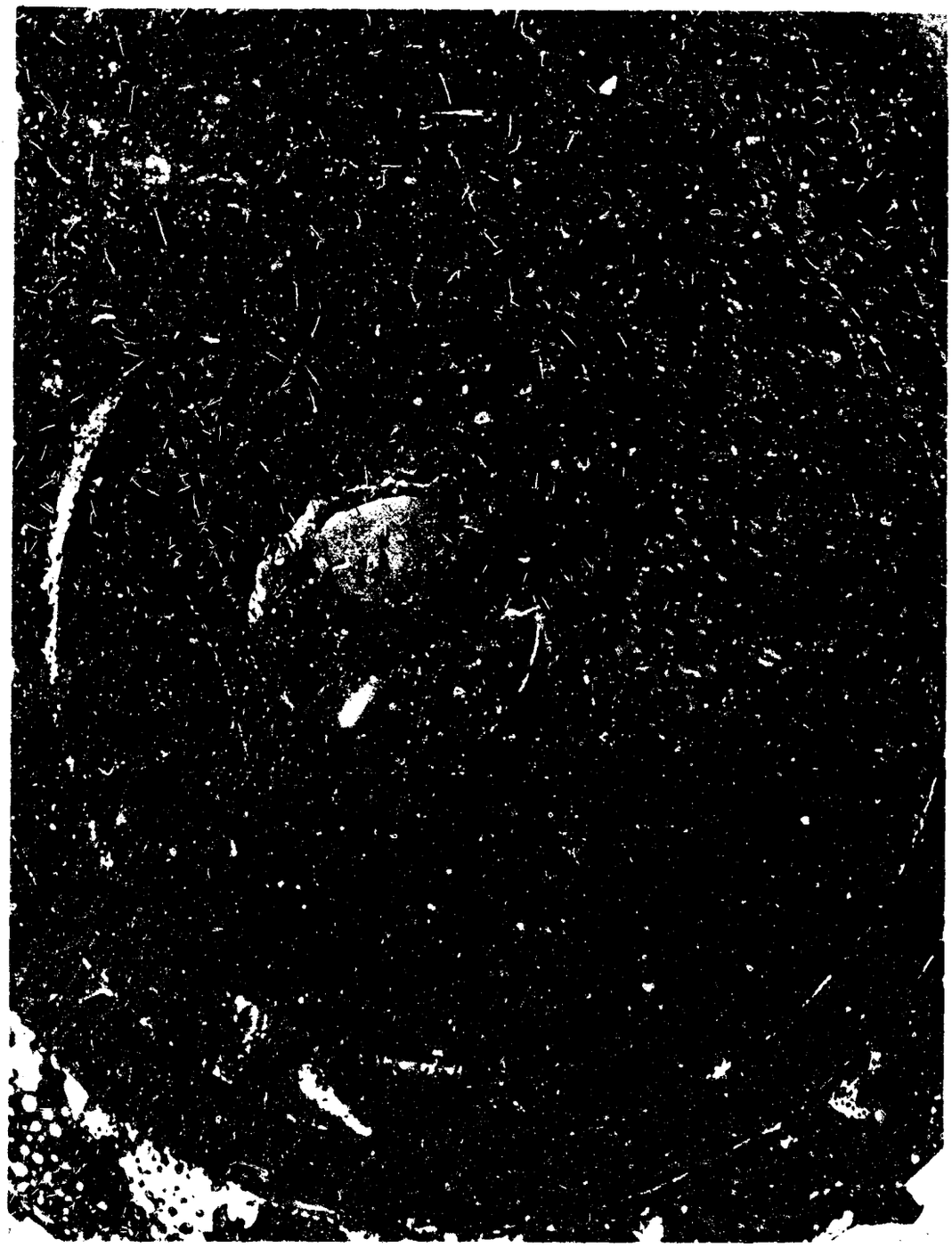

Figure 112. Exit Section View of Nozzle with a TaC-C Single Throat Insert

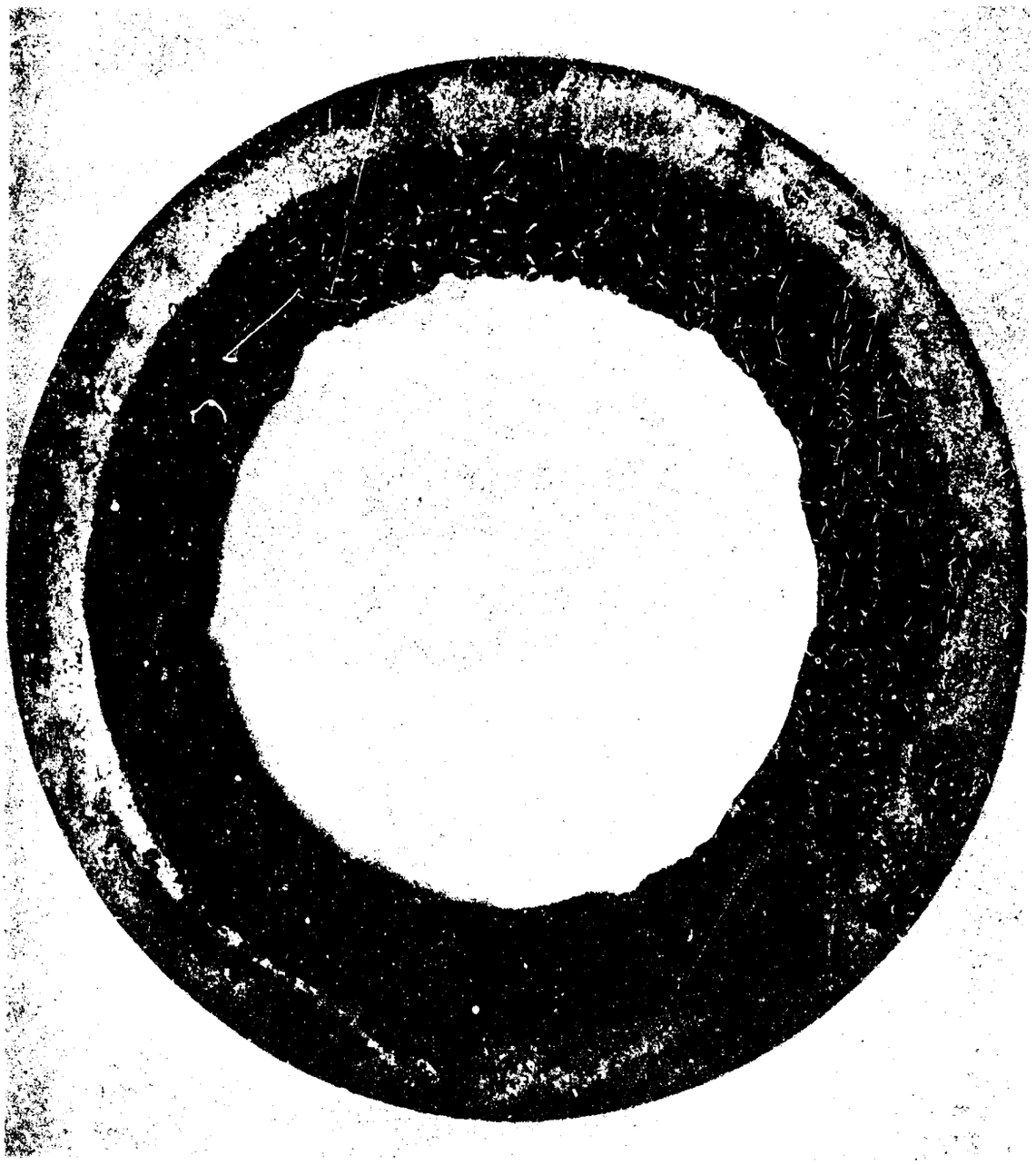

Figure 113. Entrance View of TaC-C Throat Inserts

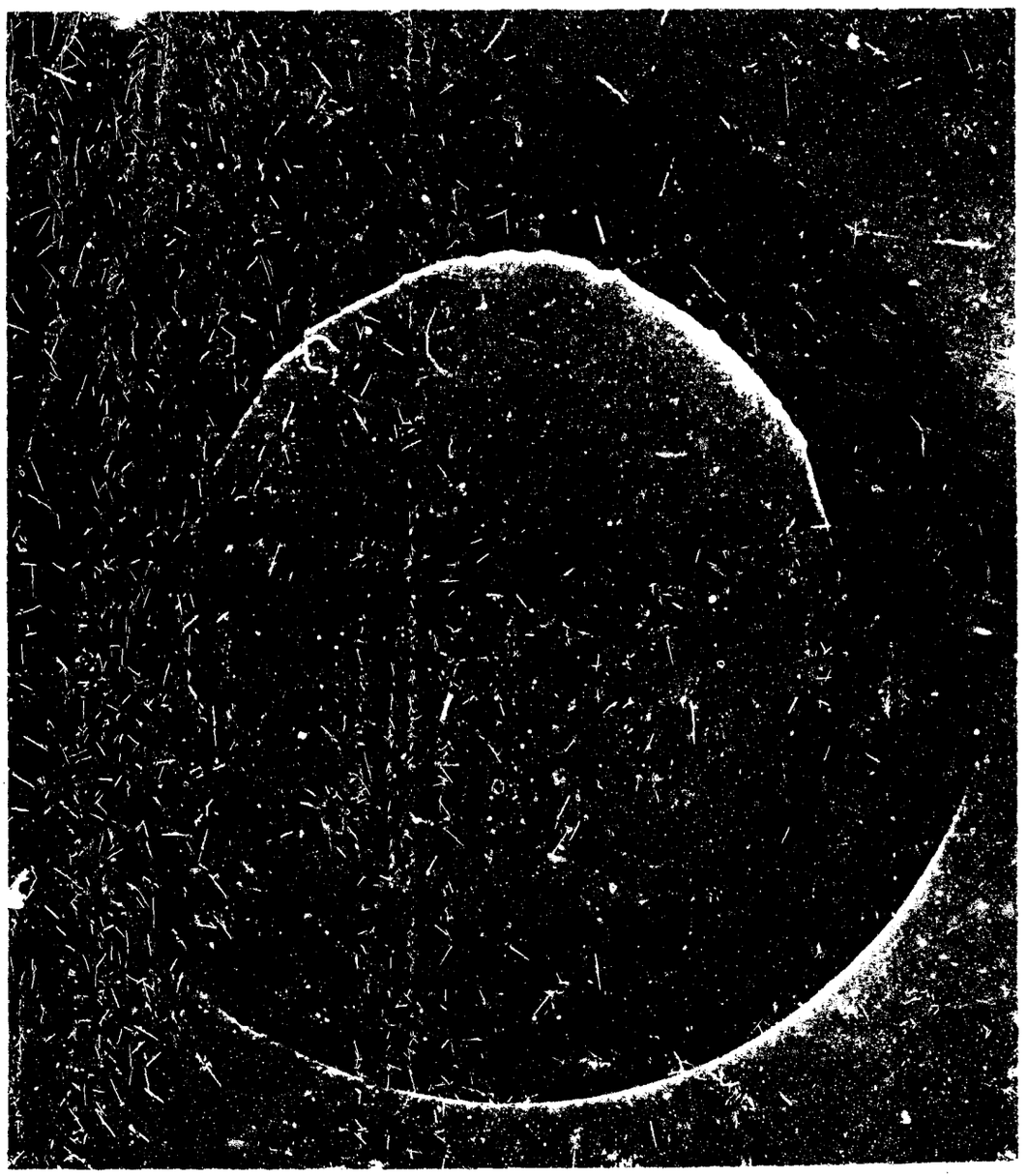

Figure 114. Exit View of TaC-C Throat Insert

Figure 115. View of TaC-C Insert Showing Circumferential Cracking

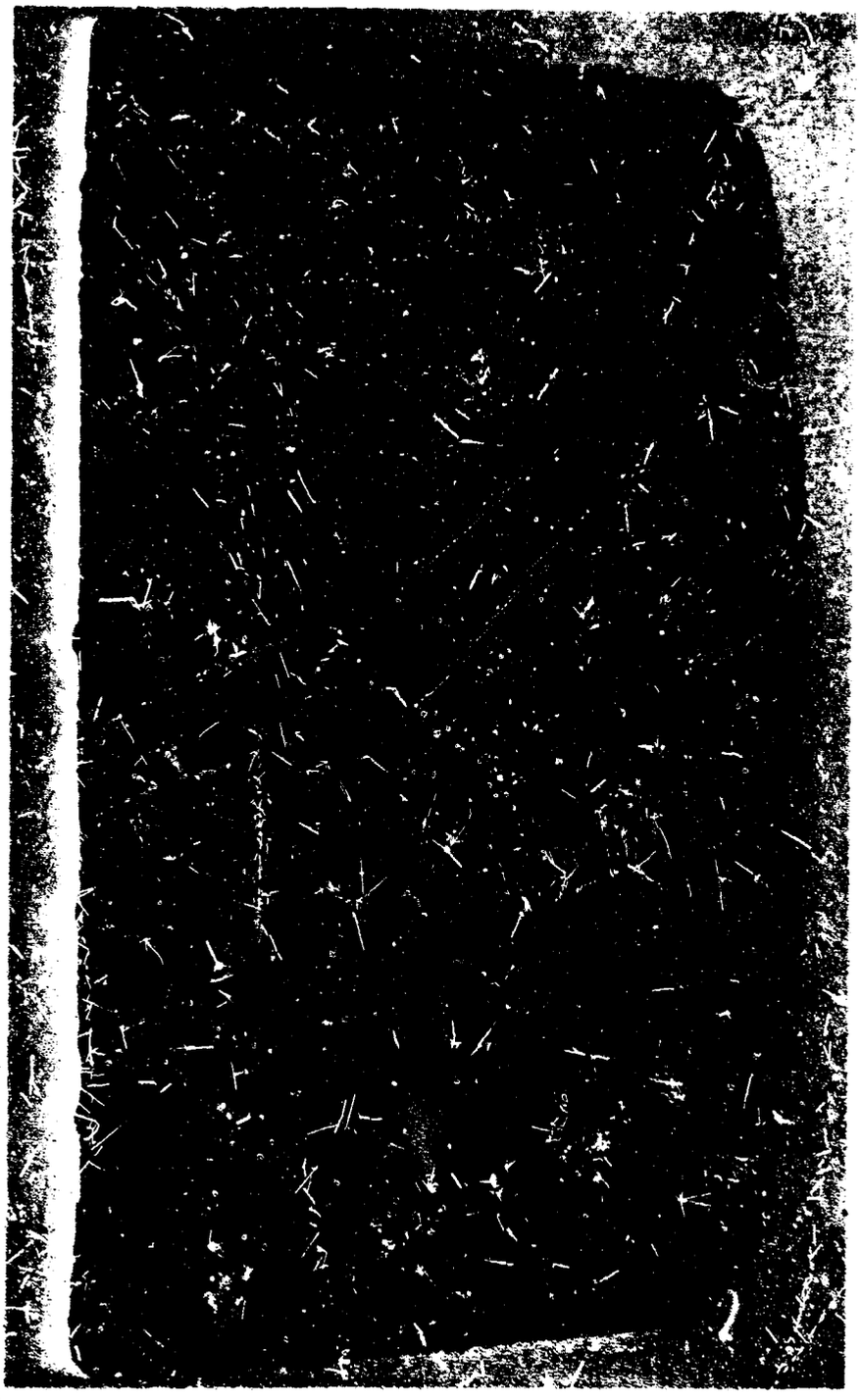

Figure 116. Opposite OD View of TaC-C Insert where only Cooling Cracks were Observed

III, E, Task 5--Demonstration of Firing Tests (cont.)

Figure 117 shows the regression profile of the nozzle components. The G-90 graphite in the entrance cap and exit cone experienced high material regression in comparison to the throat insert. The regression rates for the graphite components varied from 1.5 to 4.4 mils/sec, while the carbide insert had a regression rate which varied from 1.06 mils/sec at the throat to a maximum of 1.6 mils/sec at the exit end of the insert. This low rate makes this composite material very acceptable for the ballistic requirements of nearly all high-performance solid propellant motors.

The regression rate in the throat was slightly lower than the rates, 1.73 to 1.93 mils/sec, obtained in the HES rocket motor simulation tests for the same propellant oxidant content. This variance in regression rates is undoubtedly due to differences in boundary layer conditions and the diffusion rates of corrosive gas species across the boundary layer. The presence of aluminum oxide in the propellant exhaust did not appear to increase the regression rate in comparison to the HES tests which contained no aluminum oxide in the gas stream.

The carbide insert was sectioned longitudinally at locations 120 degrees apart. At each location, the entire cross-section of the throat was examined metallographically, and density and carbon content measurements were made. Microstructure examinations showed a uniform distribution of graphite flakes as shown by a typical microstructure in Figure 118a. Cracks were also observed to terminate upon striking a graphite flake as shown in Figure 118b.

A summary of the results of carbon analyses and density measurements to establish compositions at the three circumferential locations is shown on the following page.

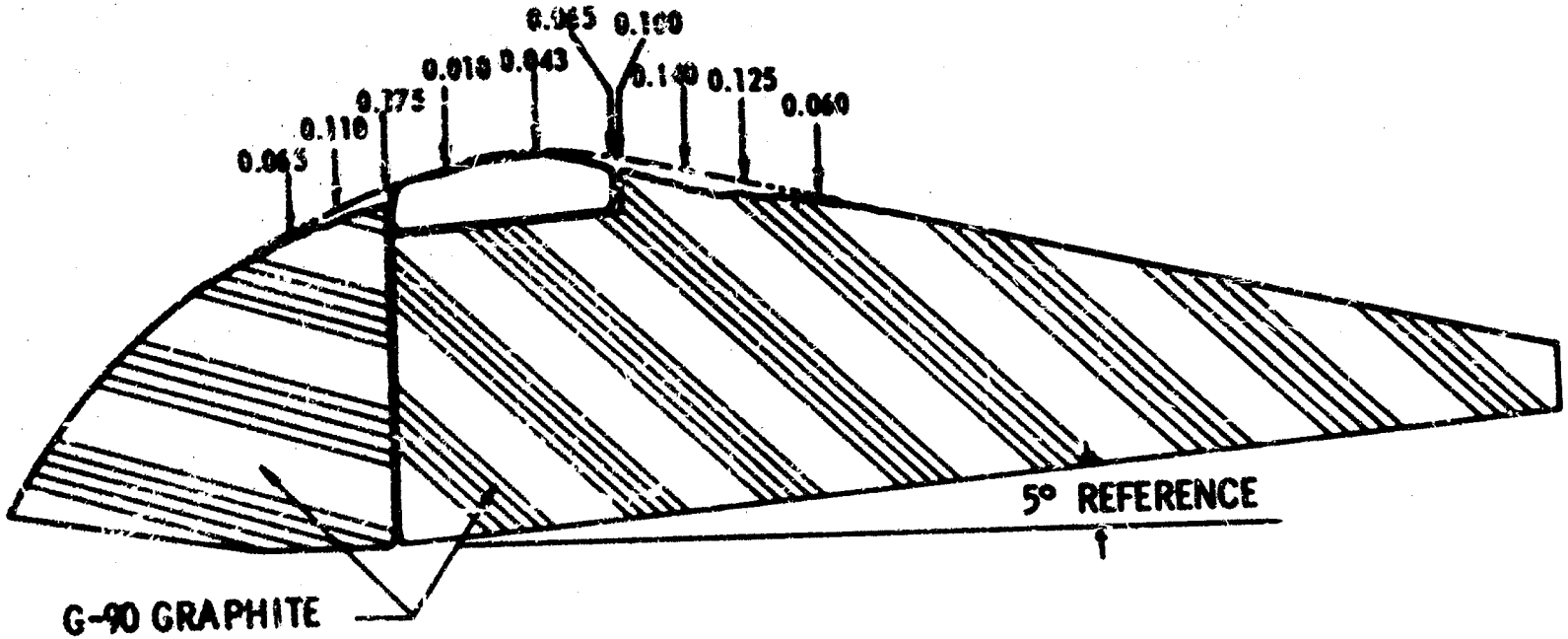

Figure 117. Regression Profile of Single TaC-C Hypereutectic Nozzle

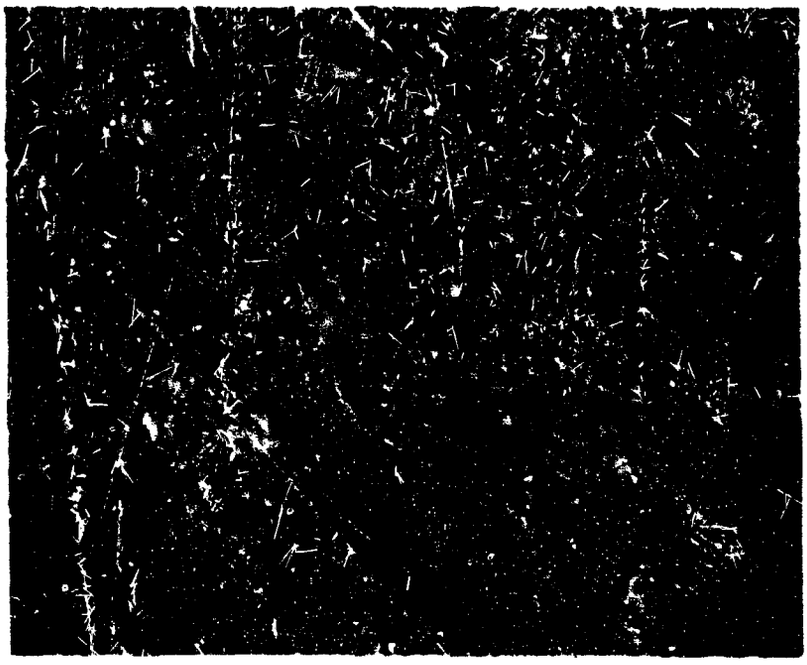

a. Typical Microstructure of TaC-C Hypereutectic Nozzle Insert. 50X

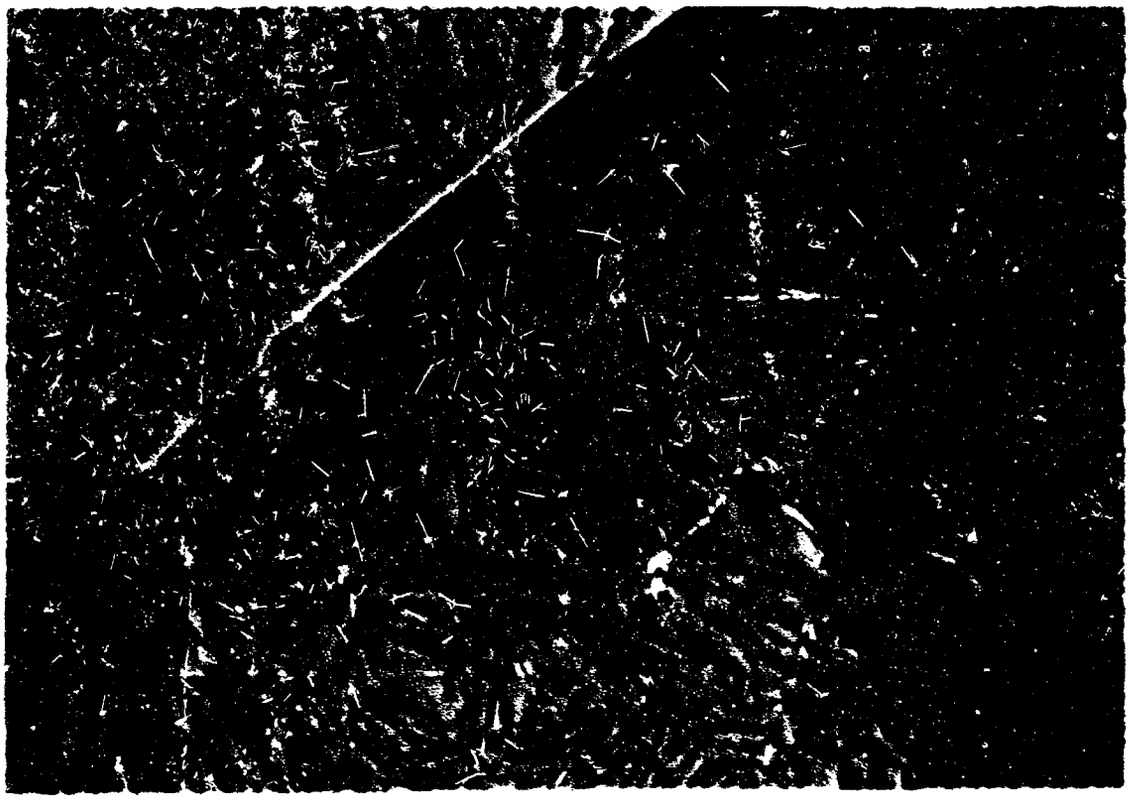

b. Termination of a Crack in Graphite Flake 100X

Figure 118. Microstructures of Single-Throat Insert

III, E, Task I--Demonstration of Firing Tests (cont.)

Circumferential Location	Segment* Location	Composition Determined from Carbon Analyses (v/o graphite flake)	Composition Determined by Density Measurements (v/o graphite flake)
0°	Entrance	5	9
	Exit	4	
120°	Entrance	3	10
	Exit	7	
240°	Entrance	3	11
	Exit	4	

The compositions derived by carbon analyses were somewhat lower than those obtained from density measurements. The effect of porosity or cracks inaccessible to water during the density measurement can cause these slight differences.

The temperature-time profile derived from a two-dimensional heat-transfer analysis of the nozzle design is shown in Figure 119. In this analysis, the flame surface of the insert reaches temperatures in excess of 5000°F shortly after ignition and approaches a near steady-state temperature of 5800°F. A large temperature gradient of over 3000°F across the insert can be noted by comparing the temperature curve for the surface of the insert with the temperature curve for the carbide/graphite interface. This large gradient is due to the relatively low thermal conductivity of the carbide composite.

As shown in Figure 119, good correlation was obtained between the theoretical heat-transfer analysis and the temperature data derived from the chromel-alumel thermocouple located in the graphite 1 in. below the flame surface at the throat.

*Location along the longitudinal cross-section of the insert.

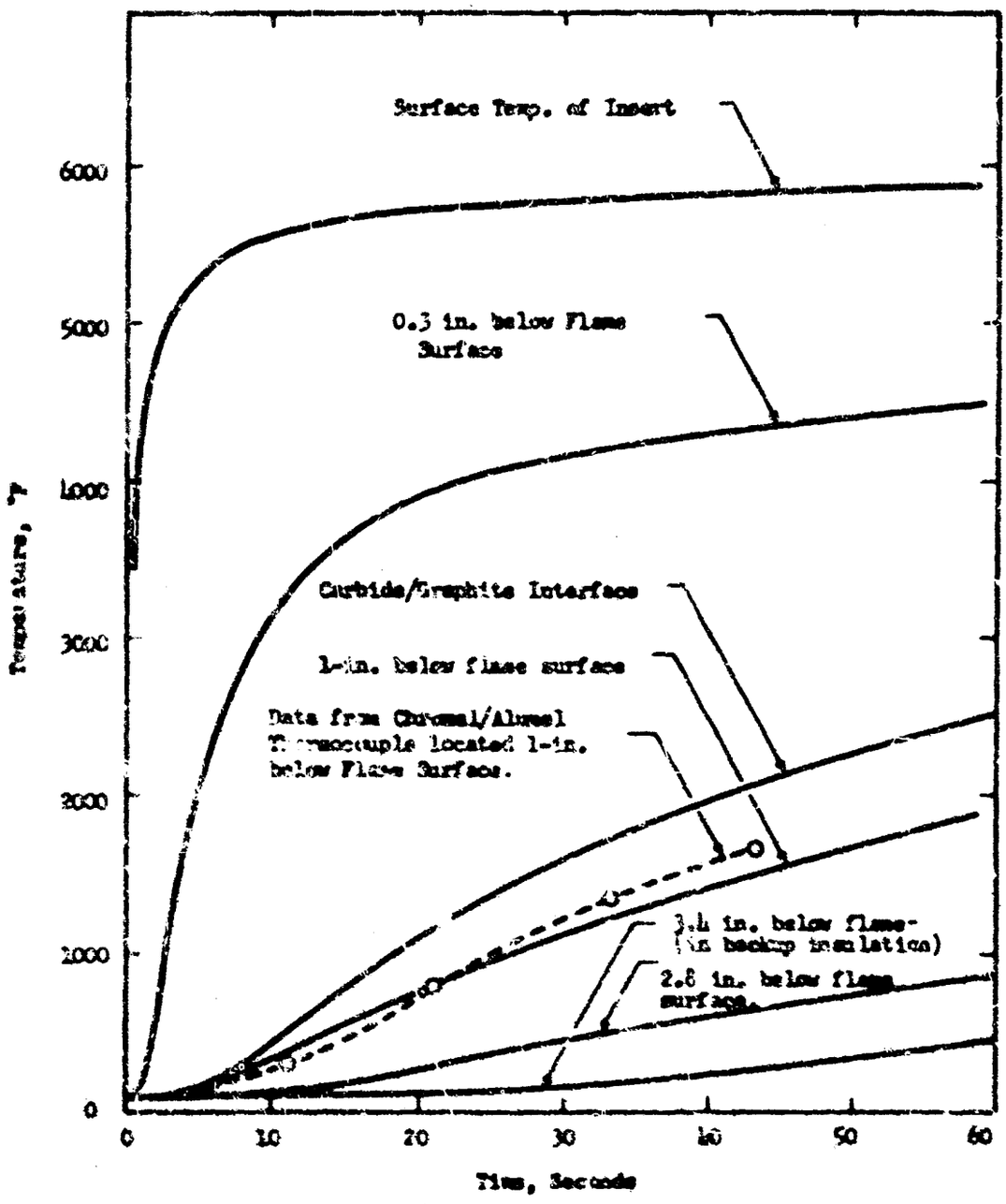

Figure 119. Thermal Profile of Single-Throat Insert Nozzle Design

SECTION IV

CONCLUSIONS AND RECOMMENDATIONS

A. CONCLUSIONS

1. Process Controls and Material Characteristics

a. Microcomposite

(1) Critical control of the impurity levels of the starting powders was required to develop the optimum metal-alloy precipitated phase. The most detrimental impurity was oxygen which inhibited diffusion of the metal into the carbide lattice. A total oxygen content of 500 ppm or less in the starting powders was found necessary.

(2) Successful fabrication of microcomposite structures is greatly dependent upon the control of the hot press parameters; temperature, pressure, time at temperature, and cooling rate.

(3) Of the microcomposites tested, the 8Ta-55Hf-37C and 8Ta-54Hf-38C offer the best potential for nozzle insert applications.

(4) Excellent resistance to crack projection in bend tests at elevated temperatures was achieved with the composition 8Ta-55Hf-37C.

b. TaC-C Hypereutectic

(1) The ability of the fusion and drop casting process to melt and cast TaC-C billets up to 4.7 in. in diameter, has been demonstrated.

(2) Strength and modulus of elasticity at ambient temperature are dependent upon carbon content. Compositions containing low carbon (8 to 9 w/o graphite flake) had high strengths (14,000 to 18,000 psi)

IV, A, Conclusions (cont.)

while compositions with high carbon contents (20 v/o graphite flake) had low strengths (2000 psi). The modulus of elasticity was found to decrease similarly with carbon content. Specimens with 9 to 10 v/o graphite flake had moduli of 30×10^6 psi. At high contents, 19 v/o graphite, the modulus values decreased to 13×10^6 psi.

(3) Elevated temperature flexure strengths for a given composition could be correlated with the morphology of the graphite flakes. Flakes that are thin, short in length, and evenly dispersed result in higher strength.

(4) Thermal expansion characteristics of the hypereutectic compositions closely followed the expansion behavior for tantalum monocarbide.

2. Environmental Capabilities

a. Thermal Shock Resistance

(1) The TaC-C hypereutectic composites from eutectic to high carbon compositions had excellent thermal shock resistance in both HES and solid propellant motor firing tests.

(2) Thermal stress cracking occurred in both micro-composite compositions during HES tests. Cracking was less severe for the 9Ta-55Hf-37C composition than the 9Ta-54Hf-38C composition.

b. Chemical Corrosion Resistance

(1) The principal mechanism responsible for material regression of both carbide composites was chemical corrosion caused by oxidants.

IV, A, Conclusions (cont.)

(2) The overall low regression rate and excellent structural integrity of the TaC-C hypereutectic composite in the solid-propellant motor firings established that this composite had excellent potential for nearly all high performance motor applications.

(3) Material regression of the TaC-C composites in motor firings was excessive in regions of high carbon content. The material removed appeared to be eroded by small fragments being cleaved along the planes of the large graphite flakes. Compositions near the eutectic provided the best resistance to material regression.

(4) Regression rates obtained on the microcomposite carbide during HES tests were significantly lower than the rates obtained from the TaC-lined TaC-C hypereutectic composites and Grade G-90 graphite.

3. Propellant Selection Criteria

a. TaC-C hypereutectic composite should be used with propellants containing low total oxidants in the exhaust gases for minimal material regression. A recommended maximum level would be 13 mol %.

b. The microcomposite has excellent resistance to corrosion because of the formation of an oxide film on the flame surface. This composite can be used with solid propellants containing high contents of oxidants in the exhaust. It appears that propellants with oxidant content up to 18 mole % could be used with the composite when minimal surface regression would be desired.

IV, A, Conclusions (cont.)

4. Carbide Nozzle Design Criteria

a. In designing carbide nozzles, provisions should be made for the high thermal expansion of carbide inserts; uniform symmetry of the throat insert must be maintained. Sufficient wall thickness must be provided to withstand high compression loading as material regression occurs, and the throat insert must be under compressive loading during entire duration of firing.

B. RECOMMENDATIONS

1. Process Refinements

a. Microcomposite

(1) A reduction in grain size would be highly desirable to increase mechanical properties and hence thermal shock resistance.

(2) An investigation of lower cost starting materials for producing the microcomposite is warranted.

(3) Further investigation is needed to refine the hot-press technique to enable the reliable fabrication of large nozzle components.

(4) Annealing, stress relieving and alloying of the metal phase are methods which should be investigated for additional improvements in ambient and elevated temperature properties.

IV, B, Recommendations (cont.)

b. TaC-C Hypereutectic

(1) An improvement in casting techniques is recommended to eliminate randomly occurring defects in cast billets. The typical type of defects found in billets are regions of porosity, "cold shut" and inhomogeneity. These types of defects become more pronounced in larger billets.

(2) Standards of quality must be established for this class of materials utilizing NDT and other quality control techniques.

2. Material Refinements

a. TaC-C Hypereutectic

(1) The control of grain size and the relationship of grain size with strength and the effect of cooling rate from the melt on grain size, and in turn, strength, should be investigated.

(2) Results of this program have shown that the morphology of the graphite flake can be varied and related to strength and possibly thermal shock resistance. Further experimentation is needed to better define this relationship and provide a material with optimized properties based upon microstructure.

(3) The investigation of alloy additions which will improve resistance to chemical attack by corrosive exhaust gas species appears promising as a means of further reducing the regression rates of the hypereutectic composites for highly oxidizing solid propellants.

REFERENCES

1. Aerospace Ceramics - Characteristics and Design Principles, Boland P. and Walton, J. D. Jr., TR-AFML-TR-65-171 (June 1965).

2. Rudy, E.: AFML-TR-65-2, Part II, Vol. I (September 1965).

3. Rudy, E.: AFML-TR-65-2, Part I, Vol. IV (September 1965).

4. "Engineering Properties of Selected Ceramic Materials", American Ceramic Society, Columbus, Ohio (1966).

5. E. S. Fisher and C. J. Renken, "Single-Crystal Elastic Moduli and the Hcp bcc Transformation in Ti, Zr, and Hf," Physical Review , 135 No. 2A, July 1964.

6. Tantalum and Tantalum Alloys, Schmidt, F. F., Defense Metals Information Center, Battelle Memorial Institute, Columbus 1, Ohio, DMIC Report 133 (July 25, 1960).

7. Research on Physical and Chemical Principles Affecting High Temperature Materials for Rocket Nozzles , Kebler, R. W., and Aspinall, S. R., Contract DA-30-069-ORD-2787, Final Report, Vol. II (Aug 1965), PXV-3.

8. T. B. Shaffer, "High Temperature Materials, No. 1", Plenum Press, New York, p. 95, (1964).

9. R. Resnick, and L. Seigle, "The Diffusion of Carbon in Tantalum Monocarbide, Transactions of the Metallurgical Society of AIME," Vol. 236, December 1966.

10. Diffusion of Carbon in Tantalum Carbides, Brisee, W. F., Report WAML-TMR-205, March 1967.

11. D. F. Kalinovich, I. I. Kovenskiy, and M. D. Smolin, "Diffusion Mobility of Carbon in Tantalum", Academy of Sciences Ukr. S.S.R., February 1964.

12. Lally, F. L. and Laverty, D. P., AFRPL-TR-68-164, (September 1968).

APPENDIX

TEST PROCEDURES

I. CHEMICAL ANALYSIS

A LECO Model 598 combustion analyzer was used to determine free and total carbon. Free carbon analyses were determined by dissolving the sample in a mixture of hydrofluoric and nitric acid. The remaining carbon was filtered and determined by combustion analyses involving absorption of the carbon-dioxide gas in KOH. The gas analysis for the total carbon was determined in a LECO conductivity cell.

II. METALLOGRAPHIC PROCEDURES

Specimens were mounted in a conductive mixture of copper-coated lucite powder and diallylphthalate. The metallographic preparation of the carbide specimen was accomplished by successive stages of grinding with silicon carbide papers ranging in grit size from 320 to 600. Final polishing was accomplished using microcloth with Linde B alumina (0.05 micron) in a 5% chromic acid solution. The samples were electro-etched using a 10% solution of oxalic acid. A dip-etch made up of a 10% solution of 6% HNO_3, 2% HCl, and 2% HF was used to clean the surface of the specimen to enhance phase contrast.

The specimens were microstructurally examined with a Zeiss Ultraphot II Metallograph.

III. DENSITY

The apparent density was measured by weighing specimens in air and suspended in water. The apparent density was calculated from the expression:

$$\text{Apparent Density} = \frac{\text{Weight (air)}}{\text{Weight (air)} - \text{Weight (water)}}$$

IV. PARTICLE-SIZE DISTRIBUTION--ANDREASON PIPET METHOD

The Andreason method depends upon the fact that, when an insoluble material is dispersed in a liquid medium and is allowed to settle freely under the force of gravity, the settling behavior is governed by Stokes' Law. According to this law, particles of a given size will settle a definite distance in a specified time interval. The distance settled will depend upon the densities of the material and of the suspending medium, the viscosity of the suspending medium, the size of the particle, and the length of time during which the particle is allowed to settle.

The Andreason method consists essentially of withdrawing a sample of definite volume from a suspension of a solid and liquid at definite intervals of time. The amount of solid material in the sample will represent all material in the suspension which is finer than a certain grain size. This grain size may be calculated from Stokes' Law, which, expressed mathematically, is as follows:

$$d = \sqrt{\frac{18\,h\,a}{g(D_1 - D_2)t}}$$

where:

- d - maximum grain diameter, cm
- a - coefficient of viscosity of suspending medium, poises
- h - distance through which the particle settles in a given time, cm
- t - time, sec
- D_1 - density of particles, gm/cc
- D_2 - density of suspending medium, gm/cc
- g - acceleration of gravity, cm/sec^2

IV, Particle-Size Distribution--Andreason Pipet Method (cont.)

By drawing samples at various intervals of time and calculating the percentage of the material in suspension finer than the grain size corresponding to those time intervals, a curve may be plotted which will represent the particle-size distribution of the material.

For these determinations, water was used as the suspending medium, which permitted determination of the fineness of powder with particles ranging from 30 to 0.5 microns. The method is not practical, however, for separations below 0.5 microns because Stokes' Law would become inoperative as a result of the time required.

V. MEASUREMENTS OF FLEXURAL STRENGTH

A. THEORY

In single-point loading, the flexural strength is expressed by the equation:

$$\sigma = \frac{3}{2} \frac{Pl}{bd^2}$$

where

P = maximum applied load, pounds
l = length of span, inches
b = width of specimen, inches
d = depth of specimen, inches

B. EQUIPMENT AND TEST PROCEDURES

Flexural strength (modulus of rupture or transverse bend strength) was measured at ambient and elevated temperatures by single point loading,

V, B, Equipment and Test Procedures (cont.)

using a graphite test fixture shown in Figure 120. Accurate alignment is maintained within the fixture by close tolerance machining to assure normal loading on the axial centerline of the specimen without eccentricity, and that the directions of loads and reactions be maintained parallel on the specimen.

The inset photograph in Figure 120 shows a closeup of the specimen positioned in the load train on two 0.25-in.-dia highly polished tungsten carbide bearing rollers. The tip at the center of the hard carbon (not capable of being graphitized) load ram contains a 1/8-in.-dia highly polished tungsten carbide roller to assure accurate centerline loading. At temperatures above 2000°F, the carbide rollers commence to plastically deform. These are then replaced with hard carbon rollers for the higher temperature tests. For ambient temperature testing, the distance between the centerlines of the two support bearing rollers was 1.500 in. and for the high-temperature testing, the distance was 1.700 in. A slightly shorter flexure specimen was machined for the room temperature testing since this specimen was used for determining the room temperature modulus of elasticity (dynamically) prior to the strength test.

A schematic view of the load train in the high temperature flexure furnace is shown in Figure 121. The graphite fixture containing the specimen is heated indirectly by radiation from a cylindrical, graphite resistance heater specifically slotted to provide a high-resistance path. The fixture is positioned on a water-cooled copper ram which transmits the loading during testing to the compression load cell. A bushing in the upper lid of the furnace provides added alignment to the carbon load ram.

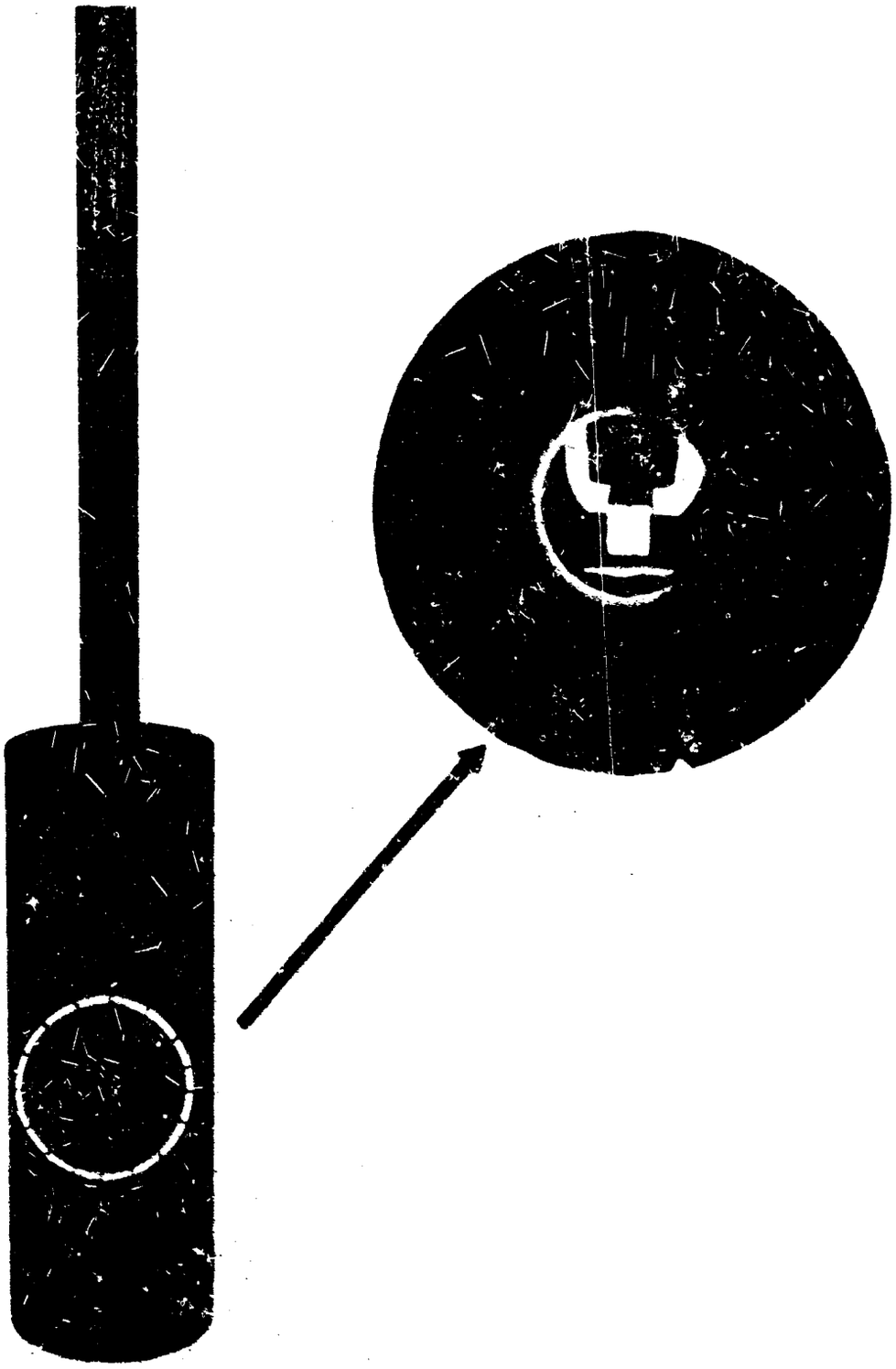

Figure 120. Graphite Flexural Strength Test Fixture

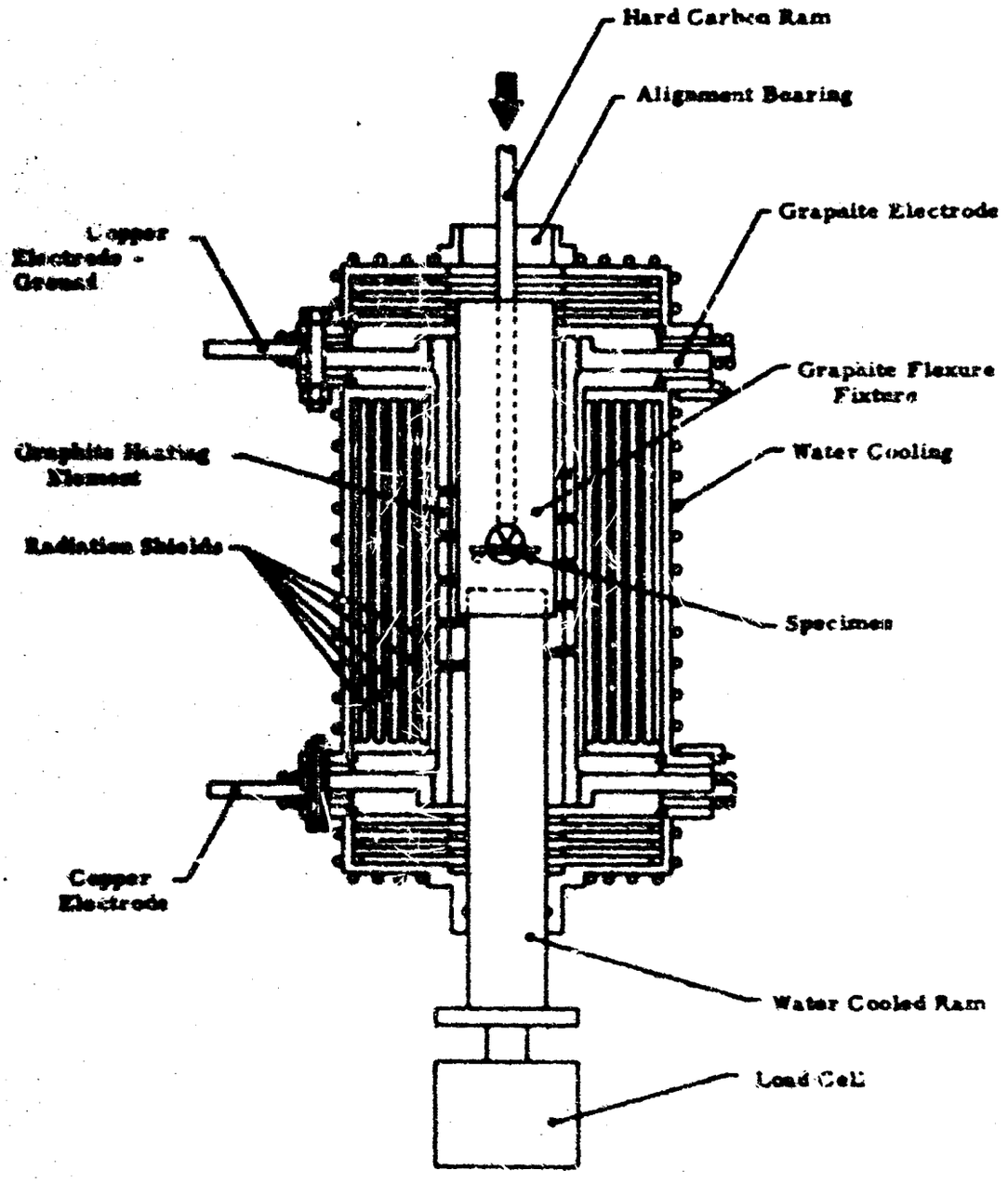

Figure 121. Schematic View of the Flexure Test Fixture and Load Train in the Furnace

V, B, Equipment and Test Procedures (cont.)

Power is supplied to the furnace by a saturable-core reactor-controlled 31 kw ac transformer. Specimen temperatures up to 1650°C are measured by a platinum/platinum-10% rhodium thermocouple and temperatures from 1650 to 2200°C a tungsten/tungsten-26% rhenium thermocouple is positioned near the surface of the specimen. Above these temperatures, a Leeds and Northrup disappearing filament optical pyrometer is used.

Figure 122 shows a view of the furnace mounted on the Instron test machine. For the elevated temperature tests, the specimen was heated in an argon atmosphere to the required test temperature and then heat-soaked for 15 minutes. The load is applied at a constant cross-head travel rate of 0.02 in./minute. The strip chart on the machine records load vs time.

VI. THERMAL DIFFUSIVITY

A. THEORY

The flash method of determining thermal diffusivity (thermal conductivity) consists essentially of the absorption of a very short pulse of radiant energy in the front of a specimen, and the recording of the resultant temperature history of the rear surface.

In the ideal case of a perfectly insulated specimen with a constant absorptivity across its surface, uniformly irradiated with a pulse of thermal energy short compared with the time required for heat to flow through the material, the back surface temperature history is given by

$$\frac{T(L,t)}{T_m} = 1+2 \sum_{n=1}^{\infty} (-1)^n \exp\left(-n^2 \pi^2 \alpha t/L^2\right) \qquad \text{(Eq 1)}$$

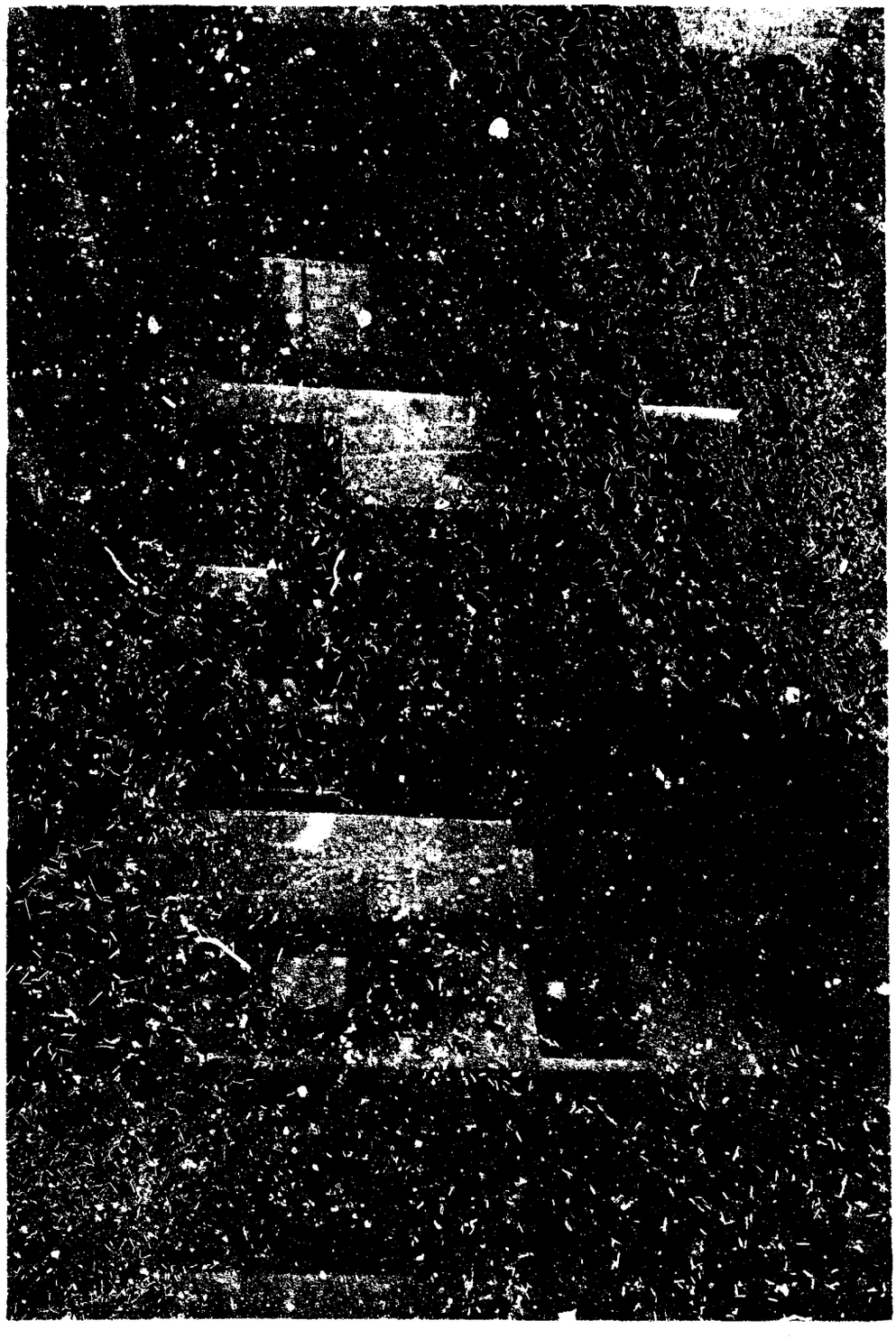

Figure 122. View of Flexure Test Furnace Mounted on the Instron Test Machine

VI, A, Theory (cont.)

where T (L,t) represents the instantaneous back surface temperature rise at time t, T_m is the maximum back surface temperature rise, α is the thermal diffusivity in cm^2/sec, L is the specimen thickness in cm, and n represents successive integers. At the time $t_{1/2}$, where T(L,t) = 0.5 T_m, Eq 1 reduces to

$$\alpha = \frac{k}{\rho C_p} = \frac{1.37L^2}{\pi^2 t_{1/2}} = \frac{0.139L^2}{t_{1/2}} \qquad \text{(Eq 2)}$$

Hence, the thermal diffusivity of a material can be determined from the specimen thickness and the time in seconds required for the back surface temperature to reach one-half of its maximum value.

The success of the method depends upon adequately meeting the boundary conditions which lead to Equation 1. Figure 123 is a dimensionless plot of Equation 1 and represents the form that the back surface temperature history of the sample will take if these boundary conditions are satisfactorily met. A departure of the data from this curve illustrates that these conditions have not been met and invalidates the data.

A condition vital in the use of Equation 1 is that the front surface of the sample must be uniformly irradiated with a pulse of thermal energy in a time which is short compared to the rise time of the back surface temperature. To accomplish this, a xenon flash lamp is used as the source of that thermal pulse. The lamp used is a General Electric type 524 through which 600 joules are discharged. The pulse is essentially completed in 500 microsec while the time to one-half of the maximum of the rear surface temperature was for the most part 50 to 300 microsec. It should be noted in Equation 2 that, for a given material, the rise time of the rear surface temperature is a function of the square of the sample thickness. A sample thickness sufficient to satisfy this condition of a short pulse duration

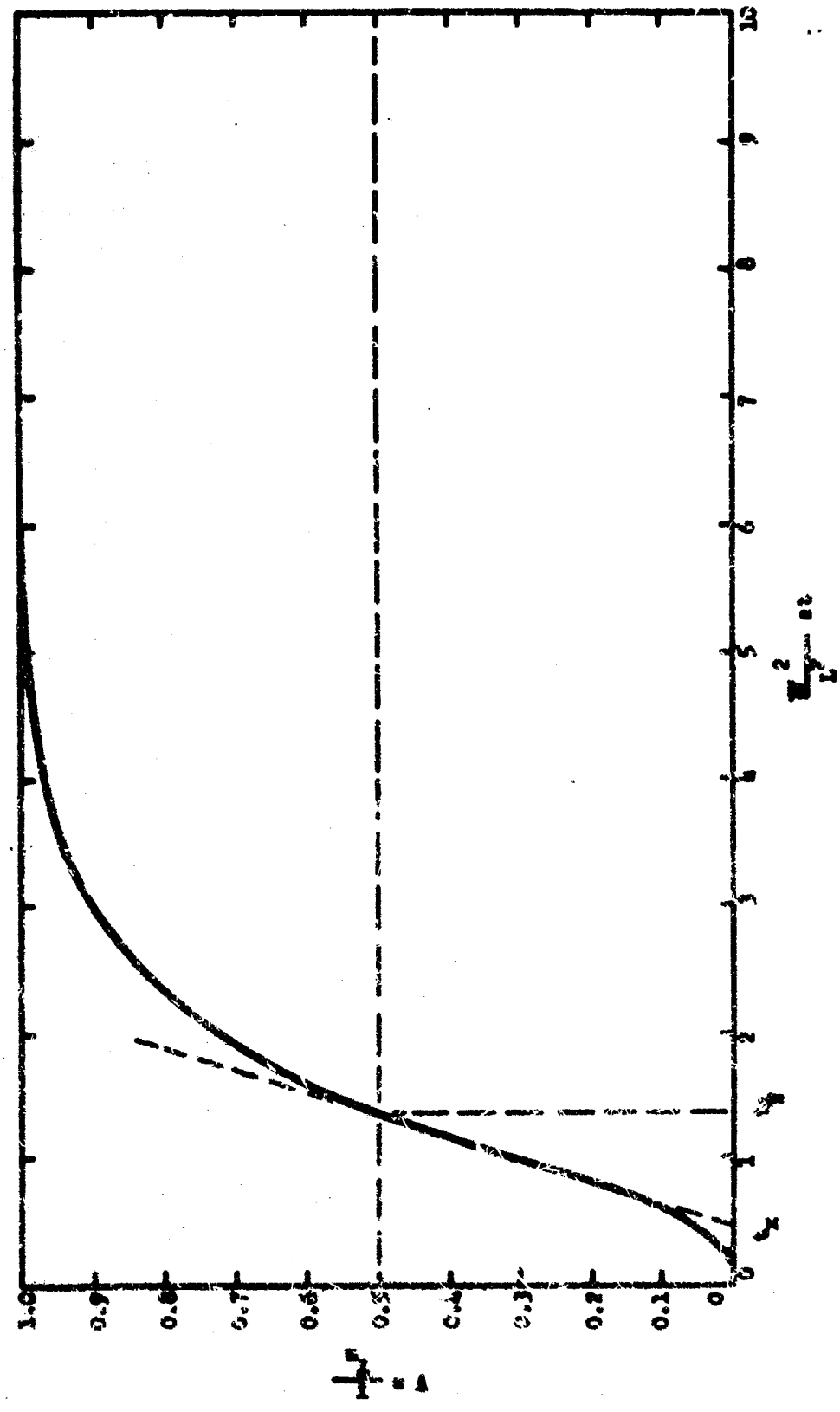

Figure 123. Dimensionless Plot of Rear Surface Temperature History

VI, A, Theory (cont.)

should be used. However, for a given amount of input energy, the maximum temperature rise attained, T_m, is an inverse function of the thickness of the sample, and to maximize the temperature of irradiance, the distribution of that irradiance on the front surface of the sample is important as noted earlier. It is a simple procedure to obtain uniform irradiation on a small flat surface from a flash lamp, but it is a boundary condition which must nevertheless be satisfied, otherwise the shape shown in Figure 1 may be distorted. The 2-in.-dia helical lamp is placed without optics only a few centimeters from the sample.

The other boundary condition imposed on Equation 1 is that the specimen be perfectly insulated. The degree to which this is satisfied within the time limits of interest is indicated by the decay rate of the back surface temperature after the maximum T_m is attained. Because of these factors, the sample holder should be designed so as to minimize all heat losses. Conductive heat losses are minimized by supporting the sample on a small area. Provided appropriate care is exercised by the experimenter, conduction heat losses, as well as convective heat losses, are negligible because of the short times involved in the flash technique. Radiative heat losses at high temperatures cannot be eliminated and, therefore, could constitute the greatest problem in the satisfaction of this boundary condition.

B. EQUIPMENT AND TEST PROCEDURES

The experimental apparatus used in these measurements is shown schematically in Figure 124. The induction heater coil leads are fed into the vacuum chamber and form a coil with an inside diameter of about one inch. The sample is held in position in the coil by a mount machined from lava and baked to a ceramic. Shields of boron nitride prevent heating of the chamber walls by radiation from the sample. Fused quartz is used for the

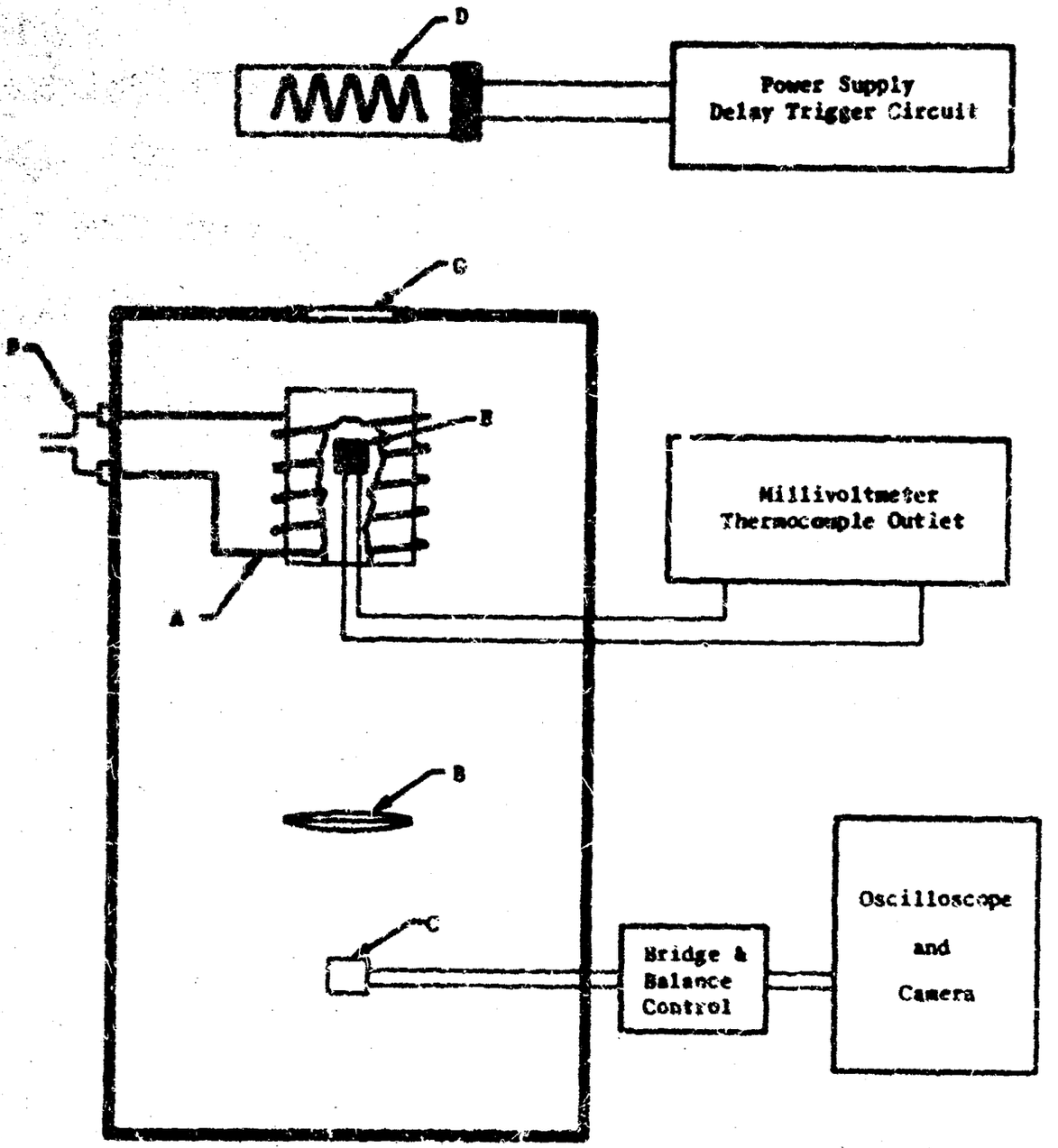

A - RF Induction Heater
B - Lens
C - Pbs Cell
D - Xenon Flash Lamp GE 524
E - Sample
F - To RF Generator
G - Window

Figure 124. Schematic Diagram of Thermal Diffusivity Apparatus

VI, B, Equipment and Test Procedures (cont.)

top window because the large thermal gradients close to the hot samples would crack glass windows. The steady-state temperature at which measurements are made is indicated by thermocouple leads fastened to the edge of the sample and fed out of the vacuum system. An optical pyrometer is used at temperatures above which platinum/platinum-rhodium thermocouples will perform. A glass lens below the sample focuses the center portion of the rear of the sample on a lead sulfide cell which measures the surface temperature history over a range from 300 to 1800°C. The linearity of the lead sulfide cell is adequate since the temperature change of the sample from the pulse is not more than a few degrees. It should be noted that a knowledge of the absolute value of detector sensitivity or the thermal input to the saple is not required because only $t_{1/2}$ is involved in Equation 2, and this time can be obtained from the calibrated sweep of the oscilloscope.

The detector is connected differentially through a load selector and balance control unit to the differential preamp of an oscilloscope. The use of differential detector circuitry is necessary to minimize the effects of the extremely high magnetic field which surrounds induction heating coils. A trigger delay circuit is used to fire the flash lamp after the oscilloscope sweep has been triggered. This is necessary to have a base line on the print from which to measure the change in the detector output voltage.

Figure 125 is a Polaroid print of the oscilloscopic delay of the detector output for a microcomposite specimen. When the shape of the temperature rise is compared with Figure 123, the agreement indicates the boundary requirements have been satisfied by the samples reported here. Since heat losses from the sample would show up as a decay in the detector output after the initial rise, it is evident from this print that the thermal pulse travels through the sample in a time which is extremely short compared with the time required for the sample to return by heat losses to the equilibrium temperature at which the measurement is made. Nonuniform illumination of the front surface could distort the knee of the curve.

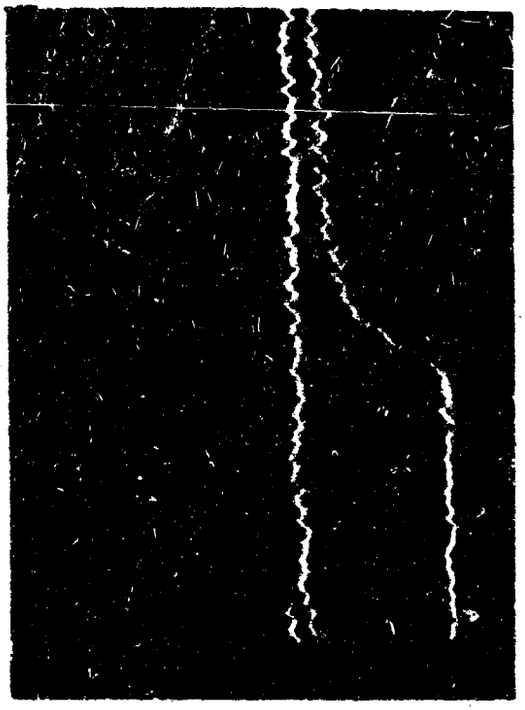

Figure 123. Polaroid Print of the Oscilloscopic Delay of Detector Output

VII. THERMAL EXPANSION

The test method used for thermal expansion measurements was similar to the optical technique reported by Conway and Losekamp (Reference 1) where distances between reference edges of a horizontal specimen are observed and measured at various steady-state temperatures by a pair of filar microscopes. Fiducial marks are ground in the specimen to provide a gage distance of 2.0 in. The specimen is heated by thermal radiation from a 6-in.-long, hollow cylindrical-type graphite heating element. The heating element completely encompasses the specimen and radiation shields minimize heat leakage and maintain a uniform specimen temperature. A 10 psig helium gas atmosphere is maintained around the specimen and heating element during all tests. The arrangement of the microscopes on the furnace is shown in Figure 126. The filar microscopes sight on the edges of the fiducial marks in the specimen. Room temperature measurements of the distance between edges of the specimen were made before each test and similar measurements during the test were made at steady-state temperatures ranging from 25 to 2760°C. The microscopes used provided a reading accuracy of 2 by 10^{-5} in. The specimen temperature is determined with an automatic recording optical brightness pyrometer, which views the specimen from the end of the furnace.

Data correction factors are applied to temperature measurements made through the quartz window using the optical pyrometer and to expansion measurements made with the microscope through a column of hot gas. Temperature corrections for the quartz window are determined by observing a hot tungsten filament lamp for conditions with and without a quartz window in front of the optical pyrometer. Optical corrections for expansion measurements are determined from tests conducted on specimens both in a vacuum and the general 10 psig helium test atmosphere. Expansion measurements in a vacuum are considered true. This latter correction is most significant and very important for accurate results. All of the corrections described are applied to the expansion data in an IBM 1130 computer program which derives a "least square fit" for the corrected data to the following equation:

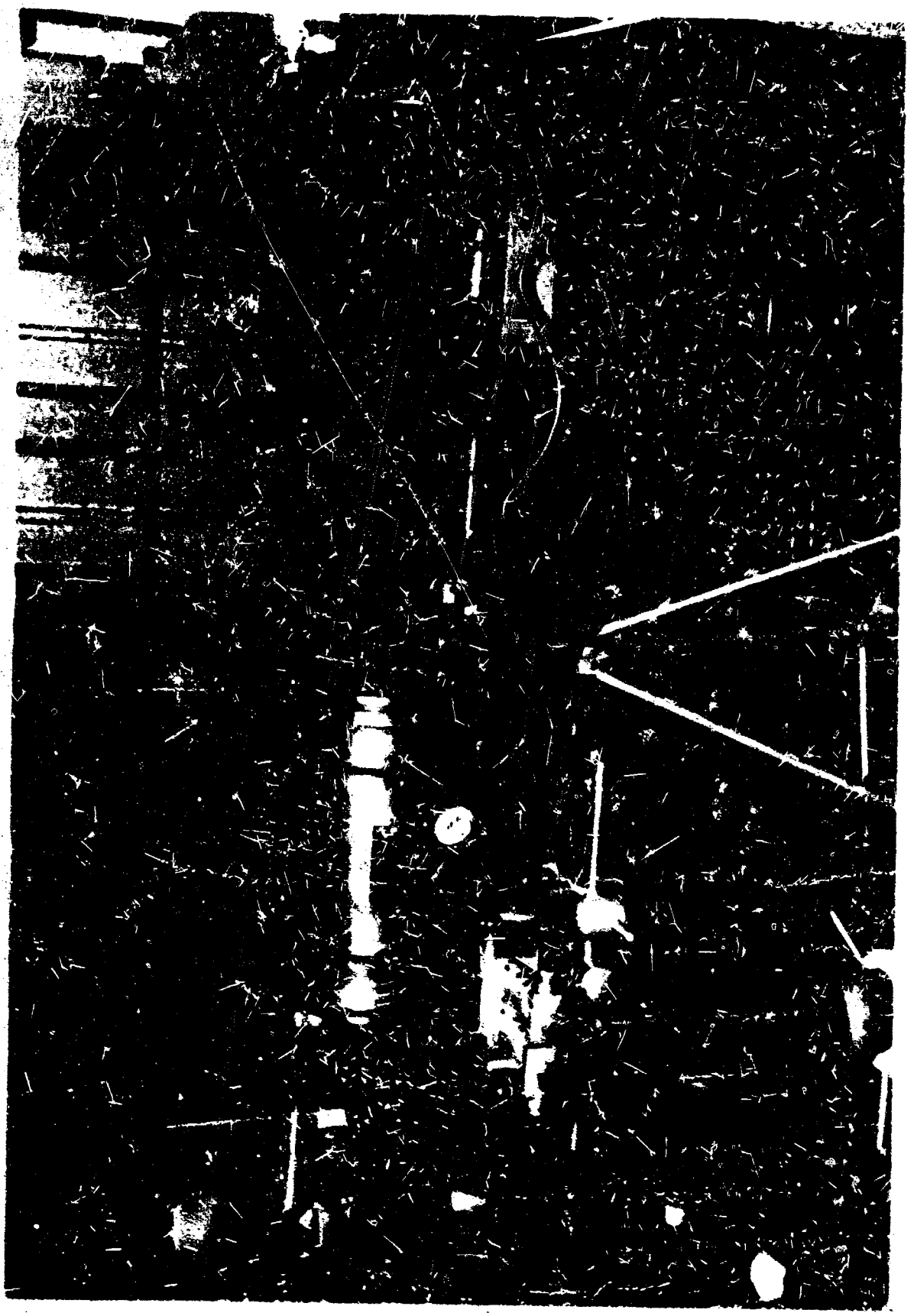

Figure 126. Equipment for Measuring Thermal Expansion

VII, Thermal Expansion (cont.)

$$\alpha = \frac{L_T - L_{21°C}}{L_{21°C}} = A_1 (T-21) + A_2 (T-21)^2$$

where:

α = thermal expansion
L_T = length between edges at T
$L_{21°C}$ = length between edges at 21°C
T = temperature, °C
$A_1 A_2$ = constants

VIII. MELTING POINT DETERMINATION

The Pirani melting point method, as described in Reference 2, is used whereby a small sample bar with a black body hole in the center is heated resistively. The temperature of the black body is measured with an optical pyrometer. Incipient melting is detected by observation of a change in emissivity within the black body hole due to the formation of melt in the center of the specimen.

The melting point furnace consists of two water-cooled copper electrodes enclosed in a double-jacketed vacuum-tight housing. The specimen, which is held between two tungsten platelets, is clamped directly onto the water-cooled electrodes (Figure 127a). A constant force, applied through a lever arm by weights (visible in Figure 127b in front of the electrodes) ensures good electrical contact between specimen and electrode. The thermal expansion of the specimen is accounted for by having one movable electrode. Figure 128 shows a typical Pirani melting point specimen produced from the microcomposite compositions.

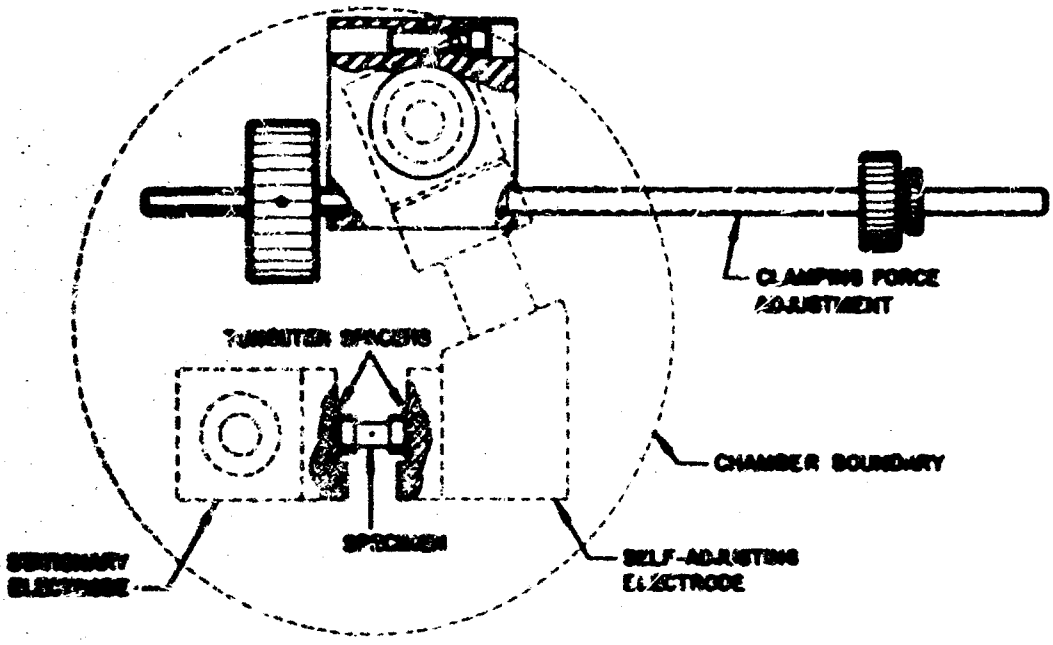

a. Face-to-Face Clamping of the Test Specimen, and Gravity Balance System

b. Interior View of Melting Point Furnace

Figure 127. Melting Point Furnace

Figure 128. Typical Pirani Melting Point Furnace

VIII, Melting Point Determination (cont.)

A gravity balancing system, firmly connected to the movable electrode on the outside of the chamber allows the specimen to be put either under axial tension or compression. The maximum axial force, which can be exerted in this way on the sample is ±2000 g and can be controlled to within ±30 g. The furnace can be operated either under vacuum or under inert gas of up to ~1/2 atmospheres.

The power supply consists of a 50 kva saturable core-reactor, step-down transformer system. The power control is effected by way of the dc-supply of the saturable reactor by means of a potentiometer with continuously variable dc-speed drive. Power application rates can be varied between 20 and 15,000 watts/sec, and are controlled by foot switches at the operator's site.

The temperature of the sample is measured optically with a disappearing-filament type micropyrometer through a quartz window in the furnace wall. A small hole, generally in the order of 0.6 to 1.0 mm in diameter, drilled or pressed into the sample, serves as the reference point for the temperature measurements. The micropyrometers are periodically calibrated against standard lamps, which were calibrated and certified by the National Bureau of Standards. As a further means of assurance of the calibration, the pyrometers are periodically checked directly against a standard pyrometer, calibrated and certified by the National Bureau of Standards.

IX. MODULUS OF ELASTICITY

A. THEORY

The dynamic modulus of elasticity was derived dynamically by the use of a composite piezoelectric resonator which operates on the theorem

IX. A, Theory (cont.)

that a linear mechanical vibrator driven by a condenser-coupled emf behaves electrically like a simple combination of circuit elements. For a multi-component resonator, the resonant frequency of a component is given by the following equation:

$$F_s = \frac{1}{M_s}\left[M_t T_t - M_r F_r\right]$$

where:

M_s, M_t, M_r = mass of sample, total resonator assembly and resonator assembly minus the sample, respectively

F_s, F_t, F_r = the corresponding resonant frequencies

The values for F_t and F_r are measured directly and F_s is then calculated from values of F_t and F_r. The modulus is then calculated as a function of temperature.

$E_s = \rho(2\ell_s F_s)^2$

ρ = specimen density

ℓ_s = specimen length

F_s = specimen resonant frequency

B. EQUIPMENT AND TEST PROCEDURES

The measurement system is shown schematically in Figure 129, and a view of the test equipment is shown in Figure 130. The driver-gage combination is a permanent assembly made by bonding two quartz rods together with beeswax. For room temperature modulus measurements, the specimen is bonded directly to the end of the driver rod with a thin film of beeswax.

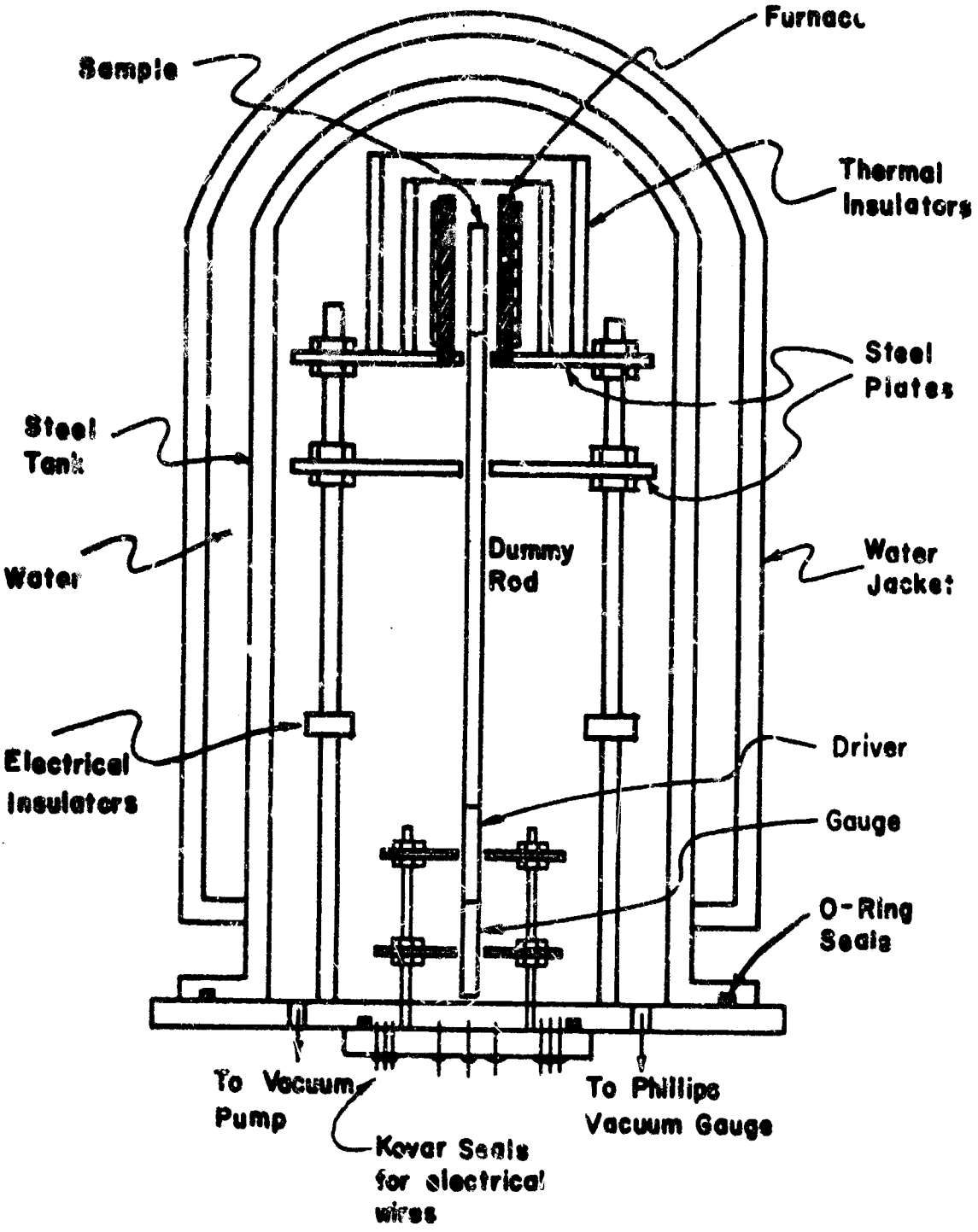

Figure 129. Schematic of Dynamic Modulus of Elasticity Apparatus

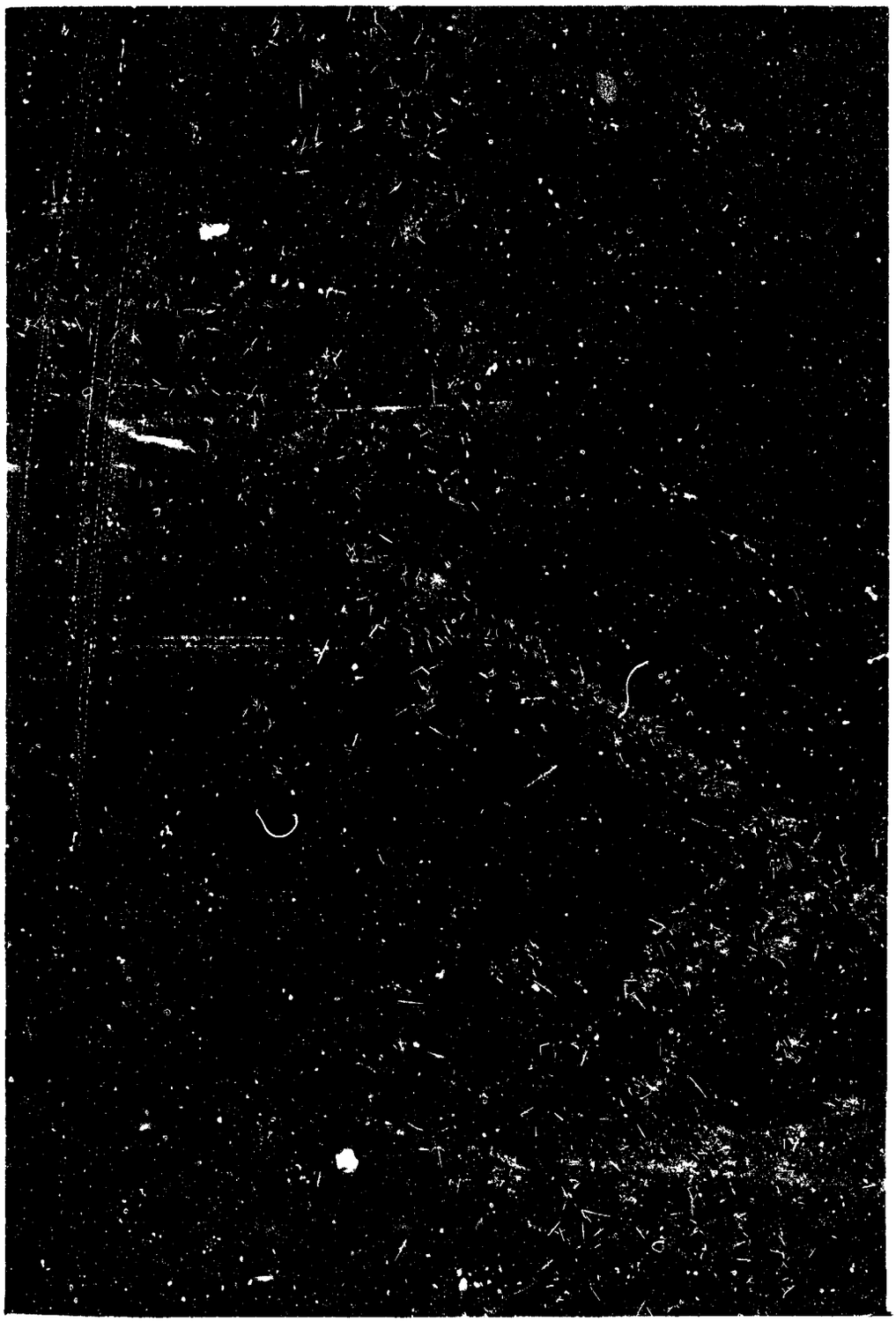

Figure 130. View of Test Equipment for Measuring Dynamic Modulus of Elasticity

IX, B, Equipment and Test Procedures (cont.)

For measurements at elevated temperatures, a long sapphire rod, cut so that it has a harmonic resonance at the fundamental frequency of the driver-gage unit, is inserted between the specimen and the driver. This permits the quartz components to be maintained near room temperature while the specimen at the end of the rod is inserted into the furnace. The major experimental difficulty for high-temperature measurements is obtaining a cement which provides sufficient bonding at the high temperature. Generally, Sauereisen cement is used for joining the specimen to the sapphire rod. The temperature limit by this technique is approximately 1200°C.

REFERENCES

1. J. B. Conway and A. C. Losekamp, "Thermal Expansion Characteristics of Several Refractory Metals to 2500°C", Transactions of the Metal. Soc. of AIME, 236, 702-709, (May 1966).

2. E. Rudy, St. Windisch, and Y. A. Chang, Technical Documentary Report No. AFML-TR-65-2, Part I, Volume I, 30-41 (Jan. 1965).

Unclassified

Security Classification

DOCUMENT CONTROL DATA - R&D

(Security classification of title, body of abstract and indexing annotation must be entered when the overall report is classified)

1 ORIGINATING ACTIVITY (Corporate author) Aerojet-General Corporation P.O. Box 15847 Sacramento, California	2a REPORT SECURITY CLASSIFICATION Unclassified 2b GROUP

3 REPORT TITLE

Advanced Composite Carbide Nozzles

4 DESCRIPTIVE NOTES (Type of report and inclusive dates)

Final Report 1 July 1966 to 12 July 1968

5 AUTHOR(S) (Last name, first name, initial)

R. P. Radtke and L. M. Swope

6 REPORT DATE	7a TOTAL NO OF PAGES	7b NO OF REFS
August 1968	246	14

8a CONTRACT OR GRANT NO.	9a ORIGINATOR'S REPORT NUMBER(S)
AF 04(611)-11608 b PROJECT NO	AFRPL-TR-68-143
c d	9b OTHER REPORT NO(S) (Any other numbers that may be assigned this report)

10 AVAILABILITY/LIMITATION NOTICES

Foreign announcement and dissemination of this report by DDC is not authorized.

11 SUPPLEMENTARY NOTES	12 SPONSORING MILITARY ACTIVITY
	Rocket Propulsion Laboratory Air Force Systems Command Edwards, California

13 ABSTRACT

The purpose of this program was to develop two thermal-shock-resistant composite carbide systems that could be reliably used with high-flame temperature solid rocket propellants. The selected systems were: (1) a microcomposite consisting of a tantalum/hafnium monocarbide and tantalum/hafnium alloy, and (2) a tantalum-carbide coated, tantalum carbide/graphite hypereutectic.

Fabrication procedures were developed, and ambient and elevated temperature properties were characterized for both the microcomposite and TaC/C hypereutectic systems. The composites were evaluated for thermal shock and chemical corrosion resistance in a hyperthermal environmental simulator using subscale inserts. The TaC/C composite exhibited outstanding thermal shock resistance, while the microcomposite showed excellent corrosion resistance.

Scale-up of the fusion casting of the TaC/C hypereutectic composite to produce 4.5-in.-dia by 3.0-in.-long billets was demonstrated. Two solid propellant motor firings using 6500°F propellant were conducted on nozzles containing TaC/C hypereutectic throat inserts.

DD Form 1473

Unclassified

Security Classification

Unclassified

Security Classification

14 KEY WORDS	LINK A		LINK B		LINK C	
	ROLE	WT	ROLE	WT	ROLE	WT
Carbide Composites Rocket Nozzle Materials Carbide Hypereutectics Ta-C Diffusion Data High Temperature Properties Motor Firings Thermal Shock Evaluation Chemical Corrosion Evaluation						

INSTRUCTIONS

1. **ORIGINATING ACTIVITY:** Enter the name and address of the contractor, subcontractor, grantee, Department of Defense activity or other organization *(corporate author)* issuing the report.

2a. **REPORT SECURITY CLASSIFICATION:** Enter the overall security classification of the report. Indicate whether "Restricted Data" is included. Marking is to be in accordance with appropriate security regulations.

2b. **GROUP:** Automatic downgrading is specified in DoD Directive 5200.10 and Armed Forces Industrial Manual. Enter the group number. Also, when applicable, show that optional markings have been used for Group 3 and Group 4 as authorized.

3. **REPORT TITLE:** Enter the complete report title in all capital letters. Titles in all cases should be unclassified. If a meaningful title cannot be selected without classification, show title classification in all capitals in parenthesis immediately following the title.

4. **DESCRIPTIVE NOTES:** If appropriate, enter the type of report, e.g., interim, progress, summary, annual, or final. Give the inclusive dates when a specific reporting period is covered.

5. **AUTHOR(S):** Enter the name(s) of author(s) as shown on or in the report. Enter last name, first name, middle initial. If military, show rank and branch of service. The name of the principal author is an absolute minimum requirement.

6. **REPORT DATE:** Enter the date of the report as day, month, year, or month, year. If more than one date appears on the report, use date of publication.

7a. **TOTAL NUMBER OF PAGES:** The total page count should follow normal pagination procedures, i.e., enter the number of pages containing information.

7b. **NUMBER OF REFERENCES:** Enter the total number of references cited in the report.

8a. **CONTRACT OR GRANT NUMBER:** If appropriate, enter the applicable number of the contract or grant under which the report was written.

8b, 8c, & 8d. **PROJECT NUMBER:** Enter the appropriate military department identification, such as project number, subproject number, system numbers, task number, etc.

9a. **ORIGINATOR'S REPORT NUMBER(S):** Enter the official report number by which the document will be identified and controlled by the originating activity. This number must be unique to this report.

9b. **OTHER REPORT NUMBER(S):** If the report has been assigned any other report numbers *(either by the originator or by the sponsor)*, also enter this number(s).

10. **AVAILABILITY/LIMITATION NOTICES:** Enter any limitations on further dissemination of the report, other than those imposed by security classification, using standard statements such as:

(1) "Qualified requesters may obtain copies of this report from DDC."

(2) "Foreign announcement and dissemination of this report by DDC is not authorized."

(3) "U. S. Government agencies may obtain copies of this report directly from DDC. Other qualified DDC users shall request through _____."

(4) "U. S. military agencies may obtain copies of this report directly from DDC. Other qualified users shall request through _____."

(5) "All distribution of this report is controlled. Qualified DDC users shall request through _____."

If the report has been furnished to the Office of Technical Services, Department of Commerce, for sale to the public, indicate this fact and enter the price, if known.

11. **SUPPLEMENTARY NOTES:** Use for additional explanatory notes.

12. **SPONSORING MILITARY ACTIVITY:** Enter the name of the departmental project office or laboratory sponsoring *(paying for)* the research and development. Include address.

13. **ABSTRACT:** Enter an abstract giving a brief and factual summary of the document indicative of the report, even though it may also appear elsewhere in the body of the technical report. If additional space is required, a continuation sheet shall be attached.

It is highly desirable that the abstract of classified reports be unclassified. Each paragraph of the abstract shall end with an indication of the military security classification of the information in the paragraph, represented as (TS), (S), (C), or (U).

There is no limitation on the length of the abstract. However, the suggested length is from 150 to 225 words.

14. **KEY WORDS:** Key words are technically meaningful terms or short phrases that characterize a report and may be used as index entries for cataloging the report. Key words must be selected so that no security classification is required. Identifiers, such as equipment model designation, trade name, military project code name, geographic location, may be used as key words but will be followed by an indication of technical context. The assignment of links, rules, and weights is optional.

Unclassified

Security Classification